UNIVERSITY OF SOUTHAMPTON

FACULTY OF ENGINEERING AND APPLIED SCIENCE

THE EFFECTS OF WHOLE-BODY VIBRATION ON THE PERCEPTION OF THE HELMET-MOUNTED DISPLAY

VOLUME II

by

Thomas Adrian Furness III

A thesis presented for the degree of
Doctor of Philosophy, 1981.

Chapter 5
DYNAMIC CHARACTERISTICS OF THE HELMET-MOUNTED DISPLAY DURING WHOLE-BODY VIBRATION

5.1 GENERAL CONSIDERATIONS

The biomechanical behaviour of subjects wearing the helmet-mounted display during whole-body vibration was investigated to explain the nature of the effects of vibration on reading performance as observed in the legibility experiments reported in Chapter 4. The main objectives of these investigations were:

a. to define the nature of the seat vibration input;

b. to determine the involuntary translational and rotational movements of the head and helmet due to sinusoidal vertical Z axis seat vibration at various frequencies;

c. to measure the rotational movements of the helmet on the head;

d. to determine the effects of operator voluntary variables (i.e., head orientation);

e. determine the magnitude of the perceived displacements of the display image in space and relative to the eye.

Eight dynamic studies were conducted to measure seat, head, helmet, and display motion during whole-body vibration at various frequencies and amplitudes. These experiments (i.e., BD.1, BD.2, BD.3, BD.4, BD.5, BD.6, BD.7, BD.8) are reported in this chapter. Reported in Chapter 6 are two other experiments (i.e., SD.1 and SD.2) in which the displacement of the helmet-mounted display image in space and relative to the eye were measured using subjective methods. Results of both dynamic and subjective displacement experiments are related to reading performance in Chapter 6. A separate dynamic study was conducted also during the helicopter field trial (i.e., H.2). This experiment is reported in Chapter 7.

5.1.1 Factors Studied in Dynamic Experiments

The dependent and independent variables considered in the dynamic experiments are listed in Table 3.1.2.

5.1.2 Coordinate System

Figure 5.1.1 shows a coordinate system for the biomechanical variables associated with head-coupled displays. The coordinate system gives the measurement axes for the translational and rotational motions of the subject, helmet-mounted display, and the environment, and includes seat, head, helmet, eye, and display motion parameters. The principal axes of translational motion of the body conform to the guidelines of ISO 2631 (1974). Since the head moves relative to the body, another set of reference axes is given for the rotational motion of the head. In this regard, the following definitions are given for the axes of rotation illustrated in Figure 5.1.1:

a) Pitch Axis. Axis of rotational motion which is parallel to a line through the ears. This axis is nominally parallel to the Y axis as defined by ISO 2631 when the subject is seated with an erect posture, looking straight ahead.

b) Yaw Axis. Axis of rotational motion which is parallel or coincident with a line through the vertex of the head (or helmet) and which bisects the line through the two ears. This axis is nominally the Z axis, as defined by ISO 2631, when the subject is seated with an erect posture, looking straight ahead.

c) Roll Axis. Axis of rotational motion which is parallel to a line through the bridge of the nose that bisects the line between the two ears. This axis is nominally parallel to the X axis, as defined by ISO 2631, when the subject is seated with an erect posture, looking straight ahead.

Figure 5.1.1 shows the relative positions of the three axes of rotation to which the various motion elements are referred (e.g., head

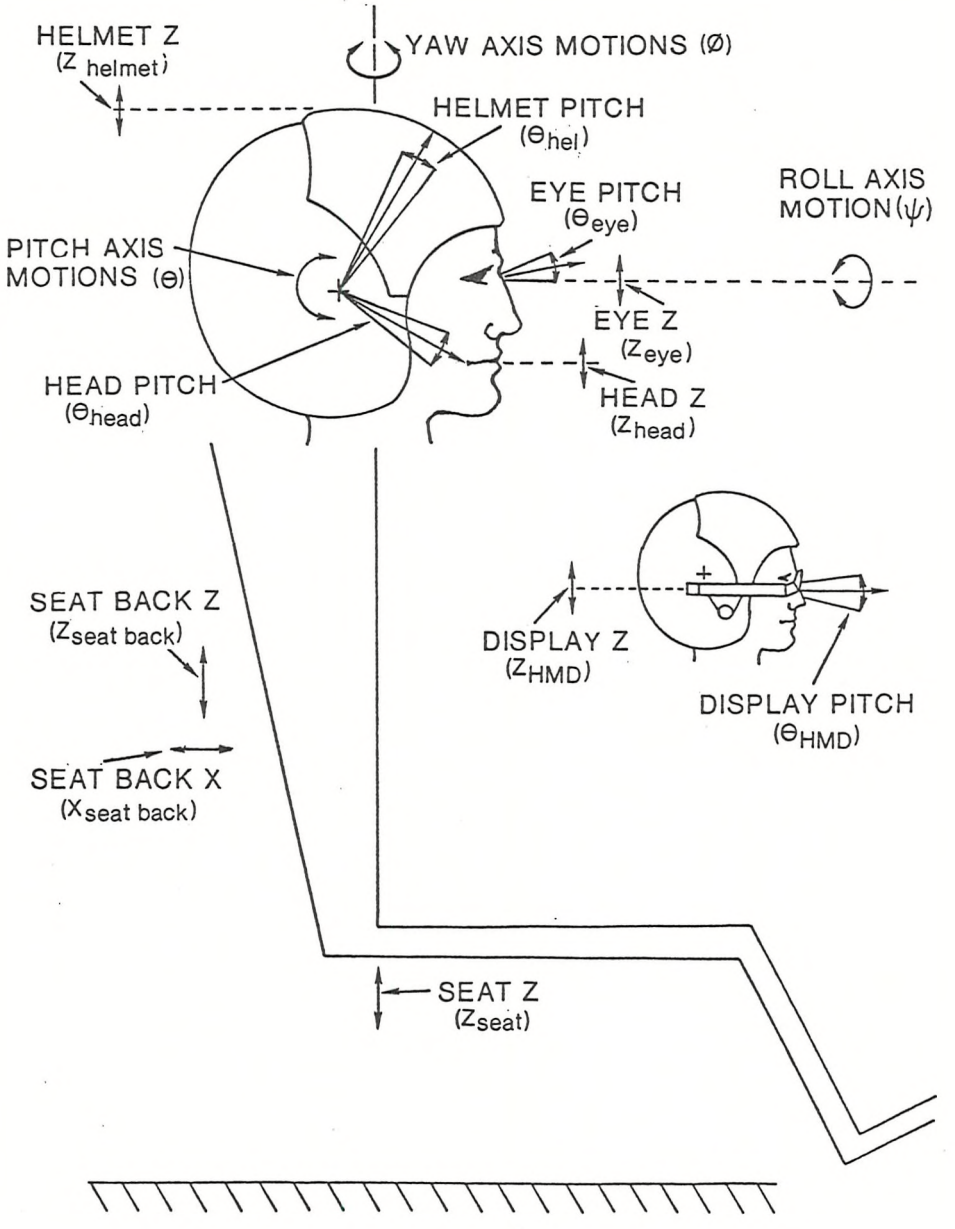

Figure 5.1.1. Coordinate System for Biodynamic Experiments

pitch, helmet pitch, etc.). This does not imply that these axes exist in an absolute sense for all the rotational motions. To the contrary, the eye, head, and helmet may have entirely different axes of rotation in pitch, roll, yaw, etc., each of which may vary in position as a function of vibration frequency and/or level (e.g., Griffin, 1975a). However, the pitch, roll, and yaw axes of each element will be assumed to be parallel with the same axes of another element; for example, the rotational axes of motion of the eye will be parallel to the rotational axes of the head and helmet. For the research reported in this thesis, the Z axis of the seat will be aligned with the vertical axis (or gravity vector) of the earth.

Table 5.1.1 lists the mathematical terms for each of the translational and rotational motions shown in Figure 5.5.1. These terms will be used in this thesis for describing the motion of the operator, display, and environment.

It should be noted that the coordinate system described above was established as a convenient framework to show the interrelationships of head, helmet, seat, etc. motions. It was not intended to be a rigorous construct in which precision mathematical transformations and biomechanical modeling could be performed.

5.1.3 Transfer Functions

The motion or response of the head, helmet, and/or helmet-mounted display were related to the input seat Z axis motion, or to each other, as transfer functions. Transfer functions are mathematical relationships between the input and output of a system which express the response of the system in terms of the modulus or amplitude ratio and the phase angle of the output and input signals for each frequency of excitation (ISO 2041, 1975). A detailed discussion of the theoretical aspects of transfer function analyses as applied to research in this thesis is contained in Appendix A.5.1.

TABLE 5.1.1. MOTION PARAMETER TERMINOLOGY

Motion Element	Axis	Acceleration	Velocity	Displacement
Seat	Z	$\ddot{Z}$ seat	$\dot{Z}$ seat	Z seat
Seat Back	Z	$\ddot{Z}$ seat back	$\dot{Z}$ seat back	Z seat back
Seat Back	X	$\ddot{X}$ seat back	$\dot{X}$ seat back	X seat back
Head	Z	$\ddot{Z}$ head	$\dot{Z}$ head	Z head
	Pitch	$\ddot{\theta}$ head	$\dot{\theta}$ head	θ head
	Yaw	$\ddot{\phi}$ head	$\dot{\phi}$ head	ϕ head
	Roll	$\ddot{\psi}$ head	$\dot{\psi}$ head	ψ head
Helmet	Z	$\ddot{Z}$ helmet	$\dot{Z}$ helmet	Z helmet
	Pitch	$\ddot{\theta}$ helmet	$\dot{\theta}$ helmet	θ helmet
	Yaw	$\ddot{\phi}$ helmet	$\dot{\phi}$ helmet	ϕ helmet
	Roll	$\ddot{\psi}$ helmet	$\dot{\psi}$ helmet	ψ helmet
Eye	Z	$\ddot{Z}$ eye	$\dot{Z}$ eye	Z eye
	Pitch	$\ddot{\theta}$ eye	$\dot{\theta}$ eye	θ eye
	Yaw	$\ddot{\phi}$ eye	$\dot{\phi}$ eye	ϕ eye
	Roll	$\ddot{\psi}$ eye	$\dot{\psi}$ eye	ψ eye
Display (HMD)	Z	$\ddot{Z}$ HMD	$\dot{Z}$ HMD	Z HMD
	Pitch	$\ddot{\theta}$ HMD	$\dot{\theta}$ HMD	θ HMD
	Yaw	$\ddot{\phi}$ HMD	$\dot{\phi}$ HMD	ϕ HMD
	Roll	$\ddot{\psi}$ HMD	$\dot{\psi}$ HMD	ψ HMD

5.1.4 Instrumentation

5.1.4.1 Transducers

The motions of the seat, head, helmet, and display were measured using translational and rotational accelerometers. The seat Z axis, seat back Z axis and X axis, the head Z axis, and display Z axis accelerations were monitored with piezo-resistive translational accelerometers (Endevco Type 2265-20). The voltage output of these accelerometers was proportional to the translational acceleration along the sensitive axis of the accelerometer. The output of the accelerometer was amplified by a special purpose instrumentation

amplifier. The rotational acceleration of the head and helmet in pitch and yaw axes (and roll when used in the field trial H.2), was measured with rotational servo accelerometers (Schaevitz ASMP-100). These accelerometers employed an induction technique for measuring acceleration, termed a "linear variable differential transformer." The output of this transducer, when biased and amplified, provided a voltage proportional to the angular acceleration of the accelerometer about its sensitive axis. The characteristics of the translational and rotational accelerometers are given in Appendix A.5.2.

5.1.4.2 Location of Accelerometers--Laboratory Experiments

Figure 5.1.2 shows the sites for locating the accelerometers during the biodynamic experiments reported in this chapter. The seat Z axis accelerometer was secured to a magnesium block mounted underneath the wooden seat platform. The seat back Z axis and X axis accelerometers were secured to another magnesium block mounted at midpoint behind the seat back. Head Z axis, roll, pitch, and/or yaw motion were measured by placing the appropriate transducer(s) in a bite-bar assembly consisting of a magnesium block secured to one end of 150 mm stainless steel bar. The bar was covered with a sterilized nylon sleeve and placed in the mouth of the subject parallel to the lateral (Y axis of the head), such that the accelerometer(s) was about 75 mm from the midsaggital plane. The mass of the bite bar assembly with the various accelerometers attached are indicated in Table 5.1.2. Helmet pitch, roll, or yaw was measured by securing a rotational accelerometer to a bracket mounted on top of the helmet at a point in line with the longitudinal (Z axis) of the body (i.e., intersection of the midsaggital and midcoronal planes). Figure 5.1.3 is a photograph showing a subject wearing the helmet-mounted display and the bite bar. A rotational accelerometer is shown mounted on top of the helmet to measure helmet pitch acceleration and, similarly, a rotational accelerometer is mounted on the bite bar to measure head pitch acceleration. A translational accelerometer is also mounted on the bite bar to measure head Z axis motion. (It should be noted that the output of the translational accelerometer measuring head Z motion will be a combination

of the vertical translational motion and the pitch rotational motion of the head for components of head pitch motion about an axis not coincident with the bite bar.)

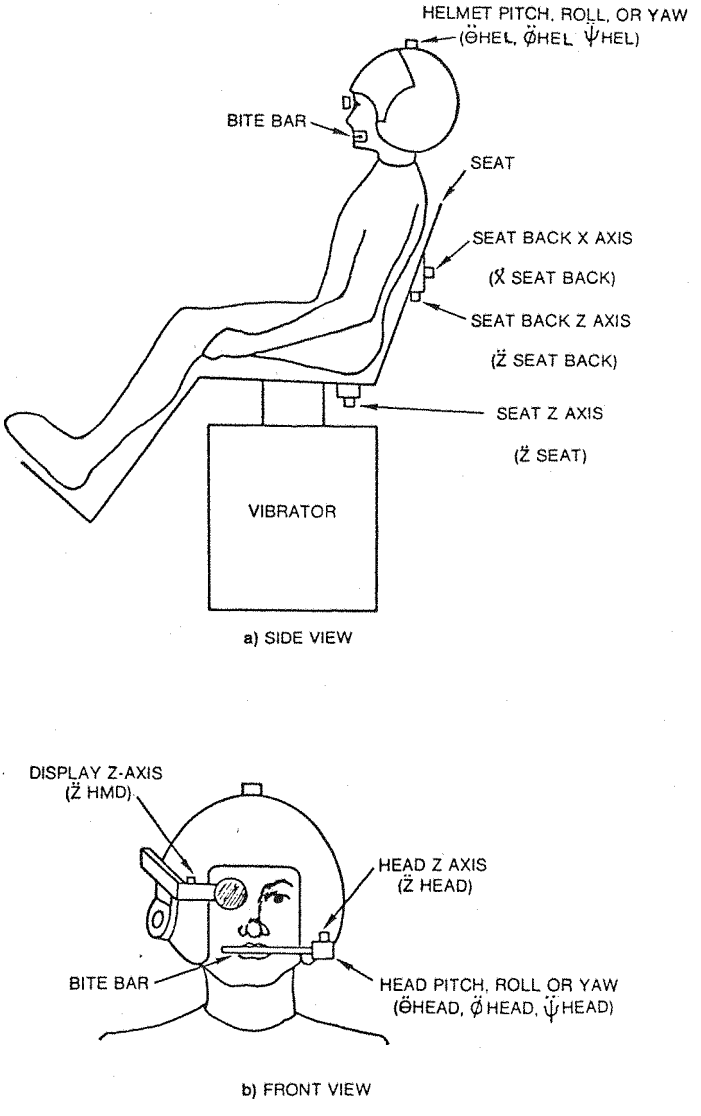

Figure 5.1.2. Location of Accelerometers in Biodynamic Experiments

TABLE 5.1.2. MASSES OF BITE BAR COMPONENTS

Component	Mass
Bite bar with attached magnesium block assembly and nylon sleeve	52 gm
Translational accelerometer (with approximately 150 mm signal lead)	10 gm
Rotational accelerometer (with approximately 150 mm signal lead)	50 gm
Total combined masses of bite bar components (including one each translational and rotational accelerometer)	112 gm

5.1.4.3 Laboratory Recording

A four channel FM instrumentation cassette tape recorder (TEAC Model R-70A) was used to record the outputs of the acceleration transducers in the laboratory studies. The input gains of the recorder amplifiers were adjusted to give the optimum signal-to-noise ratio over the dynamic ranges of the transducer outputs. Typical signal-to-noise ratios of 35 dB rms were measured. Detailed performance characteristics of the recorder are given in Appendix A.5.2. Because the recorder was limited to four channels, several experiment runs were conducted with different combinations of transducer locations.

5.1.4.4 Calibration of Transducer Measurement and Recording Systems

The gains of the transducer amplifiers were calibrated prior to each experiment. The gains of the translational accelerometer amplifiers were checked by placing the accelerometer on a horizontal surface normal to its sensitive axis and measuring the output voltage, corresponding to an acceleration of +1 g (9.81 m/s^2). The accelerometer was then turned upside down and a similar reading taken for -1 g (-9.81 m/s^2). The gain of the amplifier was set so that the

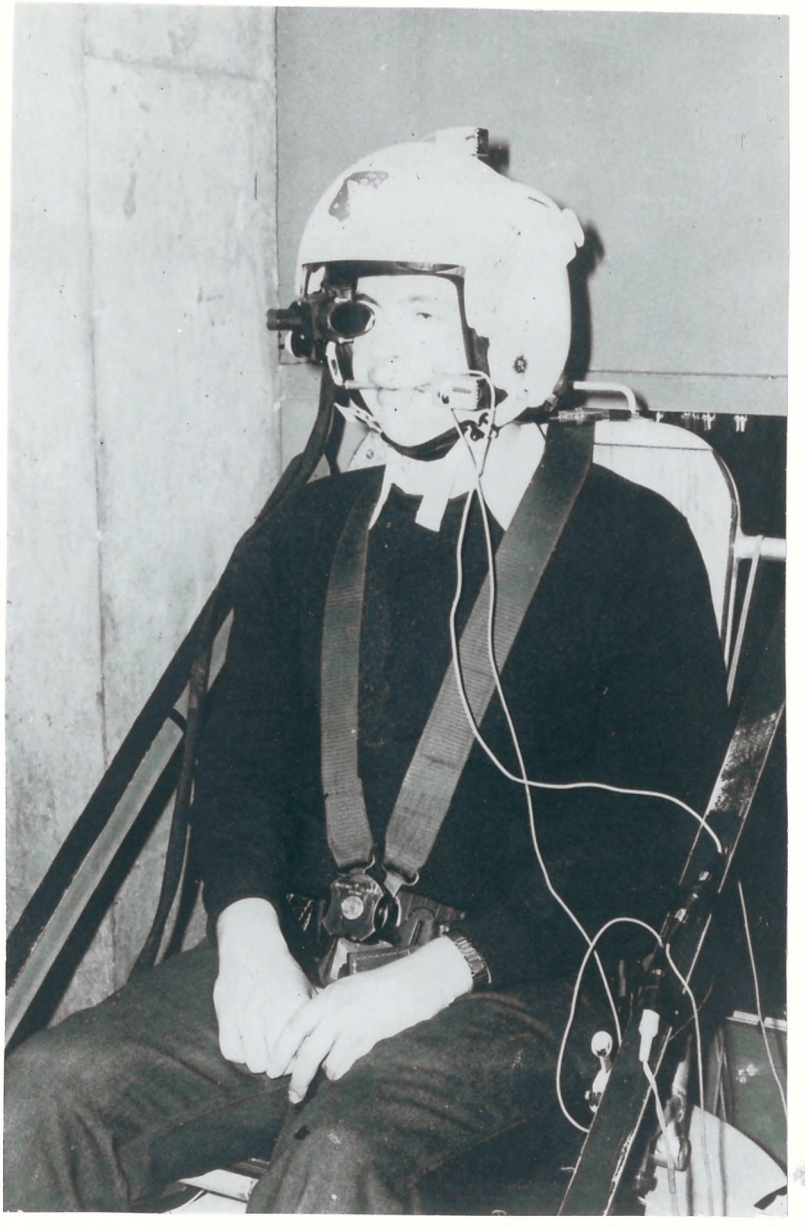

Figure 5.1.3. Subject Wearing Helmet-Mounted Display and Bite Bar (Note Accelerometers Mounted on Bite Bar and on Top of Helmet)

output voltage corresponded to 1 volt per g level. Prior to each experimental session, the accelerometer amplifier was balanced to null out the DC bias corresponding to the 1 g acceleration due to gravity. Once the initial gain of the amplifier was set, there was no measurable drift in gain. The amplifiers also exhibited a flat frequency response for transducer signals from 0 to 100 Hz.

The rotational accelerometers were calibrated by using the translational accelerometers. The rotational accelerometers were placed on a roll/pitch vibrator so that the sensitive axis of the accelerometer was parallel to the axis of rotation of the vibrator. The rotational motion of the vibrator was produced by impressing the translatory motion of a linear vibrator to a vibration platform at some distance (i.e., 0.1 m) from a pivot point (axis of rotation). A translational accelerometer measured the translatory motion of the actuator to the vibration platform. The magnitude of the rotational motion to the accelerometer was computed by multiplying the translational accelerometer reading by the distance between the application point of the vibrator to the axis of rotation.

The gains of the record and playback amplifiers of the tape recorder were set prior to each experiment. Preset voltages from an sine wave oscillator were recorded and replayed into each channel. The record gains were adjusted to achieve the desired output level when the tape was replayed for analysis by the computer. The accuracy of the overall data acquisition was measured by recording oscillator signals of preset levels on the instrumentation recorder, acquiring the signals (analogue to digital conversion) by the computer, then comparing the acquired signal levels with the original input levels. From this procedure, the calibration of the recording and acquisition system was verified. Recording and acquisition errors were always less than 10 percent, and typically less than 5 percent of the real input value.

5.1.5 Procedures

5.1.5.1 Laboratory Vibration Conditions

Vertical Z axis sinusoidal motion of the seat was used in all the laboratory biodynamic studies. Both single frequency and swept sine wave inputs were used at various acceleration levels depending upon data analyses to be performed. The range of vibration frequencies was based upon the vibration conditions in the legibility studies reported in Chapter 4 and the vibration characteristics of various fixed and rotary wing aircraft. In most of the dynamic studies, the lowest

useful vibration frequency was 1.4 Hz due to the displacement limits of the vibrator (Section 3.3.2).

Details of the vibration conditions are given in the sections to follow for the individual experiments. The duration of each vibration condition was determined by the desired frequency resolution and the degrees of freedom of the transfer function or power spectral density analysis to be performed (e.g., Section A.5.1.10). Typically, the duration of discrete frequency vibration runs was 60 s and swept sine wave runs was 100 s.

5.1.5.2 Instructions to Subjects

During the dynamic experiments, subjects were asked to maintain a relaxed upright posture while looking straight ahead. In Experiment BD.7, subjects were required to aim the helmet-mounted display at various azimuthal and elevation angles relative to a reference line-of-sight which was straight ahead. Specific instructions to subjects will be described for each experiment.

5.1.6 Analysis of Biodynamic Data

In order to analyze the seat, head, helmet, and display vibration acceleration data, the time histories obtained in the biodynamics experiments were replayed and converted into digital form using the facilities in Data Analysis Center of the Institute of Sound and Vibration Research, University of Southampton. A short description of this facility is given in Section 3.5. Using the mathematical relationships and procedures described in Appendix A.5.1, the various power spectral densities and transfer functions were computed. Figure 5.1.4 shows the flow of the data acquisition, transformation, and computational procedures used in analyzing the data from the dynamic experiments.

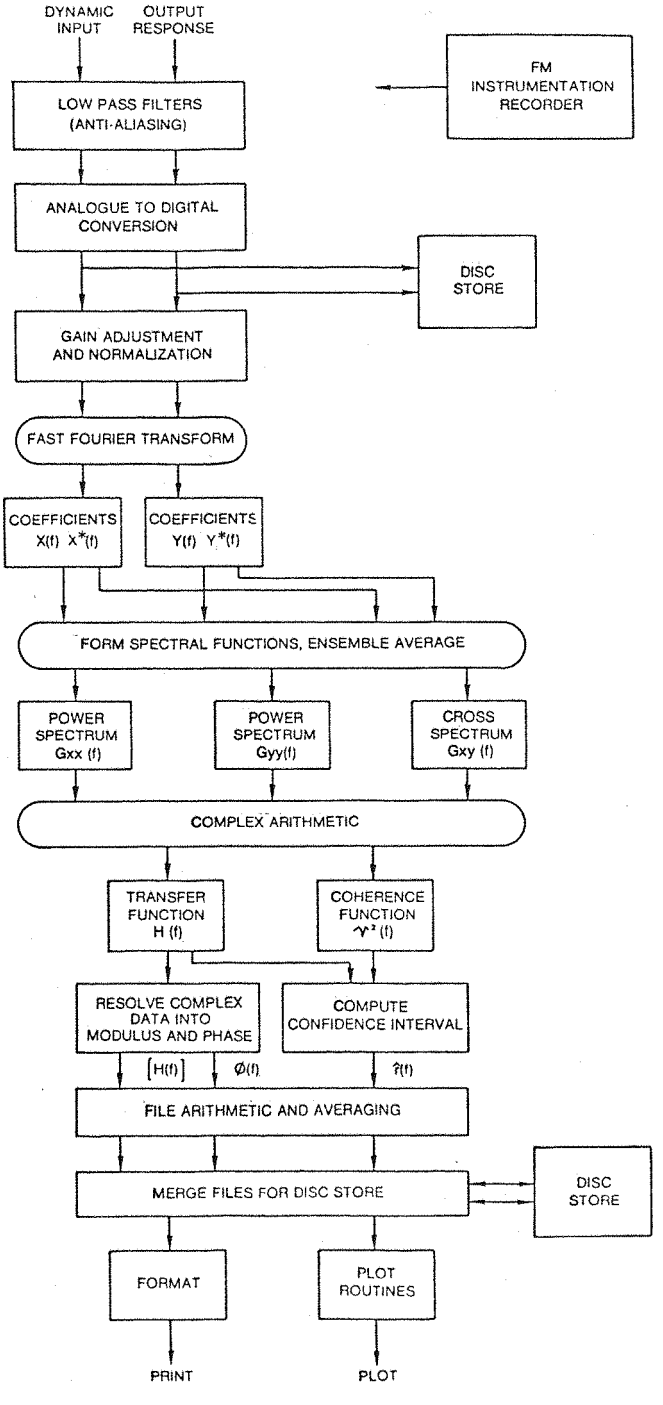

Figure 5.1.4. Data Analysis Procedures for the Dynamic Experiments

5.1.7 Harmonic Distortion

In many physical systems, the response of the system to mechanical excitation is often distorted due to nonlinearities in the system. If the mechanical excitation is a sinusoidal function of time then the response of the system may contain motions which are sinusoidal at the same frequency with an admixture of frequencies at integral multiples of the fundamental input motion. The presence of these harmonics in the response of the system is termed harmonic distortion. The magnitude of the harmonic distortion can be defined many ways. For this thesis, harmonic distortion (δ) will be defined as the percentage ratio of the rms motion of the harmonics (x_n) to the rms motion of the fundamental (x_0) or

$$\delta = \sqrt{\frac{\sum_{n=1}^{\infty} x_n^2}{x_0^2}} \times 100\%$$

where x_0^2 is the mean-squared value of that motion at the fundamental frequency (f_0) and x_n^2 is the mean-squared value of the motion of frequency f_n when $f_n = (n+1)f_0$.

5.2 EXPERIMENTS BD.1 AND BD.2: CHARACTERISTICS OF SEAT VIBRATION

5.2.1 Purpose

Two experiments were conducted to determine the characteristics of the seat vibration used in the experiments reported in Chapter 4. It was the intent of these experiments to measure the fidelity of the vibration input motion (i.e., how close it approximated a pure sinusoidal waveform) as well as to determine any artifacts in the simulated helicopter seat due to its structure (e.g., internal resonances).

5.2.2 Method

In the first experiment (BD.1), single frequency sinusoidal test signals were input to the vibration control system from the oscillator as shown in Figure 3.3.5. The total harmonic distortion (defined in Section 5.1.7) present in the oscillator had been previously measured to be less than 0.1 percent across all the test frequencies used in the experiments reported in this thesis. The acceleration of the seat in the Z axis was measured by a translational accelerometer mounted on the seat base as described in Figure 5.1.2. The experimental conditions and analysis procedures for this experiment are summarized in Table 5.2.1.

In the second experiment (BD.2), the motion of the seat back in the Z axis and X axis were measured by a swept sinusoidal vertical Z axis motion input to the seat base. Translational accelerometers were mounted on an aluminium block located at the vertical and lateral midpoints of the seat backs as shown in Figure 5.1.2. The vibration conditions in this experiment are given in Table 5.2.2.

TABLE 5.2.1. EXPERIMENT BD.1: CHARACTERISTICS OF SEAT TO VIBRATION

Purpose:	To measure the characteristics vertical vibration of the seat.
Subject:	S1
Vibration Frequency:	16 vertical Z axis, sinusoidal frequencies: 1.19 Hz - 16.0 Hz separated by 1/4 octave
Vibration Level:	0.80 m/s^2 rms @ 1.19 Hz 1.33 m/s^2 rms @ 1.33 Hz 1.50 m/s^2 rms @ 1.68 Hz - 16 Hz
Data Acquisition:	sample rate: 40 Hz sample period: 60 s filter: Rockland 1042F seat base Z: -3 dB @ 20 Hz (48 dB/octave rolloff)
Analysis:	Power Spectral distributions of seat response to each input frequency. resolution: 0.2 Hz degrees of freedom: 32 window: Hanning

TABLE 5.2.2. EXPERIMENT BD.2: CHARACTERISTICS OF SEAT BACK VIBRATION

Purpose:	To measure the motion of the seat back in fore-aft and vertical directions due to vertical vibration of the seat base.
Subject:	S1
Vibration Frequency:	linear sweep of sinusoidal motion from 1 Hz to 60 Hz, over 100 s period
Vibration Level:	1.5 m/s^2 rms
Data Acquisition:	sample rate: 120 Hz sample period: 100 s filter: Rockland 1042F seat base Z: -3 dB @ 60 Hz/48 dB/octave seat back Z: -3 dB @ 60 Hz/24 dB/octave seat back X: -3 dB @ 60 Hz/24 dB/octave
Analysis:	transfer function via cross spectral analysis resolution: 0.5 Hz degrees of freedom: 184 window: Hanning

5.2.3 Results

5.2.3.1 Power Spectral Densities of Vertical Axis Motion

Power spectral densities (PSD) of vertical Z axis seat motion were computed from the acceleration time histories for each input vibration frequency using the procedures described in Section 5.1 and Appendix A.5.1. A composite of these PSDs is shown in Figure 5.2.1. Inspection of this figure indicates that significant harmonics of the fundamental vibration frequency were present at frequencies less than 3.0 Hz. An analysis of the PSDs was performed to determine harmonic distortion at each vibration frequency using the relationship defined in Section 5.1.7. RMS levels of vibration at each frequency were obtained from the PSDs by taking the square root of the integrated power at the fundamental and each harmonic frequency within a bandwidth of 0 to 20 Hz. Figure 5.2.2 compares the rms levels of the fundamental and first three harmonics of the seat motion as a function of the input vibration frequency. Harmonic distortion of the seat acceleration and displacement is also shown. (The harmonics of seat displacement must be frequency-weighted to compute harmonic distortion.) The harmonic of seat acceleration motion at twice the fundamental frequency was greatest at the 1.88 Hz input frequency, where the rms level of this harmonic was 70.2 percent of the fundamental and 56.9 percent of the total rms value. At this frequency the harmonic distortion of seat acceleration was 72.3 percent, and of seat displacement was 35.3 percent. Harmonic distortion became less than 15.0 percent (acceleration) at vibration frequencies above 3.36 Hz. Typically, the harmonic distortion of the seat displacement was about one-half that of seat acceleration.

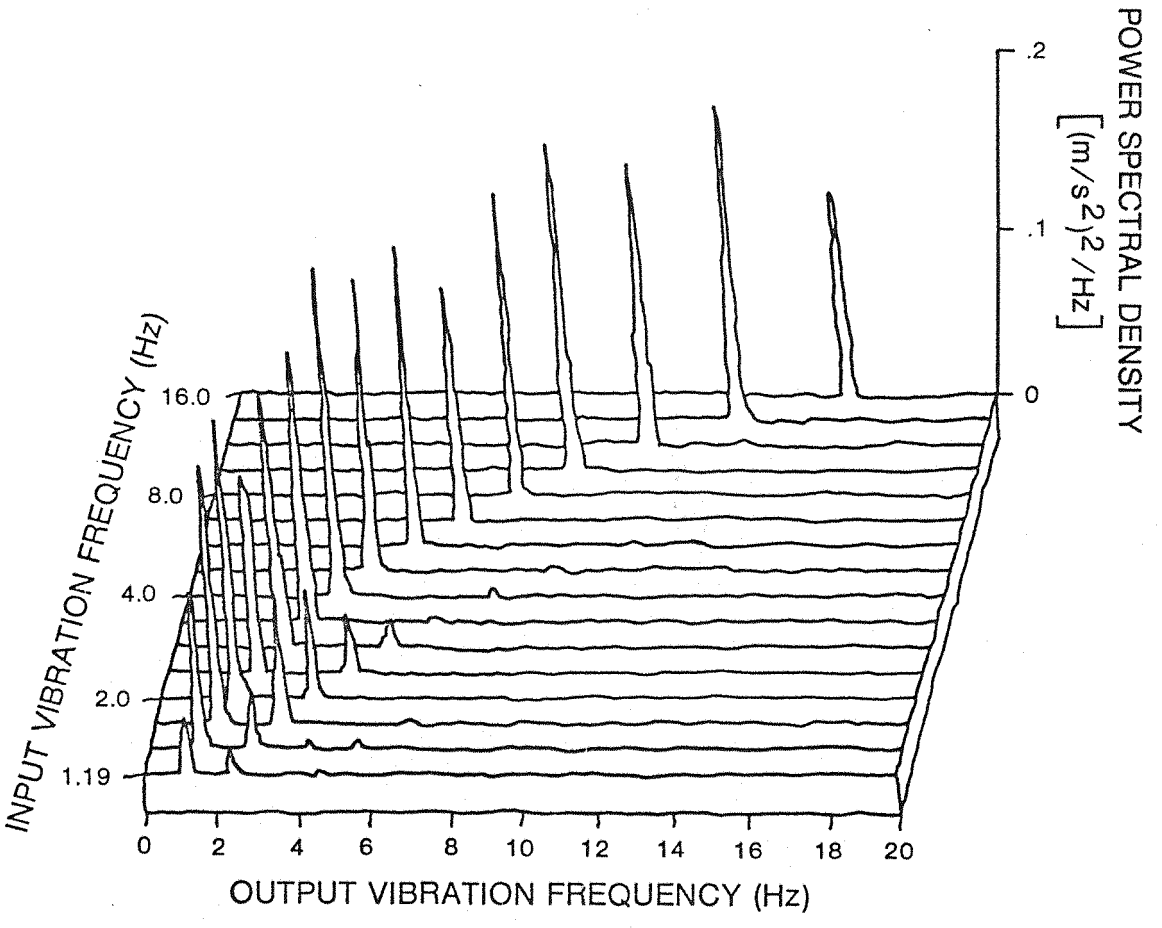

Figure 5.2.1. Composite of Power Spectral Densities of Vertical Seat (Z Axis) Acceleration due to Single Sinusoidal Input Frequencies (B_e = 0.2 Hz, DOF = 32, Experiment BD.1)

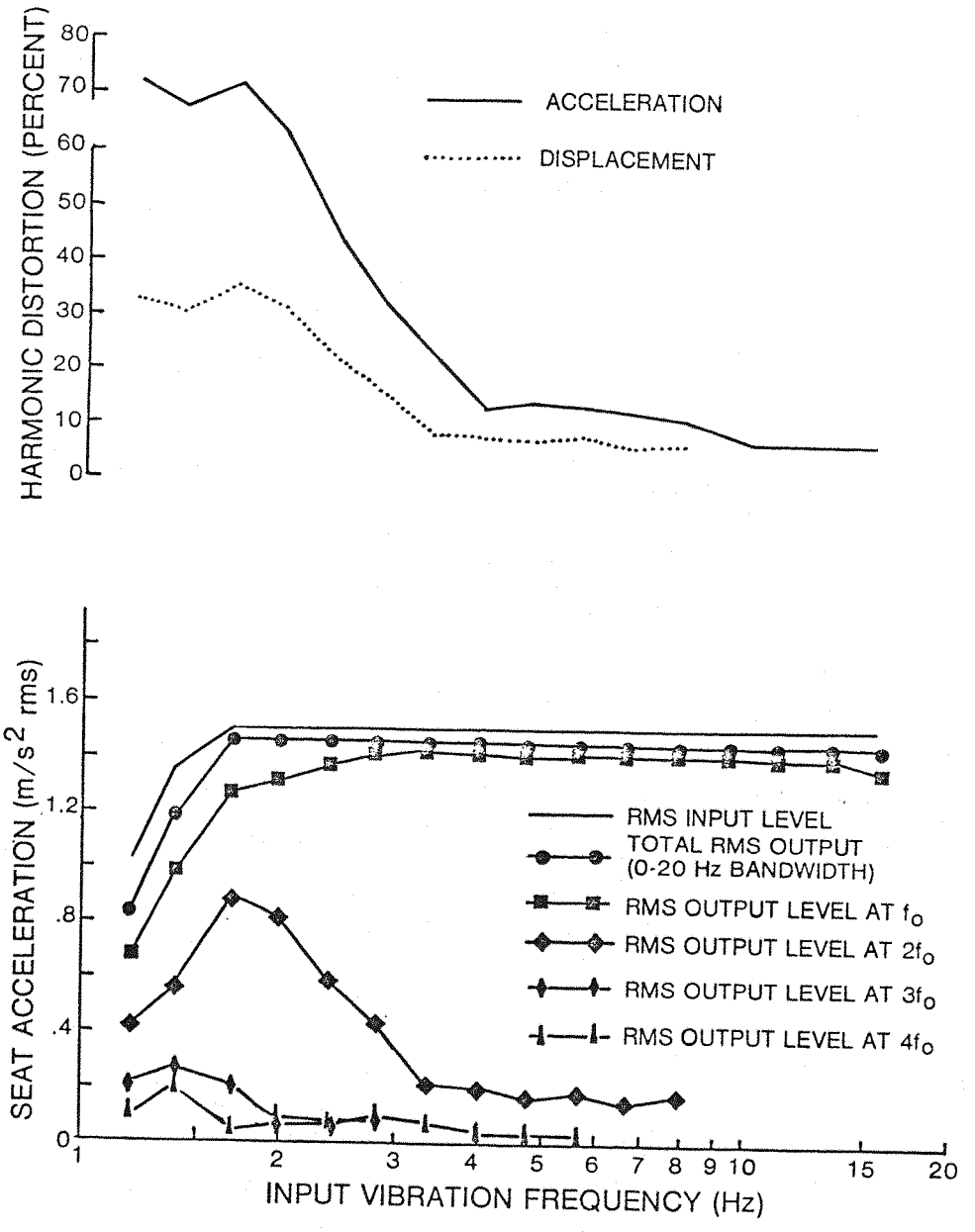

Figure 5.2.2. Analysis of Vertical Seat Vibration Response (Experiment BD.1)

5.2.3.2 Transfer Functions of Seat Back Motion to Seat Base Motion

Using the swept frequency mode of the vibration control system (Figure 3.3.5) and the cross spectral analysis procedures described in Sections 3.3., 5.1.5, and Appendix A.5.1, transfer functions were computed for vertical (Z axis) and fore-aft (X axis) motion at the seat back due to the seat base vertical motion. Shown in Figure 5.2.3

is the modulus of the seat back vertical to seat base vertical transfer function. The gain of the seat back relative to the seat base was approximately 1.0 at frequencies less than 4 Hz. Beyond 12 Hz, this gain increased to approximately 2.0 at 32 Hz. The phase of the seat back to seat base vertical motion was 0 degrees at low frequencies (i.e., less than 4.0 Hz), but increased in lag to approximately 30 degrees at 12 Hz where it remained up to 40 Hz.

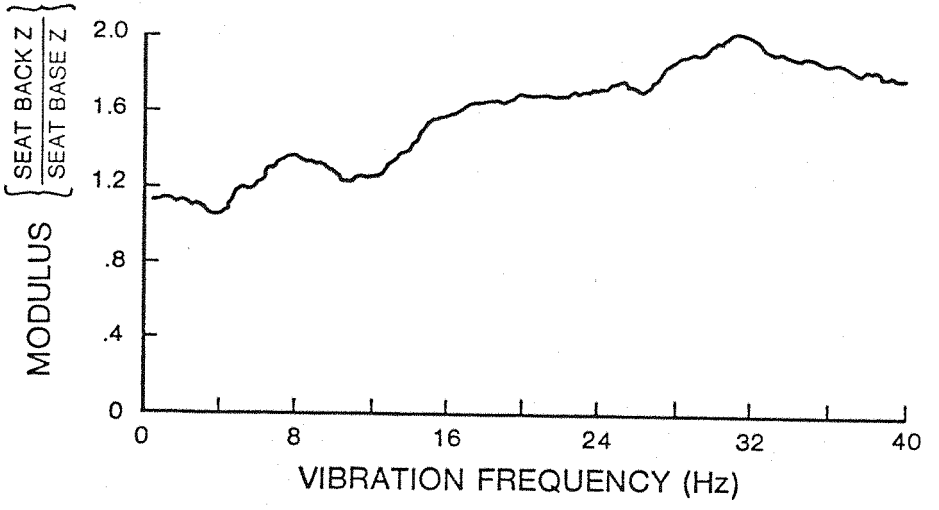

Figure 5.2.3. Modulus of Vertical Seat Base to Vertical Seat Base Transfer Function (B_e = 0.5 Hz, DOF = 184, Experiment BD.2)

The modulus of the transfer function of the seat back fore-aft motion (X axis) to the seat base vertical motion is shown in Figure 5.2.4. The large variation in seat back fore-aft motion was frequency dependent. A stable seat would exhibit zero gain in the fore-aft movement and unity gain for vertical movement across all vibration frequencies. It appears from the data that perhaps two vibration modes were present, consisting of a low frequency mode between 4 to 10 hz, an anti-resonant point at 12 Hz, and an increasing level of motion from 12 to 32 Hz. Since the fore-aft motion of the seat between 4 to 10 Hz was not accompanied by a significant change in seat back vertical motion, it can be assumed that this motion was strictly translational and may be associated with the biodynamic response of the subject. It is reasonable to postulate that the major whole-body response modes involving flexion of the back at 4 to 6 Hz and above caused a force to

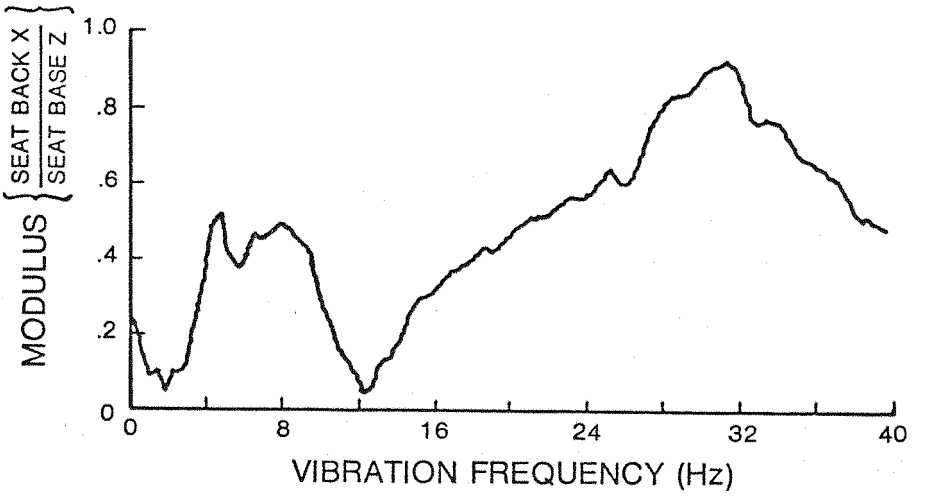

Figure 5.2.4. Modulus of Fore-Aft (X Axis) Motion of the Seat Back to the Vertical (Z Axis) Seat Base Vibration (B_e = 0.5 Hz, DOF = 184, Experiment BD.2)

be applied to seat back in the X axis (e.g., Section 2.5.3.3). Beyond 12 Hz there was a concomitant increase in seat back vertical and fore-aft movement. It is reasonable here to postulate that a rotational movement of the seat was occurring. The relatively stable increase of gains in both fore-aft and vertical seat back motion indicate that the rotational movement seemed to have the same general behaviour across the frequency range 12 Hz to 32 Hz.

5.3 EXPERIMENT BD.3: PRELIMINARY INVESTIGATION OF HEAD AND HELMET MOTION DUE TO SEAT VERTICAL (Z AXIS) VIBRATION

5.3.1 Purpose and Procedure

Two preliminary biodynamic experiments were conducted to establish the general nature of the rotational movements of head and helmet (with attached helmet-mounted display apparatus) during vertical Z axis whole-body vibration. The first of these experiments (BD.3) was conducted simultaneously and under the same vibration conditions as Experiment BD.1 (Table 5.3.1). Subjects were instructed to look straight ahead and adopt a relaxed upright posture. Head pitch was

TABLE 5.3.1. EXPERIMENT BD.3: SINGLE FREQUENCY 1/4 OCTAVE RMS TRANSMISSIBILITIES

Purpose:	To perform a preliminary study of rotational head and helmet motions due to seat base vertical vibration.
Subject:	S1
Vibration Frequency:	16 vertical Z axis, sinusoidal frequencies: 1.19 Hz - 16.0 Hz separated by 1/4 octave
Vibration Level:	0.80 m/s^2 rms @ 1.19 Hz 1.33 m/s^2 rms @ 1.33 Hz 1.50 m/s^2 rms @ 1.68 Hz - 16.0 Hz
Time Duration:	70 s per frequency
Data Acquisition:	sample rate: 40 Hz sample period: 60 s filter characteristics: seat base Z: -3 dB @ 20 Hz/48 dB/octave rolloff head pitch: -3 dB @ 20 Hz/48 dB/octave rolloff helmet pitch: -3 dB @ 20 Hz/24 dB/octave rolloff helmet yaw: -3 dB @ 20 Hz/24 dB/octave rolloff
Analysis:	Ratio of rms levels over sample period to obtain: head pitch/seat Z helmet pitch/seat Z helmet yaw/seat Z helmet pitch/head pitch PSD and integrated PSDs to analyze distortion in head and helmet movement. resolution: 0.2 Hz degrees of freedom: 32 window: Hanning

measured with a rotational accelerometer mounted on a bite bar. Helmet pitch and yaw were measured by rotational accelerometers affixed to the top of the helmet as shown in Figure 5.1.2. Head and helmet rotational motions and seat (Z axis) motion were recorded and analyzed using the facilities and instrumentation described in Sections 3.3, 3.4, 5.1, and Appendix A.5.2. The rms values of the head, helmet, and seat accelerations were derived by computing the standard deviation of the sampled time histories. These values were always in good agreement with an on-line measurement of accelerations using a true rms voltmeter.

5.3.2 Results and Discussion

5.3.2.1 Head and Helmet RMS Transmissibilities

The ratios of the helmet pitch, helmet yaw, and head pitch rms motion to seat Z rms motion were computed for each 1/4 octave vibration frequency. Plots of these ratios are shown in Figure 5.3.1. The predominant mode of helmet oscillatory rotational motion was in the pitch axis. The motion of the helmet in the yaw axis was about 20 percent that of the pitch axis.

The pitch motion of the head indicated two peaks at 5.66 Hz and 11.3 Hz similar to the results of Lewis (1979b) for head pitch motion (with a helmet) and Rowlands (1977) for head Z motion with seat back and normal posture. The helmet pitch motion generally followed the form of the head pitch motion up to about 5.66 Hz, although it was slightly less at frequencies of 4.0 Hz and below, but greater at 4.76 Hz, 5.66 Hz, and 6.73 Hz and 8.0 Hz. At vibration frequencies greater than 8.0 Hz, there was a radical departure of head and helmet motion, indicating a large amount of relative movement between the helmet and the head. Figure 5.3.2 shows the ratio the total rms motion of the helmet to that of the head in the pitch axis as a function of the seat base vibration frequencies. At 6.73 Hz, the total

rms helmet pitch motion was 40 percent greater than head pitch, but at 16 Hz was 40 percent less than head pitch. Of course, these values are rms ratios and cannot be interpreted fully without a knowledge of the spectral relationships of helmet-to-head and seat motion.

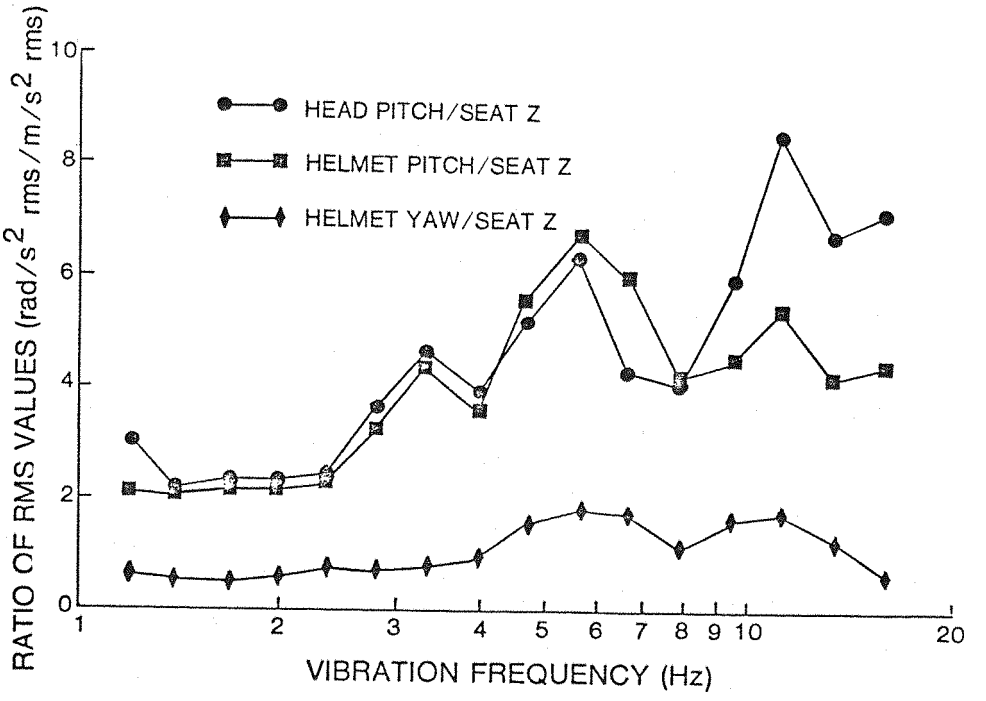

Figure 5.3.1. Ratios of rms Levels of Head and Helmet Pitch Axis and Helmet Yaw Axis Motion to Vertical Seat Z Axis Motion (Experiment BD.3)

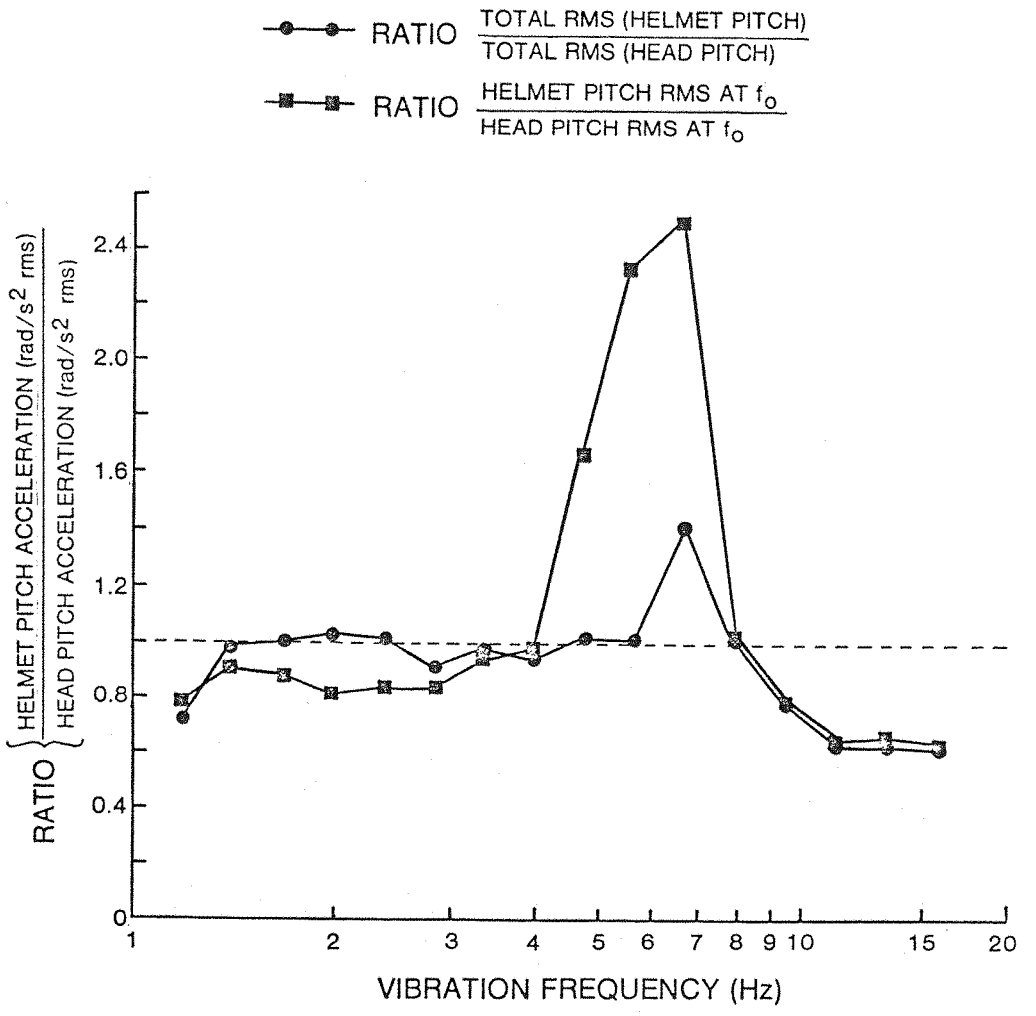

Figure 5.3.2. Ratio of rms Levels of Helmet Pitch Axis Motion to Head Pitch Axis Motion at Various Frequencies of Vertical (Z Axis) Seat Vibration (Experiment BD.3)

5.3.2.2 PSD Analysis of 1/4 Octave Data

Composite plots of the PSDs for the head and helmet pitch and helmet yaw motion are shown in Figures 5.3.3, 5.3.4, and 5.3.5, respectively. By inspection, the PSD data show that the energy in helmet and head pitch at the fundamental frequency of the seat base vibration followed the trends in the rms data shown in Figure 5.3.1. There was a large amount of harmonic activity in head pitch across vibration frequencies, but this activity was reflected in helmet pitch acceleration at only the lower frequencies. Figures 5.3.6, 5.3.7, and 5.3.8 show the relative rms vibration levels at the fundamental and harmonics derived from the integrated PSDs for helmet and head motion. Some of the harmonic behaviour of the head and helmet was probably due to the harmonic distortion in the seat motion as shown in Experiment BD.1. It would also follow, from the helmet to head rms transmissibility, that the higher frequency harmonics would be attenuated by the helmet, whereas those occurring between 4.0 Hz to 8.0 Hz would be amplified (since helmet-to-head pitch transmissibility was greater than 1.0). However, seat Z harmonics cannot be used to account for the extraordinary behaviour of the head pitch motion at 5.66 Hz where both the rms vibration levels for the second and third harmonics exceeded the fundamental by 9 percent and 61 percent, respectively. This was also the same frequency where the helmet pitch motion was the greatest, but that motion was concentrated in the fundamental (i.e., the rms level of the second harmonic was 13 percent of the fundamental rms level and the third harmonic was 6 percent of the fundamental rms level). This behaviour is reflected in Figure 5.3.2, where the ratios of the helmet pitch to head pitch rms levels at the fundamental frequency are compared to the ratios of the total rms values. There was also a significant increase in helmet yaw at 11.2 Hz which corresponded to the same frequency as the peak head pitch acceleration.

Although from one subject only, it is clear from the results above that the rotational motion of the head and helmet is complex and that relative movement of the helmet and head can be expected. The harmonic distortion aspects of head and helmet movement are discussed further in Section 5.5.4.6).

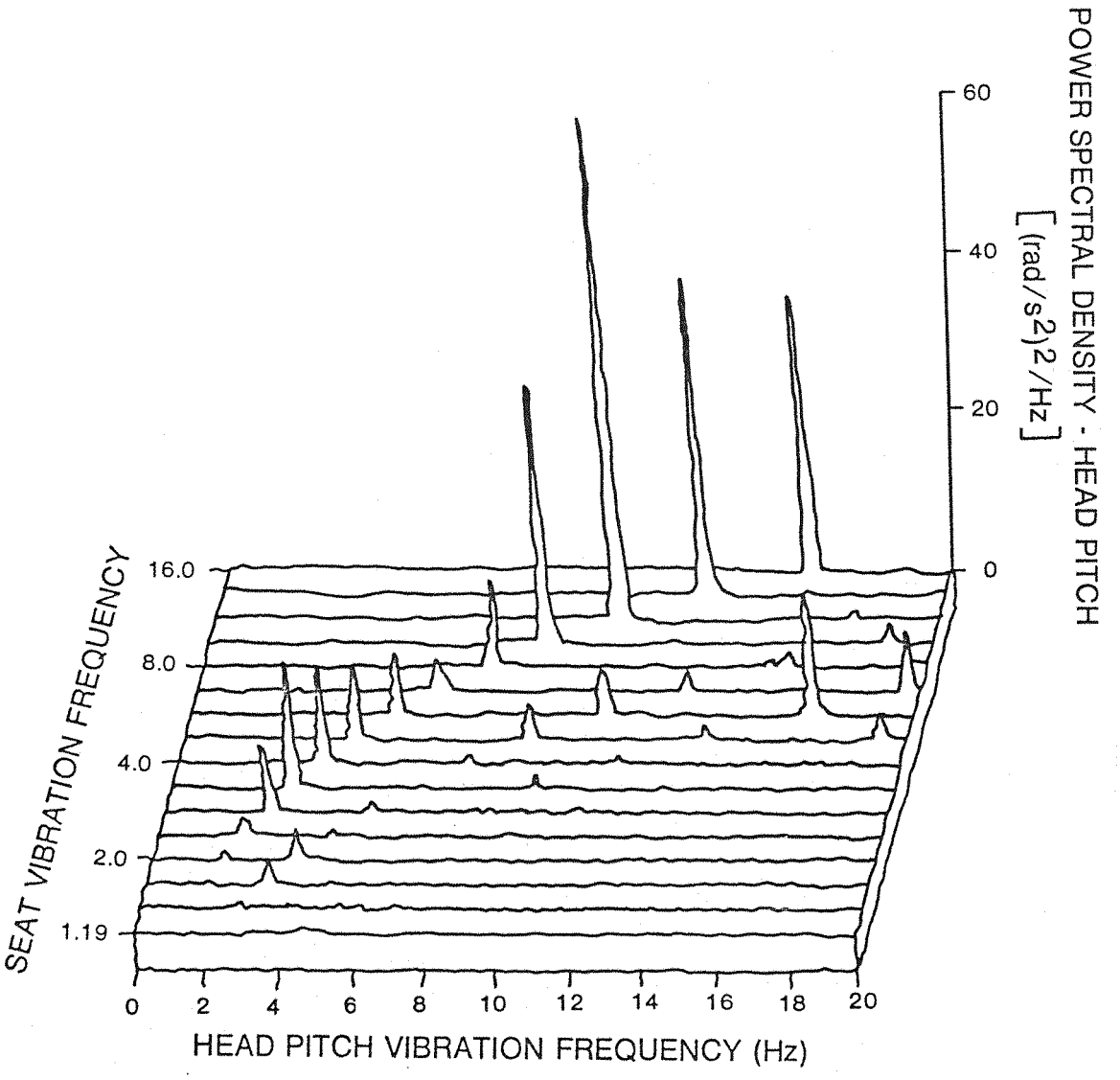

Figure 5.3.3. Composite of Power Spectral Densities of Head Pitch Axis Motion due to Vertical (Z Axis) Vibration of the Seat (B_e = 0.2 Hz, DOF = 32, Experiment BD.3)

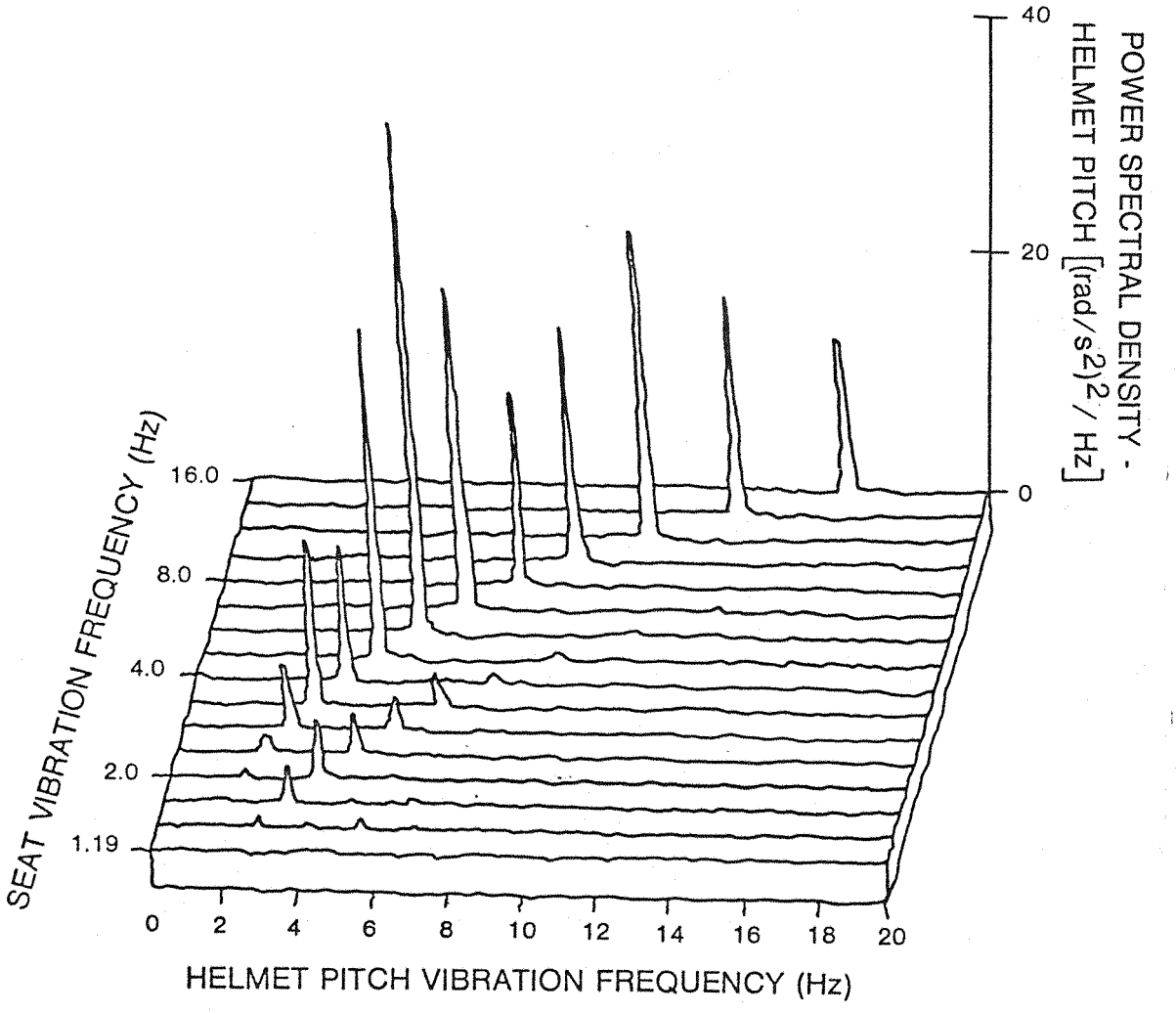

Figure 5.3.4. Composite of Power Spectral Densities of Helmet Pitch Axis Motion due to Vertical (Z Axis) Vibration of the Seat (B_e = 0.2 Hz, DOF = 32, Experiment BD.3)

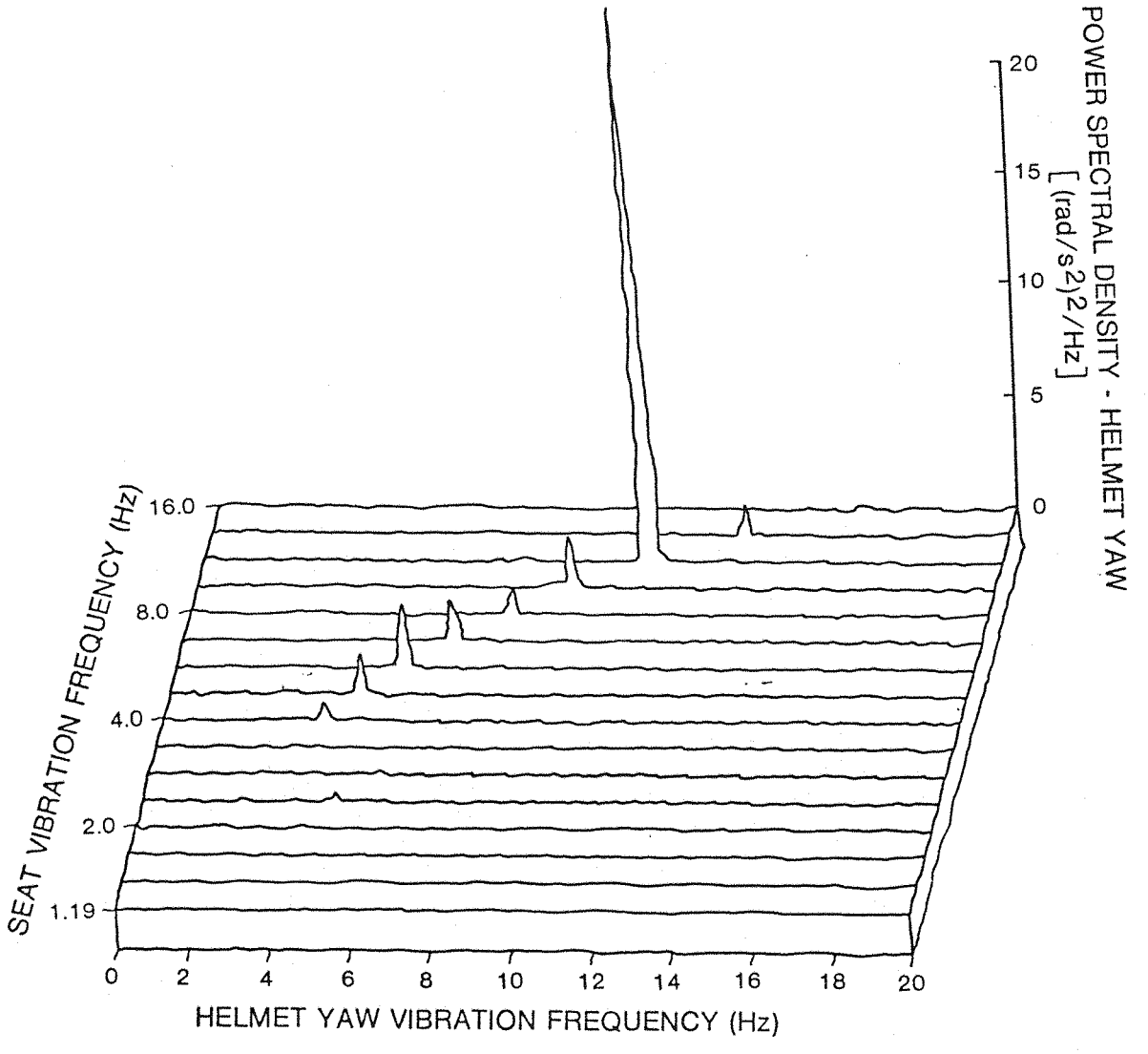

Figure 5.3.5. Composite of Power Spectral Densities of Helmet Yaw Axis Motion due to Vertical (Z Axis) Vibration of the Seat (B_e = 0.2 Hz, DOF = 32, Experiment BD.3)

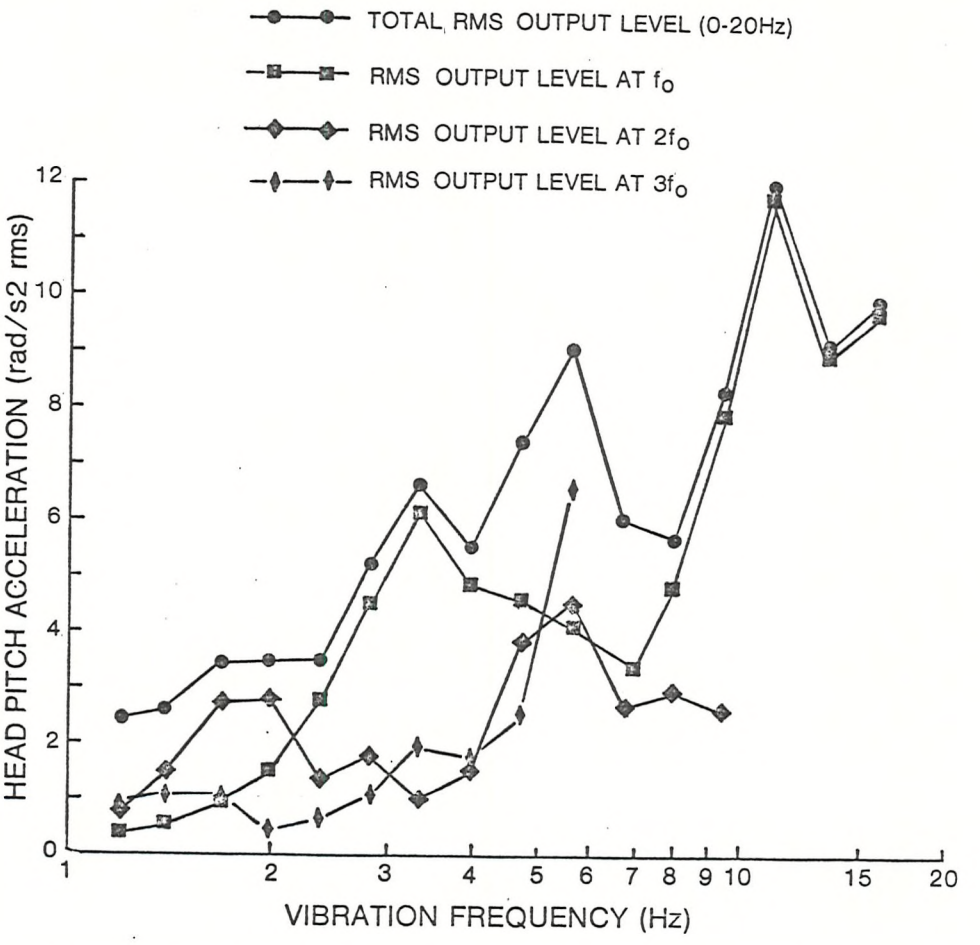

Figure 5.3.6. RMS Acceleration Levels of the Head in the Pitch Axis at Fundamental and Harmonic Frequencies due to Vertical (Z Axis) Seat Vibration (Experiment BD.3)

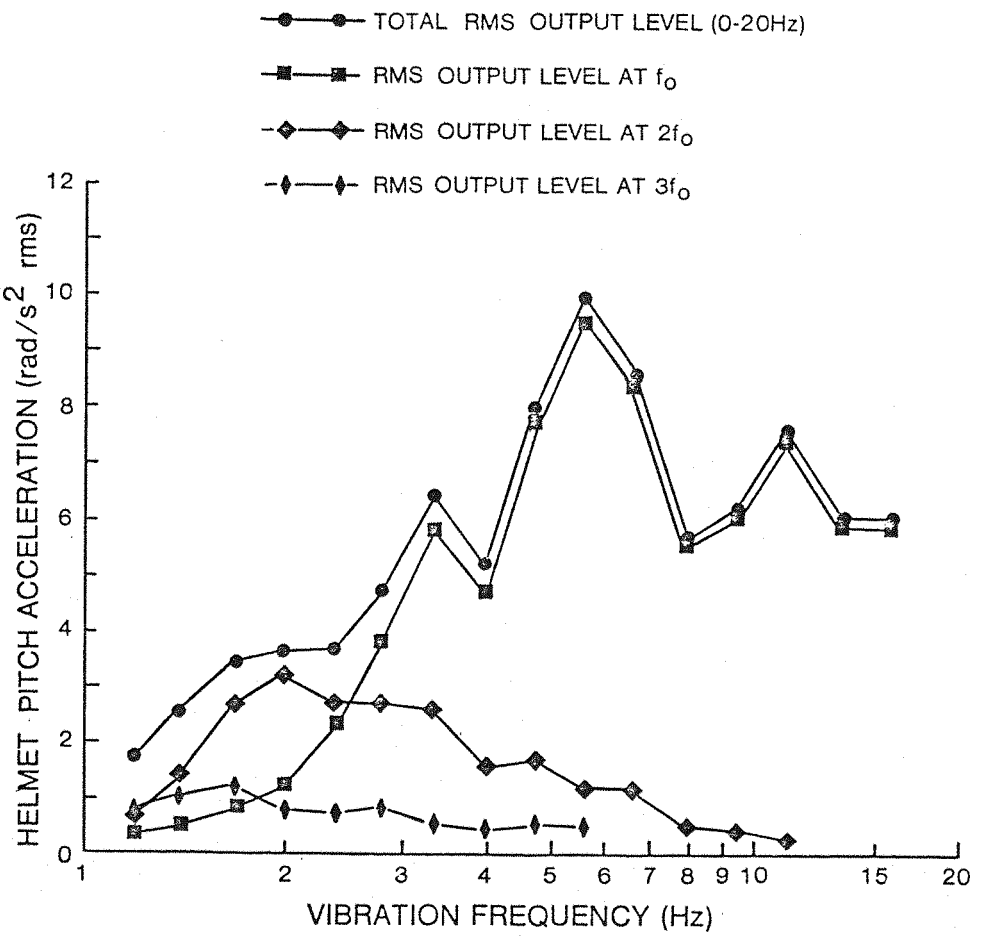

Figure 5.3.7. RMS Acceleration Levels of the Helmet in the Pitch Axis at Fundamental and Harmonic Frequencies due to Vertical (Z Axis) Seat Vibration (Experiment BD.3)

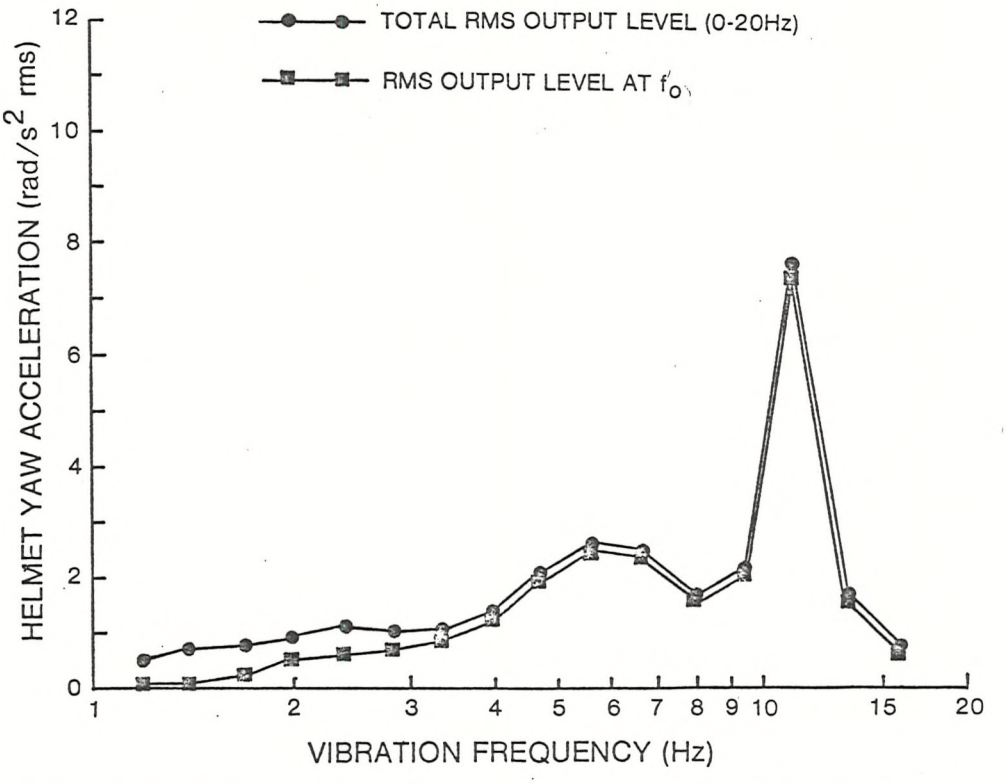

Figure 5.3.8. RMS Acceleration Levels of the Helmet in the Yaw Axis at Fundamental and Harmonic Frequencies due to Vertical (Z Axis) Seat Vibration (Experiment BD.3)

5.4 EXPERIMENT BD.4: LINEARITY OF HELMET PITCH MOVEMENT DURING VERTICAL SEAT (Z AXIS) VIBRATION

5.4.1 Purpose and Procedure

While conducting the legibility experiments reported in Chapter 4, helmet pitch motion was measured to ascertain the linearity of helmet pitch motion due to seat vertical vibration at different levels, and to determine if seat-to-helmet pitch transmissibility varied over the course of a run while the subject was performing a reading task. A rotational accelerometer affixed to the top of the helmet, as shown in Figure 5.1.2, monitored the pitch motion of the helmet over the course of the experimental runs. Seat vertical (Z axis) acceleration was also recorded. The vibration conditions in the experiment are shown in Table 5.4.1. The reading task was the same as that used in Experiment LG.1 (Section 4.2.2).

5.4.2 Results

5.4.1.1 Linearity of Helmet Pitch Motion

The standard deviation of the sampled helmet pitch motion over the reading period (approximately 50 s) was computed and divided by the standard deviation of the seat Z motion to obtain the rms helmet pitch to seat Z transmissibilities for each vibration condition. The transmissibilities are plotted in Figure 5.4.1 for each vibration frequency as a function of vibration level. The curves show that transmissibilities varied from 1.16 to 1.0 at 16 Hz, and from 1.79 to 1.0 at 11.2 Hz. Increasing vibration level tended to decrease helmet pitch transmissibility, except at 5.6 Hz and 8.0 Hz. The erratic behaviour at these frequencies may have been due to nonlinearities in helmet-to-head movement. (This possibility will be discussed in light of additional data in Section 5.9.4). In spite of these irregularities, linear regression analysis of the helmet pitch motion showed that there were significant ($p<.01$) linear correlations between helmet pitch acceleration and vertical seat (Z axis) acceleration at all

TABLE 5.4.1. EXPERIMENT BD.4: LINEARITY AND VARIABILITY OF HELMET PITCH MOTION DUE TO SEAT VERTICAL (Z AXIS) VIBRATION

Purpose: To determine the linearity of helmet pitch motion due to different levels of seat vertical vibration at different frequencies.

Subject: S1

Vibration Characteristics:

Vibration Frequency (Hz)

Vibration Level (m/s^2 rms)	2.8	4.0	5.6	8.0	11.2	16.0
	0.24	0.20	0.20	0.20	0.28	0.40
	0.48	0.40	0.40	0.40	0.56	0.80
	0.72	0.60	0.60	0.60	0.84	1.20
	0.96	0.80	0.80	0.80	1.12	1.60
	1.20	1.00	1.00	1.00	1.40	2.00

Time Duration: approximately 60 s

Data Acquisition: sample rate: 50 Hz
sample duration: 50 s
filter: Rockland
seat Z: -3 dB @ 40 Hz/48 dB/octave rolloff
helmet pitch: -3 dB @ 40 Hz/48 dB/octave rolloff

Analysis: Ratio of standard deviations (i.e., rms) of time histories at each vibration level and frequency.

Running rms computed for every 100 samples (i.e., 2 s) during 50 s period.

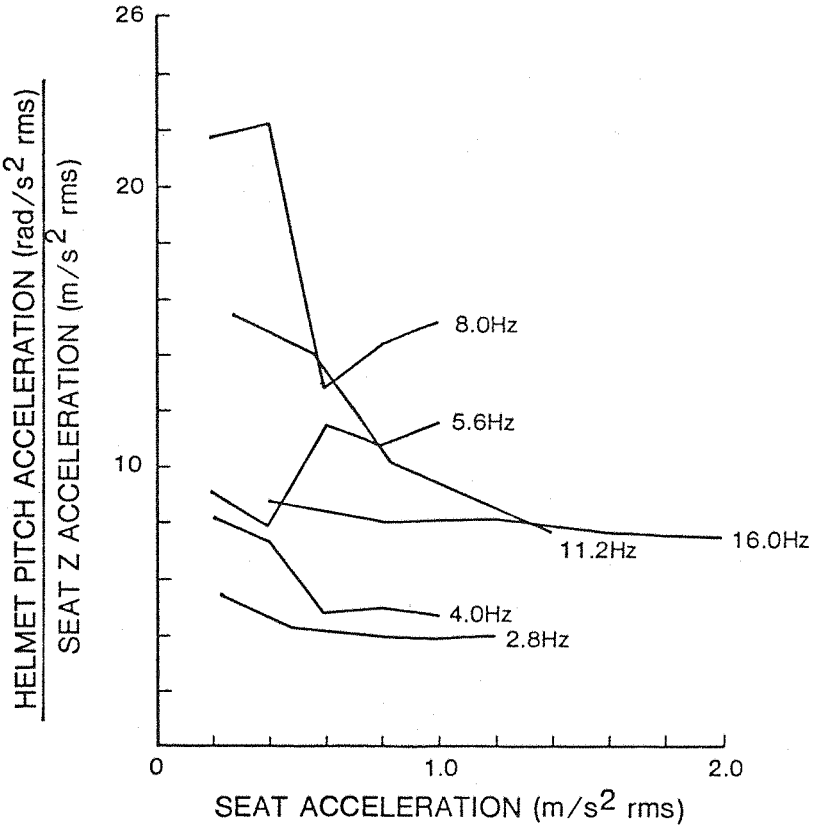

Figure 5.4.1. Ratio of Helmet Pitch Acceleration to Seat Z Axis Acceleration as a Function of Vertical (Z Axis) Seat Acceleration for Various Vibration Frequencies

TABLE 5.4.2. LINEAR REGRESSION MODELS OF HELMET-PITCH MOTION TO VERTICAL SEAT (Z AXIS) VIBRATION LEVELS

Vibration Frequency (f)	Linear Model Parameters $a_0(f)$	$a_1(f)$	Linear Correlation Coefficient (r)
2.8	-.036	3.623	0.998**
4.0	-.052	4.375	0.966*
5.6	-.038	11.138	0.992**
8.0	.118	13.309	0.962*
11.2	.159	7.412	0.942*
16.0	.023	7.667	0.999**

*p<.01

**p<.001

frequencies. Table 5.4.2 gives the parameters for linear regression models of the data:

$$\ddot{\theta}_{helmet}(f) = a_0(f) + a_1(f)\ \ddot{Z}_{seat}(f)$$

where

$\ddot{\theta}_{helmet}$ = helmet pitch acceleration (rad/s^2 rms),

$\ddot{Z}_{seat}$ = vertical Z axis seat acceleration (m/s^2 rms), and

$a_0(f)$ and $a_1(f)$ are constants for each vibration frequency.

5.4.1.2 Short Term Variation of Helmet Pitch Motion

Figure 5.4.2 shows the running rms levels of head motion for each vibration frequency as a function of the level of vertical seat vibration and time during the run. The greatest short term variability occurred at the highest vibration levels for the 2.0 Hz, 4.0 Hz, and 5.6 Hz frequencies where typically helmet pitch acceleration varied over a range of 1.4 to 1 during the 50 s run. [Note: If the motion of the head were linear (i.e., equal change in head motion for equal changes in seat motion) and did not vary during the experimental run, the data plotted in Figure 5.4.2 would consist of straight, equally spaced parallel lines for each vibration frequency.]

The variability in vibration transmission to the helmet and head was probably due to subtle changes in the posture or muscle tension of the subject. Although the data for only one subject were analyzed, nine other subjects participated in the experiment. All subjects tended to produce lower helmet pitch accelerations during the middle of the experimental runs. This behaviour seemed to be correlated with the location of the characters in the reading task. While reading either the top or bottom lines of the character array (e.g., Experiment LG.1), the helmet vibration levels were the highest, whereas when the intermediate lines were being read, helmet pitch motion was slightly less. This behaviour was especially evident at the higher vibration levels

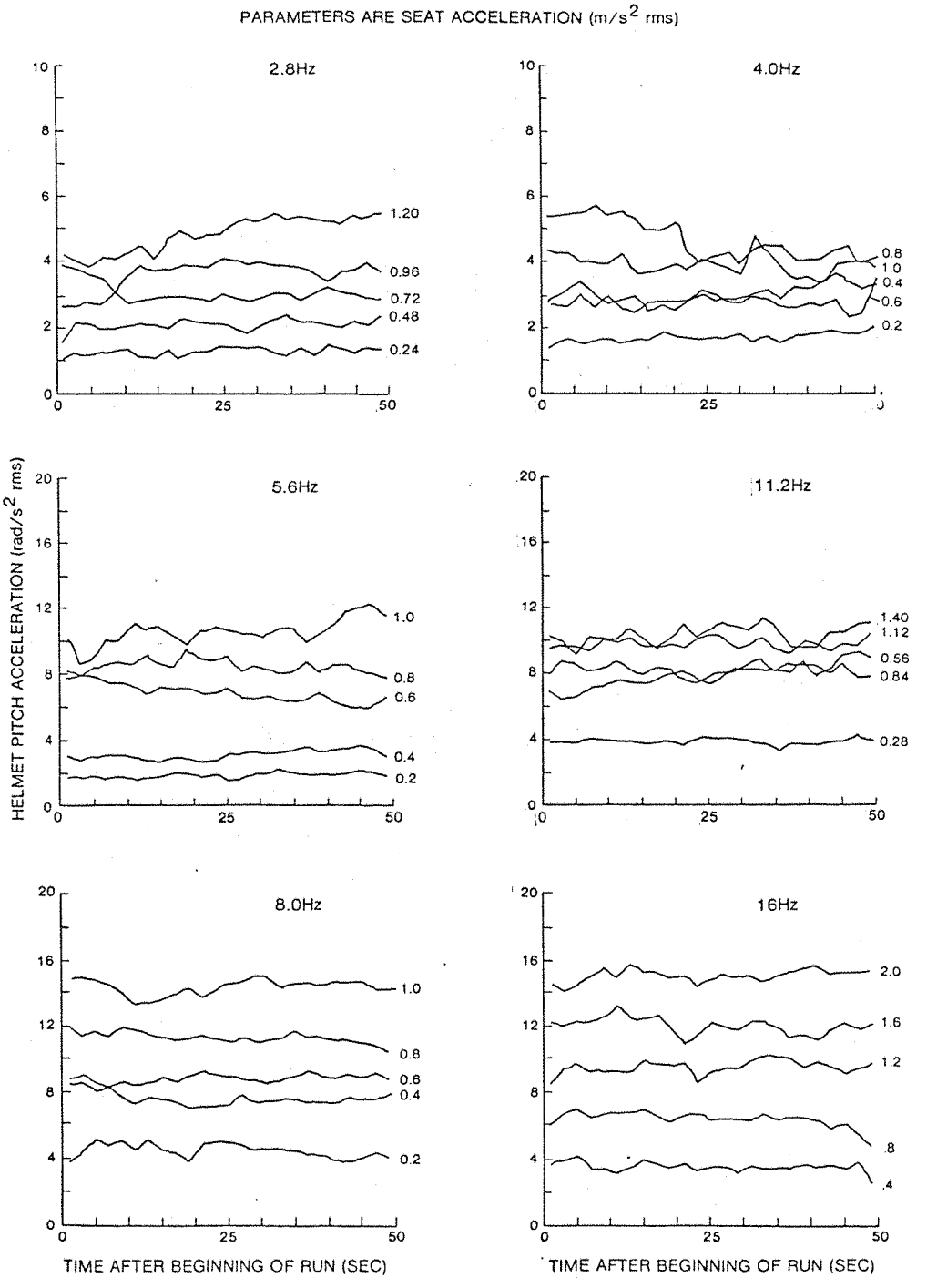

Figure 5.4.2. Running Total rms Levels of Helmet Pitch Acceleration for Various Vertical (Z Axis) Seat Vibration Levels and Frequencies During a 50 s Period (Experiment BD.4)

when the nodal images between the adjacent rows (for the intermediate lines) could be confused by becoming superimposed or at least very close to each other. It is postulated that perhaps the changes in seat to helmet pitch transmissibility were the result of subjects adjusting, unintentionally, their seating posture and/or muscle tension of the neck and head in an attempt to reduce the difficulty of the reading task.

5.5 EXPERIMENT BD.5: TRANSFER FUNCTIONS OF HEAD AND HELMET MOTION TO VERTICAL SEAT (Z AXIS) VIBRATION

5.5.1 Introduction

Up to this point, the whole-body biodynamic experiments (BD.3 and BD.4) have provided some insight into the dynamic response of a single subject at discrete vibration frequencies. These experiments have shown possible problems in the linearity and variability of transmissibilities which may be encountered in further biodynamic experiments. The power spectral distribution analyses of Experiment BD.3 have shown that head and helmet pitch motions contained harmonics which may or may not be due to the seat motion. Although an analysis of transmissibilities using the PSD approach can provide some indication of the relative contribution of harmonics, this approach does not provide any insight into the phase relationships of head, helmet, and seat motions. In order to provide an analytically sound approach for relating biodynamic response of the subjects to their reading performance in the legibility experiments, a systematic study of head and helmet response to vertical seat vibration was conducted using the subjects who participated in some of the legibility experiments. Cross spectral analysis techniques, as described in Appendix A.5.1, were used to analyze the data from these experiments.

5.5.2 Purpose

The purposes of this experiment were to gain further insight into the biomechanical nature of the helmet-to-head vibration motion and to establish head and helmet to seat transfer functions for later comparison to reading performance.

5.5.3 Method

The experimental conditions for the experiment are given in Table 5.5.1. Subjects who participated in the legibility experiments were used in this experiment (Table 3.4.1). A description of the transducer configuration used to measure seat, head, and helmet motion is given in Section 5.1. Subjects were seated and restrained as previously described (Section 3.3). The subjects were instructed to maintain a relaxed but erect posture, and to look straight ahead during each vibration run. No reading task was presented on the helmet mounted display.

5.5.4 Results

The results of the transfer function analyses are presented below for each transfer function relationship (i.e., head Z/seat Z, head pitch/seat Z, etc.). The transfer functions for the individual subjects are given in Appendix A.5.3. (Only the mean and standard deviation of the transfer functions will be shown in the text, although representative confidence intervals for single subjects will be shown.)

5.5.4.1 Coherency

In order to use the cross spectral analysis procedures to compute transfer functions, the system investigated must be linear (as defined in Appendix A.5.1). Since the subject has been shown to exhibit nonlinear biodynamic properties (e.g., Experiment BD.4), this analysis must be used with caution. Of special importance is the vibration level used to produce the data. Since some nonlinearities do exist, the transfer function, which should be valid over all vibration levels (i.e., a linear system), may have to be qualified as a "describing function" with results valid only for the specific vibration level used. (This aspect of transfer function will be discussed later in Section 5.9.) Another aspect of the cross spectral analysis approach is that the response of the system must be associated with the input (i.e., "correlated" with the input). The cross spectral density is based upon the joint power or probability of the output response to

TABLE 5.5.1. EXPERIMENT BD.5: HEAD AND HELMET TRANSFER FUNCTIONS

Purpose:	(1) To determine the transfer functions of vertical seat (Z axis) vibration to helmet pitch, head pitch, and head Z axis motion. (2) To determine head pitch to helmet pitch transfer functions.
Subjects:	S1, S3, S4, S5, S7, S8, S9, S11, S12, S13
Vibration Frequency:	0-60 Hz*, linear sweep in 100 s
Vibration Level:	1.0 m/s^2 rms
Time Duration:	approximately 200 s (two sweeps)
Data Acquisition:	sampling rate: 120 Hz sampling period: 100 s filter characteristics: seat Z: -3 dB @ 60 Hz/24 dB/octave rolloff head Z: -3 dB @ 60 Hz/24 dB/octave rolloff head pitch: -3 dB @ 60 Hz/48 dB/octave rolloff helmet pitch: -3 dB @ 60 Hz/48 dB/octave rolloff
Data Analysis:	Transfer function analysis using cross spectral distribution -coherency of input/output -confidence interval of transfer function -single subject transfer functions -mean ± standard deviation of transfer functions across subjects Transfer functions (modulus and phase)* -head Z/seat Z -head pitch/seat Z -helmet pitch/seat Z -helmet pitch/head pitch B_e = 0.5 Hz DOF = 184

*Only data for 0-40 Hz are presented due to internal resonance of the rotational accelerometer at 50 Hz.

the input. The measure of the degree that the system's output is correlated with the input is termed coherency and is defined more thoroughly in Appendix A.5.1. Coherency (viz, coherence function) is an expression of the proportion of the power in the output signal which is correlated with the input signal at a particular frequency (Bendat and Piersol, 1971). Similarly, the transfer function so computed using the cross spectral analysis approach relates only the properties of the output which are correlated with the input. If there is harmonic distortion in the input, only the outputs correlated with those frequencies will be contained in the transfer function expression.

In order to provide a measure of the coherency of the head and helmet motion to the vertical seat Z motion, the following coherency functions were computed from the time motion data from subjects S1 and S11:

head Z ($\ddot{Z}_{head}$)/seat Z ($\ddot{Z}_{seat}$)

head pitch ($\ddot{\theta}_{head}$)/seat Z ($\ddot{Z}_{seat}$)

helmet pitch ($\ddot{\theta}_{helmet}$)/seat Z ($\ddot{Z}_{seat}$)

helmet pitch ($\ddot{\theta}_{helmet}$)/head pitch ($\ddot{\theta}_{head}$)

These coherency functions are shown in Figure 5.5.1. As discussed in Appendix A.5.1, the coherency function [$\gamma^2_{xy}(f)$] should be >0.5 at any particular frequency; otherwise, the modulus and phase data may be invalid. For Subject S1, the coherency was adequate over most of the vibration frequency range above 2.5 Hz. The same was true for Subject S11, with the exception of the head pitch and helmet pitch to seat Z at approximately 10 Hz, where coherencies were 0.2. The lack of coherency at frequencies below 2.0 Hz was probably due to the severe distortion of the vibration waveform at these frequencies and the lack of adequate seat input accelerations due to the displacement limitations in the vibrator. Another possible source of noncoherency in the subjects response was voluntary control of posture (e.g., subjects may have attempted to maintain the head in an erect posture).

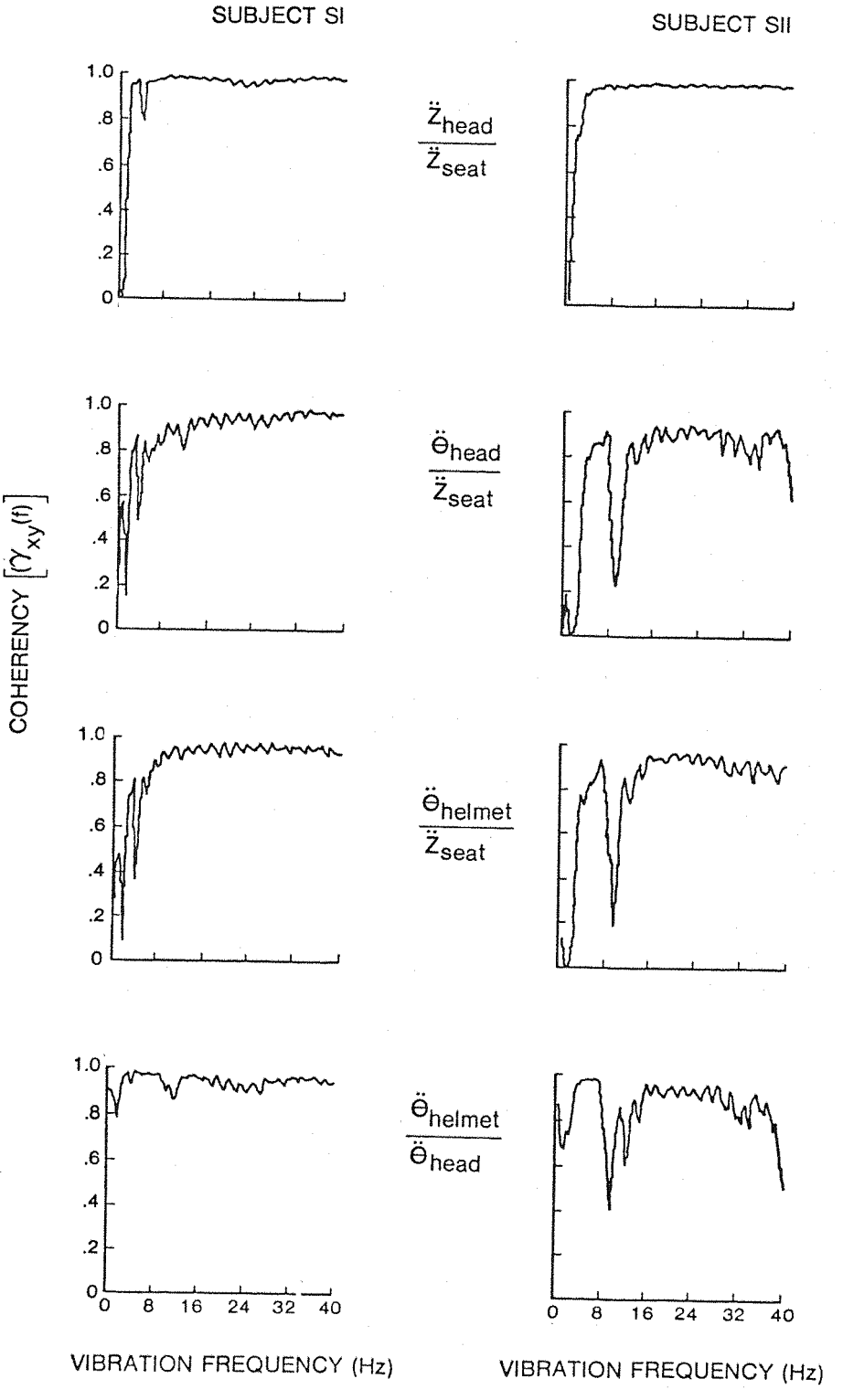

Figure 5.5.1. Coherency Functions of Head, Helmet, and Seat Accelerations for Subjects S1 and S11 (B_e = 0.5 Hz, DOF = 184, Experiment BD.5)

5.5.4.2 Head Z to Seat Z Transfer Functions

Figure 5.5.2 shows the 95 percent confidence interval about the modulus and phase for head Z to seat Z transfer functions in subjects S1 and S11. The moduli and phases of the individual transfer functions for each of the 10 subjects are contained in Appendix A.5.3. Eight of the 10 subjects exhibited the double peak for head Z to seat Z motion similar to those shown for S1 and S11 in Figure 5.5.2. These peaks were typically between 4 to 8 Hz and 12 to 16 Hz, with the exception of Subject S8. All subjects demonstrated a slight phase lead (less than 25 degrees) in head Z to seat Z motion between 4.0 Hz to 6.0 Hz, after which phase lag increased with frequency up to approximately 180 degrees at 40 Hz. There were simularities between these data and the findings of Rowlands (1977) for head Z response. However, by locating the translational accelerometer in the bite bar, the data in the present experiment were contaminated with some head pitch motion (which may account for the slight phase lead at low frequencies).

Figure 5.5.3 gives the mean and ±1 standard deviation of the moduli and the mean phase across subjects. The characteristic double peak shape of the modulus observed in most individual subjects is obscured in the averaged moduli, but can be seen as a large standard deviation between 6 Hz and 16 Hz. It is also interesting to note that the mean head Z to seat Z transmissibility was greater than one between 4 Hz and 24 Hz (cf. Figure 2.5.6).

5.5.4.3 Head Pitch to Seat Z Transfer Function

Figure 5.5.4 shows the mean and ±1 standard deviation of the modulus and the mean phase of the head pitch axis to seat vertical Z axis vibration data for the 10 subjects. Individual subject transfer functions are given in Appendix A.5.3. Representative 95 percent confidence intervals about the modulus and phase data for subjects S1 and S11 are shown in Figure 5.5.5. Figure 5.5.4 demonstrates the very large variability across subjects, even though the confidence intervals for the individual data were small. Most of the individual

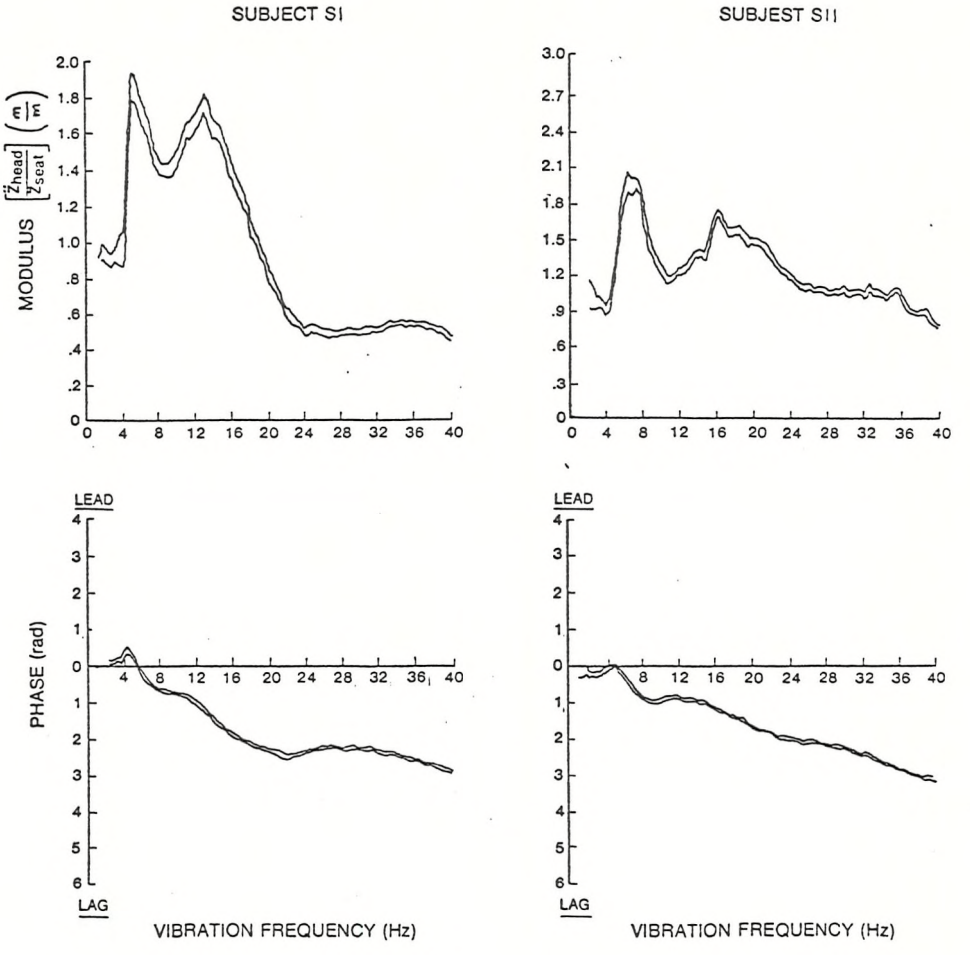

Figure 5.5.2. 95 Percent Confidence Intervals About the Modulus and Phase of the Head Z Axis to Seat Z Axis Transfer Functions for Subjects S1 and S11 (B_e = 0.5 Hz, DOF = 184, Experiment BD.5)

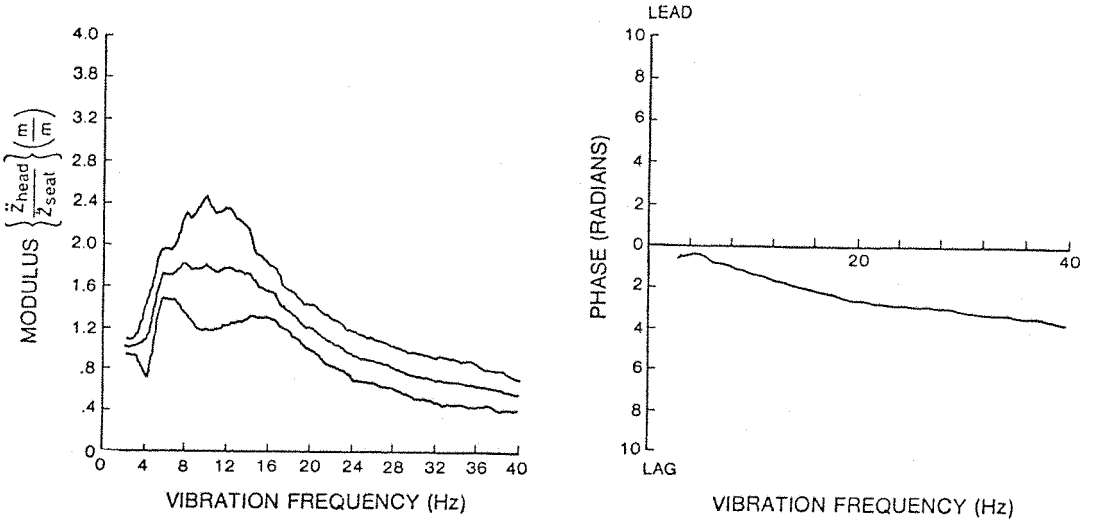

Figure 5.5.3. Mean and ±1 Standard Deviation of the Modulus and the Mean Phase of the Head Z Axis to Seat Z Axis Transfer Function for 10 Subjects (B_e = 0.5 Hz, DOF = 184, (Experiment BD.5)

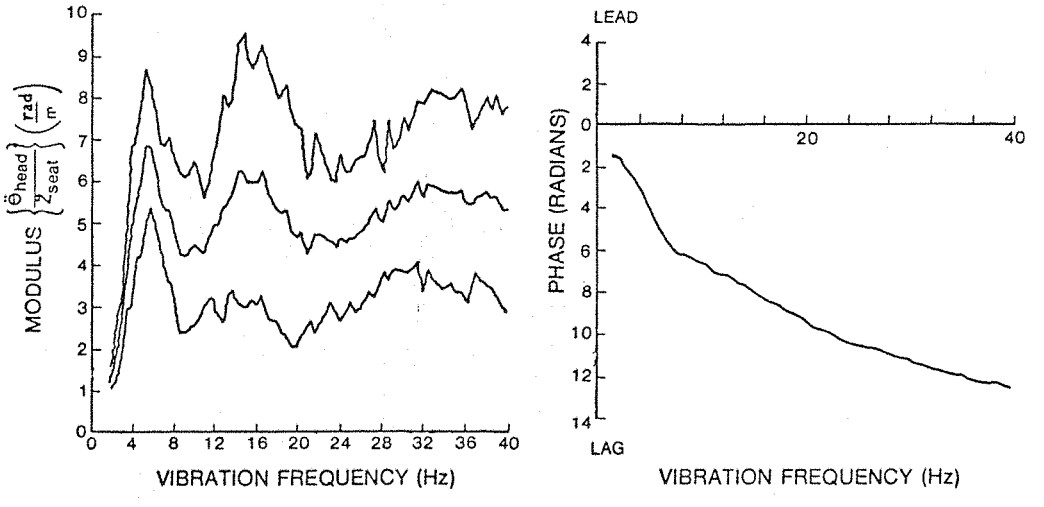

Figure 5.5.4. Mean and ±1 Standard Deviation of the Modulus and the Mean Phase of the Head Pitch to Seat Z Axis Transfer Function for 10 Subjects (B_e = 0.5 Hz, DOF = 184, (Experiment BD.5)

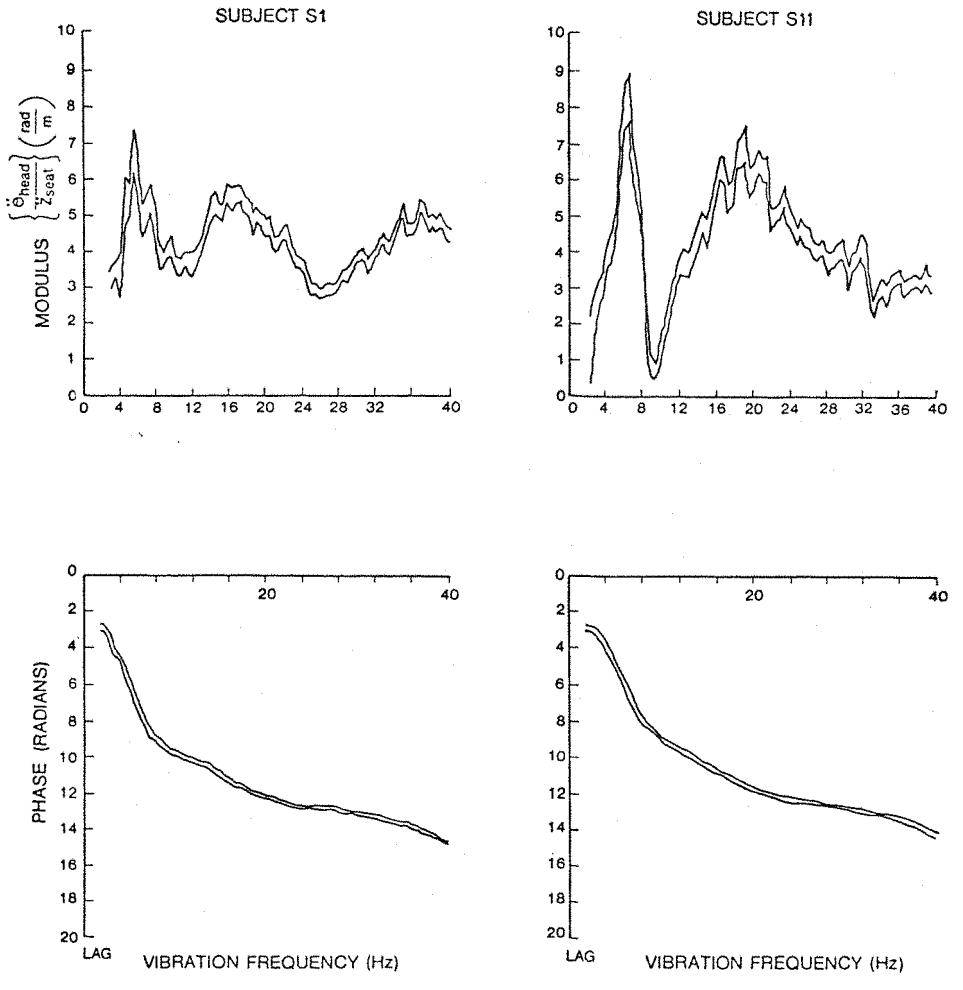

Figure 5.5.5. 95 Percent Confidence Intervals About the Modulus and Phase of the Head Pitch Axis to Seat Z Axis Transfer Functions for Subjects S1 and S11 (B_e = 0.5 Hz, DOF = 184, Experiment BD.5)

subjects exhibited a peak in the modulus of head pitch at approximately 6 to 8 Hz as well as other peaks between 14 to 18 Hz and 30 to 40 Hz. For seven out of the 10 subjects, the peaks present within the 6 to 8 Hz frequency range were accompanied by a phase shift (from the phase at 2 Hz) of approximately 90 degrees. The phase data indicated that, at very low frequency, the phase of head pitch was 180 degrees out of phase with the seat Z and motion; that is, as the seat moved upward, the head pitched downward.

The mean modulus for head pitch to seat Z at 6.8 Hz was about 7.0 rad/m, and similar to that shown by Lewis (1979b). Figure 5.5.4

and Figure 2.5.9 show data for subjects wearing different helmets, but under similar seating and vibrating conditions. Although the data were similar for the low frequencies, there was a significant departure in form and magnitude in these data at frequencies greater than 12 Hz. These differences in head pitch transmissibilities may have been due to the differences in mass distribution and suspension characteristics of the helmets.

5.5.4.4 Helmet Pitch to Seat Z Transfer Functions

Figure 5.5.6 shows the mean and ±1 standard deviation of the modulus and phase of the helmet pitch to seat Z axis transfer function. Individual subject transfer functions are given in Appendix A.5.3. Representative 95 percent confidence intervals about the modulus and phase for two subjects are shown in Figure 5.5.7. Peaks in the moduli occurred for all subjects between 6 Hz and 8 Hz and at a mean level of approximately 11 rad/m. The greatest variability in the data occurred at 10 Hz where, for some subjects (e.g., S11, S3, S9), there was a significant decrease in the helmet pitch motion. Beyond 16 Hz, the moduli of helmet pitch to seat Z motion decreased steadily for all subjects to a nominal level of about 2 rad/m at 40 Hz.

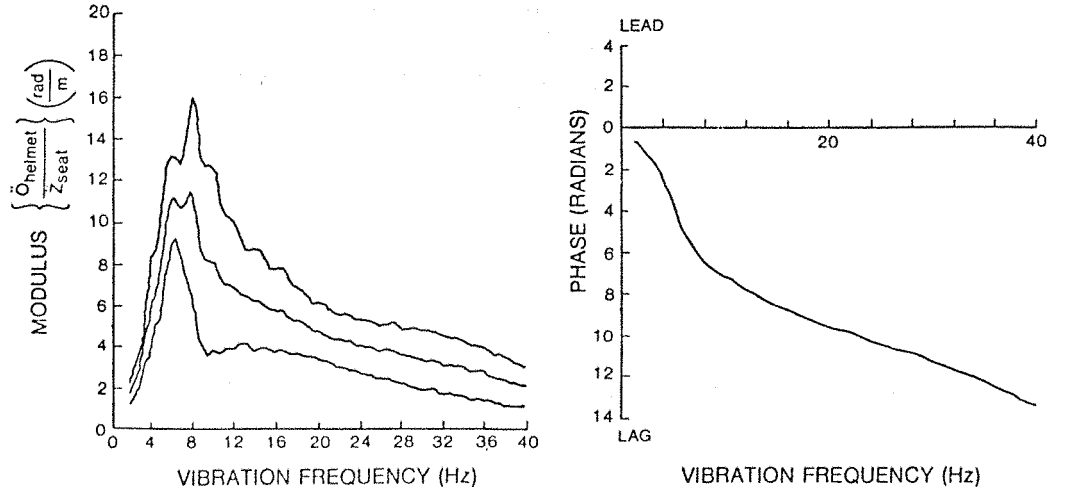

Figure 5.5.6. Mean and ±1 Standard Deviation of the Modulus and the Mean Phase of the Helmet Pitch Axis to Seat Z Axis Transfer Functions for 10 Subjects (B_e = 0.5 Hz, DOF = 184, Experiment BD.5)

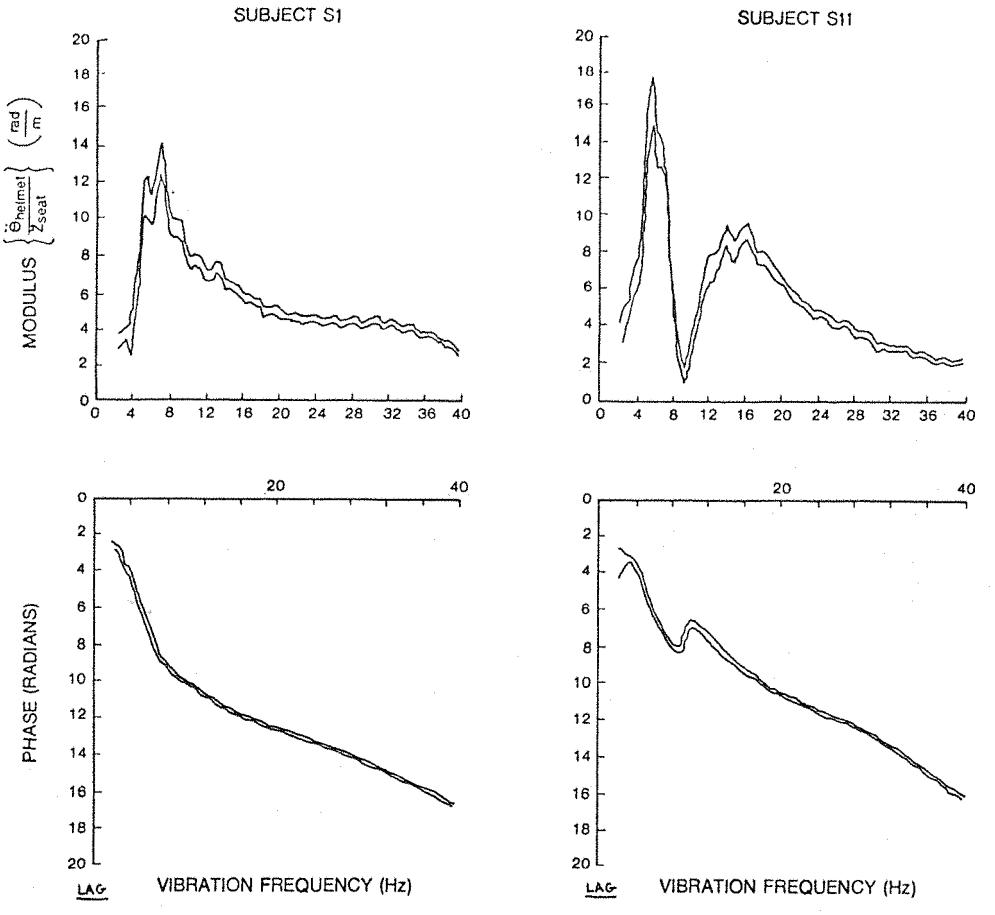

Figure 5.5.7. 95 Percent Confidence Intervals About the Modulus and Phase of the Helmet Pitch Axis to the Seat Z Axis Transfer Functions for Subjects S1 and S11 (B_e = 0.5 Hz, DOF = 184, Experiment BD.5)

5.5.4.5 Comparison of Helmet Pitch to Seat Z and Head Pitch to Seat Z Transfer Functions

Figure 5.5.8 compares the mean moduli for the head pitch and helmet pitch to seat Z axis transfer functions shown in Figures 5.5.4 and 5.5.6, respectively. At the 1.0 m/s^2 vibration level used, there were large differences in the mean amplitude of helmet motion relative to the head. At seat vibration frequencies between 4 Hz and 12 Hz, the pitch of the helmet was greater than that of the head; but at frequencies above 20 Hz, the head pitch exceeded that of the helmet. At 8 Hz,

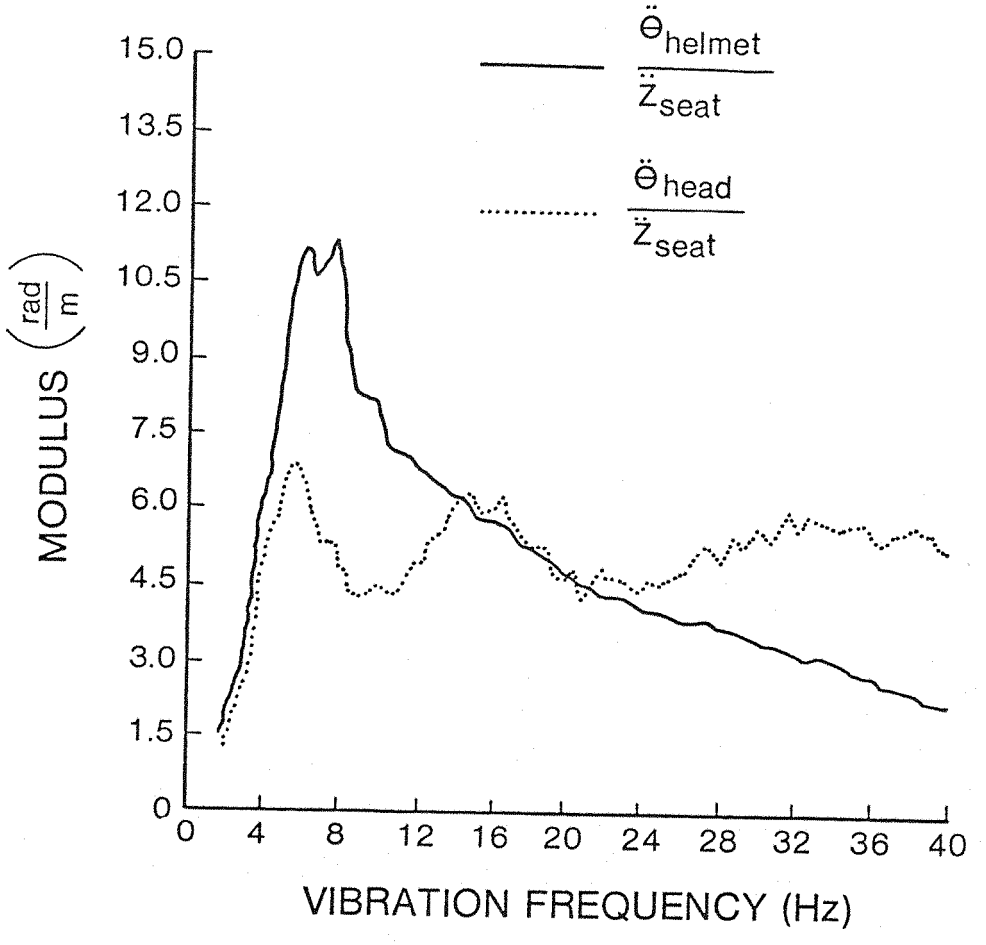

Figure 5.5.8. Comparison of Mean Moduli for Head Pitch and Helmet Pitch to Vertical Seat (Z Axis) Transfer Functions for 10 Subjects (B_e = 0.5 Hz, DOF = 184, Experiment BD.5)

the relative motion of the helmet to the head was greater than 2 to 1. Using the head pitch motion as the input, helmet pitch to head pitch transfer functions were computed for each subject and are given in Appendix A.5.3. Representative 95 percent confidence intervals about the modulus and phase for two subjects are shown in Figure 5.5.9. The mean and standard deviation of the moduli and the mean phase of the individual transfer functions are shown in Figure 5.5.10. The peak helmet to head transmissibilities in the pitch axis occurred at about 8 Hz for all subjects, but at amplitudes ranging from 1.4 (S7) to 2.6 (S5). For Subjects S5, S7, S9, and S13 there were phase lags of approximately 90 degrees, corresponding to the peaks in the moduli, which indicated possible resonances between helmet and head motion at these frequencies. Other peaks of lesser magnitudes occurred, for some subjects, at 14 to 18 Hz (Subjects S3, S5, S11, S12, S13) and also between 20 and 27 Hz (Subjects S1, S3, S4, S7, S8, S11).

5.5.4.6 Comparison of Cross Spectral and Power Spectral Determinations of Transfer Function Gains

As discussed in Appendix A.5.1, the gain of the system output, to a given input, can be determined by using either a ratio of the square roots of the PSDs of the output and input, or by using the cross spectral density of the output to the input divided by the power spectral density of the input. The attributes of both methods were also discussed in Appendix A.5.1. If the output of the system is totally correlated with the input (i.e., coherency function = 1), then the two techniques produce the same result. (It also follows that if there is power in the output not correlated with the input, the PSD method will always produce higher gains than the CSD method.) Since there were probably some nonlinearities present in the biomechanical system (which produced harmonic distortion) and some noise uncorrelated between the output and the input, a comparison of the system output to input gains determined by the two methods provides some insight into the behaviour of the overall system. Shown in Figures 5.5.11 through 5.5.13 are comparisons of the mean gains of head pitch to seat Z, helmet pitch to seat Z, and helmet pitch to head pitch using the cross spectral and power spectral methods. The most

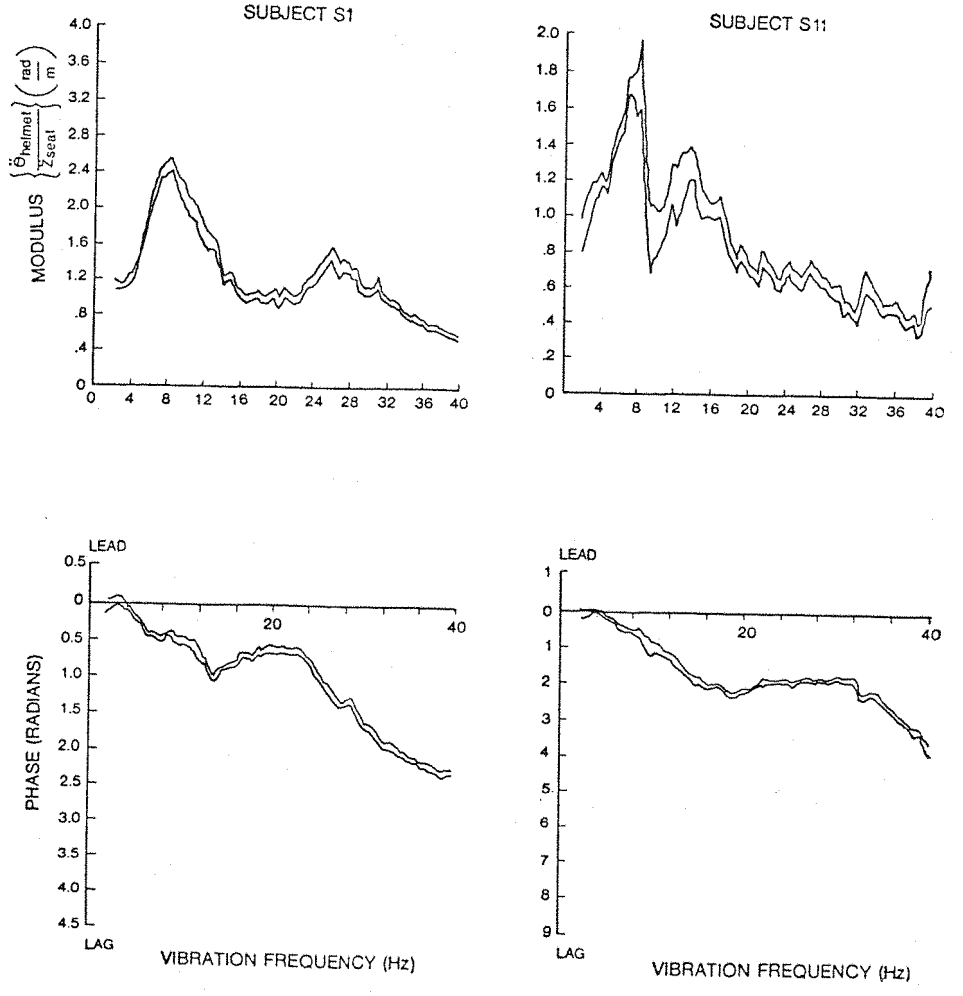

Figure 5.5.9. 95 Percent Confidence Intervals About the Modulus and Phase of the Helmet Pitch Axis to Head Pitch Axis Transfer Functions for Subjects S1 and S11 (B_e = 0.5 Hz, DOF = 184, Experiment BD.5)

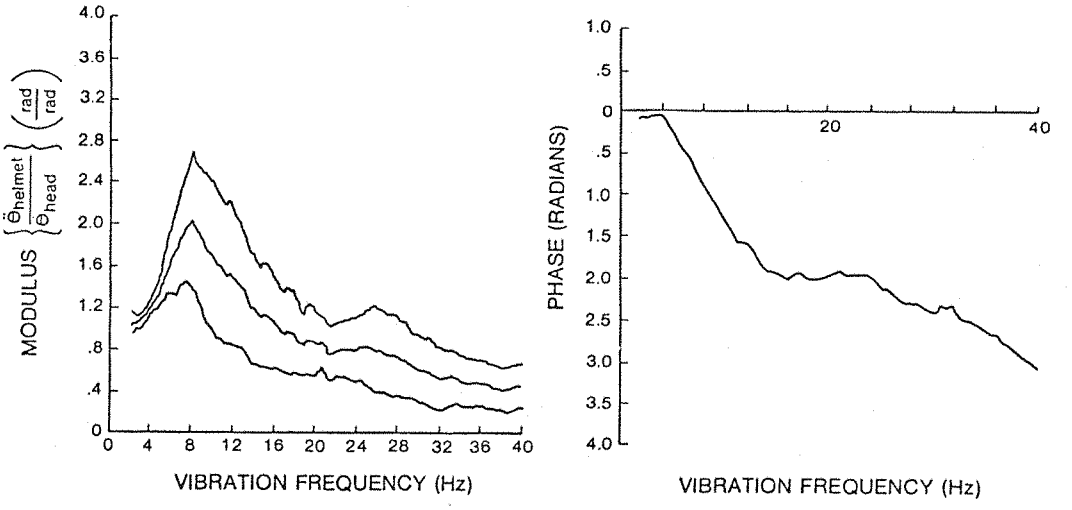

Figure 5.5.10. Mean and ±1 Standard Deviation of the Modulus and the Mean Phase of the Helmet Pitch Axis to Head Pitch Axis Transfer Functions for 10 Subjects (B_e = 0.5 Hz, DOF = 184, Experiment BD.5)

methods. The most obvious differences for the PSD and CSD determinations of output to input gains were for the head pitch to seat Z (Figure 5.5.11) and helmet pitch to seat Z (Figure 5.5.12) at frequencies of 3 Hz and below. Here the mean PSD gains were 3 to 4 times that of the CSD mean modulus. It may be recalled that, at these frequencies, coherency was also low (i.e., $\gamma_{xy}^2 < .2$) for Subjects S1 and S11 (Figure 5.5.1). Also, there were large harmonic distortions in the seat vibration motion (due to displacement limitations of the vibrator) at frequencies less than 3.66 Hz (Figure 5.2.2). These harmonics of the fundamental frequency of vibration may have produced motions of the head and helmet which were uncorrelated with the input motion. It is also possible to argue that at these frequencies (i.e., less than 3.0 Hz), there may have been some attempt by the subjects to voluntarily adjust the muscles in the neck to exert some postural control over head movement in space. The small but consistent differences in PSD to CSD gains above 3 Hz were probably due to noise inherent in the instrumentation and data acquisition systems, since the level of the noise seemed to be largely invariant with level and frequency.

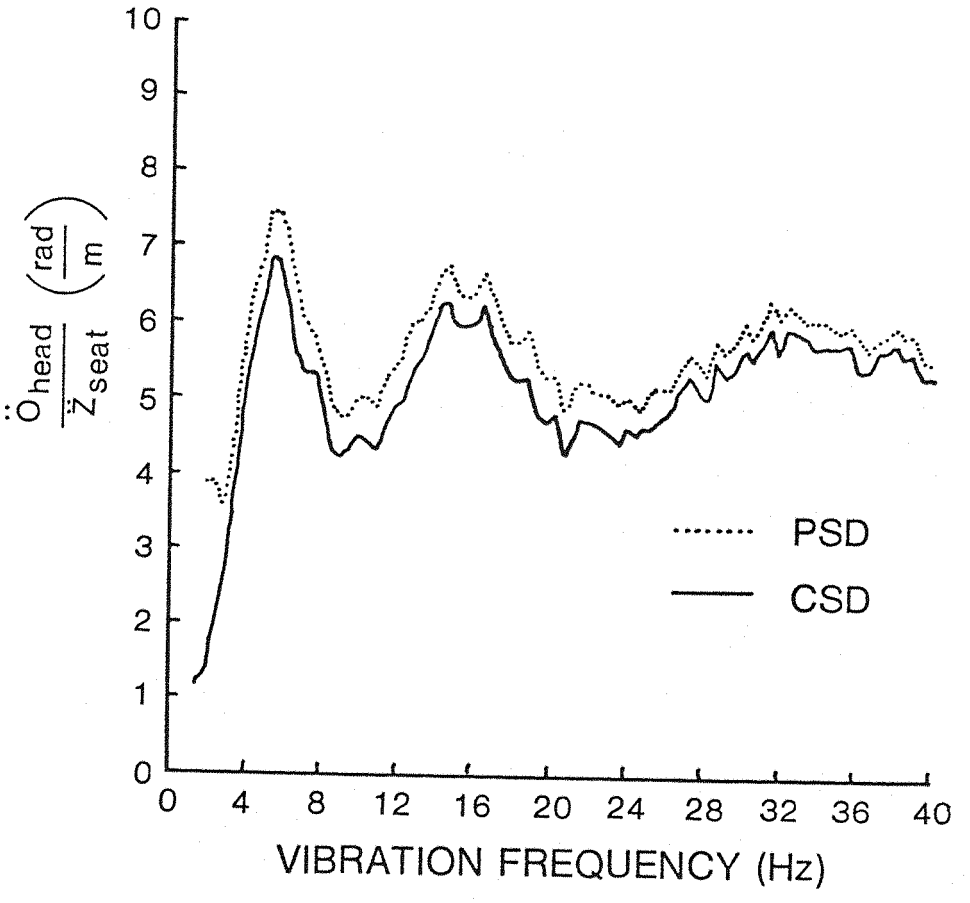

Figure 5.5.11. Comparison of Cross Spectral (CSD) and Power Spectral (PSD) Methods for Describing Head Pitch Axis to Vertical Seat (Z Axis) Transfer Functions Means for 10 Subjects (B_e = 0.5 Hz, DOF = 184, Experiment BD.5)

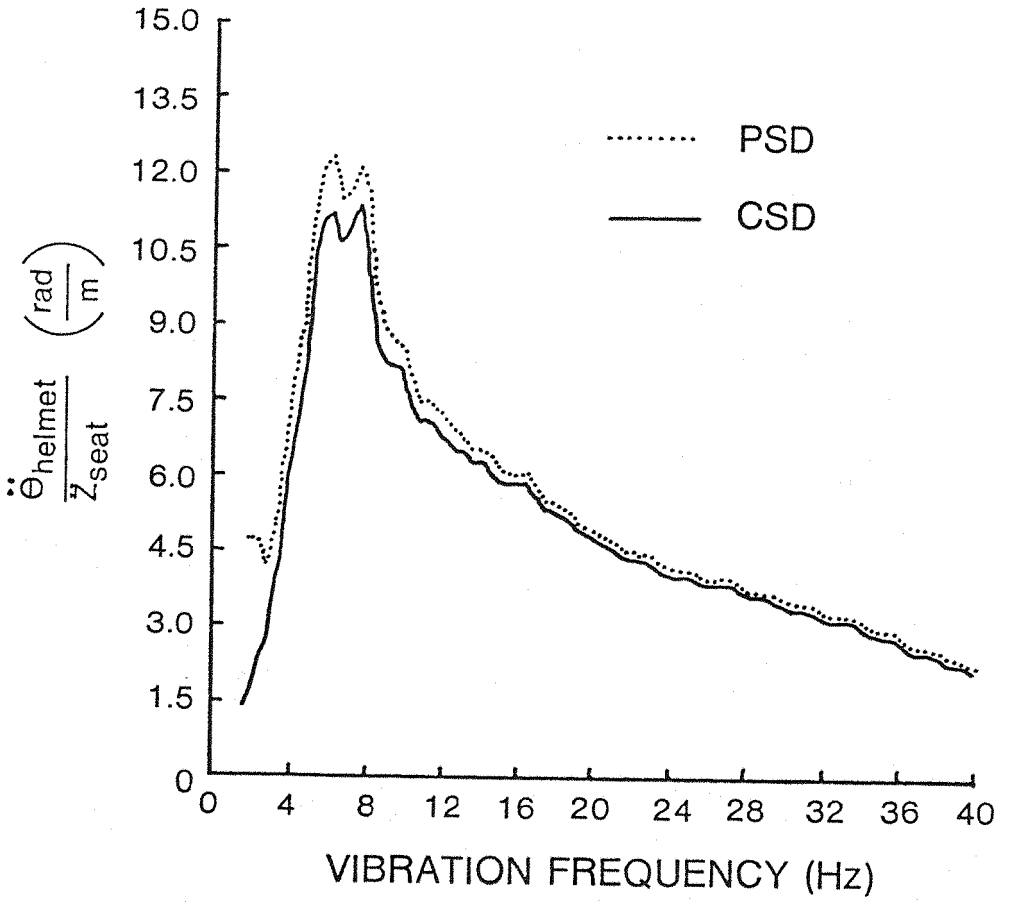

Figure 5.5.12. Comparison of Cross Spectral (CSD) and Power Spectral (PSD) Methods for Describing the Helmet Pitch Axis to Vertical Seat (Z Axis) Transfer Functions for 10 Subjects (B_e = 0.5 Hz, DOF = 184, Experiment BD.5)

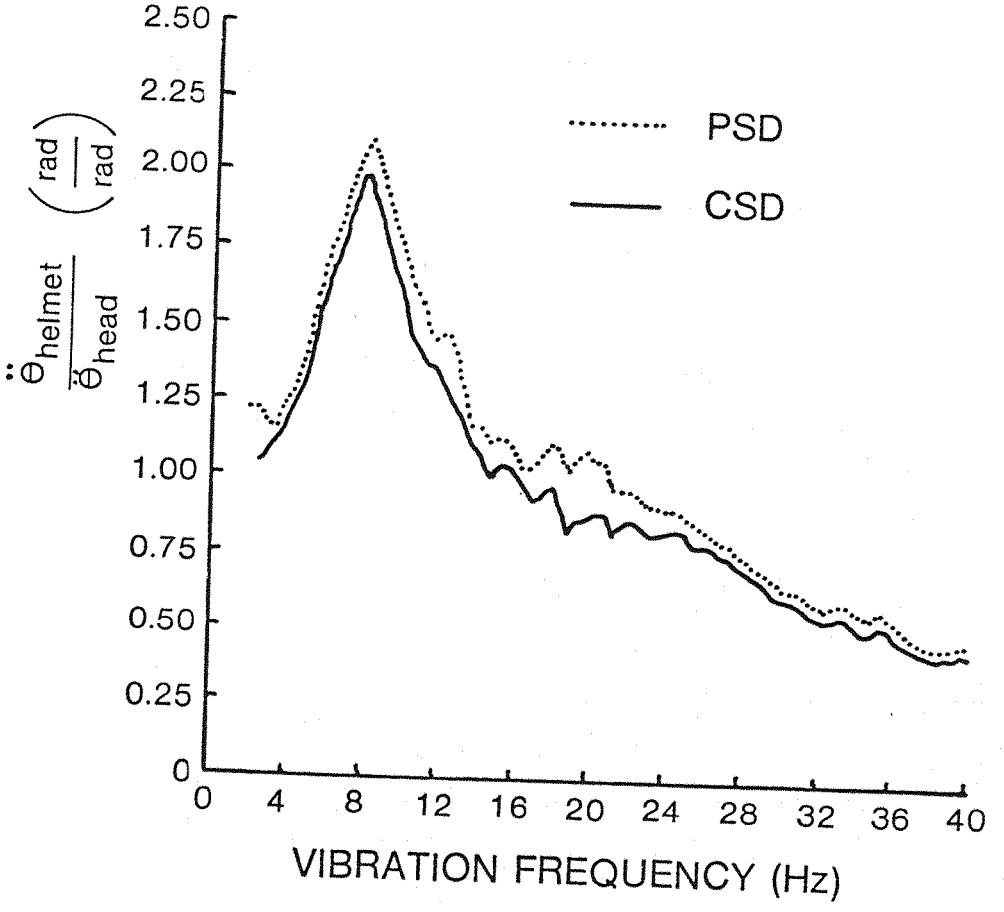

Figure 5.5.13. Comparison of Cross Spectral (CSD) and Power Spectral (PSD) Methods for Describing the Helmet Pitch Axis to Head Pitch Axis Transfer Functions Means for 10 Subjects (B_e = 0.5 Hz, DOF = 184, Experiment BD.5)

5.6 EXPERIMENT BD.6: HEAD MOTION IN THE ROLL AXIS

5.6.1 Introduction and Method

A small study was conducted to provide some indication of the levels of head roll motion which would occur (with the helmet-mounted display) during whole-body vertical vibration of the seat. Two subjects (S1 and S12) were used in the experiment with the vibration conditions shown in Table 5.6.1. The vibration levels used in the sinusoidal sweep input are shown in Figure 5.6.1. Increased acceleration levels

at the very low frequencies (<4.0 Hz) and high frequencies (>16.0 Hz) were used in order to have a sufficient input vibration level to compute transfer functions. (Based upon preliminary experiments, it was anticipated that the levels of head roll motion would be low compared to head pitch motion.) The roll motion of the head was measured by a rotational accelerometer mounted in a bite bar (Figure 5.1.2). Subjects were instructed to look straight ahead.

TABLE 5.6.1. EXPERIMENT BD.6: HEAD ROLL TO SEAT Z TRANSFER FUNCTIONS

Purpose:	To determine the modulus and phase of the roll movement of the head due to vertical seat Z axis sinusoidal vibration.
Subjects:	S1, S12
Vibration Frequency:	0-82 Hz* linear sweep of sinusoidal waveform in 100 s
Vibration Level:	See Figure 5.6.1
Time Duration of Exposure:	approximately 200 s
Data Acquisition:	sampling rate: 160 Hz sampling period: 100 s filter: seat Z - none head roll - none
Data Analysis:	transfer function analysis using cross spectral density (B_e = 1.0 Hz, DOF = 276) -head roll/seat Z

*Only 0 to 40 Hz are presented due to resonance of rotational acceleration at 50 Hz.

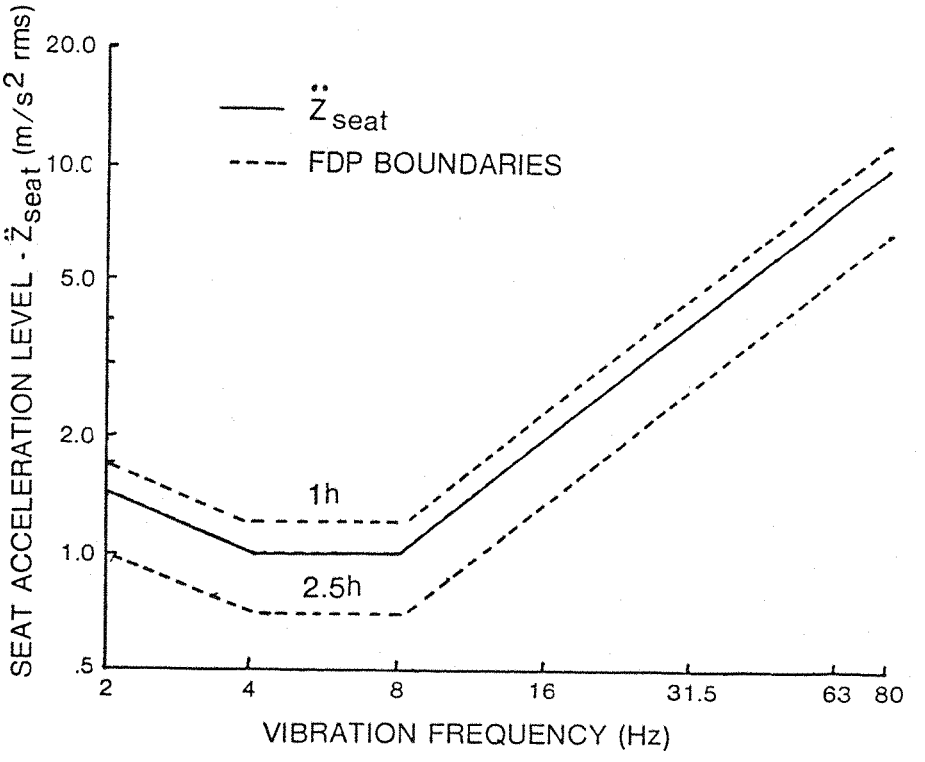

Figure 5.6.1. Seat Z Axis Acceleration Levels Used in Experiment BD.6 Compared to 1 h and 2.5 h Fatigue-Decreased Proficiency Boundaries [ISO 2631-1974(E)]

5.6.2 Results

Figure 5.6.2 shows the modulus and phase curves for the head roll to seat Z transfer functions. The greatest transmissibility of seat Z vibration to the head occurred at 8 Hz for S12 and 10 Hz for S1. The maximum moduli for head roll for the two subjects were about an order of magnitude lower than their moduli for head pitch (Figure A.5.3.2) at the same frequencies.

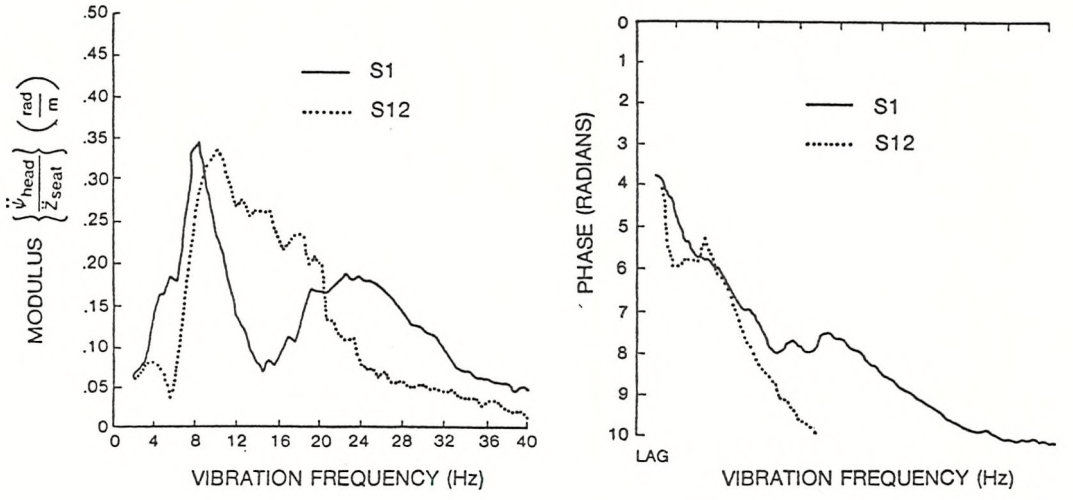

Figure 5.6.2. Modulus and Phase of the Head Roll Axis to Seat Z Axis Transfer Functions for Subjects S1 and S12 (B_e = 1.0 Hz, DOF = 276, Experiment BD.6)

5.7 EXPERIMENT BD.7: EFFECT OF HEAD POSITION ON HEAD AND HELMET TO SEAT TRANSFER FUNCTIONS

5.7.1 Introduction and Purpose

As discussed in Section 2.5.3.5, the transmissibility of vibration from the seat to the head has been shown to vary with the orientation of the head. Voluntary movement of the head also was shown to influence relative movement of the helmet on the head (Section 2.5.3.12). Since it can be expected that the operator will adopt various head orientations when using the helmet-mounted display (especially if a head position sensing system is used in conjunction with the helmet-mounted display to visually direct sensors, etc.), the influence of head orientation on the transmission of vibration to the head and helmet is particularly relevant. The purpose of this experiment was to establish transfer functions describing the transmissibility of seat vibration to the head and from the head to the helmet at various helmet orientation angles.

5.7.2 Method

In order to establish a particular helmet orientation during an experimental run, targets were positioned at various angles relative to a straight ahead (i.e., 0 degrees azimuth and 0 degrees elevation) orientation. The targets consisted of six circular black discs, 2 cm in diameter on a 7.6 cm by 12.7 cm rectangular white cards. The cards were also numbered 1 through 6. The viewing distance of the cards varied according to orientation angle, but in all cases was greater than 3 m. The particular orientation angles used in the experiment were selected as representing the practical limits of the head search envelop which may be expected during an operational task. During the course of the experiment, an aiming reticle was presented on the helmet-mounted display, consisting of bisecting horizontal and vertical lines subtending a visual angle of approximately 5 degrees in each dimension. Subjects were instructed to orient their heads so as to superimpose the reticle from the display over the target which had been specified by the experimenter, and to maintain aiming of the reticle to the best of their ability during the data run. During the data runs, helmet pitch, helmet yaw, and head pitch were measured with rotational accelerometers and vertical seat Z axis vibration was measured with a translational accelerometer as shown in Figure 5.1.2. The vibration conditions for the experiment are given in Table 5.7.1. The order of presentation of target orientations was randomized for each subject.

5.7.3 Results and Discussion

The moduli of the transfer functions relating helmet pitch, head pitch, and seat motion for each subject and head orientation are given in Appendix A.5.4. Composites of the transfer function moduli at the different helmet orientation angles are shown for the two subjects in Figure 5.7.1. From this figure the following general observations can be made.

TABLE 5.7.1. EXPERIMENT BD.7: OFF-AXIS TRANSFER FUNCTIONS

Purpose: To define head and helmet to seat transfer functions for different head orientation angles.

Subjects: S3, S8

Helmet Orientation Angles (degrees):

Azimuth	Elevation
0	0
0	+36.9 (up)
0	-36.9 (down)
45 (left)	0
45 (left)	+36.9
45 (left)	-36.9

Vibration Frequency: 0-20 Hz linear sweep of sinusoidal waveform in 100 s

Vibration Level: 1.5 m/s^2 rms

Data Acquisition: sampling rate: 40 Hz

sampling period: 115 s

filter:

seat Z: -3 dB @ 20 Hz 48 dB/octave
head pitch: -3 dB @ 20 Hz 48 dB/octave
helmet pitch: -3 dB @ 20 Hz 24 dB/octave
helmet yaw: -3 dB @ 70 Hz 24 dB/octave

Data Analysis: transfer function analysis:

head pitch/seat Z
helmet pitch/seat Z
helmet yaw/seat Z
helmet pitch/head pitch

resolution: B_e = 0.2 Hz

degrees of freedom: DOF = 68

window: Hanning

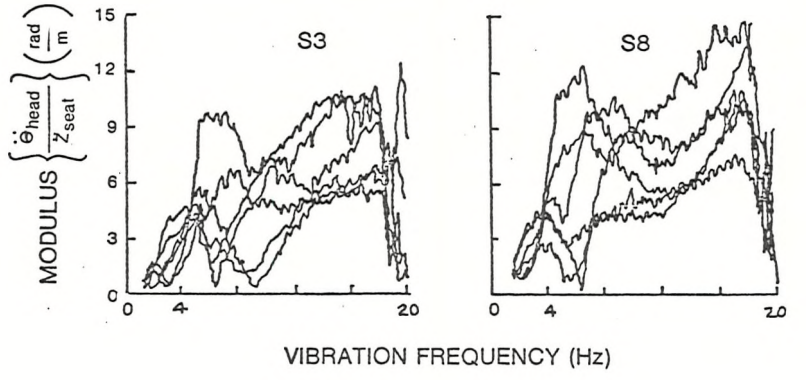

a) HEAD PITCH/SEAT$_Z$

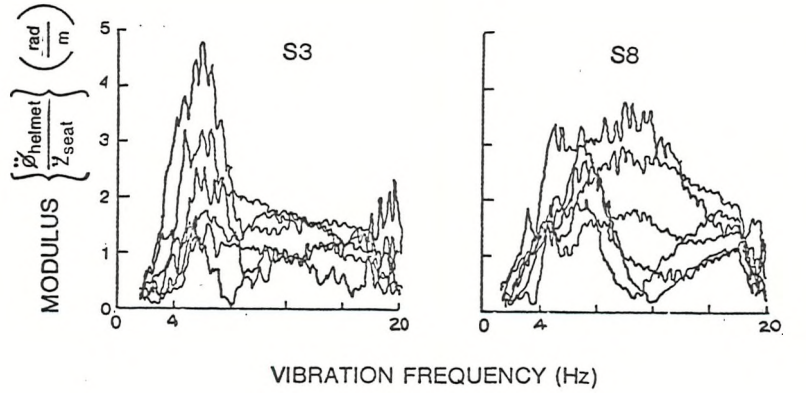

b) HELMET YAW/SEAT Z

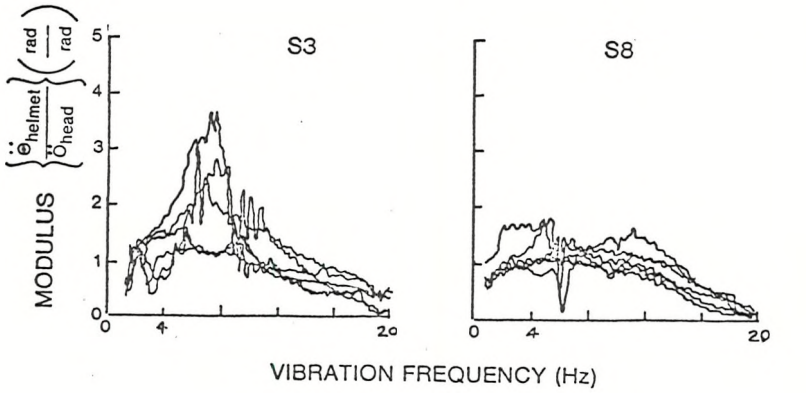

c) HELMET PITCH/HEAD PITCH

Figure 5.7.1. Composites of Moduli of Head Pitch to Seat Z, Helmet Yaw to Seat Z, and Helmet Pitch to Head Pitch Transfer Functions for Subjects S3 and S8 and 6 Head Orientation Angles (B_e = 0.2 Hz, DOF = 68, Experiment BD.7)

5.7.3.1 Head Pitch

For Subject S8, off-axis orientations tended to increase the transmissibility of vibration from the seat to the head. Although this was not always true for Subject S3, transmissibilities did increase for both subjects above 16 Hz for the off-axis conditions. For example, when Subject S3 aimed his head to the left by 45 degrees and upward by 36.9 degrees from the straight ahead orientation, head pitch to seat Z gain doubled at 16 Hz. The off-axis orientation of the head caused the greatest effect for Subject S8 at 7 Hz, where a 45 degree left and 36.9 degree downward orientation caused a three-fold increase in head pitch to seat Z gain over a straight ahead orientation. The form (frequency distribution) of the transfer function changed for both subjects when looking downward, with a notable "dip" in the moduli at 6 Hz for both subjects.

5.7.3.2 Helmet Pitch

The helmet motion in the pitch axis was always greater than that of the head at low frequencies (i.e., less than 12 Hz), but less than the head at higher frequencies for all orientations; however, the cross-over frequency (i.e., where helmet pitch equals head pitch) did vary widely as a function of head orientation. The greatest disparity in helmet pitch to head pitch transfer function occurred at 8.0 Hz when Subject S3 changed his helmet orientation from 45 degrees (left) and 36.9 degrees (upward) to 45 degrees (left) and 0 degrees (elevation), causing the helmet pitch to head pitch gain to change from 1.0 to 3.7. Similarly, when looking from 36.9 degrees upward (at 0 degrees azimuth) to straight ahead, a gain change of 1.2 to 2.8 was observed at 8 Hz. In both of these cases, orienting the head upward reduced the helmet to head transmissibility in the pitch axis. This behaviour also occurred to a lesser extent for Subject S8 at 7 Hz.

5.7.3.3 Helmet Yaw

The motion of the helmet in the yaw axis was also shown to be affected by helmet orientation primarily between 4 Hz and 8 Hz. Data for both

subjects indicated that orienting their helmets to the 45 degree azimuthal position and either upward or downward by 36.9 degrees caused the greatest increases in helmet yaw to seat Z axis gains relative to the straight ahead position. For example, when Subject S3 aimed his helmet to the 45 az, -36.9 el orientation there was greater than a threefold increase in helmet yaw to seat Z gain. Typically, helmet yaw to seat Z axis gains were less than one-third of the helmet pitch to seat Z axis gains across the frequency range of 0 to 20 Hz.

5.8 EXPERIMENT BD.8: EFFECT OF THE FLIGHT HELMET ON THE TRANSMISSION OF VIBRATION FROM THE SEAT TO THE HEAD

5.8.1 Purpose

Most of the experiments reported in the literature relating display visibility to the biodynamic response of the head during vertical seat vibration have been conducted without a flight helmet. As discussed in Section 2.5.3.12, Lewis (1979b) has shown that the flight helmet can affect the way in which vibration is transmitted to the head. The purpose of this experiment was to define the effect on head motion when using the flight helmet with an attached helmet-mounted display.

5.8.2 Method

The experiment was conducted simultaneously with Experiment BD.6. The vibration experimental conditions were the same for both experiments. Table 5.8.1 lists other pertinent factors in the experiment. The head pitch motion was measured using a rotational accelerometer mounted on a bite bar as described in Section 5.1.4.2. The USAF HGU 2A/P helmet with helmet-mounted display attached was used in the experiment.

TABLE 5.8.1. EXPERIMENT BD.8: EFFECT OF FLIGHT HELMET ON HEAD MOTION

Purpose:	To measure the differences in head pitch axis to vertical seat Z axis transfer functions with and without the helmet-mounted display.
Subjects:	S1, S2, S3, S4, S5, S6, S7, S8, S9, S10, S12
Vibration Frequency:	0 to 82 Hz, linear sweep of sinusoidal waveform in 100 s.
Vibration Level:	See Figure 5.6.1
Time Duration of Exposure:	approximately 200 s
Data Acquisition:	sampling rate: 160 Hz sampling period: 100 s filter: seat Z - none head Z - none head pitch - none
Data Analysis:	transfer function analysis using cross spectral density head pitch/seat Z, with and without helmet resolution: 1.0 Hz degrees of freedom: 276 window: Hanning

5.8.3 Results

5.8.3.1 Head Pitch Axis Motion

Figure 5.8.1 shows a comparison of means of the moduli of the head pitch to vertical seat Z axis vibration transfer functions for the helmet and no helmet conditions. Representative single subject transfer functions are shown in Figure 5.8.2. In the case of the pitch motion of the head, the effect of the helmet was to reduce by greater than 50 percent the head pitch motion within the frequency region of 6 Hz to 10 Hz. There was also a decrease of approximately 30 percent in the mean modulus between 20 Hz and 32 Hz with the helmet. The dynamic behaviour for individual subjects was not consistent, however, as can be seen in Figure 5.8.2. The two moduli for Subjects S4 and S12 were similar to the head pitch behaviour observed by Lewis (1979b) and shown in Figure 2.5.16. Generally, the addition of the helmet on the head attenuated head pitch axis motion at frequencies less than 12 Hz. In some cases, the helmet tended to amplify pitch at frequencies above 12 Hz (e.g., Subject S4 between 12 Hz and 20 Hz and Subject S12 between 28 Hz and 38 Hz).

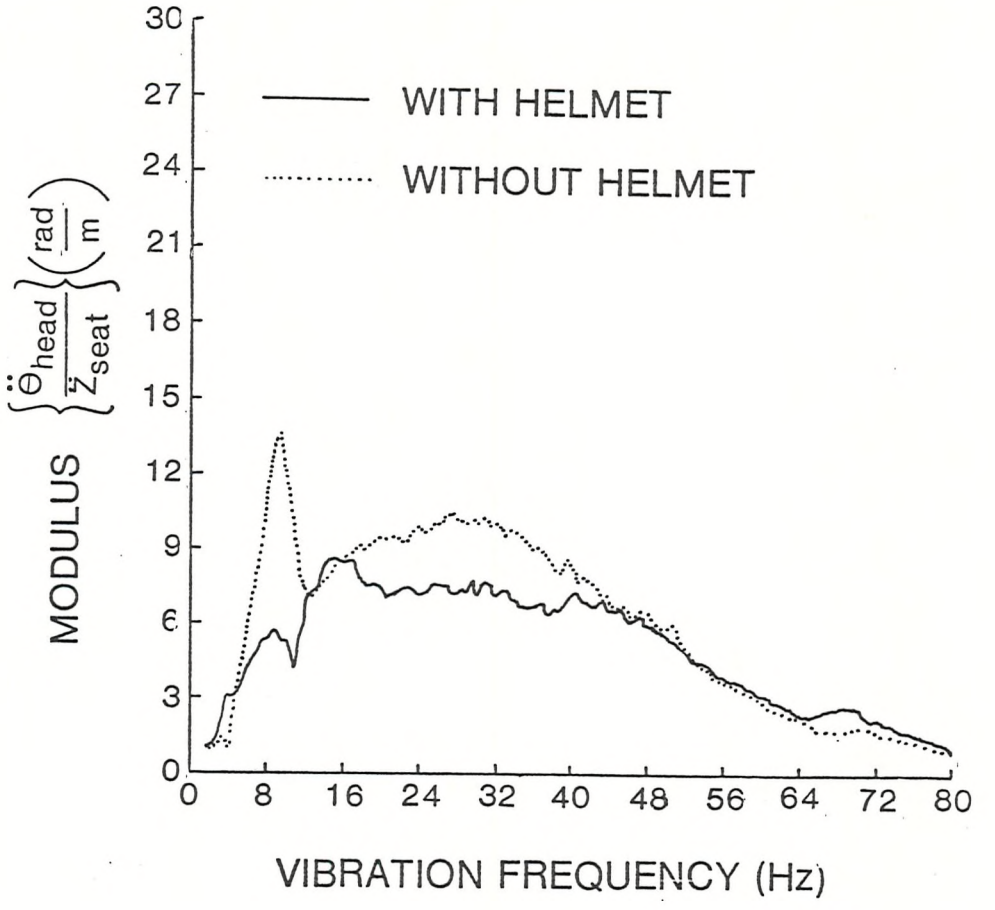

Figure 5.8.1. Comparisons of Mean Moduli of the Head Pitch to Seat Z Axis Transfer Functions With and Without the USAF Flight Helmet-Mean for 10 Subjects (B_e = 1.0 Hz, DOF = 276, Experiment BD.8)

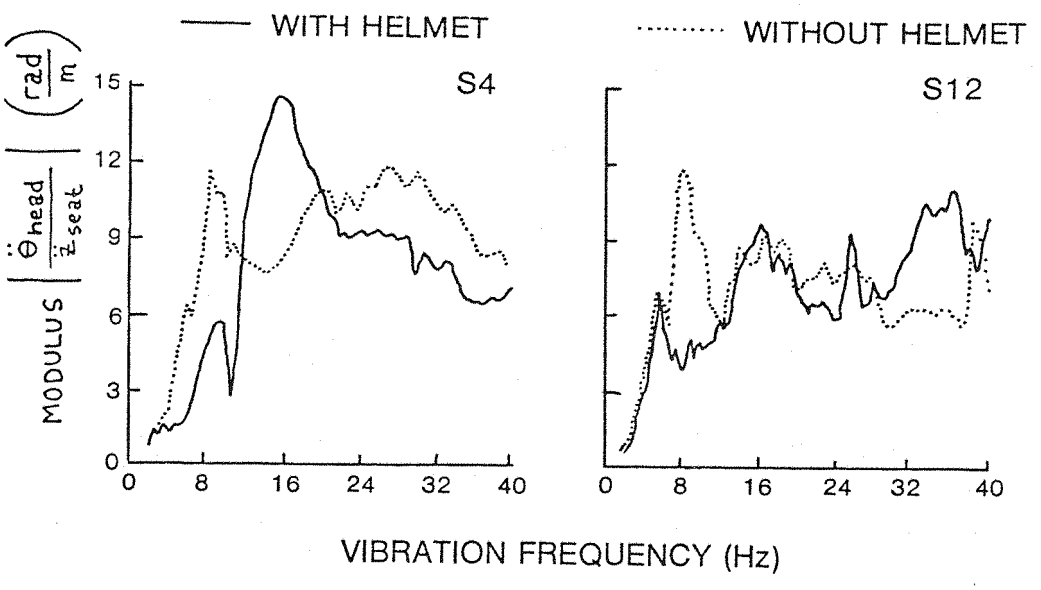

Figure 5.8.2. Comparison of the Moduli of Head Pitch Axis to Seat Z Axis Transfer Functions for Subjects S4 and S12 With and Without the Flight Helmet (B_e = 1.0 Hz, DOF = 276, Experiment BD.8)

5.9 DISCUSSION OF OVERALL BIODYNAMIC RESULTS

5.9.1 The Nature of the Input Motion

The harmonic distortion observed in the acceleration motion of the seat at the low frequencies (i.e., < 2.8 Hz) can been attributed to the displacement limits of the electrodynamic vibrator. Because this aspect of vibrator performance may also affect subject dynamic behaviour, the reading performance data obtained at frequencies less than 2.8 Hz may have been affected by the harmonic distortion in the seat motion and may not represent accurately the effects of single frequency vibration (e.g., Experiment LG.1). However, the rapid decrease of harmonic distortion at 2.8 Hz and above allowed the input seat motion to be considered a discrete sinusoidal frequency for these higher frequencies.

5.9.2 Transmission of Seat Vibration to the Head

The behaviour of the vertical motion of the head due to the vertical (Z axis) motion of the seat was consistent with the general findings in the literature. In particuar, the double peaks in transmissibilities at 4 to 8 Hz and 14 to 18 Hz were consistent with the findings of Rowlands (1977) and Lewis (1979b) involving a seat back. The data shown in Figures 5.5.2 and 5.5.3 must be considered only as estimates of head translation motion due to vertical Z axis seat motion because the position of the translation accelerometer in the bite bar allowed the pitch motion of the head also to contribute to measurement of the vertical motion.

5.9.3 Nature of Head Pitch Motion

The experiments reported in this chapter have shown again that vertical Z axis vibration of the body produces rotational motions of the head. The motion of the head in the pitch axis was probably the result of the vertical acceleration field acting upon the mass of the head, whose center of mass was offset from the head to neck pivot point or points. The acceleration field, therefore, produced a torque around the pivot point, causing a rotational acceleration of the mass of the head about the pivot point (or point of rotation). The finding that pitch motion of the head predominates that of the roll and yaw axes is also consistent with the findings of others (e.g., Rance, 1978, and Lewis, 1979b).

The magnitudes of head pitch motion observed in Experiment BD.5 (Figures 5.5.4 and 5.5.5) were also comparable to those observed by Lewis (1979b) at low frequencies (<12 Hz), but differed remarkably at the higher frequencies, perhaps due to the difference in flight helmets used during the two experiments (i.e., Lewis used a MK 1A flying helmet). The frequencies of seat Z vibration causing the greatest pitch movement of the head in Experiment BD.5 were between 6 and 8 Hz and 14 and 18 Hz. It is reasonable to assume that these sensitivities of head pitch to seat Z motion were associated with the major body

response and head/neck response reported in the literature (Section 2.5.3.3). The harmonic distortion observed in the head pitch motion indicated that the biomechanical mechanisms and perhaps postural effectors were introducing nonlinearities in the transmission of vibration to the head. Some of the harmonic content can be attributed to the harmonic distortion in the seat motion especially below 3 Hz. Rance (1978) also observed significant levels of head pitch energy at twice the fundamental frequency under low distortion motion inputs. The frequency-doubling nature of head pitch motion will possibly have a great impact on viewing the head-coupled display information due to the stimulation of the semicircular canals, eliciting the vestibulo-ocular reflex. For example, the head pitch and VOR may respond to a 4.0 Hz excitation frequency even though the seat vibration frequency is only 2.0 Hz. This behaviour would tend to lower the seat vibration frequency for which the pursuit reflex can be expected to aid perception of a moving display image.

The addition of the helmet to the head proposes a conundrum. Normally, increasing the rotational moment of inertia of a mass lowers its resonant frequency, assuming an offset spring-dash pot coupling of the mass to a pivot point. The effect observed in Experiment BD.8 was that the helmet tended to attenuate the predominant frequency of head pitch rotational motion between 4 Hz and 8 Hz, but perhaps increase head pitch at higher frequencies. In this situation, the helmet at the lower frequencies was acting as a rotational vibration absorber. Another possible explanation was that the helmet did, indeed, shift the natural frequency of head pitch movement downward, which caused a "detuning" of the head from the major body response at 4 to 6 Hz. While attenuating the head movement at 6 to 8 Hz, the helmet simultaneously caused an increase of pitch motion of the head at 16 Hz. This finding may mean that the helmet caused a greater coupling of head and neck to the upper body resonances at this frequency. Another possibility was that the helmet, with its additional mass and elastic coupling (i.e., foam pads and scalp) to the head may have acted as a dynamic absorber system for the head, having its own resonance at about the same frequency (i.e., about 16 Hz). The lack of consistent behaviour in head-to-helmet movement across subjects may have been due

to differing fitting quality of the helmet on the heads of the subjects.

5.9.4 Behaviour of the Helmet on the Head

There was a consistent peak in helmet to head pitch moduli (i.e., between 6 and 10 Hz) for all subjects. Subjects S5, S7, S9, and S13 also had phase lags of approximately 90 degrees accompanying these peaks. With the exception of these subjects, there was no consistent indication of a helmet-to-head resonance at any frequency. It is possible that the reason that the helmet pitch to head pitch was greatest between 6 and 10 Hz was that the input energy (i.e., head pitch angular acceleration) was also greatest at these frequencies, and that nonlinearities in the helmet pitch to head pitch motion caused the modulus of the helmet-to-head transfer function to peak. This hypothesis is reasonable based upon the results of Jarrett (1978). From his results, it can be expected that a large rotational input to the head will cause not only a displacement of the scalp relative to the skull, but a displacement of the helmet relative to the scalp, the latter occurring only at very high angular accelerations of the head. The peaks in helmet-to-head pitch moduli may, therefore, have been an effect of a nonlinearity in helmet-to-head pitch motion which was amplitude dependent. This effect also occurred at about 16 Hz, where head pitch accelerations were also high. Recent experimental results by Wells (1980), using the same helmet and seating conditions as in Experiment BD.5, have shown that large amplitude dependent helmet to head gains may be present. For example, shown in Figure 5.9.1 are three helmet pitch-to-head pitch transfer functions obtained by Wells for one subject during vertical Z axis sinusoidal vibration swept from 0 to 32 Hz at three vibration levels (0.7, 1.4, and 2.8 m/s^2 rms). The curves show that an increase in vibration level from 0.7 to 2.8 m/s^2 rms increased head to helmet transmissibility by 46 percent at 6.4 Hz and decreased it by 120 percent at 9.6 Hz!

It is also possible to argue against the "nonlinearity" hypothesis above. If indeed, nonlinearities in helmet-to-head pitch transmissibilities were completely amplitude dependent, then it would follow

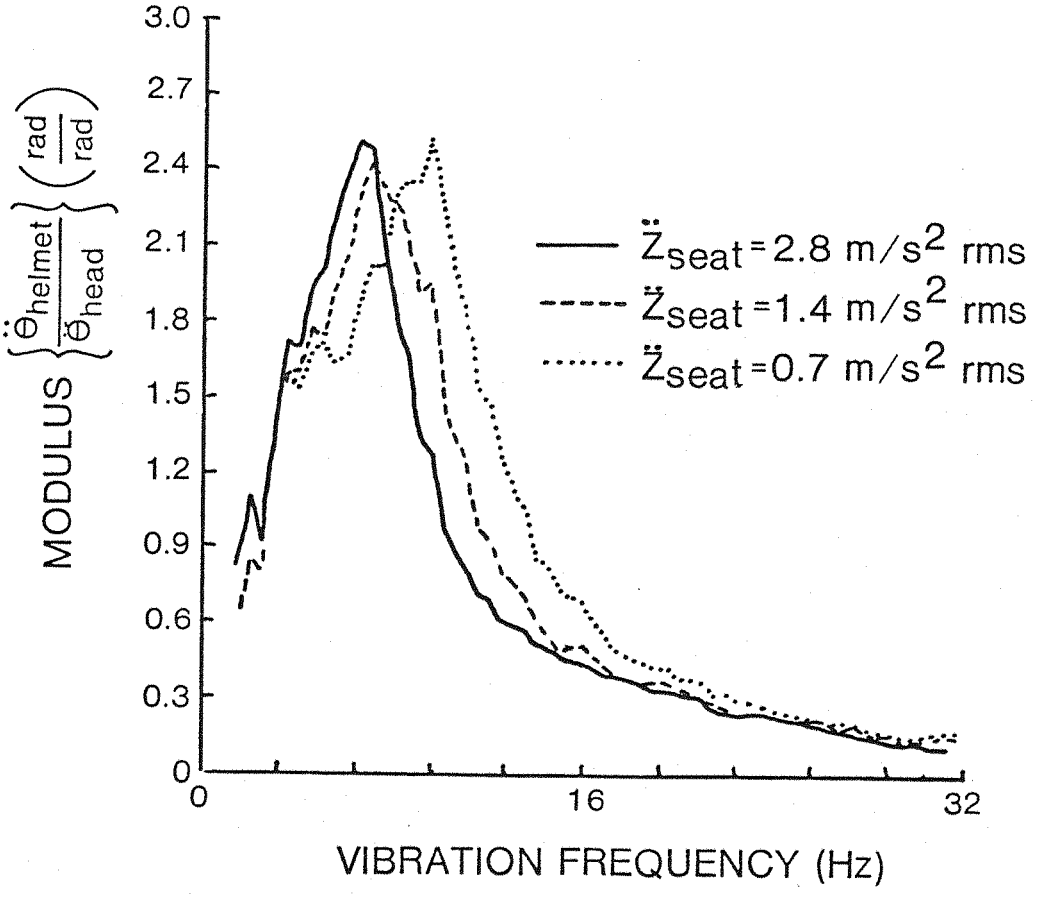

Figure 5.9.1. Comparison of Moduli of Helmet Pitch to Head Pitch Transfer Functions Obtained for One Subject at Three Levels of Seat Acceleration (B_e = 0.5 Hz, DOF = 48, Data From Wells, 1980)

that the head-to-helmet transmissibility should be correlated to head pitch acceleration. Both regression analyses and Spearman rank order correlation analyses showed that this relationship did not exist (at least statistically) across subjects. The failure of these tests to reach statistical significance then, of course, could have been due to the variability of helmet to head transmissibilities resulting from differing helmet fit across subjects. Also, it was observed that the peak pitch motion of the head and helmet-to-head transmissibility did

not occur at the same frequency for all subjects. Indeed, the vibration frequency of peak helmet-to-head transmissibility was consistently greater by 2 Hz to 3 Hz than the peak head pitch motion. This behaviour may be possible if the gain in helmet to head pitch gain were dependent upon head "jerk" (i.e., the rate of change of instantaneous head pitch acceleration). Jerk may be a controlling factor in causing the helmet to slip relative to the scalp. The true nature and causes of helmet and head behaviour can perhaps be determined only after more extensive investigations wherein the coupling of the helmet to the head can be controlled. (It is the author's opinion that a resonance between the helmet and the head at a frequency between 8 and 10 Hz may be too low for the masses and coupling involved, and it is more likely that the true resonance may be greater than 20 Hz. Since there is no question about the existence of a nonlinear effect, it must surely be a factor in explaining the bizarre behaviour of the helmet on the head at the low frequencies.)

5.9.5 Sources of Variability

The data from the biodynamic experiments reported above exhibited a large variability across subjects. This aspect of the data was anticipated based upon the nature of biodynamic responses of the observer to whole-body vibration generally reported in the literature. The sources of the variability can be considered to be due to effects across subjects and within subjects. The variabilities across subjects are reflected in the mean and standard deviation of the tranfer functions shown in Figures 5.5.3, 5.5.4, 5.5.6, and 5.5.10. One source of intersubject variability was the different biomechanical attributes of each subject. The transmission of vibration through the body to the head has already been shown to be highly variable, but dependence upon specific physical characteristics of subject has not been well examined in the literature. In the present studies, no correlations of significance (Spearman rank order correlations) were found between the magnitude or frequency of head pitch gain (in regions of 6 to 8 Hz and 8 to 16 Hz) and the physical height, weight, or ages of subjects. There were also no apparent relationships

between the transmissibilities of head pitch to seat Z at the two main frequencies of greatest pitch (i.e., 4 to 8 Hz and 14 to 18 Hz). (In other words, the magnitude of the head pitch at 4 to 8 Hz did not correlate with head pitch at 14 to 18 Hz.)

As mentioned above, another possible source of intersubject variability was the differing fits of the helmets on the heads of subjects. One helmet was used for all subjects. It was necessary to fit the helmet to the subject's head using foam pads of differing thicknesses. This technique did not produce consistent helmet-to-head stability or comfort amongst subjects. It was necessary for several subjects to overcome deficiencies in helmet fit by tightening the chin strap on the helmet. A Spearman rank order correlation test across subjects produced no significant correlations between the gains of the moduli of helmet-to-head pitch transfer functions and the head pitch to seat Z transfer functions (at the 4 to 8 Hz peaks). This result implied that an external factor, such as helmet fit, was primarily the source of the intersubject variability in helmet to head movements.

Sources of variability within subjects included posture and muscle tension, nonlinearities and head orientations. The large variation in the ratio of helmet pitch to seat Z motion during an experimental run (as shown in Figure 5.4.2), was surprising, especially since the subjects were restrained by a tight harness. Only very limited movement of the subject on the seat was possible. Since the changes in the magnitude of helmet pitch may have been task related (e.g., Section 5.4.2.2), it was possible that the subjects unconsciously used their neck muscles to adjust the vibration transmitted to the head to promote the greatest legibility of the visual material. Perhaps another manifestation of postural and muscle tension effects was the nonlinear behaviour of helmet pitch to seat Z as shown in Figure 5.4.1. The results reported in Section 5.4.2, as well as the findings reported by Griffin (1975a) for head pitch motion, indicated that for some vibration frequencies, the magnitude of the transmissibility of helmet (and most likely head) pitch motion to seat motion varied inversely with the level of seat Z motion. It can be conjectured that at these frequencies the operator attempted to limit the

maximum level of vibration at the head/helmet, perhaps again by unconscious adjustments of posture and/or muscle tension.

In Section 5.7, the orientation of the head was shown to affect seat-to-head and head-to-helmet transmissibilities. Transmission of vibration to the head at different orientations were probably affected by the stiffness of neck muscles (especially at the extreme positions used) and the orientation of the cervical vertebrae. The orientation of the helmet also adjusted the center of mass of the head relative to the neck pivot point or points, thereby changing the influence of the Z axis acceleration field on the torque produced by the head and helmet mass about the point of rotation. It was also possible that the different orientations of the helmet produced differing modes and centers of rotation of the head and helmet pitch motion relative to the body. It is logical that in an elevated head orientation (positive elevation), movement of the head on the neck would probably be restricted from occiput to condyles, and perhaps OC_1 and OC_2, whereas at the head-depressed orientation, movement about OC_6 and the thoracic spine may be included. It follows that the differing modes of vibration and centers of rotation probably had a marked effect on the differing centers of mass of the head and helmet (especially with the helmet-mounted display attached), thereby causing not only a change in seat to head transmissibility, but also head to helmet transmissibility with the differing head orientations. It was unlikely that small changes in head orientation had a significant effect on the data in Experiments BD.3, BD.4, BD.5, and BD.6, while subjects were attempting to look straight ahead. However, in an operational setting, large head orientations can be expected from crewmembers and, therefore, the coupling of the head to the helmet, under these conditions, may affect perception of the helmet-mounted display.

5.10 SUMMARY OF BIODYNAMIC STUDIES

The following items were considered to be the key findings of the biodynamic experiments:

a. The vibration motion response of the seat contained significant harmonic components for input frequencies less than 3.36 Hz. Harmonic distortion of acceleration was greatest at 1.68 Hz (i.e., 72.3 percent). Above 3.36 Hz, harmonic distortion of the seat acceleration was less than 15 percent (BD.1).

b. Vertical Z axis motion of the seat produced rotational motions of the head and helmet primarily in the pitch axis. Helmet yaw acceleration was typically 20 percent of helmet pitch and head roll was about 10 percent of head pitch (BD.3, BD.6).

c. Harmonics were observed in the helmet and head pitch motion (BD.3).

d. Some nonlinearities in helmet pitch to seat Z axis rms transmissibilities were observed at 5.6 Hz, 8.0 Hz, and 11.2 Hz (BD.4).

e. Transfer functions (modulus and phase) were computed for individual subjects and averaged across subjects, showing the relationships of head Z axis, head pitch axis, and helmet pitch axis motion to seat Z axis motion and helmet pitch axis motion to head pitch axis motion (BD.5).

f. The transmissibility of vertical Z axis seat vibration to the head, causing pitch motion of the head, was frequency-dependent and showed peaks for almost all subjects at between 4 Hz to 6 hz, 14 Hz to 18 Hz, and 30 Hz to 40 Hz (BD.5).

g. Helmet pitch motion was generally greater than head pitch motion at seat vibration frequencies between 4 Hz and 12 Hz, but less than head pitch above about 16 Hz (BD.5).

h. The orientation of the head relative to the body significantly affected the form and magnitude of the transmission of vibration from the seat to the head and helmet and affected as well the nature of the head to helmet coupling (BD.7).

i. The addition of a flight helmet to the head caused both an attenuation and amplification of head pitch motion, depending upon the subject and vibration frequency (BD.8).

j. Large within subject (BD.4, BD.7) and between subject variabilities in biodynamic responses to whole-body vibration were observed (BD.5, BD.7).

Chapter 6
RELATIONSHIPS OF READING PERFORMANCE AND DYNAMIC BEHAVIOUR OF THE HEAD, HELMET, AND EYES

6.1 INTRODUCTION

The purpose of this chapter is to investigate how helmet-mounted display reading performance may be related to the nature of head, helmet, and eye movement during whole-body vibration. From the literature summarized in Chapter 2, it was shown that previous investigators have observed decrements in reading performance during both whole-body vibration and object vibration which were attributable to the relative oscillatory motion of the image (of the reading material) on the retina. In the legibility experiments reported in Chapter 4, whole-body vibration also affected the reading of numeric characters presented on the helmet-mounted display, depending upon the frequency and amplitude of the seat vibration. Generally, there was a linear relationship between the seat vibration amplitude and reading error at each of the 1/2 octave frequencies (i.e., 1.42 Hz to 45 Hz), although there was also a wide variation in the magnitude of the reading errors across subjects. The vertical Z axis sinusoidal vibration of the seat at frequencies of 4.0 to 8.0 Hz caused the greatest reading difficulty for most subjects. The dynamic experiments in Chapter 5 indicated that the vertical vibration motion of the seat produced rotational movements of the helmet and head predominantly in the pitch axis. These motions were shown to be mostly sinusoidal for frequencies of 4.0 Hz and greater. In these experiments, the mean seat vibration frequency causing the maximum head pitch motion (while wearing the helmet) was approximately 5.5 Hz. Similarly, a mean frequency of 6.4 Hz caused the most helmet pitch to seat Z movement and 7.5 Hz the greatest movement of helmet relative to the head.

Although the dynamic experiments were successful in delineating many aspects of helmet and head behaviour during vertical seat vibration, up to this point very little can be confirmed about the dynamic nature of the image perceived on the helmet-mounted display. In this regard, two special experiments were conducted. The first experiment (SD.1)

investigated the nature of the movement of the display image in space whereas the second experiment (SD.2) explored the nature of the movement of the display image on the retina of the eye. These experiments will be described in detail in the next two sections of this chapter. The results of these experiments and the effect of the dynamic behaviour of head, helmet, and eye movement on reading performance will then be discussed at the end of the chapter.

6.2 EXPERIMENT SD.1: DISPLACEMENT OF THE HELMET-MOUNTED DISPLAY IMAGE IN SPACE

6.2.1 Introduction to Experiment

As discussed previously, the helmet-mounted display produces a virtual image which is perceived at optical infinity. The optical axis of this image is presumed to be stationary with the axis of the helmet (i.e., with a hard stiff mounting of the display optics unit to the helmet). Because the display image is collimated, translational movements of the eye relative to, but within the exit pupil of the display optics, should not cause a displacement of the display image in space, nor cause a displacement of the image on the retina of the eye. On the other hand, any rotational movement of the helmet in space should be perceived as an angular displacement of the display image in space, regardless of the movement of the eye and/or head relative to the display optical axis. Experiment SD.1 was conducted in order to test this hypothesis and investigate the nature of the movement of the display image in space.

6.2.2 Method

The approach used in the experiment was to measure the apparent displacement of the display image at different viewing distances.

A diagram showing the apparatus for the experiment is shown in Figure 6.2.1. The helmet-mounted display used in the experiment was the same as that described previously. The variable transmission filter over the optical combiner on the helmet-mounted optics unit was

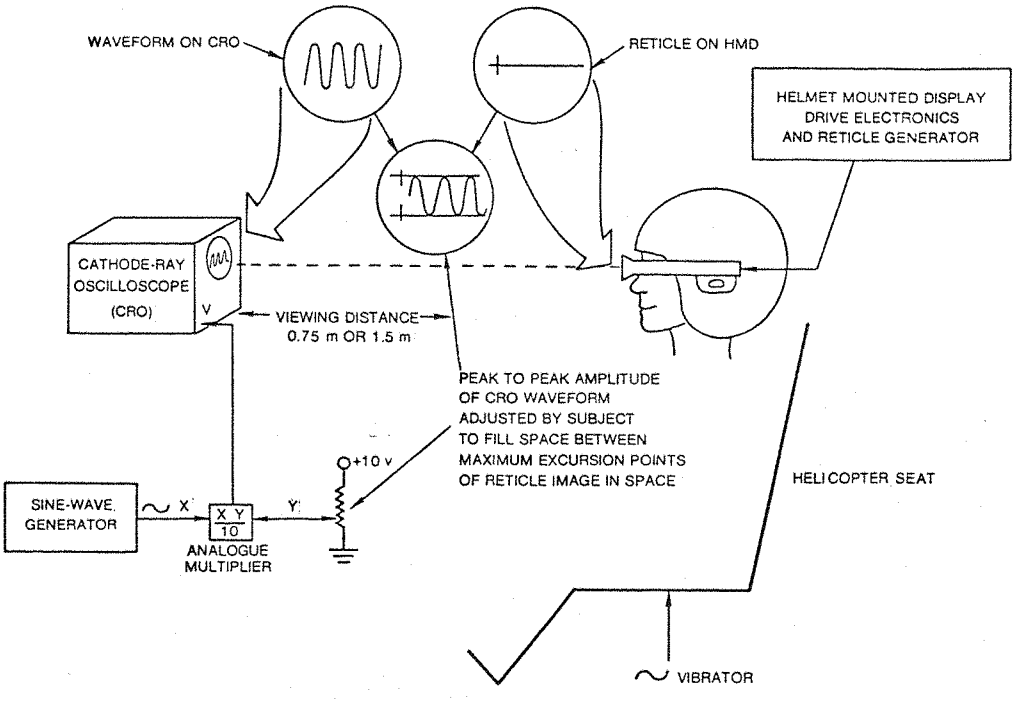

Figure 6.2.1. Apparatus and Illustration of Task used in Measurement of Helmet-Mounted Display Image Displacement in Space (Experiment SD.1)

adjusted to allow a 14 percent light transmission. A special electronic reticle was presented on the helmet-mounted display as shown in Figure 6.2.2. The reticle was presented with a luminance of approximately 48 cd/m^2 and was collimated to optical infinity. With the introduction of vertical Z axis sinusoidal vibration of the seat, the vibration transmitted to the head caused the head and helmet to oscillate in the pitch axis causing the subject to perceive a vertical movement of the reticle image in space. A cathode-ray oscilloscope (CRO) was used as a means of measuring the amplitude of the angular displacement of the reticle image as seen by the observer. The CRO had a screen size of 10 cm and a yellowish-green phosphor over which an orange filter had been placed. A 1000 Hz sinusoidal waveform from a sine wave oscillator was input into the vertical amplifier of the CRO. The time base of the CRO was set at 1.0 ms/cm to allow ten complete cycles of the waveform to be displayed horizontally on the CRO screen. The vertical peak-to-peak magnitude of the input waveform was adjustable by a remote potentiometer held by the subject. The

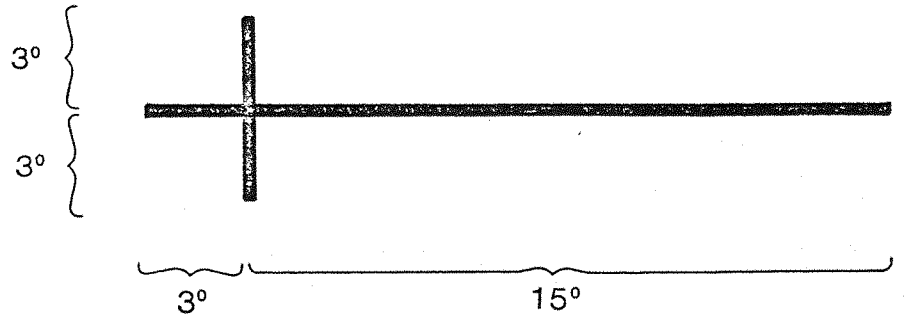

LINE WIDTH ≈4 MINUTE-OF-ARC

Figure 6.2.2. Format and Visual Angles Subtended by the Helmet-Mounted Display Reticle used in Experiment SD.1

rms input voltage level of the vertical waveform was measured by a digital voltmeter (Sinclair Model DM2). The luminance of the waveform on the CRO was set at approximately 120 cd/m^2. The CRO was located either at 0.75 m or 1.5 m from the subject, depending upon the experimental condition.

The task performed by the subjects was to superimpose images of the helmet-mounted display reticle over the CRO screen, then adjust (beginning at zero) the vertical height of the sinusoidal waveform until it was just equal to the distance between the maximum excursion points of the reticle. This procedure is illustrated in Figure 6.2.1. The subjects indicated when this adjustment had been completed and a reading of the vertical input voltage to the CRO was taken by the experimenter. These readings were later converted into displacement distances. (Note: Even though the helmet-mounted display image was collimated to optical infinity, there was sufficient depth of focus in the subjects eyes under these luminance conditions to observe the superimposed reticle and CRO images as in focus at both the 0.75 m and 1.5 m viewing distances.)

Nine subjects were used in the experiment. These were taken from the same group of subjects as used in Experiment LG.1. The subjects were presented with eight vibration frequency conditions at each of the two CRO viewing distances of .75 m and 1.5 m. The vibration conditions corresponded to eight of the ten frequencies and maximum seat acceleration level conditions used in Experiment LG.1. (The 1.42 Hz and 2.0 Hz vibration frequencies were not used in this experiment due to the large amount of harmonic distortion measured in the seat motion in Experiment BD.1.) The order of presentation of vibration conditions was randomized across subjects at the two viewing distances. The subjects were given several practice trials prior to beginning the experiment. As an ancillary condition, Subject S1 was presented with additional levels of seat Z vibration at one-fifth and three-fifths of the maximum level at all frequencies. Table 6.2.1 summarizes the conditions for the experiment.

6.2.3 Results

The heights (peak-to-peak amplitude) of the sinusoidal waveformson the CRO for the individual subjects and experimental conditions are given in Tables 6.2.2 and 6.2.3. The subtended visual angle (α) of the vertical displacement of the reticle images was computed from the data for the 2.8 Hz, 4.0 Hz, and 5.6 Hz vibration frequencies using the formula below:

$$\alpha = 2 \tan^{-1} \left(\frac{H_{150} - H_{75}}{150} \right) \qquad (6.1)$$

where H_{150} is the height (cm) of the CRO waveform at 150 cm, and H_{75} is the height (cm) of the CRO waveform at 75 cm. This formula allows the effect of vertical head displacement resulting from seat displacement to be removed from the displacement amplitudes of the CRO. However, the application of the formula assumes that α is constant between the experimental conditions involving the two CRO viewing distances.

TABLE 6.2.1. EXPERIMENT SD.1: DISPLACEMENT OF HELMET-MOUNTED DISPLAY IMAGE IN SPACE

Purpose:	To perform a subjective measure of the peak-to-peak angular displacement in space of a helmet display image as a function of vibration frequency and level.
Method:	Subjects adjusted height of CRO waveform to equal superimposed displacement of helmet-mounted display reticle image. 75 cm and 150 cm viewing distances used.
Subjects:	9S (S1, S2, S3, S4, S6, S7, S8, S9, S10)
Seat:	Helicopter (unmodified)
Vibration Conditions:	Vertical Z axis sinusoidal

Frequency (Hz)	Level* (m/s^2 rms)
2.8	1.2
4.0	1.0
5.6	1.0
8.0	1.0
11.2	1.4
16.0	2.0
22.4	2.8
45.0	5.6

Analysis:	Subtended angle of reticle displacement computed for each vibration condition and compared with helmet pitch displacement from Experiment BD.5.

*Corresponds to maximum seat acceleration levels in Experiment LG.1

TABLE 6.2.2. VERTICAL DISPLACEMENT (CM) OF HELMET-MOUNTED DISPLAY RETICLE AT 75 CM VIEWING DISTANCE

Frequency (Hz)	2.8	4.0	5.6	8.0	11.2	16.0	22.4	45.0
Level (m/s^2 rms)	1.2	1.0	1.0	1.0	1.4	2.0	2.8	5.6
Subject								
S1	0.75	1.33	1.49	0.89	0.19	0.08	0.00	0.09
S2	2.87	4.32	1.57	1.17	0.34	0.11	0.00	0.00
S3	3.68	1.37	0.96	1.89	1.23	0.34	0.28	0.41
S4	1.27	2.73	1.63	1.60	0.77	0.28	0.14	0.09
S6	2.55	1.72	0.88	0.29	0.18	0.11	0.09	0.02
S7	2.07	1.40	1.84	0.94	0.09	4.49	0.09	0.18
S8	1.67	2.88	1.57	0.43	0.11	0.09	0.15	0.30
S9	2.68	1.44	0.60	0.28	1.63	2.56	0.49	0.12
S10	1.59	2.46	0.96	0.75	0.71	0.54	0.00	0.00

TABLE 6.2.3. VERTICAL DISPLACEMENT (CM) OF HELMET-MOUNTED DISPLAY RETICLE AT 150 CM VIEWING DISTANCE

Frequency (Hz)	2.8	4.0	5.6	8.0	11.2	16.0	22.4	45.0
Level (m/s^2 rms)	1.2	1.0	1.0	1.0	1.4	2.0	2.8	5.6
Subject								
S1	2.85	3.04	2.45	2.12	0.86	0.18	0.12	0.17
S2	6.07	6.12	4.11	1.97	1.19	0.00	0.00	0.00
S3	4.66	3.55	2.92	4.63	2.00	1.23	0.90	0.65
S4	4.15	4.58	4.06	2.49	1.81	0.32	0.31	0.24
S6	4.53	5.85	1.12	0.22	0.11	0.28	0.33	0.07
S7	4.75	1.88	2.50	1.74	0.14	6.62	2.48	0.14
S8	3.25	4.82	1.57	2.00	0.85	0.09	0.54	0.65
S9	4.62	3.39	2.84	0.81	5.04	4.70	0.76	0.13
S10	2.78	3.45	1.86	1.87	0.84	0.66	0.00	0.00

For the remaining frequencies (i.e., 8.0 Hz, 11.2 Hz, 16.0 Hz, and 22.4 Hz), the subtended visual α' was computed using the formula below:

$$\alpha' = 2 \tan^{-1} \frac{H_{150}}{H_{300}}$$

This formula was considered to be more reliable for the higher frequencies since only one CRO reading was used to compute α'. At these frequencies, the vertical head displacement was less than 5 percent of the CRO displacements and was, therefore, considered to be an acceptable level of experimental error.

Table 6.2.4 gives the resulting subtended angles of the reticle image displacements in space using the data in Table 6.2.2, Table 6.2.3, and the formulae above. The mean and standard deviation of these data are plotted in Figure 6.2.3.

6.2.4 Data Variability

The data exhibited a large variance across all vibration frequencies, with the most notable differences in subtended angle occurring at the higher frequencies. For example, at 16.0 Hz, Subject S7 indicated an angular displacement of the display reticle of 151.7 minutes-of-arc while Subject S2 indicated an angular displacement of zero. (Several subjects noted a greater difficulty in performing the tasks at frequencies greater than 11.2 Hz.) Some intersubject variability was anticipated due to individual subject dynamic characteristics observed in the previous chapter. In addition, there were perhaps two other contributing factors to variability in this experiment.

The first was that the reticle image displacements in space at the 2.8 Hz, 4.0 Hz, and 5.6 Hz frequencies were computed from displacement data acquired during separate runs in the experiment. It was shown in Section 2.5.3.4 that only minor changes in body posture, muscle tension, etc. could cause marked changes in transmission of vibration. Since data from the two runs (i.e., viewing distance) were compared to

TABLE 6.2.4. ANGULAR DISPLACEMENTS (MINUTES-OF-ARC) OF HELMET-MOUNTED DISPLAY RETICLE IN THE PITCH AXIS

Frequency (Hz)	2.8	4.0	5.6	8.0	11.2	16.0	22.4	45.0
Level (m/s^2 rms)	1.2	1.0	1.0	1.0	1.4	2.0	2.8	5.6
Subject								
S1	96.2	78.5	43.9	48.6	19.7	4.1	2.8	3.9
S2	146.4	82.4	116.3	45.1	27.3	0.0	0.0	0.0
S3	44.6	100.2	90.0	106.1	45.8	28.2	20.6	14.9
S4	132.1	84.6	111.4	57.1	41.5	7.3	7.1	5.5
S6	90.8	188.9	10.9	5.0	2.5	6.4	7.6	1.6
S7	122.5	21.6	30.0	39.9	3.2	151.7	56.8	3.2
S8	72.6	89.1	79.9	45.8	19.5	2.1	12.4	14.9
S9	89.0	89.3	102.4	18.6	115.5	107.7	17.4	3.0
S10	54.5	45.3	41.1	42.9	19.3	15.1	0.0	0.0
$\bar{x}$	94.3	86.7	69.5	45.5	32.7	35.2	13.9	5.2
σ	34.5	45.7	38.8	27.9	34.3	55.0	17.7	5.8

obtain the angular displacements, changes in subject intrinsic conditions between the runs may have contributed to variability in these results. The second factor was related to the task. Ideally, several samples would have been obtained during each data run, then averaged to improve the reliability of the data point. This approach, however, would have necessitated an extended exposure of subjects to high level vibration conditions. Instead, a short training session involving several trial runs was conducted at the beginning of each experimental session.

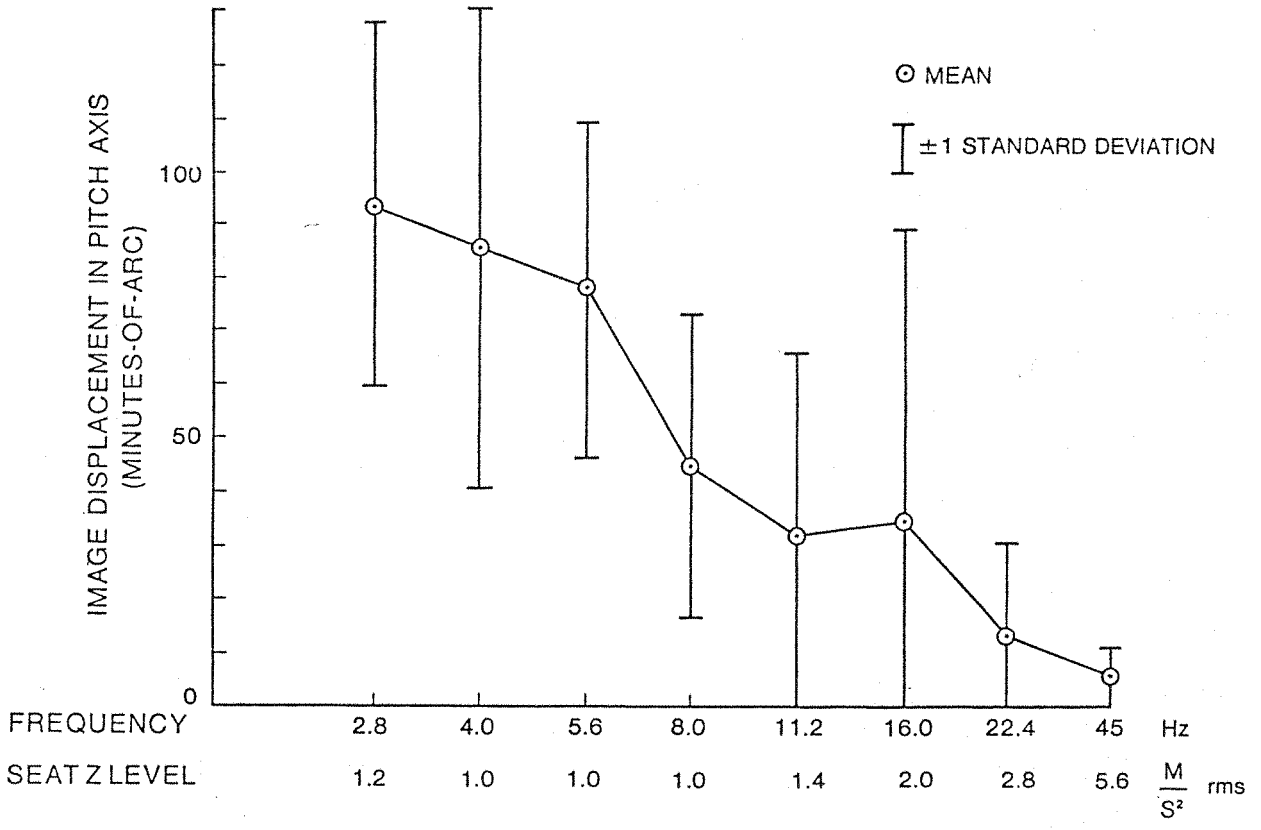

Figure 6.2.3. Mean and Standard Deviation of Pitch Angular Displacement of the Helmet-Mounted Display Reticle Image as a Function of Vertical Z Axis Whole-Body Sinusoidal Vibration Conditions, Experiment SD.1

Practice trials were repeated until the subjects were confident that they could perform the task. In spite of the variability of the data across subjects, there was a significant correlation of the subtended angles with helmet pitch behaviour observed in Experiment BD.5. This aspect of the results will be discussed later in Section 6.2.6.

6.2.5 Effect of Vibration Level

In a separate session, Subject S1 performed the reticle image displacement task under vibration conditions which included seat Z axis acceleration levels which were one-fifth and three-fifths the magnitude of that used for each frequency in the main experiment. The angular displacements of the reticle for these conditions are given in Table 6.2.5 and plotted in Figure 6.2.4. The image displacement of

TABLE 6.2.5. ANGULAR DISPLACEMENTS OF HELMET-MOUNTED DISPLAY RETICLE AT THREE SEAT Z ACCELERATION LEVELS (SUBJECT 1)

Frequency (Hz)	Pitch Angular Displacements (minutes-of-arc)					
	Low-Level		Medium Level		High Level	
	Seat Z (m/s^2 rms)	α (minutes-of-arc)	Seat Z (m/s^2 rms)	α (minutes-of-arc)	Seat Z (m/s^2 rms)	α (minutes-of-arc)
2.8	0.24	24.0	0.72	52.7	1.2	96.2
4.0	0.20	14.5	0.60	40.2	1.0	78.5
5.6	0.20	15.9	0.60	16.9	1.0	43.9
8.0	0.20	16.2	0.40	39.4	1.0	48.6
11.2	0.28	7.8	0.84	13.5	1.4	19.8
16.0	--	--	1.20	2.4	2.0	4.2
22.4	--	--	--	--	--	--
45.0	--	--	3.36	3.8	5.6	3.8

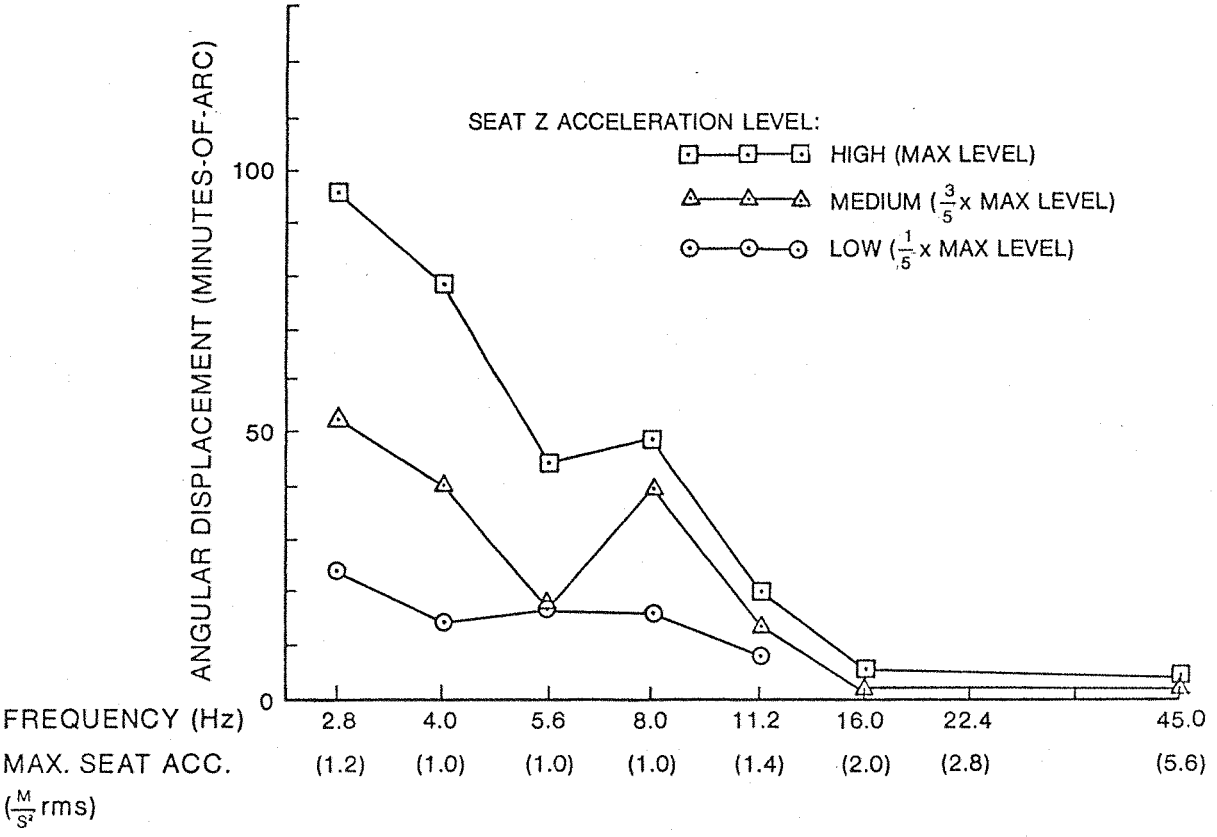

Figure 6.2.4. Comparison of Angular Displacements of Helmet-Mounted Display Reticle at Three Seat Acceleration Levels for Subject 1, Experiment SD.1

the reticle at the three levels of seat Z acceleration is mostly linear across the vibration frequencies as shown. Some deviations from linearity were expected between 4.0 Hz and 8.0 Hz, given the helmet pitch behaviour of the same subject (S1) as shown in Figure 5.4.1 (Experiment BD.4).

6.2.6 Comparison of Reticle Image Displacement and Dynamic Head and Helmet Behaviour

Table 6.2.6 gives reticle image displacement data of Table 6.2.4 normalized to a seat Z axis acceleration of 1.0 m/s^2 rms. Figure 6.2.5 shows the mean data from Table 6.2.6 compared with the mean pitch angular displacement (peak-to-peak) of the helmet in space as estimated from the individual helmet pitch to seat Z transfer functions for the same subjects (Experiment BD.5). Inspection of Figure 6.2.5 suggests that there was good correspondence between the image displacement and helmet displacement in space, at least up to a vibration frequency of 8.0 Hz. Beyond 8.0 Hz (i.e., 11.2 and 16.0 Hz), the mean image displacement was more than twice that of the helmet displacement.

Selected individual subject data (S1, S3, S4, S7, S8, S9) showing the same comparisons of image displacement and helmet pitch displacement are plotted in Figure 6.2.6. As can be seen from Figure 6.2.6, Subject S8 exhibited the most consistent agreement between the helmet pitch and image displacement between Experiments BD.5 and SD.1. Subjects S1, S4, and S9 also tended to show good agreement, with exceptional discrepancies at some frequencies. In spite of the variability in correspondence of these data across subjects, some general observations can be made. First, the general order of magnitude of the image displacement in space in Experiment SD.1 was similar to the helmet pitch displacement estimated from the helmet pitch to seat Z transfer functions in Experiment BD.5. This correspondence in the results of the two experiments is remarkable, especially considering that the data were obtained under different vibration and task conditions. There were, however, some notable exceptions. For example, Subjects S7 and S9, within in the frequency range of 8.0 to 22.4 Hz, showed radical increases in observed image displacement over helmet

TABLE 6.2.6. ANGULAR DISPLACEMENTS (MINUTES-OF-ARC) OF HELMET-MOUNTED RETICLE NORMALIZED TO SEAT ACCELERATION LEVELS OF 1.0 M/S^2 RMS

Frequency (Hz)	2.8	4.0	5.6	8.0	11.2	16.0	22.4	45.0
Subject								
S1	80.2	78.5	43.9	48.6	14.1	2.1	1.0	0.7
S2	122.0	82.4	116.3	45.1	19.5	0	0	0
S3	37.2	100.2	90.0	106.1	32.7	14.1	7.4	2.7
S4	110.1	84.6	111.4	57.1	29.6	3.7	2.5	1.0
S6	75.7	188.9	10.9	5.0	1.8	3.2	2.7	0.3
S7	102.1	21.6	30.0	39.9	2.3	75.9	20.3	0.6
S8	60.5	89.1	79.9	45.8	14.0	1.1	4.4	2.7
S9	74.2	89.3	102.4	18.6	82.5	53.9	6.2	0.5
S10	45.4	45.3	41.1	42.9	13.8	7.6	0	0
$\bar{x}$	78.6	86.7	69.5	45.5	23.4	17.6	5.0	0.9
σ	28.85	45.7	38.8	27.9	24.5	27.5	6.3	1.0

displacement. These increases were greater than 20 to 1 (S7) and 12 to 1 (S9) at 16.0 Hz. These exceptional levels of image displacement may have indicated that there were large differences in the movement of the display optics relative to the helmet, perhaps due to a resonance or a loose coupling between the optics and helmet. This factor may also account for the large differences between image displacement and helmet displacement in space for Subject S8 at 8.0 Hz, 11.2 Hz, 16.0 Hz, and 22.4 Hz. The fact that this type of behaviour did not occur for the other subjects indicates that the behaviour was more likely due to a loose coupling rather than a resonance. Although no independent dynamic study of display to helmet mechanical behaviour was conducted, an inspection of the connection assembly between the helmet and display optics revealed that a registration insert had become worn which may have caused the optics to move relative to the head for some subjects.

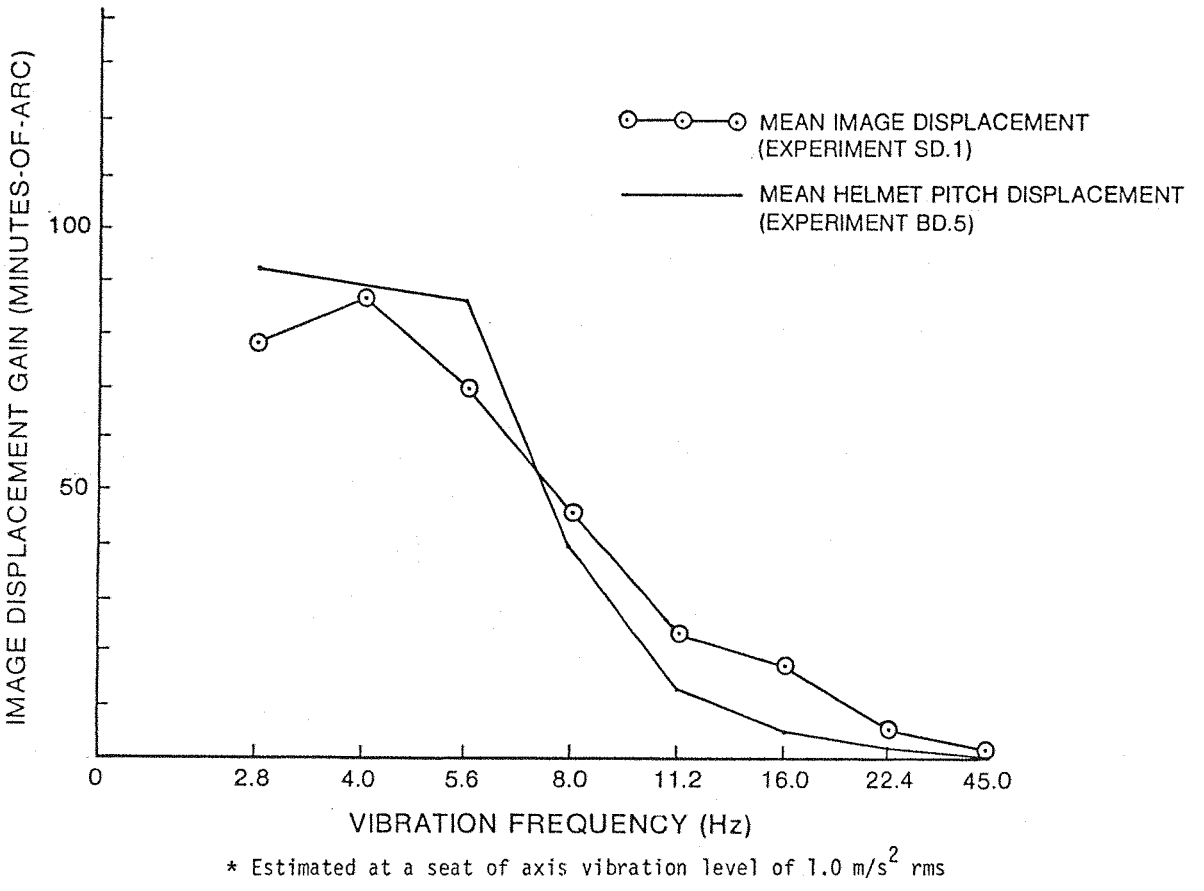

Figure 6.2.5. Comparison of Estimated Mean Image Displacement to Mean Helmet Pitch Displacement for Vertical Seat Acceleration Level of 1.0 m/s^2 rms

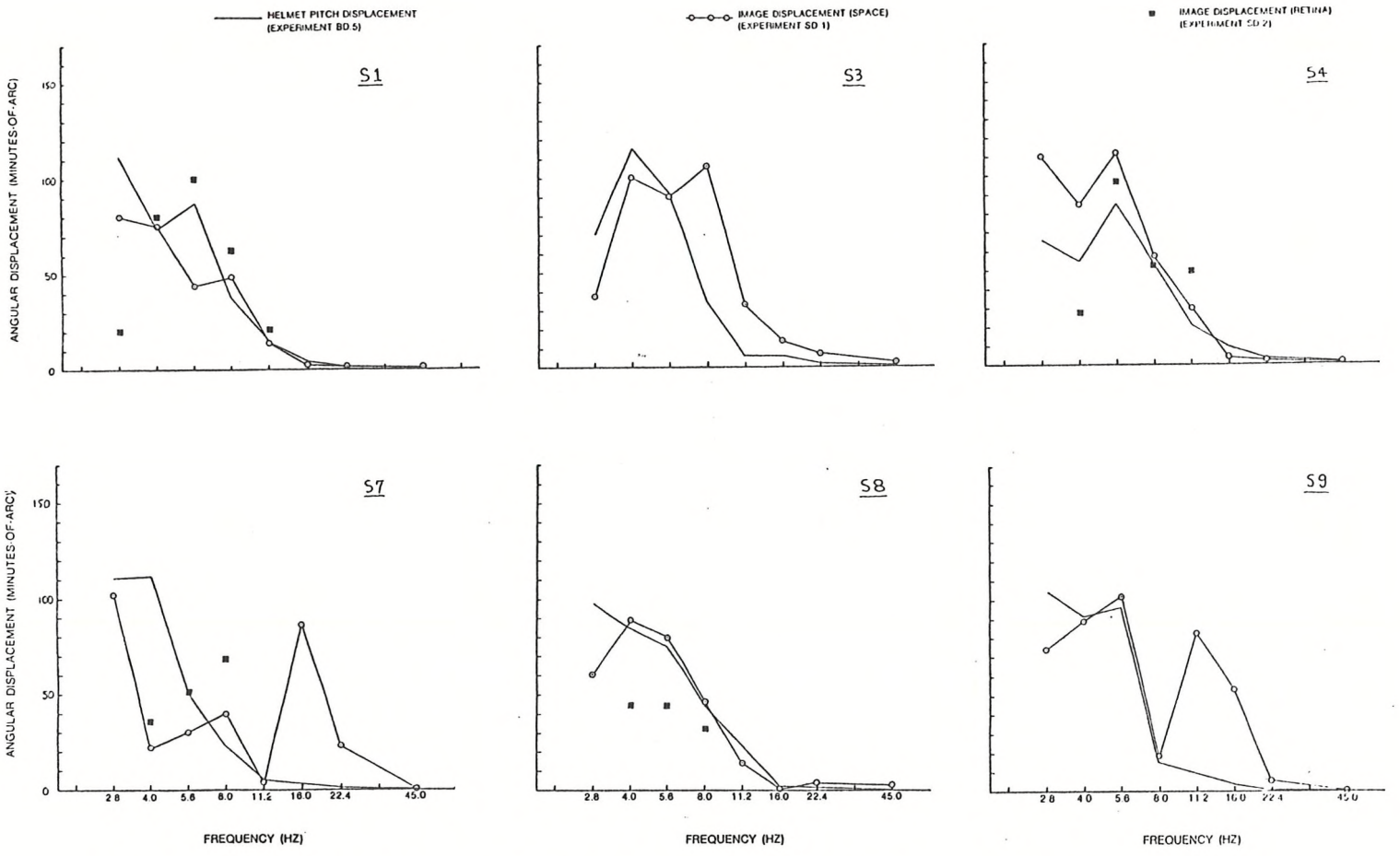

Figure 6.2.6. Comparison of Image Displacement in Space, Helmet Pitch Displacement in Space, and Image Displacement on the Retina for Individual Subjects at Seat Acceleration Level of 1.0 m/s^2 rms

With the major exceptions noted above, the peak-to-peak displacement of the image in space for Subjects S1, S4, S8, and S9 generally corresponded with the helmet pitch displacement estimated from the transfer functions. At least for these subjects, it can be concluded that rotational movements of the helmet in space will be perceived as equivalent angular displacements of the display image in space.

6.3 EXPERIMENT SD.2: DISPLACEMENT OF THE HELMET-MOUNTED DISPLAY IMAGE ON THE RETINA

6.3.1 Introduction to Experiment

The movements of the eyes relative to the helmet and head can only be assumed in the dynamic and legibility experiments discussed thus far in this thesis. It has been found from these experiments that vertical Z axis seat motions produce oscillatory rotational motions of the helmet which are perceived also as angular oscillations of the helmet-mounted display image in space. From the literature cited in Chapter 2 (e.g., Section 2.5.5.2), the rotational movements of the head in the pitch axis at frequencies greater than 1.0 Hz to 1.5 Hz can be expected to produce reflexive eye movements (i.e., the vestibulo-ocular reflex) which cannot be suppressed by the pursuit tracking reflex. Above 1.5 Hz and less than about 8.0 Hz (e.g., Benson and Barnes, 1978), the vestibulo-ocular reflex will compensate involuntarily for the rotational movements of the head, producing eye movements which maintain the optical axis of the eye (i.e., fovea centralis) at or near a space-referenced line-of-sight. Accordingly, while the VOR is operative, the displacement of a helmet-mounted display image on the retina should be equivalent to the angular displacement of the helmet in space. Furthermore, under these conditions wherein there is relative oscillatory movement between the helmet display and the eye, distinct images should appear at the zero velocity points or nodes of the image transition across the retina. The visual angle subtending the two nodal images, therefore, should be equivalent to the peak-to-peak angular displacement of the display image on the retina and, likewise, the optical axis of the display relative to the optical axis of the eye. The purpose of this experiment (SD.2) was to

determine the magnitudes of the displacement of the helmet-mounted display image on the retina during selected vibration conditions and to ascertain the presence or absence of the VOR by comparing these data to helmet pitch (BD.5) and image displacement in space (SD.1) obtained under similar vibration conditions.

6.3.2 Method

The approach used in the experiment was to measure the angular separation distances of the nodal images to determine the peak-to-peak magnitude of the angular displacement of the display image on the retina. Seven subjects were selected from the group of subjects which participated in Experiment SD.1 (S1, S2, S4, S7, S8) and/or Experiment BD.5 (S1, S4, S7, S8, S11, S12). These subjects were presented with a 5 x 10 array of numeric characters as described in Chapter 4. The subtended angle of each character was adjusted to 13.75 minutes-of-arc. The subtended angle of the vertical separation of adjacent rows of the characters was 55.25 minutes-of-arc (from the centers of characters). The luminance of the characters on the HMD was approximately 19 cd/m^2 on an almost totally dark background. The background luminance of the room was approximately 1.0 cd/m^2. The 14 percent transmission visor was in place over both eyes, making the transmitted luminance of the room approximately .14 cd/m^2 to the left eye and approximately .06 cd/m^2 to the right eye.

Subjects were presented with vertical seat Z sinusoidal vibration at vibration frequencies of 4.0 Hz, 5.6 Hz, and 8.0 Hz. In addition, Subjects S1 and S12 were presented with a 2.8 Hz vibration condition and Subject S1 a 16.0 Hz vibration condition. The seat vibration level was adjusted by the subject using a 10 turn potentiometer which he held in his hands during each vibration run. During each experiment run (i.e., for each vibration frequency), the subjects were instructed to observe the nodal images formed by the array of numeric characters presented on the helmet-mounted display and to adjust the seat vibration level for each of the three nodal image viewing conditions below:

Condition 1: Nodal images of each character just separated from itself (no overlap). (Equivalent to an image displacement on the retina of 13.75 minutes-of-arc.)

Condition 2: Nodal images of adjacent vertical rows just touching each other. (Equivalent to an image displacement on the retina of 41.5 minutes-of-arc.)

Condition 3: Nodal images of adjacent vertical rows completely overlapped. (Equivalent to an image displacement on the retina of 55.25 minutes-of-arc.)

These image viewing conditions are illustrated in Figure 6.3.1.

Prior to beginning the experiment, explanations and illustrations of the three nodal image viewing conditions were given to the subjects. Subjects were then allowed several practice trials to achieve these conditions until they were confident they could perform the tasks. During the experiment, the experimenter adjusted the appropriate vibration frequency and instructed the subject as to which nodal image condition was desired. When the nodal image viewing condition had been achieved by the subject (by adjusting the seat vibration level), he signaled the experimenter and a reading was taken of the rms seat acceleration level (i.e., m/s^2 rms). A summary of the conditions for the overall experiment are given in Table 6.3.1.

6.3.3 Results

Table 6.3.2 gives the seat Z vibration levels adjusted by each subject in order to produce the three nodal image viewing conditions. The means of the seat vibration levels for these conditions are shown plotted as a function of vibration frequency in Figure 6.3.2. These results indicate that the displacement of nodal images was most sensitive to seat vibration at the 5.6 Hz and 8.0 Hz frequencies. Figure 6.3.3 shows the mean image displacement presented as a function of seat acceleration level for each vibration frequency. Although the number of data points for each frequency was limited to three (four if assumed there is zero image displacement at zero vibration level), image displacement appeared to be linearly related to seat vibration level for image displacements of 13.75 minutes-of-arc and greater.

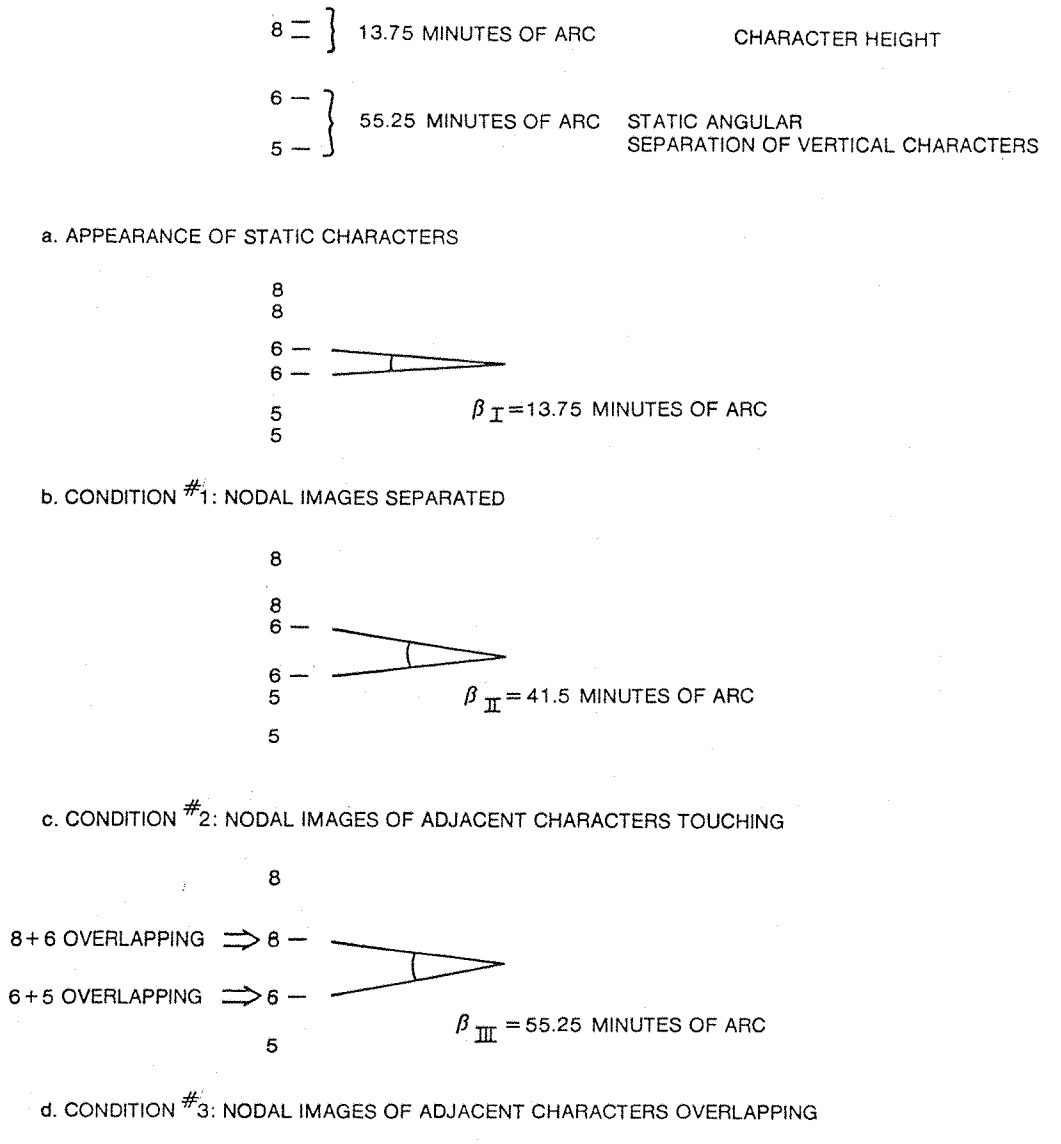

Figure 6.3.1. Illustration of Nodal Image Viewing Conditions and Corresponding Retinal Image Angular Displacements for Experiment SD.2. (Note that only three characters in the column are illustrated when actual display presentation was fifty characters arranged in 10 vertical columns by 5 horizontal rows.)

TABLE 6.3.1. EXPERIMENT SD.2: DISPLACEMENT OF HELMET-MOUNTED DISPLAY IMAGE ON THE RETINA

Purpose: To measure the peak-to-peak angular displacement of helmet-mounted display images on the retina as a function of vibration frequency.

Method: Subjects adjusted vertical seat Z axis acceleration level to achieve specific nodal image viewing conditions of helmet-mounted display presentation.

Subjects: 7S (S1, S2, S4, S7, S8, S11, S12)

Seat: helicopter (modified)

Vibration Conditions: Vertical, Z axis, sinusoidal

Frequency	Subjects	Level
2.8	S1, S12	*
4.0	all except S2	*
5.6	all	*
8.0	all	*
11.2	S1, S2, S4, S12	*
16.0	S1	*

Analysis: Seat acceleration level for each frequency and nodal image viewing condition obtained and compared with helmet pitch (BD.5) and image displacement (SD.1) in space.

*Subjects adjusted seat acceleration level to achieve specfied nodal image viewing conditions.

TABLE 6.3.2. VERTICAL SEAT Z AXIS VIBRATION LEVELS (m/s^2 rms) REQUIRED TO PRODUCE THREE NODAL IMAGE ANGULAR DISPLACEMENTS (β)

Frequency (Hz)	2.8	4.0	5.6	8.0	11.2
β_I = 13.75 (minutes-of-arc)					
S1	1.52	.43	.33	.29	1.15
S2	--	--	.46	.37	.68
S4	--	--	--	--	--
S7	--	.63	.50	.38	--
S8	--	.72	.39	.72	--
S11	--	--	--	--	--
S12	--	.65	.44	.45	1.20
$\bar{x}$	1.52	.61	.42	.44	1.01
σ	--	.12	.07	.17	.29
β_{II} = 41.50 (minutes-of-arc)					
-S1	1.76	.50	.41	.40	1.57
S2	--	--	.50	.43	1.08
-S4	--	1.51	.43	.79	--
-S7	--	.97	.70	.56	--
-S8	--	.86	.46	1.01	--
-S11	--	.69	.50	.64	--
-S12	--	.72	.55	.66	2.06
$\bar{x}$	1.76	.88	.51	.64	1.57
σ	--	.35	.10	.21	.49
β_{III} = 55.25 (minutes-of-arc)					
S1	2.0	.58	.50	.94	2.48
S2	--	--	.54	.55	1.41
S4	--	--	--	.66	1.13
S7	--	1.55	1.04	0.80	--
S8	--	1.05	.62	1.67	--
S11	--	.85	.69	1.11	--
S12	--	1.07	.98	.98	2.55
$\bar{x}$	2.0	1.02	.73	.96	1.89
σ	--	.36	.23	.37	.73

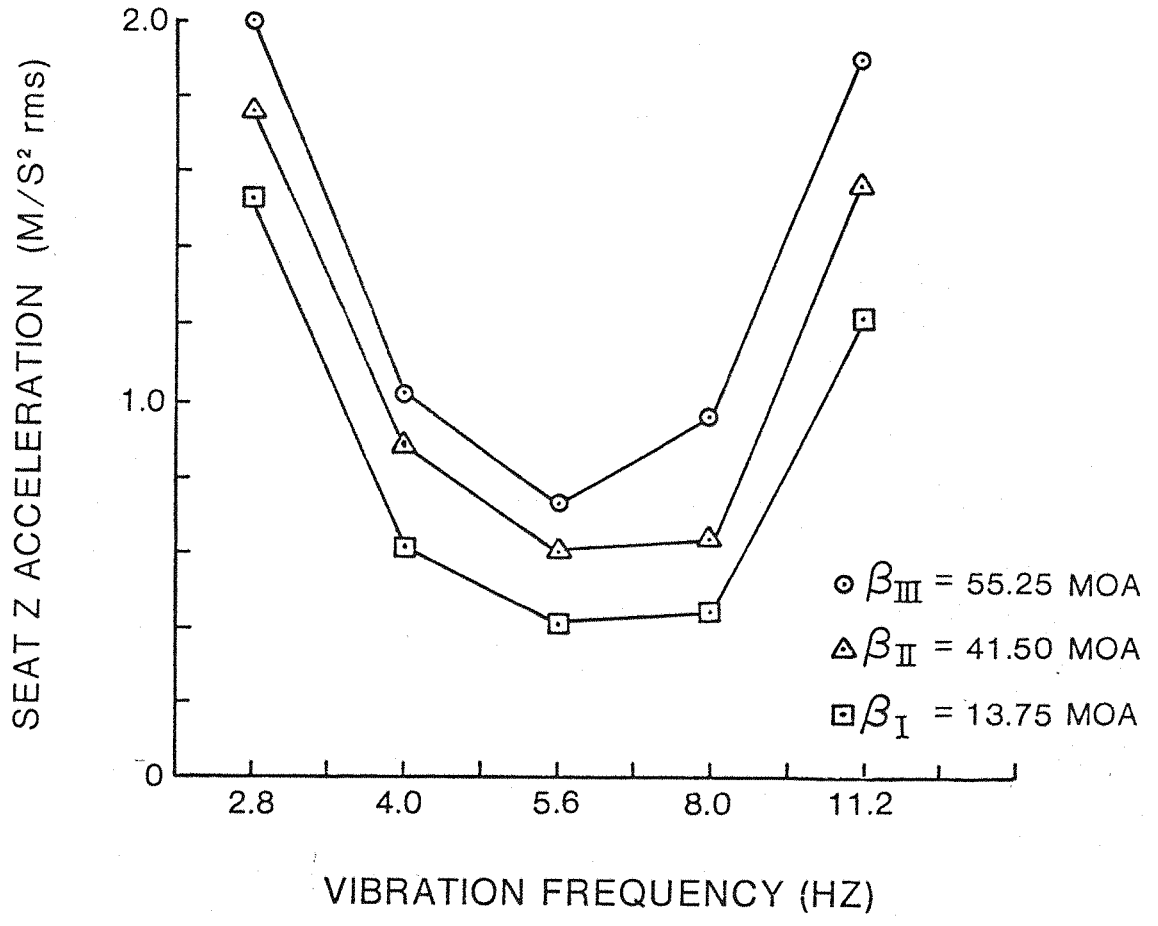

Figure 6.3.2. Mean Vertical Seat Z Vibration Level Required to Produce Three Nodal Image Angular Separations (β), Experiment SD.2

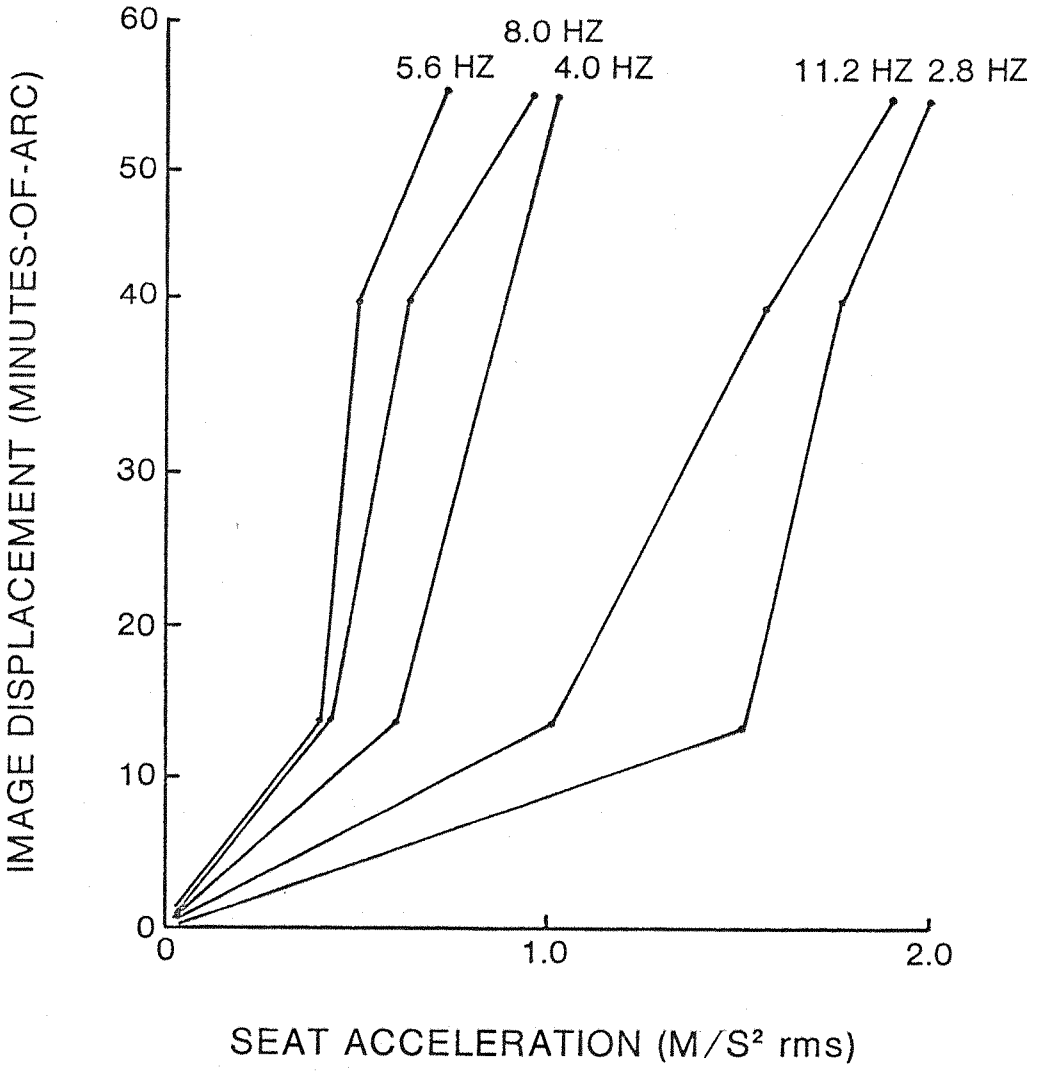

Figure 6.3.3. Peak-to-Peak Displacement of Helmet-Mounted Display Image on the Retina as a Function of Seat Vibration Level and Frequency, Experiment SD.2

6.3.4 Comparison of Image Displacements on the Retina to Helmet and Image Displacements in Space

As postulated in Section 6.3.1 above, if the vestibulo-ocular reflex causes the eyes to remain stabilized in space, then the image displacement on the retina and, hence, the angular separation of the nodal images should equal the displacement of the helmet display image in space. In order to compare the retinal image displacement data measured in the experiment with that of Experiments BD.5 and SD.1, the

magnitudes of retinal image displacement for a seat vibration level of 1.0 m/s^2 rms were estimated from the data in Table 6.3.1. These estimates were found by first constructing linear models of the individual subject data for each frequency and then calculating the equivalent displacement for a vibration level of 1.0 m/s^2 rms. The data from this analysis are given in Table 6.3.3. These data are compared with SD.1 and BD.5 results in Figure 6.2.6 for Subjects S1, S4, S7, and S8.

TABLE 6.3.3. ESTIMATED PEAK-TO-PEAK ANGULAR DISPLACEMENT OF HELMET-MOUNTED IMAGE ON THE RETINA AT A SEAT ACCELERATION LEVEL OF 1.0 m/s^2 rms

	Angular Displacement (minutes-of-arc)					
Frequency (Hz)	2.8	4.0	5.6	8.0	11.2	16.0
Subject						
S1	19.9	80.1	99.8	62.8	20.6	9.3
S2	--	--	78.3	90.6	36.0	--
S4	--	27.5	96.5	52.5	48.9	--
S7	--	35.6	52.1	68.4	--	--
S8	--	44.4	44.4	32.9	--	--
S11	--	63.2	81.0	53.4	--	--
S12	8.5	47.6	47.6	55.9	17.7	--
$\bar{x}$	14.2	49.7	71.4	59.5	30.8	9.3
σ	--	19.1	23.3	17.6	14.5	--

Another comparison of the retinal image movements and helmet pitch movements is shown in Figure 6.3.4 for Subjects S1, S4, S7, S8, S11, and S12. Here the ratio of the angular acceleration of the display image on the retina (rad/s^2 rms) to the vertical seat Z acceleration level (m/s^2 rms) is plotted with the modulus of the helmet pitch to seat Z transfer function. (Note that the values of the helmet pitch gain were sampled from the original individual subject moduli in Appendix A.5.3.) Figure 6.3.4 shows that between 2.8 Hz and 5.6 Hz, retinal image accelerations were either approximately equal or less than those for helmet pitch for most subjects, thereby indicating that most of the image movement on the retina at these frequencies can be

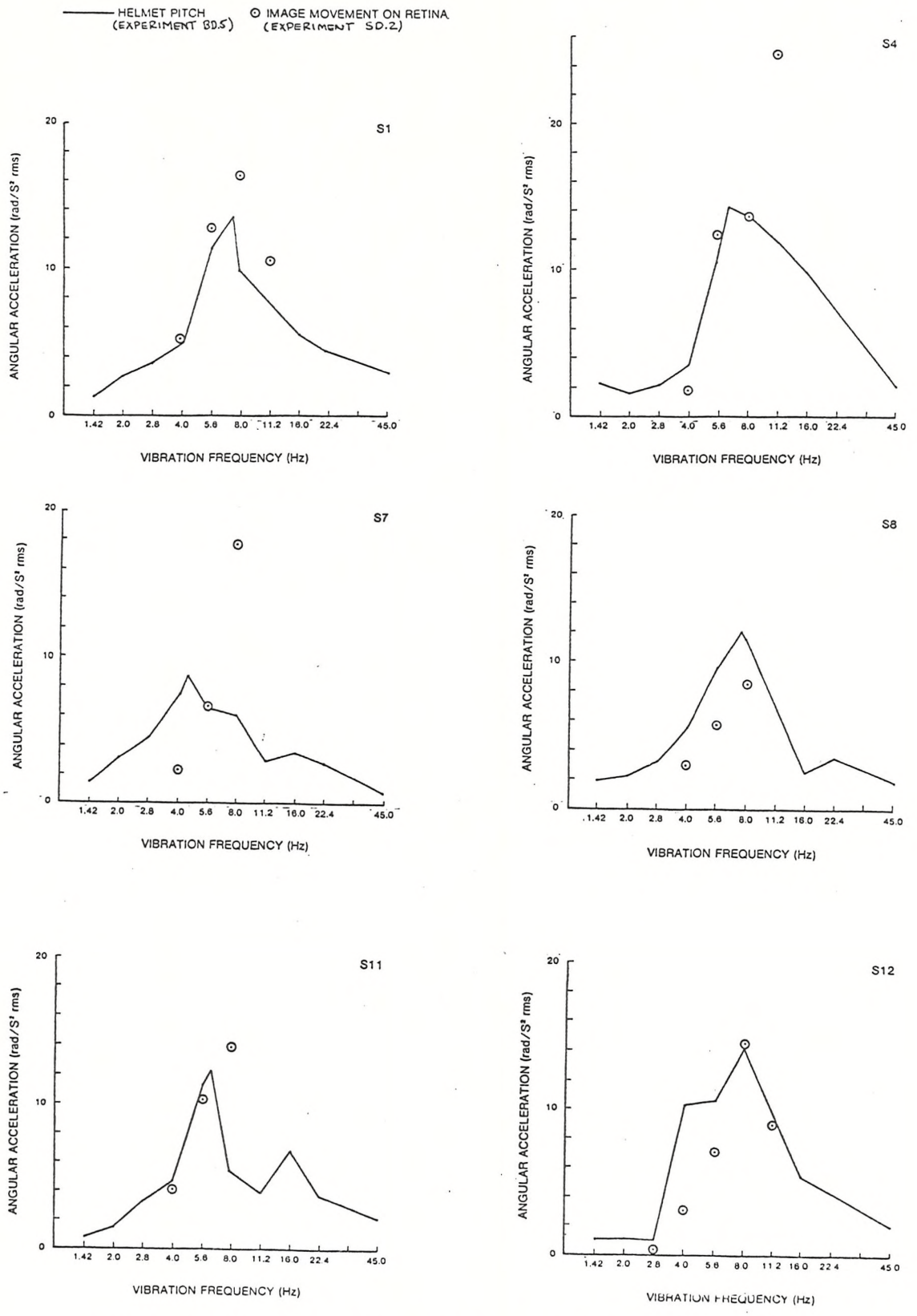

Figure 6.3.4. Comparison of Helmet Pitch Acceleration and Estimated Retinal Image Acceleration for a Seat Acceleration Level of 1.0 m/s^2 rms

attributed to the oscillation of the display image relative to a space stabilized eye. The combination of the slight phase lags in helmet to head movement and the eye to head gains of less than 1.0 may have caused gains of image accelerations on the retina to be less than helmet pitch accelerations for some subjects. The large increase in the gain of retina image movement relative to helmet pitch for Subjects S1, S4, S7, and S11 at 8.0 Hz or 11.2 Hz suggests that the VOR may have become inoperative at these frequencies. These increases in gain can be accounted for by the gain and phase relationships of helmet to head pitch motion for these subjects derived from the BD.5 data. In this case, the motion of the helmet relative to the head was actually greater than the motion of the helmet in space. Under helmet pitch conditions wherein the bandwidth of the VOR had been exceeded, the eyes probably became "head referenced" rather than "space referenced" and the movement of display image on the retina increased beyond that of helmet pitch oscillation in space. The seemingly high VOR bandwidth (up to 11.2 Hz) for S12 may be a misnomer. Inspection of the gain and phase relationships of helmet-to-head movement for this subject indicated that approximately equal image accelerations on the retina would occur with either the eyes stabilized in space or referenced to the head.

Caution must be exercised in any extensive interpretation of these results since the data for the helmet pitch and image movement were obtained under different vibration conditions and experimental studies. Nevertheless, the results are remarkably consistent with each other and with the literature.

6.4 RELATIONSHIPS OF HEAD, HELMET, AND EYE MOVEMENTS TO READING PERFORMANCE

6.4.1 Introduction to Analysis

The dynamic experiments of BD.5, SD.1, and SD.2 indicate that the pitch oscillatory (i.e., sinusoidal) movements of the head and helmet during vertical whole-body vibration also produce oscillatory movements of the helmet display image on the retina. The magnitudes of these oscillatory retinal movements were measured in Experiment SD.2,

and depending upon the frequency of oscillation, were attributed to either the oscillation of the helmet in space (and hence the display image as per Experiment SD.1) and/or the relative movement of the helmet on the head. These results were consistent with the general nature of the vestibulo-ocular reflex as reported in the literature.

Since the oscillation of the helmet and head were found to be sinusoidal (Experiment BD.3), it can be assumed that the oscillation of the display image on the retina was also sinusoidal. Under these conditions, the translation of the display image on the retina should be similar to that of an object oscillating with equivalent peak-to-peak magnitude and frequency being viewed by a static eye. According to O'Hanlon and Griffin (1971), the reading error (E) of Landolt "Cs" produced by such a sinusoidal displacement of the display image on the retina should be inversely proportional to the maximum duration of the image over a small retinal area, or $E \propto f, \sqrt{d}$ where f is the frequency of sinusoidal oscillation (Hz) and d is the peak-to-peak displacement of the image on the retina.[1]

6.4.2 Comparison of Reading Performance and Dynamic Behaviour

In order to test the relationship of dynamic behaviour and reading performance, the pitch displacement of the helmet in space was estimated using the transfer functions from Experiment BD.5 and compared to reading performance from Experiment LG.1 via the model above. Specifically, the peak-to-peak amplitude of image displacement on the retina (β) during each reading condition was estimated first by computing the peak-to-peak helmet pitch displacement (θ_{helmet}) using the helmet pitch to seat Z transfer functions for each subject from BD.5 at the appropriate vibration frequency and level corresponding to the conditions producing the reading error in Experiment LG.1. Since only

[1]The application of this model to a helmet-mounted display viewing situation assumes that the psychophysical effects of a static eye viewing an oscillating scene will be the same as those of a space-stabilized eye (while the head is moving) viewing an oscillatory scene of equivalent retinal image displacement.

seven of the ten subjects in Experiment BD.5 participated in Experiment LG.1 (i.e., S1, S3, S4, S5, S7, S8, S9), data for these subjects only were used in the analysis. Table 6.4.1 gives the results of this analysis showing the estimated helmet pitch displacement and the value of the model $E \propto f\sqrt{\theta_{helmet}}$ compared to the mean reading errors for these subjects in Experiment LG.1. (Note: The vibration frequency of 45.0 Hz was not used in this analysis since there was no significant effect of vibration level on reading error at this frequency in Experiment LG.1.)

The data summarized in Table 6.4.1 are plotted in Figure 6.4.1. By inspection, several observations can be made from these data. First, the number of reading errors does appear to be related to the square root of the helmet pitch amplitude regardless of the vibration frequency. The grouping of the data for the 1.42 Hz, 2.0 Hz, 2.8 Hz, and 4.0 Hz vibration frequencies indicates that the perception of the helmet-mounted display tends to follow the model (using helmet pitch displacement) across these frequencies and, therefore, may be mediated by the same dynamic mechanism. This would be the case if the eyes were truly space-stable at these frequencies and reading error were due to the displacement of the image in the retina caused by the displacement of the helmet in space as the data from Experiment SD.2 would tend to confirm.

The data for the 5.6 Hz, 8.0 Hz, and 11.2 Hz vibration frequencies are grouped somewhat also with similar slopes. At these higher frequencies of head rotational oscillation, the bandwidth of the VOR may have been exceeded thereby causing the eyes to move with the head. If this were the case, the behaviour of the image in the retina would be described better by the movement of the helmet on the head. In order to test this premise, the model $E \propto f\sqrt{\theta}$ was recomputed using the relative displacement of the helmet on the head (ϕ). These data are plotted in Figure 6.4.2. It becomes apparent here that the grouping and slopes of the data using helmet-on-head movement becomes a better predictor using the model and mean data for the frequencies 5.6 to 22.4 Hz. The two methods for estimating reading performance (i.e., $f\sqrt{\theta}$ and $f\sqrt{\phi}$) are combined as shown in Figure 6.4.3 wherein helmet pitch

TABLE 6.4.1. RELATIONSHIP OF MEAN READING ERRORS (E) (EXPERIMENT LG.1) TO HELMET PITCH DISPLACEMENT (θ_{HELMET}) (EXPERIMENT BD.5) VIA MODEL $E \propto F\sqrt{\theta_{HELMET}}$

Vibration Frequency (f) (Hz)	Seat Z Level (m/s^2 rms)	Mean Helmet Pitch Modulus (rad/m)	Estimated Helmet Pitch Displacement (θ_{helmet}) (minutes-of-arc)	Model $f\sqrt{\theta_{helmet}}$	Mean Reading Errors (E)
1.42	.28	1.381	47.24	9.76	1.71
	.56		94.47	13.80	6.71
	.84		141.71	16.90	12.14
	1.12		188.94	19.52	12.86
	1.40		236.18	21.82	16.71
2.0	.28	2.112	36.42	12.07	4.71
	.56		72.83	17.07	6.29
	.84		109.25	20.90	9.29
	1.12		145.66	24.14	12.14
	1.40		182.08	26.99	17.86
2.8	.24	2.948	22.23	13.20	4.86
	.48		44.46	18.67	10.29
	.72		66.69	22.87	14.86
	.96		88.91	26.40	20.00
	1.20		111.14	29.52	22.14
4.0	.20	5.809	17.89	16.92	8.43
	.40		35.77	23.92	12.29
	.60		53.66	29.30	16.57
	.80		71.54	33.83	19.00
	1.00		89.43	37.83	24.29
5.6	.20	10.984	17.25	23.26	2.29
	.40		34.51	32.90	8.14
	.60		51.76	40.29	13.00
	.80		69.02	46.52	15.00
	1.00		86.27	52.01	19.00
8.0	.20	10.517	8.10	22.76	5.43
	.40		16.19	32.19	15.29
	.60		24.29	39.42	13.57
	.80		32.38	45.52	18.14
	1.00		40.48	50.90	19.14
11.2	.28	6.813	3.75	21.68	3.29
	.56		7.49	30.66	7.00
	.84		11.24	37.55	9.71
	1.12		14.98	43.35	13.43
	1.40		18.73	48.47	14.71
16.0	.40	5.482	2.11	23.24	3.57
	.80		4.22	32.87	5.14
	1.20		6.33	40.25	5.86
	1.60		8.44	46.48	7.86
	2.00		10.55	51.97	7.86
22.4	.56	4.234	1.16	24.17	1.14
	1.12		2.33	34.18	2.14
	1.68		3.49	41.86	2.43
	2.24		4.66	48.33	5.71
	2.80		5.82	54.04	3.57

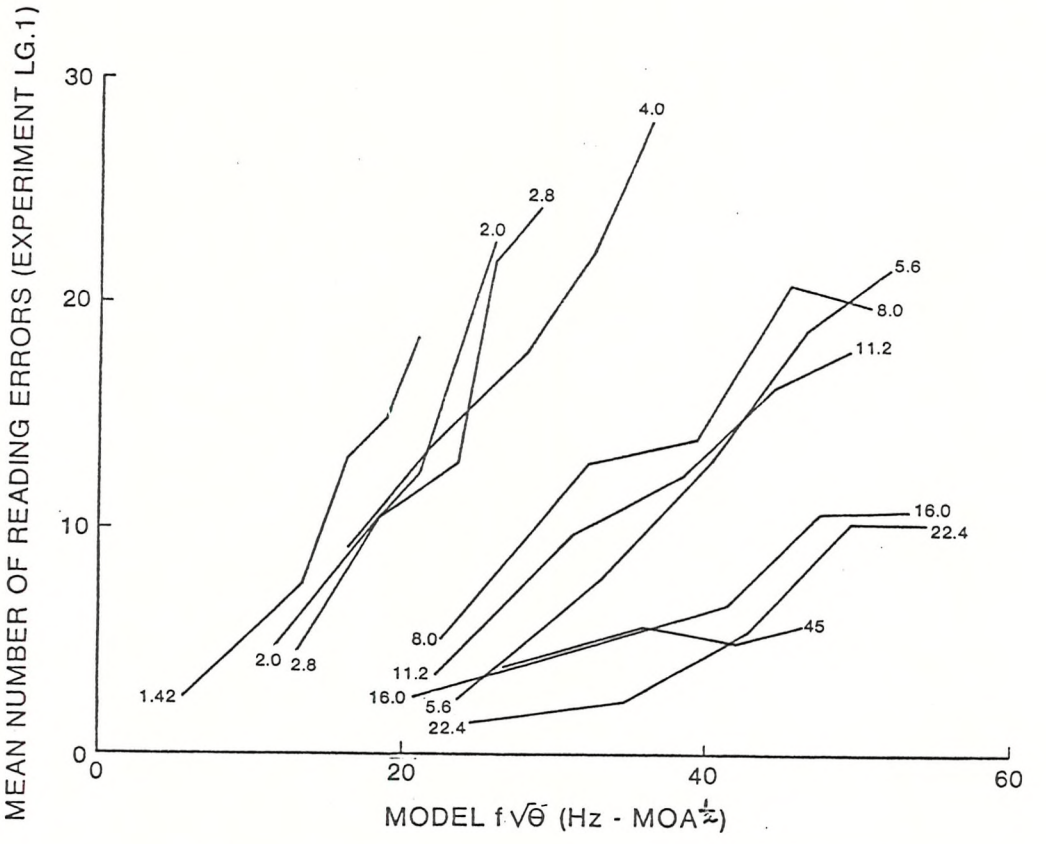

Figure 6.4.1. Relationship of Mean Reading Errors From Experiment LG.1 to Model of Reading Performance $f\sqrt{\theta}$ Where f is the Seat Vibration Frequency and θ is the Peak-to-Peak Angular Displacement of the Helmet in Space as Estimated from Experiment BD.5

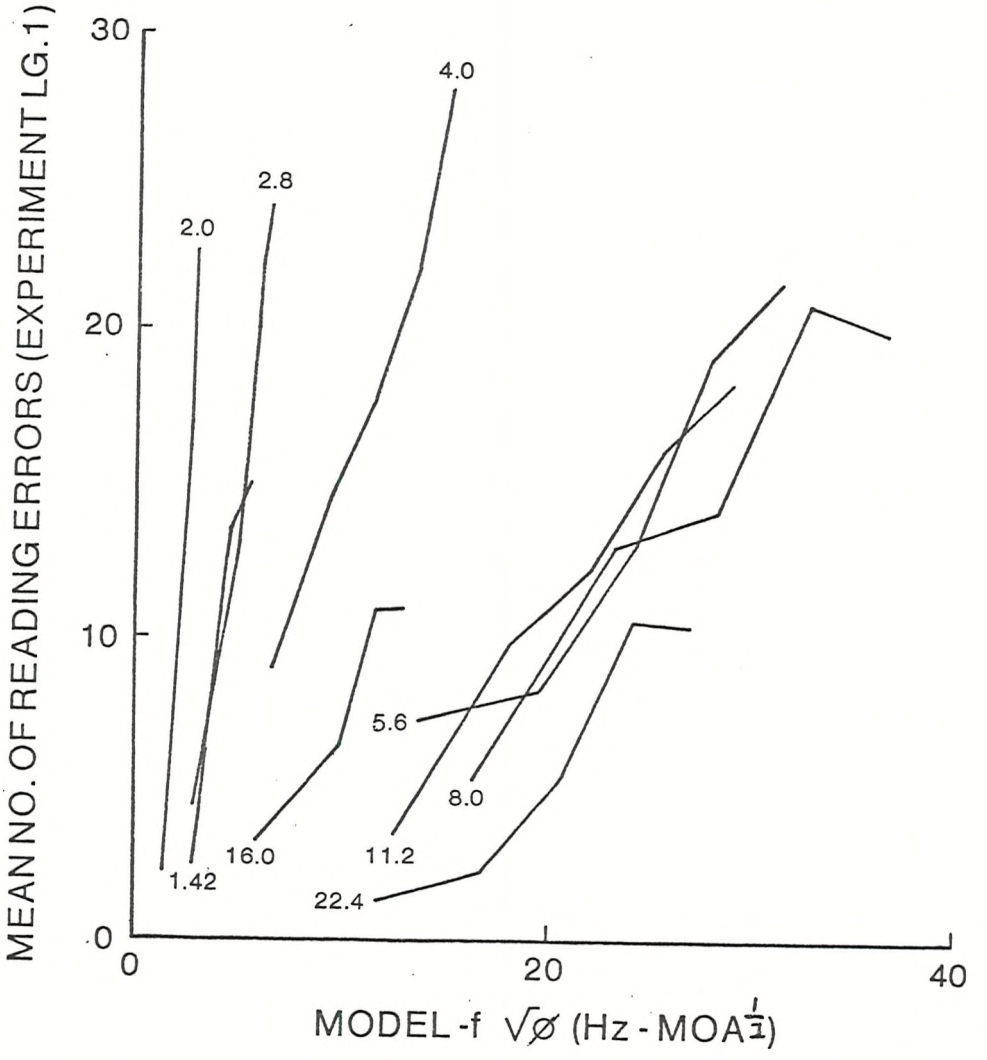

Figure 6.4.2. Relationship of Mean Reading Errors From Experiment LG.1 to Model of Reading Performance $f\sqrt{\phi}$ Where f is the Seat Vibration Frequency and ϕ is the Peak-to-Peak Angular Displacement of the Helmet on the Head

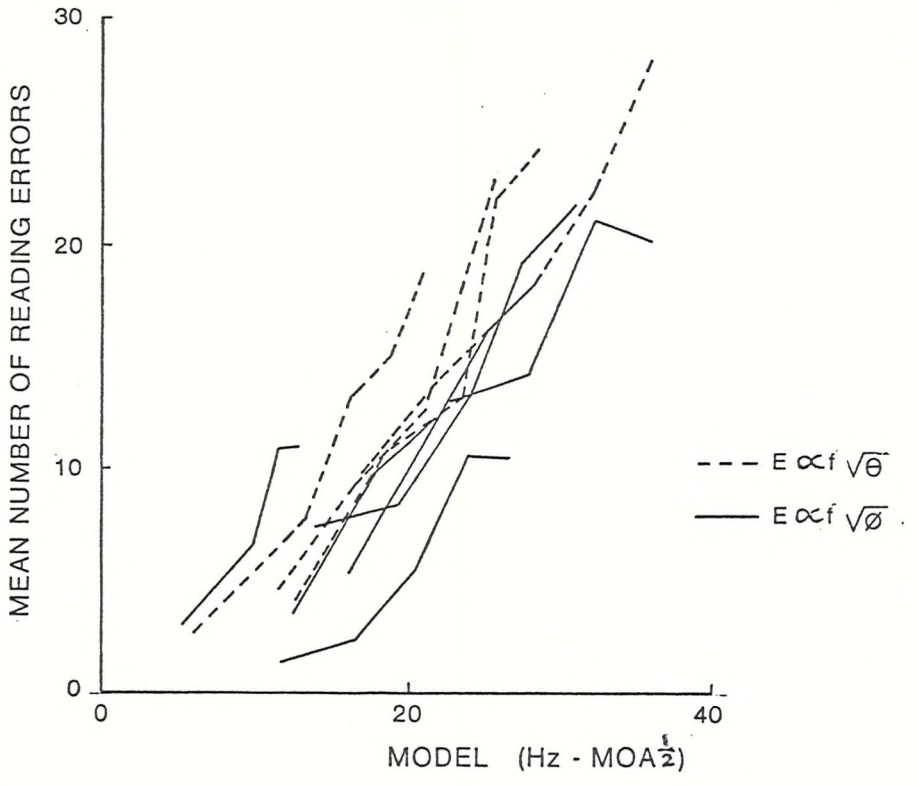

Figure 6.4.3. Combination of Models for Relating Reading Performance to Head and Helmet Dynamic Behaviour. Dashed Lines Represent the Predicted Reading Performance for the Vibration Frequencies of 1.42 Hz, 2.0 Hz, 2.8 Hz, and 4.0 Hz Computed Using $f\sqrt{\theta}$ (θ = Helmet Pitch Displacement). Solid Lines Represent the Predicted Reading Performance for the Vibration Frequencies of 5.6 Hz, 8.0 Hz, 11.2 Hz, 16.0 Hz, and 22.4 Hz Computed using $f\sqrt{\phi}$ (ϕ = Helmet Displacement on the Head).

motion is used for 1.42 Hz to 4.0 Hz, and helmet-on-head pitch motion is used for 5.6 Hz to 22.0 Hz. The coefficient of correlation of these data is highly significant (r_0 = .871, $p<.001$), indicating that there is generally good agreement across all frequencies and levels between the mean legibility and mean dynamic data. These findings are further substantiated by individual subject data using O'Hanlon and Griffin's model. With the exception of Subject S7, the individual reading errors for each subject (Experiment LG.1) correlated ($p<.001$) with the performance predicted to the models. The coefficients of correlation and linear regression models depicting these relationships are given in Table 6.4.2.

TABLE 6.4.2. COEFFICIENTS OF CORRELATION (r_0) AND LINEAR REGRESSION MODELS RELATING READING ERRORS TO PREDICTED PERFORMANCE USING $E \propto f\sqrt{\theta}$ AND $E \propto f\sqrt{\phi}$ FOR INDIVIDUAL SUBJECTS

Subject*	Coeficient of Correlation (r_0)	Linear Regression Model*		
		Intercept (a_0)	Slope (a_1)	95% Confidence Interval of Slope
S1	.592**	.007	.346	.146
S3	.526**	-.032	.676	.340
S4	.700**	-.136	.331	.105
S5	.800**	.466	.586	.137
S7	-.203	--	--	--
S8	.596**	.190	.467	.196
S9	.658**	-.235	.706	.252
Overall	.871**	-.255	.740	.128

*Regression statistics computed with 45 samples per subject.
**p<.001

Since the analysis above supports the relationship of reading performance to dynamic behaviour via the model $E \propto f\sqrt{d}$, a question arises as to the appropriateness of the original regression models used to describe the legibility data in Experiment LG.1.[1]

Even though the linear component of the analysis of simple main effects (Table 4.2.5) accounted for the majority of the sums of squares of seat acceleration level on reading error at each vibration frequency, a vibration analysis using orthogonal contrasts of the relationship of reading to the square root of seat vertical Z axis acceleration was not performed.

[1] In the regression analysis in Experiment LG.1 (Section 4.2.3), linear models of the reading error were obtained showing error (E) to be directly proportional to the rms seat Z acceleration level (a). It would follow from the analysis above, that if the model $E \propto f\sqrt{d}$ is valid, and there is a linear relationship between helmet pitch displacement and seat Z acceleration level (a), then a more appropriate model would have been $E \propto \sqrt{a}$ (for each individual vibration frequency).

In order to explore further the nature of the reading error as a function of vibration seat acceleration, regression analysis was performed on the original mean data from Experiment LG.1 using a and $\sqrt{a}$. As can be seen in Table 6.4.3, the coefficients of correlation of the model employing $\sqrt{a}$ yields a slightly higher correlation on all but the 2.0 Hz and 4.0 Hz frequencies. Although this analysis is not conclusive, it does indicate that the data from Experiment LG.1 can be appropriately modeled with the equation $E \propto \sqrt{a}$.

TABLE 6.4.3. COMPARISON OF CORRELATIONS OF MEAN READING ERRORS (E) (EXPERIMENT LG.1) TO SEAT ACCELERATION LEVEL (a) AND SQUARE ROOT OF SEAT ACCELERATION LEVEL ($\sqrt{a}$)

Vibration Frequency	Coefficients of Correlation E with a	Coefficients of Correlation E with $\sqrt{a}$
1.42	.976	.988
2.0	.976	.947
2.8	.991	.997
4.0	.995	.988
5.0	.986	.996
8.0	.880	.911
11.2	.990	.995
16.0	.970	.978
22.4	.763	.779

If it is accepted that the model established by O'Hanlon and Griffin is valid for the oscillatory retinal image motion produced by viewing the helmet-mounted display during whole-body vibration, then the analysis above contains some implications regarding eye movement behaviour. Specifically, it appears from the data above that the reading performance at 5.6 Hz does not correspond with the predicted performance using only helmet pitch in space. The implication here is that the eyes were not completely stabilized (i.e., VOR gain<1.0). On the other hand, the predicted performance was achieved using the data relating helmet on head movement, implying that at 5.6 Hz and above, the eyes were more or less moving with the head.

The implied reduction in the gain of the vestibulo-ocular reflex between 4.0 Hz and 5.6 Hz would occur at a frequency less than that which would normally be predicted from the findings of Benson (1972), Griffin (1976b), and Benson and Barnes (1978) [although Benson (1972) did show an increasing number of reading errors in a space-stable display above 4.0 Hz with head oscillation in the yaw axis]. The observed nature of reading error and helmet/eye movement dynamics above is consistent with the results of Experiment LG.1 for the large panel-mounted display viewed at a distance of 1.5 m (Section 4.2.3). There, the significant increases in reading errors for the 5.6 Hz and 8.0 Hz vibration conditions corresponded with increases in head pitch (without the helmet) at the same frequencies in Experiment BD.8 (e.g., Figure 5.8.3). Again, these results imply that a general reduction in VOR gain may have occurred at 5.6 Hz and above.

6.5 SUMMARY

The purpose of this chapter was to explore the relationships between helmet display reading performance and the dynamic behaviour of the head, helmet, and eyes under whole-body vibration conditions. The main conclusion emerging from this analysis was that helmet-mounted display reading performance can be related to the magnitude and frequency of the angular displacement of the display images formed on the retina using the model established by O'Hanlon and Griffin (1972). The observed nature of the movement of the display image on the retina was explained by the dynamic interaction of the helmet, head, and eyes. It was found that retinal image movements can be estimated from the helmet pitch transfer function for frequencies between 1.42 and 5.6 Hz and the helmet pitch on the head at the frequencies between 5.6 Hz and 22.4 Hz.

Clearly, the nature of the movements of the helmet display image on the retina during whole-body vibration is very complex. The results of the experiments and analysis in this chapter cannot be considered as conclusive. More research is needed to delineate the full nature of the retinal image motion as it relates to legibility of the helmet-mounted display. Furthermore, a more robust demonstration of the

viability of the O'Hanlon and Griffin model as it may relate to helmet-mounted display viewing is needed. It is suggested here that any further experiments provide simultaneous measurements of helmet, head, and eye dynamic behaviour in conjunction with reading performance so that variability between experiments (e.g., BD.5, SD.1, SD.2, and LG.1) can be eliminated.

Chapter 7

IN-FLIGHT INVESTIGATIONS OF HELMET-MOUNTED DISPLAY LEGIBILITY AND HEAD AND HELMET MOVEMENT BEHAVIOUR

7.1 INTRODUCTION

The experiments reported in Chapters 4 and 5 have considered the legibility of the helmet-mounted display and the biodynamic response of the head and the helmet during single axis, discrete frequency, sinusoidal vibration conditions within the laboratory. As reported in Section 2.5.2, these vibration conditions are not realistic when compared to the multiple axis, random and/or multiple frequency deterministic motion encountered in fixed and rotary wing aircraft. In order to test the validity of the laboratory experiments relative to the airborne environment, two in-flight experiments were conducted aboard a representative helicopter. The purpose of the first experiment was to measure the legibility of the helmet-mounted display under various flight conditions. The second experiment was conducted to measure the response of the helmet and head to the vibration caused by the same flight conditions. The two experiments will be described separately with their results, then discussed together in context with the previous laboratory studies.

7.2 EXPERIMENT H.1: HELMET-MOUNTED DISPLAY LEGIBILITY IN A HELICOPTER

7.2.1 General Considerations

The general character legibility task described in Chapter 4 served as the basis for this experiment. The intent of the study was to duplicate the visual material presentations used in experiment LG.3 under various helicopter flight conditions, while measuring the accuracy of reading the numeric characters.

7.2.2 Method

7.2.2.1 Aircraft

A prototype SEA KING helicopter (tail number XV 371) manufactured by Sikorsky Aircraft Company was used as the flight test vehicle. The helicopter was furnished and supported by the Royal Aircraft Establishment, Farnborough. Characteristics of the aircraft are given in Table 7.2.1.

TABLE 7.2.1. CHARACTERISTICS OF SEA KING FLIGHT TEST HELICOPTER

Aircraft Type/Model	SEA KING (CH-53)
Manufacturer	Sikorsky
Number of Hours Operated	1603
Number of Main Rotor Blades	5
Diameter of Main Rotor	18.9 m
Number of Tail Rotor Blades	6
Diameter of Tail Rotor	3.15 m
Height to Top of Tail Rotor	5.13 m
Overall Length (rotors turning)	22.15 m
Unladen Weight	5923 kg
Weight (fully fueled)	9299 kg
Engines: port	R/R Gnome Type 54002 28/1/76
starboard	R/R Gnome Type 50006 30/10/75
Engine RPM	18966
Main Rotor RPM	203
Tail Rotor RPM	1238.3
Main Rotor Pass Frequency	16.9 Hz
Tail Rotor Pass Frequency	123.8 Hz

7.2.2.2 Aircraft Installation

The helmet-mounted display system (Hughes Model 212) used in the laboratory experiments was also used in the helicopter tests. The display electronics unit was located in an equipment rack in the

helicopter cabin with the display control panel continuously accessible to the experimenter. The cable from the HMD electronics to the helmet-mounted unit was routed overhead along the aircraft fuselage and supported near the copilot's head (left seat), leaving approximately 0.3 m of the cable free of any support. A video tape recorder (IVC Model 826) was also mounted in the equipment rack and used to input prerecorded video information into the helmet-mounted display. A portable audio recorder was interfaced to the aircraft intercommunication system to record voice communication between the copilot (subject), experimenter, pilot, and other crewmembers.

7.2.2.3 Visual Stimulus Material

A video tape recording of the numeric presentations (in the 5 x 10 array format) used in experiment LG.1 (Chapter 4) was replayed on the video tape recorder for input to the HMD during flight. A total of five character sizes (12, 15, 22, 29, and 36 minutes-of-arc) were used. The display luminance was adjusted to approximately 19 cd/m^2. The HMD was operated with the visor (15 percent transmission) in place over both eyes and the variable transmission filter over the display eye. Ambient light transmission was approximately 15 percent to the left eye and 0.008 percent to the right (display) eye. The ambient luminances were not measured directly, but from previous flight tests under similar conditions (i.e., same area, time of year, and weather conditions), the ambient luminance was estimated at 3000 cd/m^2 for the 1000 foot altitude flight condition and 1500 cd/m^2 for the ground and 20 foot altitude conditions.

7.2.2.4 Flight Conditions

In order to present the different aircraft vibration conditions which may be encountered during flight operations, seven repeatable flight conditions and one static (no vibration) condition were used as shown in Table 7.2.2. The aircraft was flown by the pilot (right seat) at these conditions while the copilot served as the experimental subject.

TABLE 7.2.2. FLIGHT CONDITIONS USED IN EXPERIMENTS H.1 AND H.2

Condition	Altitude (feet)	Velocity (knots)	Altitude
Static (no Vibration)	0	0	level
Rotor	0	0	level
Hover	20	0	level
20	20	20	level
70	1000	70	level
90	1000	90	level
110	1000	110	level
Bank	1000	70	20° bank

7.2.2.5 Subjects

Two experienced helicopter test pilots were used as subjects in the experiment. One pilot operated the aircraft while the other pilot served as the subject, then the two pilots switched positions. The physical characteristics of the subjects are given in Table 7.2.3.

TABLE 7.2.3. PHYSICAL CHARACTERISTICS OF PILOT/SUBJECTS

Characteristics	Pilot A (KA) (AD)	Pilot B
Age	32	35
Height	176.5 cm	188.0 cm
Weight	63.5 kg	78.0 kg
Visual Acuity	6/12 (uncorrected) 6/4 (corrected with 0.5 diopter lenses)	6/4 (uncorrected)
Number of Flight Hours	2874 3004	

7.2.2.6 Procedure

Table 7.2.4 gives the order of presentation of the display stimuli and flight conditions for Subject A. The order of presentation was reversed for Subject B, and the 12 minutes-of-arc character size was substituted for the 36 minutes-of-arc character size. During each experiment run, the experimenter instructed the pilot (right seat) as to the flight condition which was needed. The HMD character size was adjusted by the experimenter. When the pilot indicated that the desired flight condition was achieved and stabilized, the experimenter started the video tape recorder and unblanked the HMD presentation to the subject. The subject was required to read the numeric array aloud (into the intercom system) at a self-paced rate of approximately one character per second. During this time the experimenter recorded the reading errors (an audio recording of the subject response was used later as a verification of the scoring accuracy).

TABLE 7.2.4. ORDER OF STIMULUS PRESENTATION (PILOT A)

Flight Condition	Character Size				
	12*	15	22	29	36
Static		1	2	3	4
Rotor		8	7	6	5
Hover		9	10	11	12
20		16	15	14	13
70		17	18	19	20
90		24	23	22	21
110		25	26	27	28
Bank		32	31	30	29
Static		33	34	35	36

*Note: For Pilot B, order of presentation was reversed and 12 minutes-of-arc character size substituted for 36 minutes-of-arc size.

All helicopter flights were made in the local Farnborough and Salisbury Plain areas during the period of 10-20 August 1978. Flight times were from approximately 1100 to 1500 hours. Weather conditions were clear with scattered clouds and light winds of 5-7 knots.

7.2.3 Results

No reading errors were committed by either subject during any of the character size or static or flight conditions. The pilots were interviewed following the flights. Table 7.2.5 gives a summary of pilot comments. Generally, the pilots complained about the difficulty of reading smaller character sizes (i.e., 12 and 15 minutes-of-arc), and were surprised that they had committed no errors. They made no statement as to which flight condition produced the subjectively more difficult reading task. It can be surmised from these comments that even though the reading accuracy was good, there was some uncertainty in the subject responses at the smaller character sizes. The subjects preferred the 22 minutes-of-arc character size stating that the 12 and 15 minutes-of-arc sizes were too small and the 29 and 36 minutes-of-arc sizes too large for comfortable reading. In the latter case, the subjects stated that too much eye movement was required to fixate upon the characters in the large format sizes. Again, the flight conditions appeared to have had no significant effect on reading performance.

7.3 EXPERIMENT H.2: HEAD AND HELMET MOVEMENT IN HELICOPTER FLIGHT ENVIRONMENT

7.3.1 General Considerations

In order to interpret the results of Experiment H.1 in light of the laboratory findings in Chapter 4, it was necessary to measure the movement of the head and helmet induced by the helicopter vibration. The purpose of this experiment was to quantify these responses during the same flight conditions as used in Experiment H.1 above.

TABLE 7.2.5. SUMMARY OF PILOT COMMENTS

Pilot A (KA)

- The large format (i.e., 36 minutes-of-arc character size) more difficult to read:
  - had to scan (more spread out)
  - would reduce reading speed in actual aircraft operations
- Green characters OK.
- Helmet uncomfortable.

Pilot B (AD)

- Pain behind right eye.
- Chin strap uncomfortable.
- After use for approximately 20 minutes, saw display break through into outside scene.
- When another aircraft entered scene, lost concentration.
- Middle two character sizes (i.e., 15 minutes-of-arc and 22 minutes-of-arc) easiest to read.
- No observed effect of helicopter vibration.

7.3.2 Vibration Instrumentation

In order to measure the vibration levels present in the SEA KING helicopter, a special purpose instrumentation package was used. This vibration measurement system was the same as that developed and reported by Griffin (1972a) and described later by Parsons (1979). The vibration recording system consisted of six vibration accelerometers, six accelerometer amplifiers, a six-channel frequency division multiplexed encoding unit, and a two-channel portable direct record tape recorder. Upon playback, the taped signals were decoded three channels at a time and analyzed using the procedures described in Chapter 5 and Appendix A.5.1.

7.3.2.2 Accelerometer Mounting

Six simultaneous vibration acceleration measurements were made during flight: the X axis and Z axis translatory motion of the seat pilot interface; the translatory motion of the seat back in the axis normal to the plane of the seat back; rotational motion of the helmet in the pitch axis; rotational motion of the head in the pitch and roll axis. The X axis and Z axis vibration input of the seat to the subjects was measured by a rigid sit-bar positioned between the helicopter seat cushion and the ischial tuberosities of the pilot subjects. The sit-bar incorporated orthogonally positioned translational accelerometers (Endevco 2265-20) in the center of the sit-bar. The vibration input of the seat back to the subject was measured by a similar pad with a translational accelerometer (Endevo 2265-20) located with its sensing axis normal to the seat back. (This method and apparatus for recording seat base and seat back translational acceleration were described in detail by Parsons, 1979). The pitch rotational acceleration of the helmet was transduced by a rotational accelerometer (Shaevitz ASMP-100) affixed on the helmet as described in Section 5.1. The roll and pitch rotational accelerations of the head were measured using a bite-bar containing two rotational accelerometers (Shaevitz ASMP-100) as described in Section 5.1.

7.3.2.2 Procedure

Vibration levels were recorded using the same aircraft, flight conditions, and subjects as in Experiment H.1. The measurements were made with the helmet-mounted display attached to the helmet. Records of 120 s duration were made for each flight condition and each pilot. During each recording period, the subject was instructed to look straight ahead as if he were reading the characters on the helmet-mounted display. The accelerometers/amplifiers were calibrated before each flight and rechecked at the completion of the test flight. (The calibration procedures for the vibration measurement system are described in detail by Parsons, 1979.)

7.3.3 Results

7.3.3.1 RMS Time History

The recorded accelerometer measurements of the X and Z axis of the seat, the normal axis of the seat back, the pitch and roll axes of the head, and the pitch axis of the helmet for one pilot/subject were low pass filtered, with a bandwidth of 0 to 40 Hz, and sampled at a rate of 128 samples/s over a 60 s period. The standard deviations of the magnitude of the samples over 1 second periods (i.e., every 128 samples) were computed and output as the RMS vibration level (within the 40 Hz bandwidth) as a function of time. (The standard deviation of the sampled time history corresponds to the RMS vibration acceleration level excluding any constant terms such as the acceleration due to gravity.) Running records of the RMS vibration levels for the seat Z axis and the helmet pitch axis are shown in Figure 7.3.1 for the various flight conditions. As can be seen during the hover and 20 knot flight conditions, variations in the seat Z axis vibration level were large (e.g., greater than factor of 2 over the mean value during the hover condition).

The means of the RMS readings and their standard deviations over the 60 s time histories are given in Table 7.3.1. Figure 7.3.2 is a plot of the mean RMS value as a function of the flight conditions for the six parameters measured. Generally, there was an increasing trend in the total seat X and Z axis and seat back motions with increasing forward velocity of the helicopter. The seat back motion was always observed to have a larger mean than the seat base (X and Y axis). Simultaneously, there was little effect of flight condition on helmet pitch or head roll, but a marked effect on head pitch, especially during the 70 knot, 90 knot, 110 knot, and bank conditions.

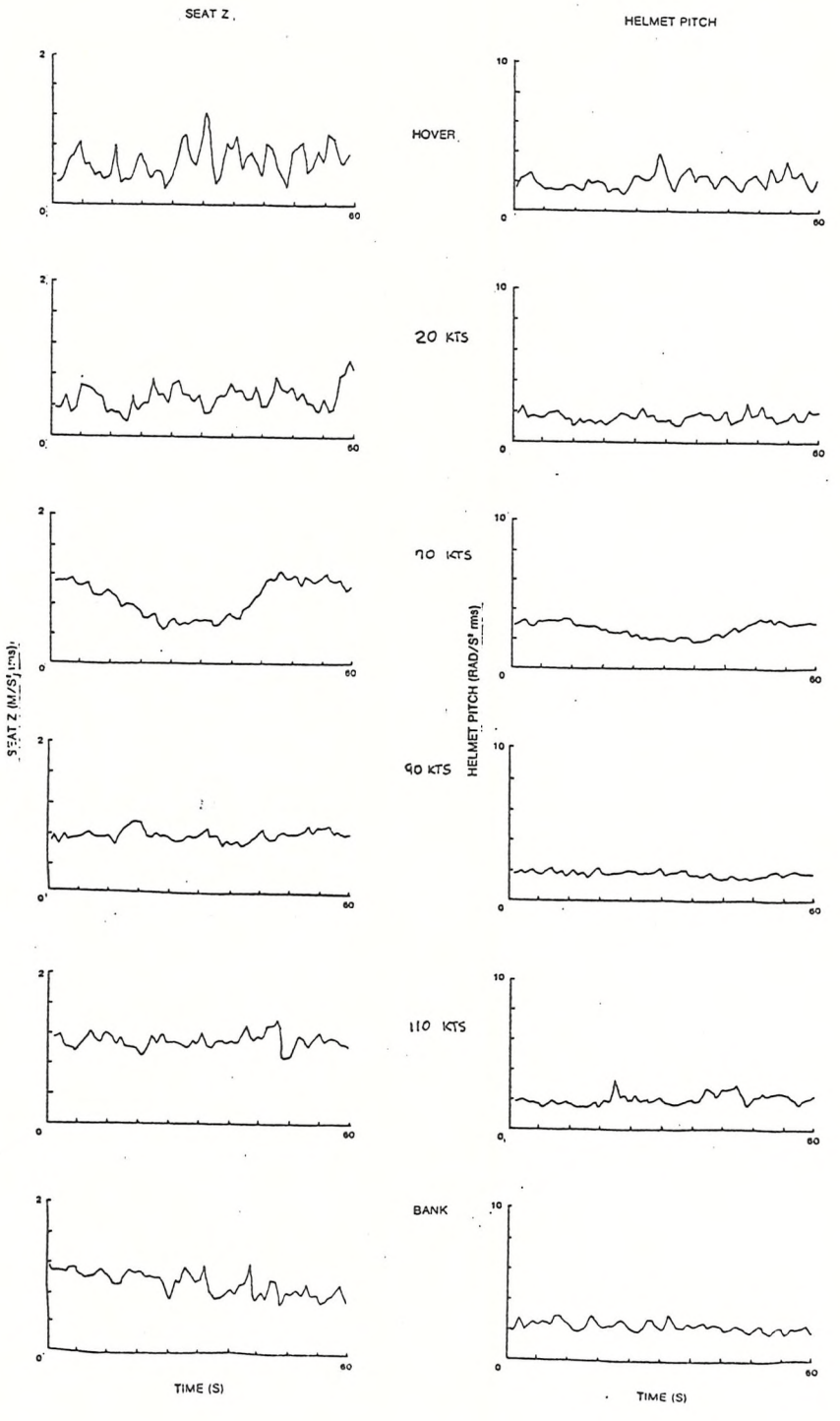

Figure 7.3.1. RMS Levels of Seat Z Axis and Helmet Pitch Axis Acceleration During a 60 s Interval for Six Flight Conditions, Pilot A (Experiment H.2)

TABLE 7.3.1. MEANS AND STANDARD DEVIATIONS OF RMS VIBRATION TIME HISTORIES (PILOT A)

Flight Condition	VIBRATION MEASUREMENT					
	Seat Z Axis	Seat Back	Seat X Axis	Head Pitch	Helmet Pitch	Head Roll
	m/s^2 rms	m/s^2 rms	m/s^2 rms	rad/s^2 rms	rad/s^2 rms	rad/s^2 rms
Rotor	0.283 (0.088)	0.449 (0.135)	0.258 (0.046)	1.8037 (0.4885)	1.0082 (0.2743)	1.1894 (2.525)
Hover	0.578 (0.220)	0.771 (0.293)	0.342 (0.077)	3.2130 (0.9166)	2.0443 (0.5445)	0.9135 (0.2605)
20 Knots	0.516 (0.160)	0.743 (0.253)	0.291 (0.065)	2.9922 (0.9070)	1.6860 (0.3309)	0.9975 (0.3192)
70 Knots	0.868 (0.249)	1.167 (0.290)	0.484 (0.105)	18.3778 (5.4543)	2.7010 (0.4922)	1.2020 (0.2643)
90 Knots	0.786 (0.074)	1.253 (0.096)	0.470 (0.043)	12.9459 (2.7280)	1.8006 (0.1937)	1.6085 (0.2417)
110 Knots	1.100 (0.100)	1.525 (0.152)	0.854 (0.099)	10.0861 (2.0571)	2.0319 (0.3751)	1.6913 (0.2735)
Bank	0.934 (0.139)	1.453 (0.186)	0.618 (0.090)	11.2128 (2.9453)	2.2908 (0.3101)	1.6702 (0.3695)

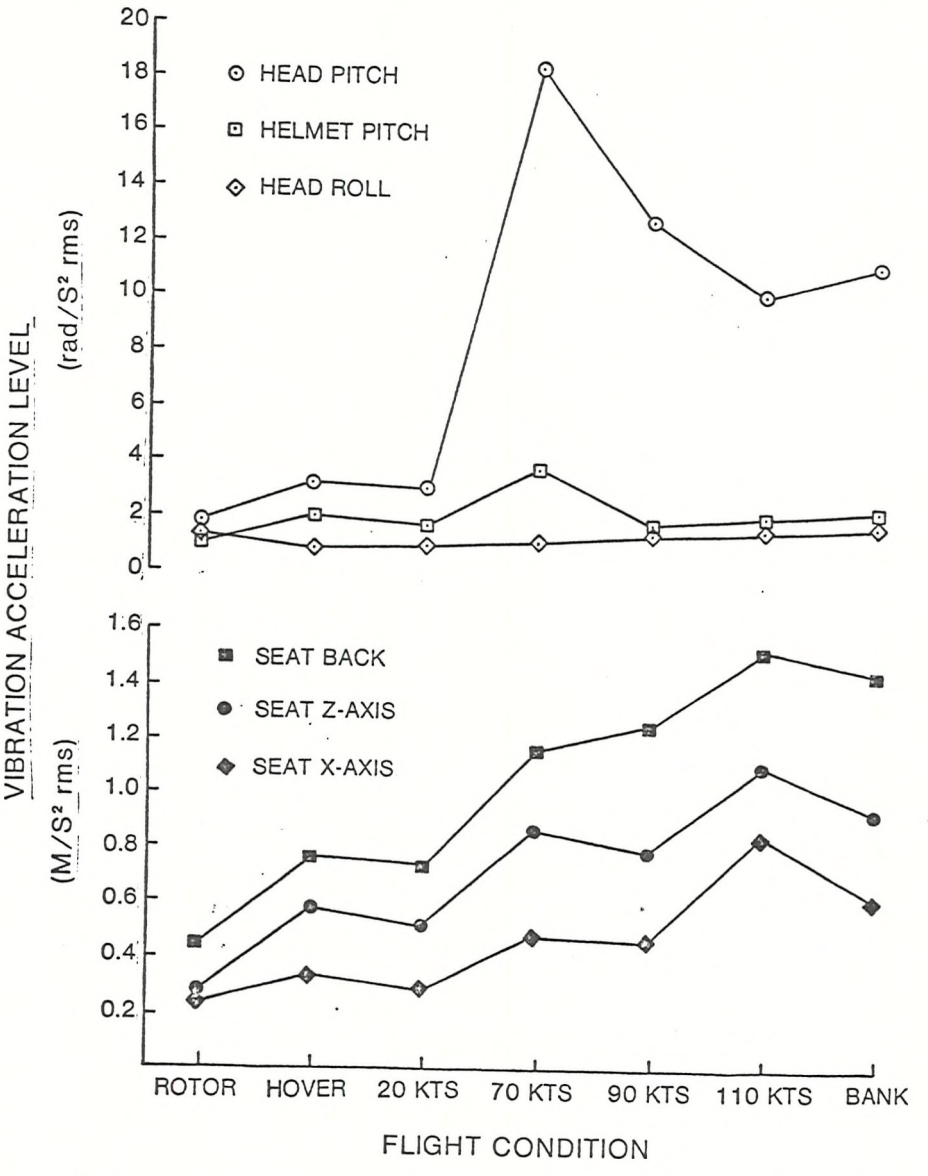

Figure 7.3.2. Mean Total RMS Vibration Levels of Head, Helmet, and Seat Motion as a Function of Flight Condition for Pilot A (Experiment H.2)

7.3.3.2 PSD Analysis

Power spectral densities (PSDs) were computed from the vibration acceleration time histories for the head, helmet, and seat motions described above. Representative PSDs are shown in Figures 7.3.3 and 7.3.4 for the seat, and head and helmet motions during the hover, 70 knots, 110 knots, and bank flight conditions. By inspection, it can be seen that the vibration responses of all parameters exhibited

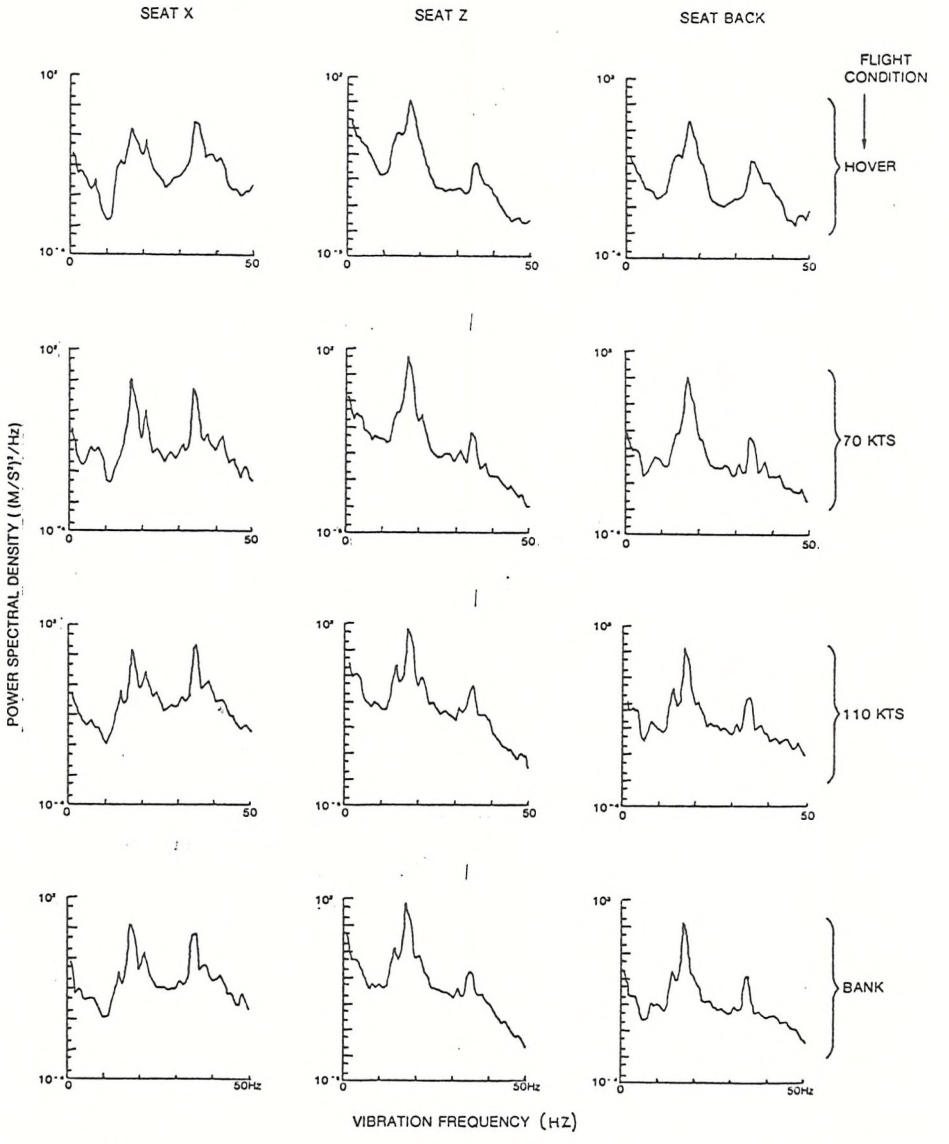

Figure 7.3.3. Power Spectral Densities of Seat X and Z Axes and Seat Back Vibration Acceleration for Pilot A During Four Helicopter Flight Conditions (B_e = 1.0 Hz, DOF = 100, Experiment H.2)

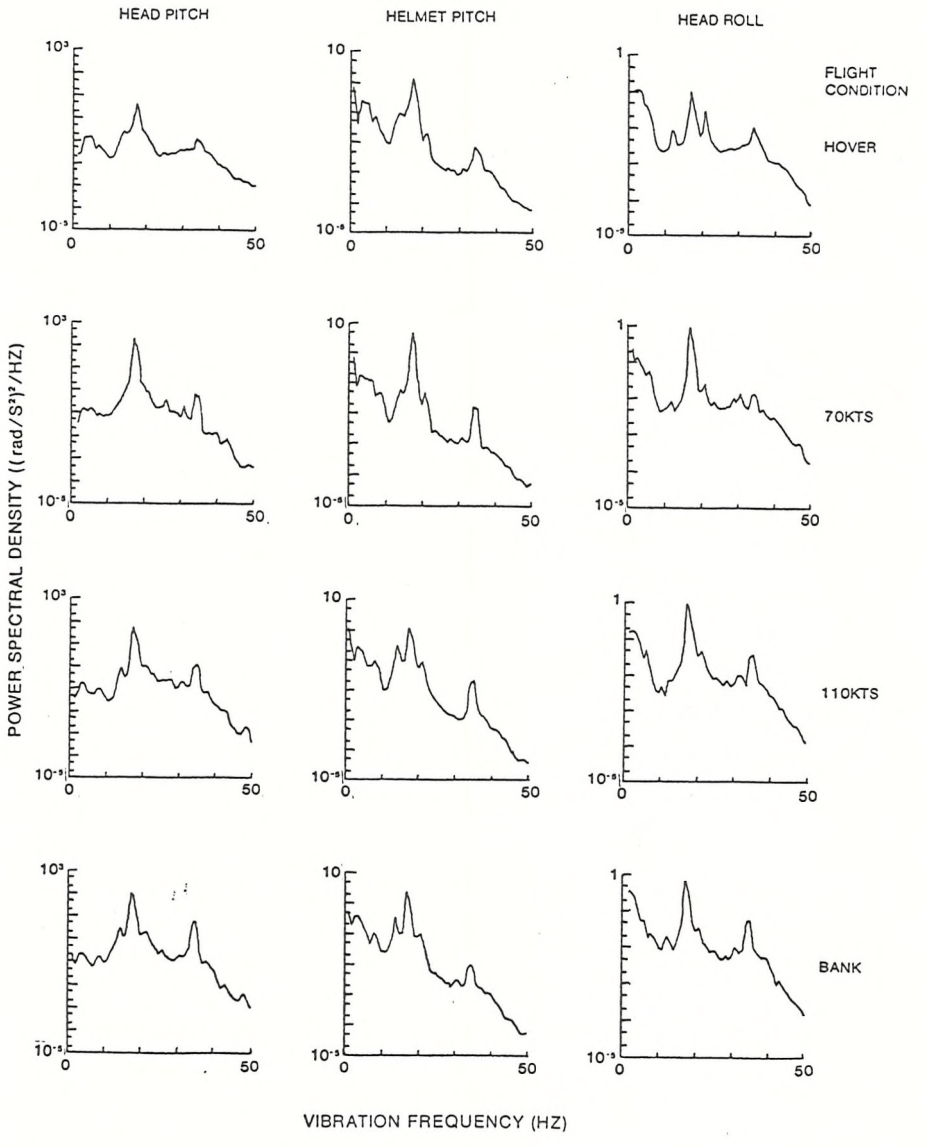

Figure 7.3.4. Power Spectral Densities of Head Pitch Axis, Head Roll Axis, and Helmet Pitch Axis Vibration Acceleration for Pilot A During Four Helicopter Flight Conditions (B_e = 1.0 Hz, DOF = 100, Experiment H.2)

deterministic properties (i.e., there was a concentration of vibration energy at approximately 17 Hz and 34 Hz). This response was present in the seat Z axis and seat back under all the flight conditions. The 17 Hz frequency corresponds to the main rotor blade passage frequency, i.e., the rate that main rotor blades pass over the fuselage. Under some flight conditions, the 34 Hz harmonic of the 17 Hz frequency predominated in the seat X axis motion. Head pitch and roll axis motion and helmet pitch motion also exhibited peak accelerations at 17 Hz; but, in addition, helmet pitch motion contained components of similar magnitude at frequencies less than 5 Hz.

An analysis of the PSDs was conducted by separating the 0 to 40 Hz frequency range into seven bands which isolated the main components of energy observed in the vibration spectra. The equivalent RMS vibration level within each frequency band was computed and the amount of power in that band related to the total power for that flight condition. A summary of this analysis is given in Table 7.3.2. Inspection of Table 7.3.2 shows that the spectral distribution of the vibration response was affected by the flight condition. While this effect was small for the three seat parameters, it was more pronounced for head roll and head pitch. For example, when the forward velocity of the helicopter increased from 20 knots to 70 knots, the head pitch acceleration at 17 Hz increased over 6 times from 2.45 to 15.9 rad/s^2 rms. However, additional increases in forward velocity reduced helmet pitch.

TABLE 7.3.2. SEAT, HEAD, AND HELMET VIBRATION LEVELS AT SELECTED FREQUENCIES IN SEA KING HELICOPTER

Flight Condition	Seat X							Seat Z							Seat Back						
	0-6 Hz		16-20 Hz		33-37 Hz		Total RMS	0-6 Hz		16-20 Hz		33-37 Hz		Total RMS	0-6 Hz		16-20 Hz		33-37 Hz		Total RMS
	m/s^2 rms	(% TP)*	m/s^2 rms	(% TP)	m/s^2 rms	(% TP)	m/s^2 rms	m/s^2 rms	(% TP)	m/s^2 rms	(% TP)	m/s^2 rms	(% TP)	m/s^2 rms	m/s^2 rms	(% TP)	m/s^2 rms	(% TP)	m/s^2 rms	(% TP)	m/s^2 rms
Rotor	0.13	(20.0)	0.10	(13.0)	0.18	(40.0)	0.28	0.22	(35.0)	0.28	(57.0)	0.05	(1.7)	0.37	0.12	(5.5)	0.44	(79.3)	0.10	(<.1)	0.49
Hover	0.09	(7.6)	0.17	(25.0)	0.24	(51.0)	0.34	0.25	(23.0)	0.44	(69.0)	0.03	(0.3)	0.53	0.20	(9.1)	0.59	(77.8)	0.13	(3.6)	0.66
20 Knots	0.07	(6.3)	0.14	(24.0)	0.20	(53.0)	0.28	0.19	(14.2)	0.45	(78.8)	0.03	(0.4)	0.50	0.18	(6.9)	0.64	(84.7)	0.08	(1.2)	0.70
70 Knots	0.10	(3.8)	0.36	(52.0)	0.30	(36.8)	0.49	0.22	(6.2)	0.85	(91.4)	0.04	(0.2)	0.89	0.15	(1.5)	1.17	(95.5)	0.10	(0.7)	1.20
90 Knots	0.12	(6.5)	0.33	(50.0)	0.25	(29.0)	0.47	0.34	(15.7)	0.76	(80.7)	0.02	(0.1)	0.84	0.16	(1.7)	1.22	(95.0)	0.08	(0.4)	1.26
110 Knots	0.14	(2.8)	0.48	(32.6)	0.62	(53.4)	0.85	0.36	(9.9)	1.04	(84.7)	0.09	(0.6)	1.13	0.24	(2.5)	1.45	(92.0)	0.18	(1.4)	1.51
Bank	0.17	(7.5)	0.44	(49.3)	0.35	(32.2)	0.52	0.37	(11.8)	0.97	(84.1)	0.06	(0.3)	1.06	0.23	(2.3)	1.50	(94.0)	0.17	(1.2)	1.54

Flight Condition	Head Pitch							Helmet Pitch							Head Roll						
	0-6 Hz		16-20 Hz		33-37 Hz		Total RMS	0-6 Hz		16-20 Hz		33-37 Hz		Total RMS	0-6 Hz		16-20 Hz		33-37 Hz		Total RMS
	rad/s^2 rms	(% TP)	rad/s^2 rms	(% TP)	rad/s^2 rms	(% TP)	rad/s^2 rms	rad/s^2 rms	(% TP)	rad/s^2 rms	(% TP)	rad/s^2 rms	(% TP)	rad/s^2 rms	rad/s^2 rms	(% TP)	rad/s^2 rms	(% TP)	rad/s^2 rms	(% TP)	rad/s^2 rms
Rotor	0.58	(9.6)	1.44	(58.6)	0.28	(2.2)	1.88	1.48	(77.1)	0.64	(14.5)	0.11	(0.4)	1.68	2.58	(39.0)	1.20	(8.4)	0.87	(4.5)	4.13
Hover	0.71	(5.6)	2.60	(74.7)	0.55	(3.4)	3.01	1.69	(53.1)	1.42	(37.8)	0.14	(0.4)	2.33	0.71	(63.7)	0.37	(17.6)	0.16	(3.3)	0.89
20 Knots	0.95	(11.3)	2.45	(75.6)	0.44	(2.5)	2.81	2.32	(76.6)	1.16	(19.1)	0.10	(0.1)	2.65	1.40	(88.2)	0.29	(3.7)	0.13	(0.7)	1.49
70 Knots	0.81	(0.3)	15.9	(97.0)	1.12	(0.5)	16.15	2.37	(42.4)	2.66	(53.6)	0.19	(0.3)	3.64	1.41	(56.2)	1.13	(36.0)	0.18	(1.0)	1.88
90 Knots	0.82	(0.5)	11.1	(94.2)	0.86	(0.6)	11.44	2.17	(62.6)	1.47	(28.8)	0.08	(0.1)	2.74	1.24	(53.2)	1.03	(36.8)	0.14	(0.6)	1.70
110 Knots	0.69	(0.7)	8.0	(88.2)	1.40	(2.7)	8.52	1.93	(54.9)	1.42	(29.6)	0.20	(0.6)	2.61	0.90	(32.3)	1.16	(53.5)	0.27	(2.9)	1.59
Bank	1.16	(0.8)	12.1	(86.4)	3.21	(6.1)	13.01	1.91	(45.2)	1.83	(41.6)	0.14	(0.3)	2.84	2.12	(75.3)	1.02	(17.4)	0.34	(2.0)	2.44

*Figures in brackets represent the percentage of total power over a bandwidth of 0 to 40 Hz contained in the specific frequency band.

7.3.3.3 Relationships of Seat, Head, and Helmet Motions

The relationships[1] of helmet pitch, head pitch, and seat Z motion are shown in Figures 7.3.5, 7.3.6, and 7.3.7 for four flight conditions. These curves were obtained by computing the ratios of the square roots of the appropriate PSDs.

It should be noted from these curves that, while there was little effect of flight condition on the ratio of helmet pitch to seat Z motion (at those frequencies of 2 to 6 Hz and 17 Hz wherein the helmet pitch and seat Z vibration energy were the greatest), there was a large effect of flight condition in the head-pitch to seat Z axis motion. For example, when going from the hover to the 70 knots flight condition, the head pitch to seat Z transmissibility ratio varied from 5.4 to 18.7 rad/m while helmet pitch to seat Z ratio remained approximately constant at 2.6 rad/m. These differences are reflected in the helmet pitch to head pitch ratio curves in Figures 7.3.7.

As a check on the validity of the helmet pitch to head pitch ratio curves obtained above using the PSD analysis, the coherency functions between helmet pitch and head pitch where computed using the time histories for the four flight conditions. From the coherency function, it can be surmised that the movements of the helmet were correlated [i.e., $\gamma^2(f) \geq 0.5$] with the movements of head within the frequency regions of 2 to 10 Hz, 14 to 18 Hz, and 33 to 35 Hz. (These are the same regions as shown in Figure 7.3.4 wherein the head pitch energy levels were the greatest.)

[1]Note: These ratios cannot be assumed to be transfer function relationships in that the correlation between the output (e.g., head pitch) relative to an input (e.g., seat Z) was not established. Furthermore, the magnitudes of the relationships will contain noise, uncorrelated movements, and can only be considered as valid estimates within those vibration frequency regions wherein sufficient vibration energy was available in the seat (i.e., less than 20 Hz).

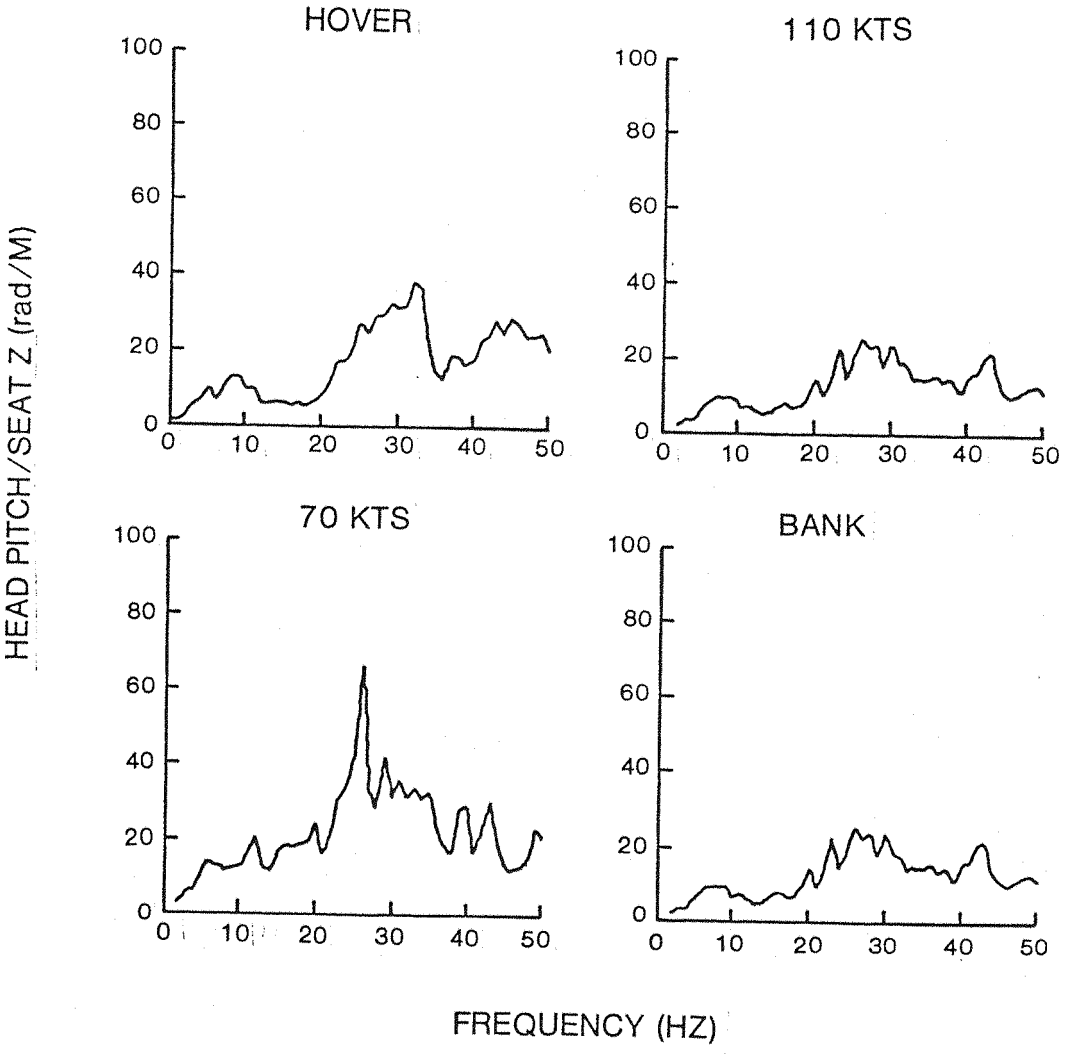

Figure 7.3.5. Ratio of the Square Roots of the PSDs for Head Pitch Acceleration and Seat Z Axis Acceleration for Four Flight Conditions (B_e = 1.0 Hz, DOF = 100, Experiment H.2). (Note: The Ratios of Head Pitch Axis to Seat Z Axis at Frequencies Above 20 Hz are Probably Inaccurate due to Very Low Measured Vibration Levels, see Text.)

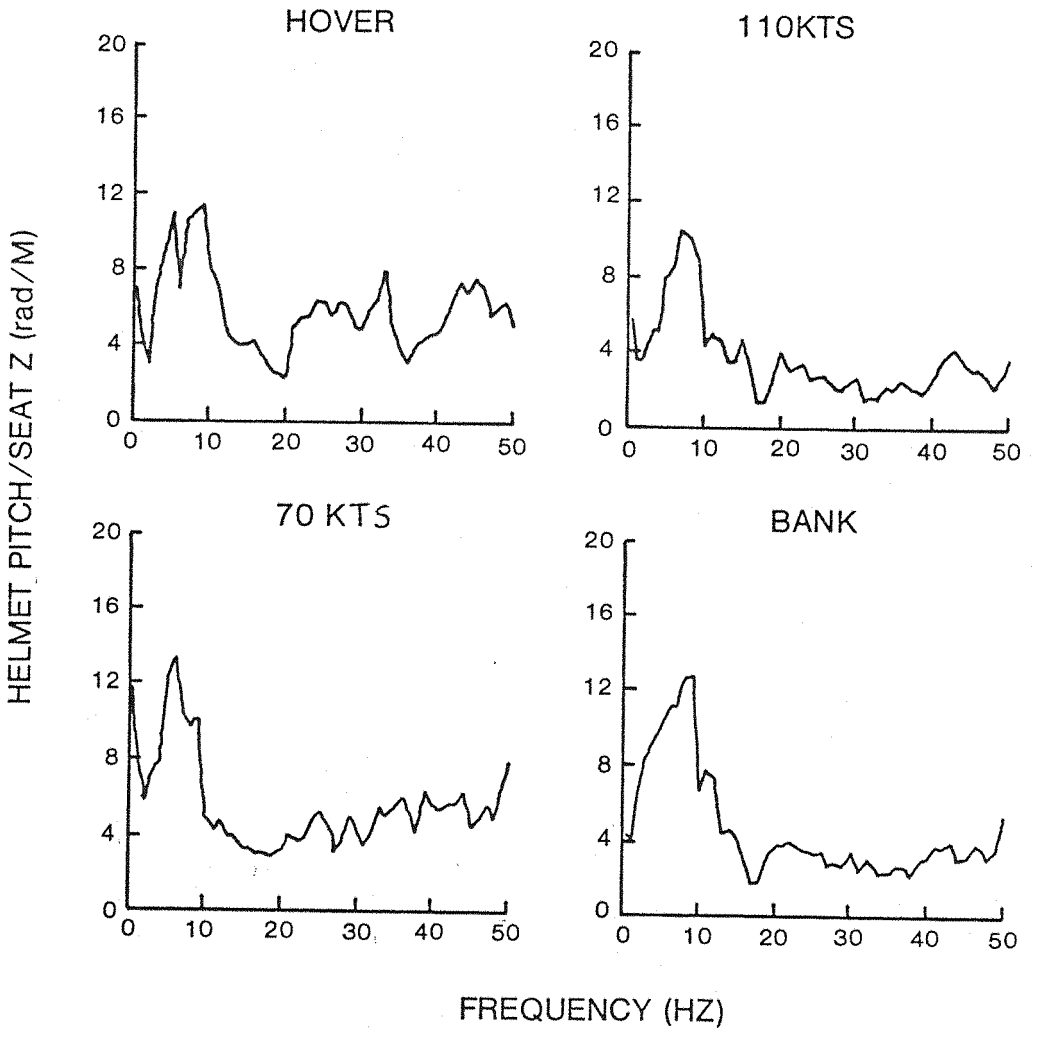

Figure 7.3.6. Ratio of the Square Roots of the PSDs for Helmet Pitch Acceleration and Seat Z Axis Acceleration for Four Flight Conditions (B_e = 1.0 Hz, DOF = 100, Experiment H.2) (Note: Ratios of Helmet Pitch to Seat Z Axis at Frequencies Above 20 Hz are Probably Inaccurate due to Very Low Measured Vibration Levels, see Text.)

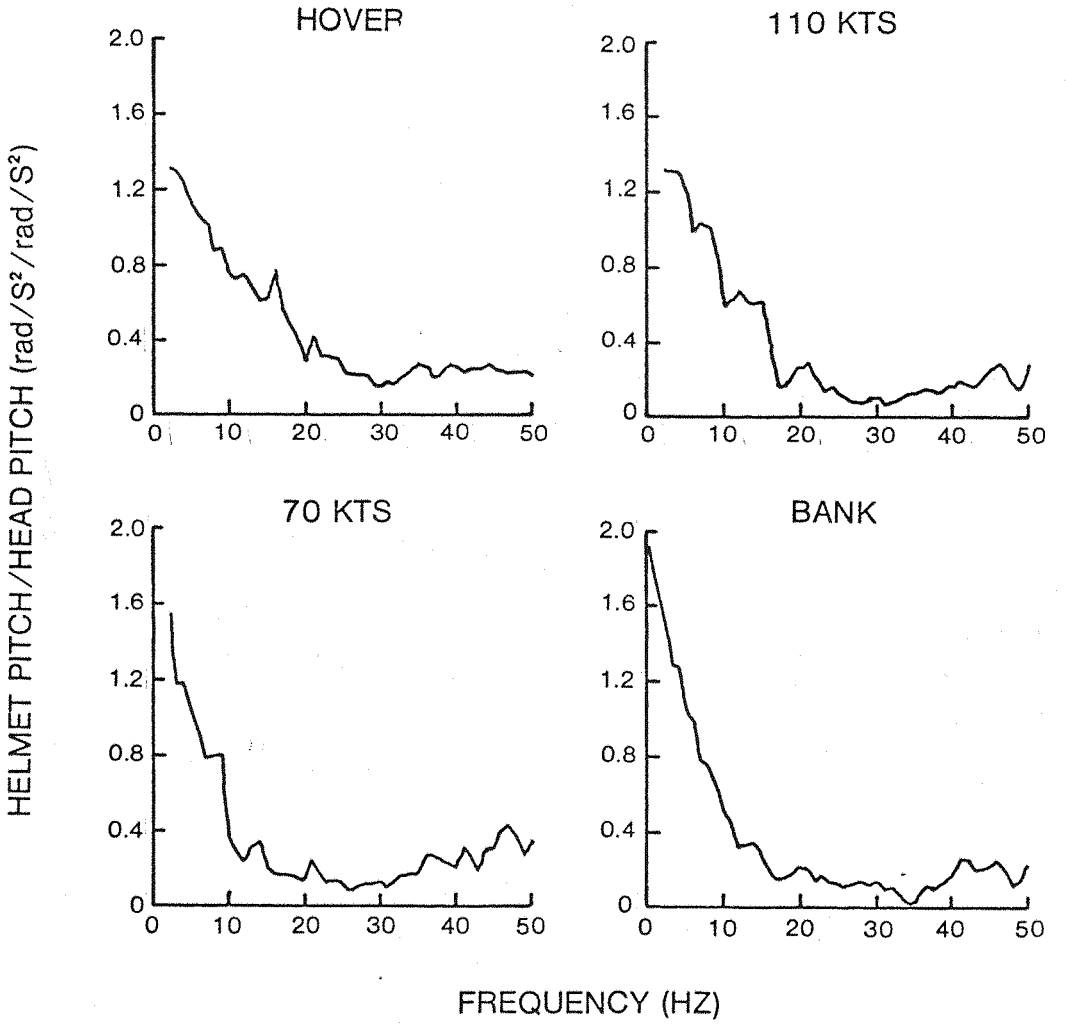

Figure 7.3.7. Ratio of the Square Roots of the PSDs for Helmet Pitch Acceleration and Head Pitch Acceleration for Four Flight Conditions (B_e = 1.0 Hz, DOF = 100, Experiment H.2)

Transfer functions of the helmet pitch to head pitch were then computed using the cross spectral distribution method (Appendix A.5.1). The moduli of the helmet pitch to head pitch transfer functions are shown in Figure 7.3.8 for four flight conditions. (Note: The modulus values are indicated only for those frequencies wherein the coherency functions were determined to be equal or greater than 0.5. Within those regions the estimates of the actual modulus values were considered to be statistically reliable, that is, assuming system linearity).

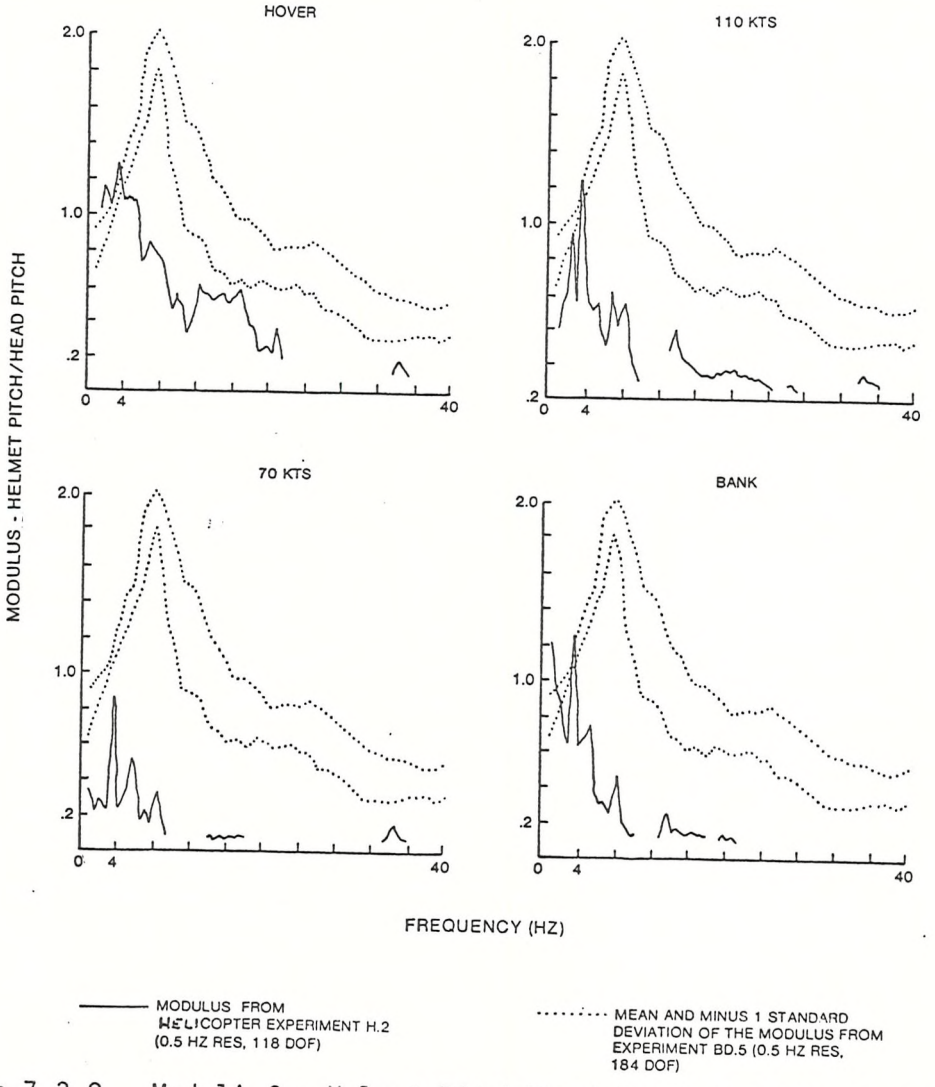

Figure 7.3.8. Moduli for Helmet Pitch/Head Pitch Transfer Functions for Four Flight Conditions in Experiment H.2 Compared with the Mean and Minus One Standard Deviation of the Helmet Pitch/Head Pitch Modulus from Experiment BD.5

Also shown in Figure 7.3.8, for comparison, are the mean moduli and -1 standard deviation of the helmet pitch/head pitch transfer functions

obtained under laboratory conditions in Experiment BD.5 (Section 5.5). Except for the peak in head to helmet pitch transmissibility at approximately 4 Hz, the gain of helmet to head transmissibilities generally were far less in flight than within the laboratory. (Of course, these data were obtained with different subjects.) One explanation for the dichotomy of laboratory and in-flight helmet to head coupling may have been due to nonlinearities in the helmet to head motion. Figure 7.3.9 shows that at approximately 17 Hz, the various head pitch vibration accelerations obtained during the seven flight conditions produced different helmet pitch to head pitch ratios. (For the system to be linear, the data should have remained on a line of constant slope.) The smaller head pitch accelerations during the hover, rotor, and 20 knots flight condition produced helmet to head ratios approximately linear and almost within ±1 standard of the same magnitude as the laboratory data from Experiment BD.5. However, further increases in head pitch acceleration at 110 knots, 90 knots, and bank produced very little increase in helmet pitch acceleration. Figure 7.3.9 also shows a large difference between the helmet pitch/head pitch ratio of power spectra and the transfer function gain at 70 knots. This indicates that a relatively large part of the helmet motion was not correlated with the head motion. Similarly, as shown in Figure 7.3.10, nonlinearities were observed for the seat Z to head pitch motion at 17 Hz during the various flight conditions. Although the rotor, hover, 20 knots, and 110 knots conditions produced head pitch to seat Z ratios commensurate with the laboratory data, the 70 knots, 90 knots, and bank conditions caused head pitch accelerations, which relative to the seat Z accelerations present, exceeded the laboratory data. While the helicopter data for head pitch to seat Z at 17 Hz did not correspond to the laboratory data, the helmet pitch to seat Z response during flight in vibration frequencies less than 10 Hz agreed well with the laboratory data. The helmet pitch to seat Z ratio previously shown in Figure 7.3.6 is reproduced in Figure 7.3.11 along with the mean ratio data (square roots of ratio of PSDs) from Experiment BD.5. (Note that here is a difference in the resolution of the two sets of data.)

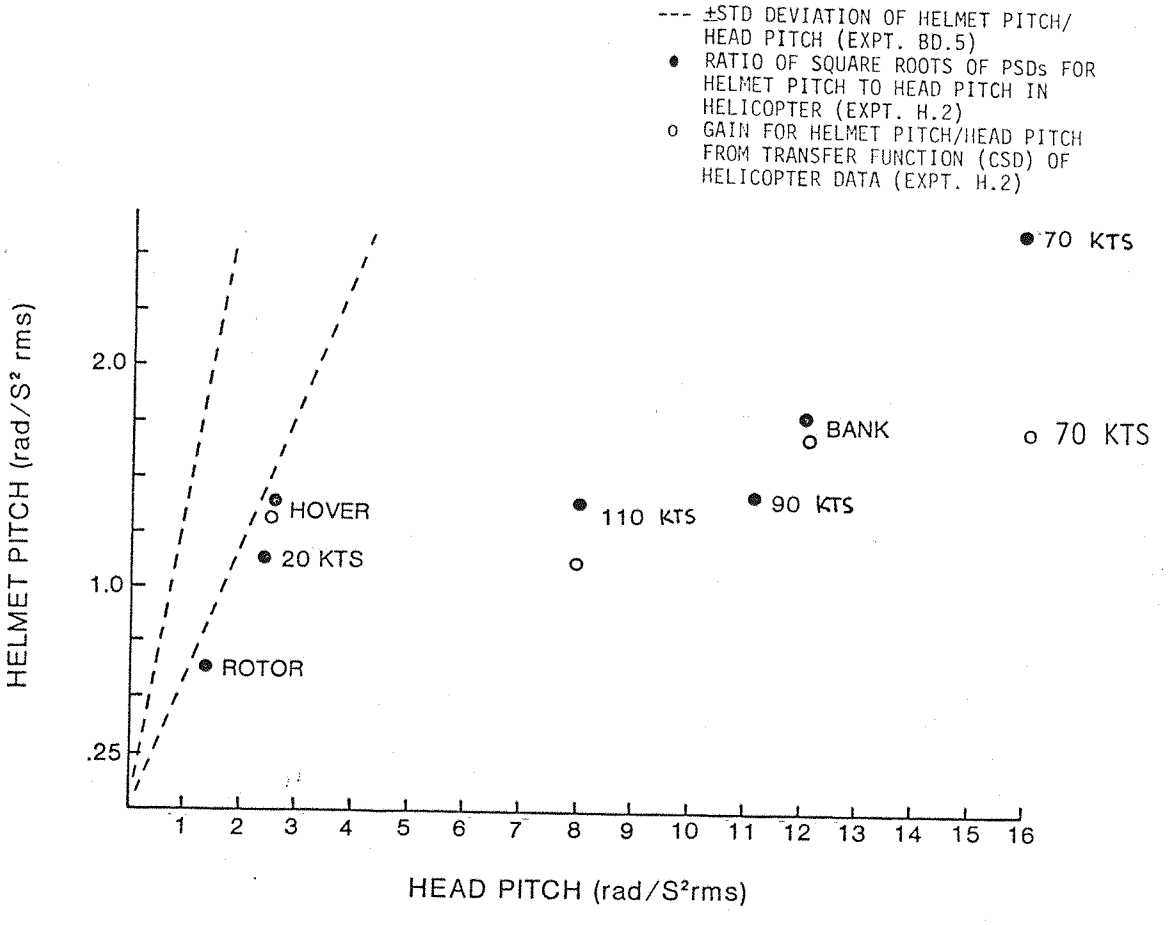

Figure 7.3.9. Relationships of Helmet Pitch to Head Pitch RMS Vibration Levels at 17 Hz for all Helicopter Flight Conditions Compared to ±1 Standard Deviation of the Helmet Pitch/Head Pitch Transfer Function Gain at 17 Hz from Experiment BD.5 (Also Shown are Gains at 17 Hz from the Helmet Pitch/Head Pitch Transfer Functions During the Four Flight Conditions in Figure 7.3.8

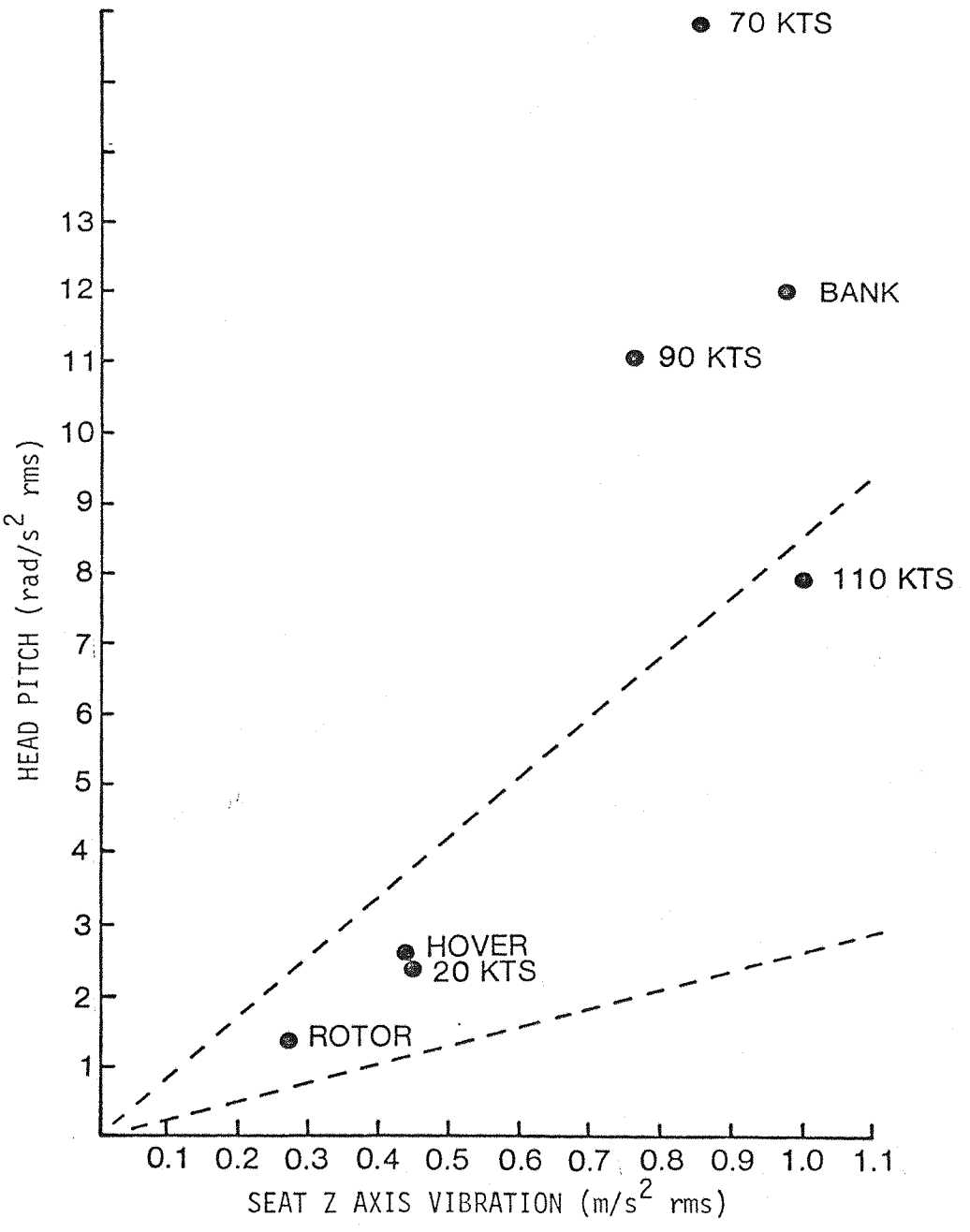

Figure 7.3.10. Relationships of Head Pitch to Seat Z Axis rms Vibration Levels at 17 Hz for all Helicopter Flight Conditions Compared to ±1 Standard Deviation of the Head Pitch/Seat Z Axis Transfer Function Gain at 17 Hz from Experiment BD.5

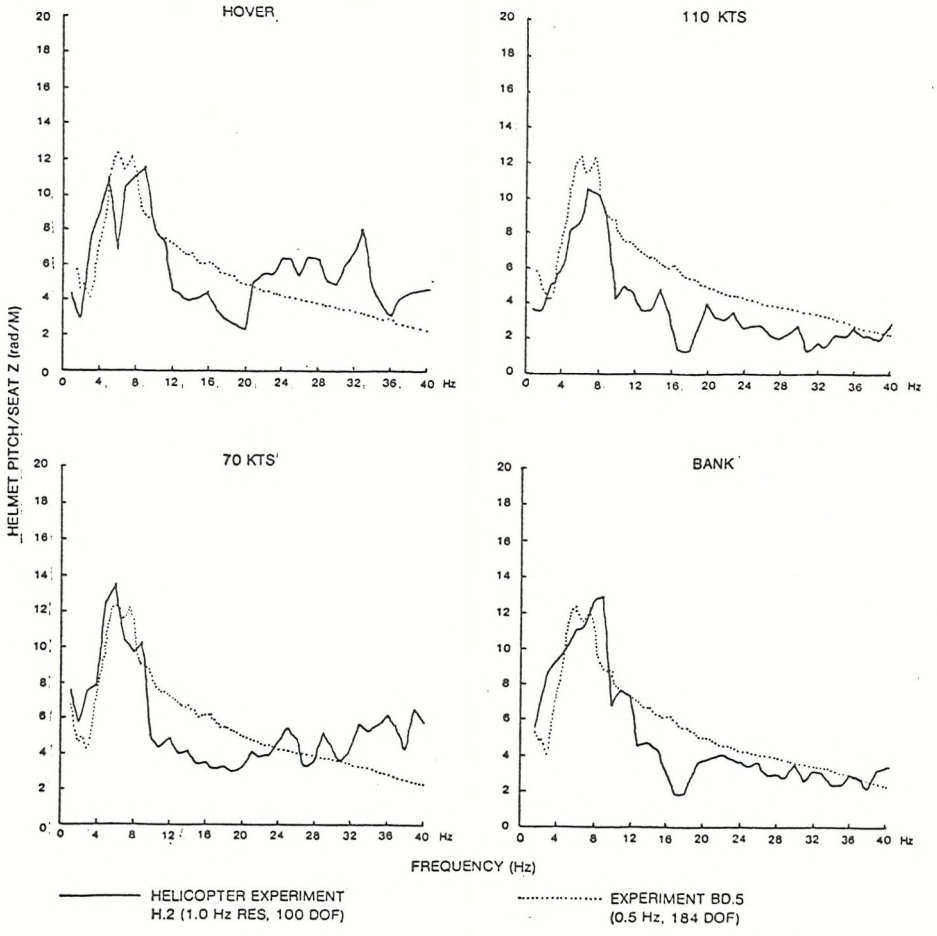

Figure 7.3.11. Ratio of the Square Roots of the Power Spectral Densities of Helmet Pitch to Seat Z Axis Vibration for Four Helicopter Flight Conditions as Compared to Similar Data From Experiment BD.5

7.4 DISCUSSION

7.4.1 General Observations

The nature of the vibration measured at the seat of the SEA KING helicopter under the various flight conditions was typical of that measured in similar aircraft during other experiments (e.g., Grimster et al., 1974). The predominant vibration frequency was approximately 17 Hz, which can be attributed to the effect of the main rotor blade passage above the fuselage. The low frequency vibration "lumped" into the 2 to 6 Hz frequency region can be ascribed to artifacts in the

main rotor frequency (i.e., approximately 3.4 Hz) and to the aerodynamic properties of the aircraft and the effect of wind, ground buffet, and other external factors. Since the dynamic and legibility experiments were conducted during separate flights in the aircraft, it was also possible that the biodynamic measurements did not completely reflect the vibration conditions during which the reading tasks were performed. Differences in the weather conditions and fuel load may have changed slightly the helicopter vibration motions between the two experiments.

7.4.2 Biodynamics Experiment

The Experiment H.2 reported above was one of the first to record the rotational movements of the head and helmet during flight in a helicopter. It was not surprising that the dynamic response of the head in the pitch axes during flight was dissimiliar to that measured in the laboratory during Experiment BD.5 and others. As discussed in Section 2.5.3.11, factors which may have contributed to differences between the in-flight and laboratory biodynamic responses may have been due to the nature of the seat, seating posture, multiple vibration paths, multiple axis seat motion, and multiple frequency vibration. Some aspects of these factors are discussed below.

Since the seat vibration in the helicopter was measured at the interface to the subject, the fact that the main paths of vibration were coupled to the subject through seat cushions should not have affected the measurement of the effective vibration input to the subject. However, two other paths of vibration input were present in the floor vibration input to the feet of the subject and the vibration of the cable to the helmet-mounted display. While it is unlikely that these paths had any significant influence in the rotational behaviour of the head and helmet, the multiple axis nature of the seat motion probably had a great influence on head motion dynamics.

As was seen from the data presented in Table 7.3.2, motion of the seat back (predominantly in the fore-aft X axis) was consistently greater than that of the seat base in either the vertical Z axis or fore-aft X axis directions. Based upon the findings reported by Lewis (1979b)

and discussed in Section 2.5.3.7, one would predict that the combined vibration input of the seat base in the X axis and Z axis and the seat back caused greater head pitch motion than if only the seat Z axis motion were present, as in Experiment BD.5. Furthermore, the seat back tended to "amplify" (typically by a factor of 4) the motion observed in the X axis of the seat base. It is postulated that the combined motion of the seat base and seat back in the X and Z axes caused the increase in head pitch motion for 70 knots, 90 knots, 110 knots, and bank flight conditions over that observed under similar vertical Z axis vibration levels in the laboratory.

Since the biodynamic data from only one subject was analyzed, individual subject effects could not be assessed. Seating posture is one individual factor which, according to the evidence presented in Section 2.5.3.4, can significantly affect the transmission of vibration to the head. Both pilot subjects commented that they usually adopted a posture during flight which maximized visibility from the cockpit. This postural position changed as a function of flight condition since the attitude of the helicopter changed. Typically, according to the aircrew, this posture involved sitting forward in the seat, often with the back not in complete contact with the seat back.

While the relationship of head pitch motion to seat motion was expected to be somewhat different in the helicopter than in the laboratory, a significant difference in the helmet pitch to head pitch was not expected. The nonlinear behaviour of the helmet on the head in the pitch axis was seen in Figure 7.3.9 for the vibration frequency at 17 Hz. Also, as shown in Figure 7.3.9, the modulus of the helmet pitch to head pitch was far below that measured in the laboratory, nor was there any characteristic peak at 8 Hz as observed in Experiments BD.5 and BD.7. Using the present data, it is possible to speculate only as to the reasons for the differences between the laboratory and flight results regarding head and helmet pitch relationships:

1. The helmet may have had a rather loose fit on the head;

2. The axis of rotation of the head and, hence, its affect on the helmet was different during flight, especially with the vibration input of the seat back;

3. The motion of the helmet on the head was nonlinear at lower vibration levels, which was not apparent in the laboratory experiments when higher vibration levels were used.

Using the argument in 3 above and the findings of Jarrett (1978), it is possible to divide the helmet to head pitch movement into three regions:

Region I: Helmet pitch to head pitch motion due to the rotational compliance of the scalp.

Region II: Slip of helmet on the head causing lower helmet pitch/head pitch gain.

Region III: Effect of head movement restraints to limit movement of helmet on the head (i.e., chin strap, nape strap, etc.).

Since the data reported was for only one subject, further experimentation is required to verify that a real nonlinearity exists and to investigate its causes.

7.4.3 Legibility Experiments

The intent of the helicopter legibility experiment (H.1) was to duplicate the stimulus presentation of Experiment LG.3 using an array format. In neither the static nor the helicopter vibration conditions were errors produced, even though the aircrew expressed difficulty and uncertainty in reading the 12 and 15 minutes-of-arc characters. The results under static conditions were generally consistent with those obtained in Experiment LG.3. The luminance conditions in the laboratory versus the aircraft were slightly different in that the background

luminance for the characters in the airborne experiment consisted of the ambient luminance (approximately 3000 cd/m^2) attenuated by the visor and variable transmission filter to approximately 0.24 cd/m^2, as opposed to the 0.50 cd/m^2 background luminance presented by the raster in Experiment LG.3. Another difference was the luminance presented to the left eye. In the case of the airborne experiment, this luminance was approximately 450 cd/m^2 whereas in the laboratory Experiment LG.3, the luminance presented to the left eye was zero. (Note: the left eye in the airborne experiment was not occluded for safety-of-flight purposes, and to present a realistic cockpit display viewing task.) In any case, the ambient, or background luminance, of the display was sufficient to provide good visibility of the characters under both static and in-flight vibration conditions. In this regard, the character and background luminances and contrast were close to the ideal display presentation conditions found in Experiment LG.4.

Since the predominant frequency of vibration in the helicopter was 17 Hz, the data for the 16 Hz vibration condition in Experiment LG.3 (Figure 4.4.2) would normally provide a proximate basis for comparing the laboratory and flight test results. The seat Z axis vibration in the laboratory was set at 1.0 m/s^2 rms. The seat Z axis acceleration in the helicopter achieved this level only during the 110 knots flight condition. However, due to the influence of the seat back motion as discussed above, the head pitch motion induced by the multiple axis seat motion was greater than that in the laboratory. It is, therefore, more reasonable to estimate the magnitude of image displacement occurring during flight based upon the results of Experiment SD.2 in Chapter 6.

The maximum pitch accelerations of the helmet and head occurred at 17 Hz during the 70 knots flight condition, corresponding to 0.23 degree peak-to-peak (15.9 rad/s^2 rms) and 0.04 degree peak-to-peak (2.7 rad/s^2 rms) angular displacements of the head and helmet, respectively. To determine the displacement of the display image relative to the retina of the eye, the magnitude and phase relationships of eye-to-head movement and helmet-to-head movement must be known. Since these data are not available, the image displacement on

the retina can only be estimated, given some assumptions. In accordance with the eye movement behaviour discussed in Chapter 6.0, it is likely that at 17 Hz, the vibration induced movement of the eyes approximated that of the head (i.e., the bandwidth of the VOR being limited beyond 10 Hz). Depending upon the phase relationships of helmet to head movements, the angular displacement of the optical axis of the display to the eye could range from 11.4 minutes-of-arc to 16.2 minutes-of-arc, depending upon phase relationships.

When compared with the mean estimated subjective displacement of 17.6 minutes-of-arc obtained in Experiment SD.2 (Table 6.2.6) for a 16 Hz seat vibration frequency, the image displacement data calculations for the present experiment appear to be reasonable. It can be surmised then that under the helicopter flight conditions, the attendant background luminance, combined with the helmet and head vibration levels, were insufficient to produce viewing conditions which would cause reading errors, even though a 16.2 minutes-of-arc image displacement would be greater than that subtended by the height of the smallest character.

7.5 SUMMARY AND CONCLUSIONS

The helicopter experiments reported above provided a basis for comparing the results of the laboratory biodynamic and legibility experiments with those in-flight. Since the results above were obtained for only two subjects, these findings cannot be considered as conclusive, but more as a possible indication of trends. The key findings of the helicopter biodynamic experiment were that: (1) the vibration energy input of the seat and seat back and response of the head and helmet was concentrated at 17 Hz, corresponding to the main rotor passage frequency; (2) the biodynamic experiments also showed that the vibration level of the seat was affected by the flight condition which, in turn, caused different levels of head and helmet rotational vibration; and (3) the relationship of helmet to head vibration was also shown to be affected by the flight condition. Differences in the ratios of the helmet pitch to head pitch between in-flight and laboratory findings were attributed to the multi-axis nature of the seat motion in-flight,

and especially the contribution of the seat back in increasing the pitch axis motion of the head. This experiment probably represented the first time that the in-flight rotational movements of the head and helmet have been reported in the literature.

In spite of the vibration levels experienced by the subjects in the helicopter legiblity experiment, no reading errors were committed, regardless of the character size or flight condition. The smallest and largest character sizes were subjectively the most difficult to read on the helmet-mounted display. The main complaint about the largest character sizes (i.e., 29 and 36 minutes-of-arc) was the difficulty of searching the total field-of-view or format size of the display, and not the legibility of the individual characters. Given the vibration levels measured in the helicopter and the luminance and contrast characteristics of the visual stimulus, it would be predicted from the laboratory findings (Experiments LG.3 and LG.4) that very few reading errors, if any, would be produced. From this standpoint, the flight data agrees with the laboratory data. It is apparent that the ambient background luminance to the display eye was within the range to improve the visibility of the characters (especially for the 12 minutes-of-arc characters) and reduce the effects of vibration on display perception commensurate with the findings of Experiments LG.3 and LG.4.

It can be concluded from the experiment that, at least for the flight conditions and luminance conditions experienced in the SEA KING helicopter during this experiment, the visibility of this helmet-mounted display will not be seriously degraded. From the subject comments, character sizes of at least 22 minutes-of-arc are recommended. More study is necessary to quantify the nature of the interaction of head and helmet motion during flight or any complex multiple-axis vibration environment.

Chapter 8
EFFECTS OF VIBRATION AND IMAGE STABILIZATION ON THE PERCEPTION OF TARGET IMAGERY PRESENTED ON THE HELMET-MOUNTED DISPLAY (EXPERIMENT ST.1)

8.1 BACKGROUND AND EXPERIMENTAL CONSIDERATIONS

In the laboratory experiments described above, the legibility of the helmet-mounted display was determined by measuring the accuracy of reading numeric characters, presented with a homogeneous (uncluttered) background. During whole-body vibration, the perception of these characters was facilitated by the formation of nodal images at the zero velocity points of the relative movement between the optical axes of the eye and the display.

Because the appearance of nodal images of continuous half-tone scenes may be different than for discrete information, there is some question about the applicability of character legibility results to display presentations of pictorial information should the helmet-mounted display be used with an imaging sensor (e.g., Section 2.2.4).

8.1.1 Vibration Effects on Sensor Imagery

The presentations of sensor images may be described as continuous two dimensional distributions of luminances representing spatial and spectral (reflective or emissive) aspects of the world as transduced by the sensor. Information of high interest (e.g., targets) in this imagery will probably consist of spatially complex arrangements of luminances presented on backgrounds which are also spatially complex. Typically, targets are recognized by distinguishing features which may appear as low contrast and high spatial frequency details in the display scene. It can be anticipated that whole-body vibration causing the formation of nodal images of such scenes will obscure some of the essential low contrast detail due to overlap of the target with itself and with a complex background. There have been no experiments reported in the literature on the effects of object or whole-body vibration on the perception of sensor imagery.

8.1.2 Display Stabilization Considerations

In Chapter 6 the reduction in the legibility of the helmet-mounted display was shown to be related to the relative movement of the eye and display causing a displacement of the image on the retina. The magnitude of the vertical displacement was approximately equal to the angular displacement of the helmet in the pitch axis for vibration frequencies up to about 5.6 Hz. (This apparently corresponded to the approximate bandwidth of the vestibulo-ocular reflex.) It follows from these findings that reducing the displacement of the image on the retina by some means may improve performance. If the helmet display image is made to appear stable in space (i.e., independent of head and helmet movement) for frequencies wherein the vestibulo-ocular reflex is operative, it is postulated that reading performance will improve.

8.1.3 Methods of Helmet-Mounted Display Stabilization

Ideally, a stabilization approach should align the display image dynamically to the involuntary movements of the eye produced by the whole-body vibration. To accomplish such an ideal stabilization system, a dynamic measurement of eye movements must be made across a range of vibration frequencies and used to control the orientation of the display image relative to the eye. To date, suitable methods for measuring eye movement under whole-body vibration frequencies greater than 5.0 to 6.0 Hz have not been developed (e.g., Young and Sheena, 1975). Since the movements of the eyes have been shown in the experiments reported above and by others (e.g., Benson and Barnes, 1978) to be almost stable in space for head rotational movements between approximately 1.5 Hz and 8.0 Hz, proximate stabilization of the display image relative to movements of the eyes can be derived from the pitch motion of the helmet.

In the experiment described below, a simplified stabilization method was used which approximated the space stabilization of the helmet-mounted display image. This method, though not ideal, used simple components which were readily available and required only minor modification to the display electronics. Details of Experiment ST.1 and the stabilization system are given below.

8.1.4 Objectives of Experiment

The objectives of the current experiment were twofold: the first objective was to investigate the effects of vertical Z axis whole-body vibration on the perception of pictorial imagery presented on the helmet-mounted display. The second objective was to assess the use of a simple stabilization technique for reducing image displacement on the retina. For this experiment, simulated sensor images were used as visual material instead of the numeric characters reported for earlier experiments.

8.2 METHOD

8.2.1 Visual Material

The visual material presented on the helmet-mounted display consisted of video tape replays (IVC Model 826P) of simulated airborne approaches (i.e., optical zoom) to ground military targets. Six targets (Sherman tank, M-60 tank, uncovered truck, covered truck, half-track, and mobile gun) were presented in a random sequence at four different orientations. Photographs of the targets and immediate background are shown in Figure 8.2.1. The horizontal and vertical dimensions of the raster on the cathode-ray tube were adjusted so that the target length subtended a visual angle of 0.64 degrees at the observer's eye at the beginning of the zoom run and 6.40 degrees at the end of the zoom run. The maximum duration of each target approach was 20 seconds. The average target luminance was 2.1 cd/m^2, and average background luminance was 48.4 cd/m^2, for an average target-to-background contrast of approximately 96 percent for all the targets. The visual material was presented on the same helmet-mounted display as described previously.

8.2.2 Vibration

Vertical, Z axis sinusoidal motion was presented to the subjects during the experimental runs using the electrodynamic vibrator described previously. Subjects were seated and restrained in the modified helicopter-type seat also described previously.

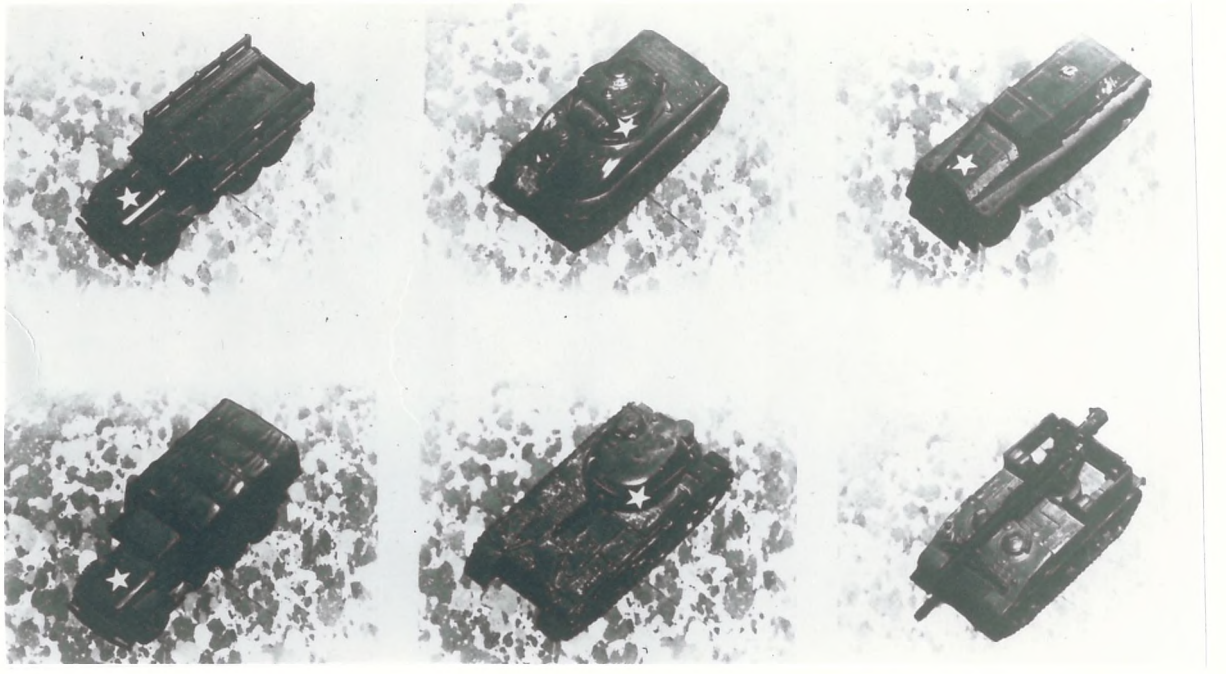

Figure 8.2.1. Targets and Target Backgrounds used in Experiment ST.1

For this experiment, the frequency of oscillation of the seat was set at 4.0 Hz with an amplitude of 1.0 m/s^2 rms. This vibration frequency was shown in previous experiments (i.e., LG.1 and LG.2) to produce the greatest degrading effects in character legibility when using the same helmet-mounted display.

8.2.3 Image Stabilization System

Proximate stabilization of the helmet-mounted display image in space was accomplished by displacing the raster vertically on the cathode-ray tube as a function of the signals received from an angular servo accelerometer (Schaevitz Engineering Model ASMP-100) mounted on the helmet. The sensitive axis of the accelerometer was aligned with the pitch axis of the helmet. The feedback network from the accelerometer performed a 180 degree phase shift of the acceleration measurements and allowed manual adjustment of feedback gain to the vertical deflection amplifier in the helmet-mounted display electronics. The stabilization network "simulated" a double integration of the accelerometer

signals in order to obtain some instantaneous measure of helmet rotational displacement in space; however, the gain adjusted in the stabilization system was only valid for one discrete frequency of helmet pitch motion at a time. Harmonic distortion in helmet pitch motion would, therefore, degrade the quality of the stabilization system. (True space stabilization under other than these ideal conditions must be accomplished by performing a continuous double integration of the accelerometer output.) Angular displacements of the display image of up to 4.6 degrees (peak-to-peak) could be provided by this stabilization system. Figure 8.2.2 shows a diagram of the helmet-mounted display stabilization and vibration equipment used in the experiment.

8.2.4 Subjects

Ten subjects were used in the experiment (S1, S3, S4, S5, S7, S8, S11, S12, S13, S14). Physical characteristics of the subjects are given in Table 3.4.1.

8.2.5 Experiment Design

There were four main conditions used in the experiment; two control (no vibration) conditions, one vibration condition without image stabilization, and one vibration condition with image stabilization. The subjects task during all conditions was to identify each "zoom target" as soon as possible during each zoom run. The independent variables in the experiment were vibration/stabilization conditions, target type, and target orientation. Dependent variables were target subtended angle at the time of identification and accuracy of identification.

The subjects were divided into two groups of five subjects each. Both groups received the control conditions for the first and last conditions. For the second condition, one group received the vibration without stabilization and the other group the vibration with stabilization. For the third condition, the groups were reversed, (i.e., the first group received the vibration with stabilization and the second group received the vibration without stabilization). Each condition

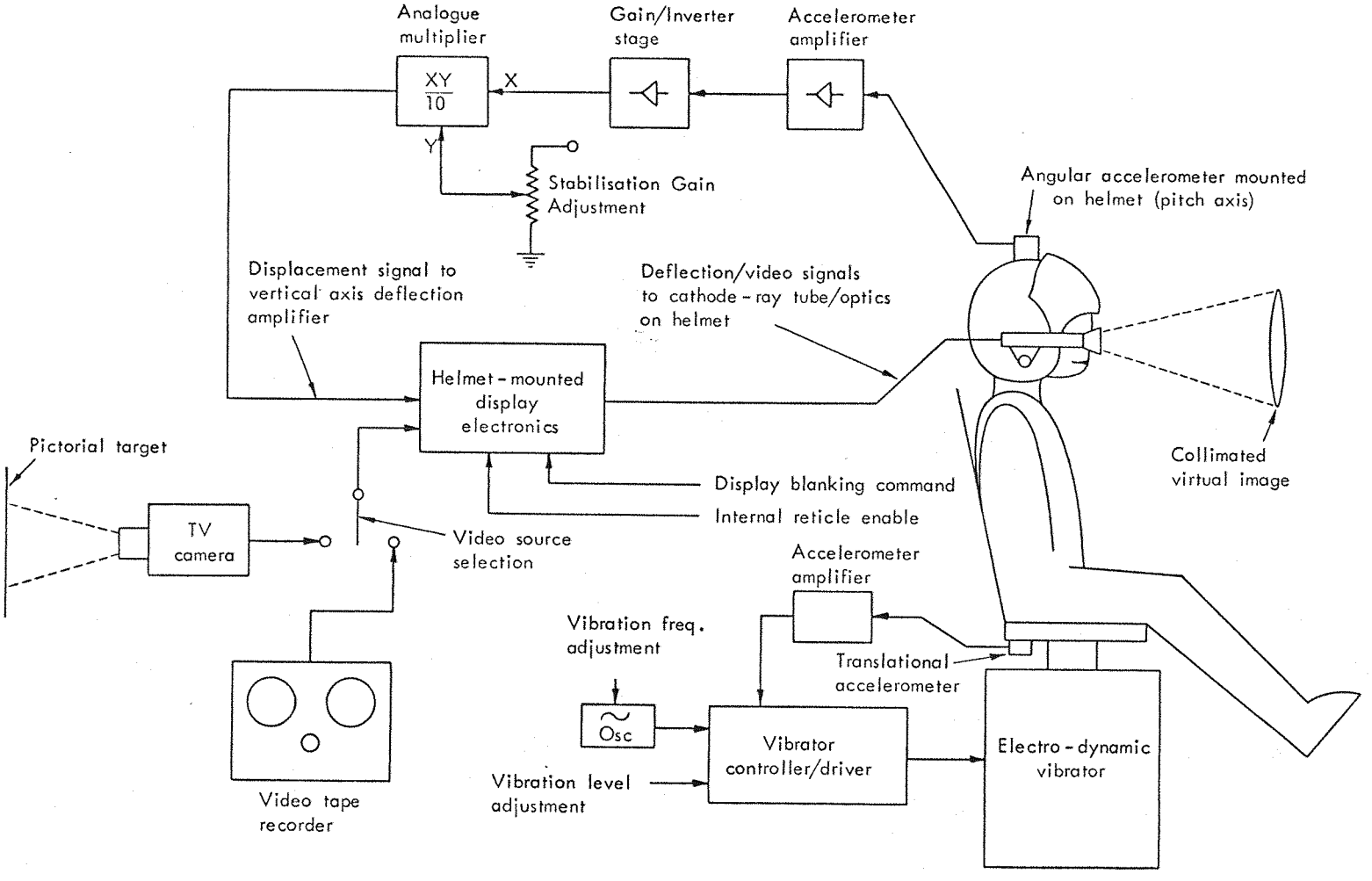

Figure 8.2.2. Diagram of the Helmet-Mounted Display, Image Stabilization and Vibration Apparatus used in Experiment ST.1

consisted of 24 runs during which each of the six targets was presented in four orientations.

The duration of each target run was a maximum of 20 s with an interval of 10 s between target runs. The subjects were given a 2 minute break between conditions one and two, and three and four, and a 5 minute break between conditions two and three.

8.2.6 Procedures

Prior to beginning the experiment, each subject was given still photographs of the targets (in one orientation only), and was required to study the photographs until certain that he could correctly identify each target. The subject was then tested by the experimenter using the same photographs to ascertain that he had learned to recognize the targets.

The subject was then seated on the vibration seat and fitted with the helmet-mounted display. The helmet was fitted to the subject to minimize any helmet slippage on the head by using the insertable foam rubber pads. The position of the display optics was adjusted on the helmet to locate the center of the exit pupil within the center of the subject's visual field.

In order to adjust the gain of the stabilization circuit, each subject was presented with a still pictorial image obtained from a TV camera (Sony Model AVC 3250) aimed at a photograph of an aircraft. While being vibrated at a sinusoidal frequency of 4.0 Hz and level of 1.0 m/s^2 rms, the subject was asked to adjust the level of the stabilization gain until the image was the "clearest" or "best defined." The subject was given four trials during which the gains were recorded by the experimenter and averaged to set the stabilization gain for that subject in the experiment.

At the beginning of each target run, the experimenter simultaneously activated the vibrator (if used in that condition), unblanked the image on the helmet-mounted display, and started an elapsed time

counter (counting in increments of 0.1 s). The target subtended angle increased until the target could be recognized by the subject. The subject then shouted "stop" to the experimenter, at which time the vibration motion and elapsed time counter were stopped and display image blanked. The subject would then report the identity of the target which, along with the elapsed time, was recorded by the experimenter. The start point on the video tape was varied from condition to condition to prevent subjects from becoming familiar with the presentation sequence of the targets on the video tape.

Prior to beginning the four conditions described above, each subject was given verbal instructions and a practice condition (no vibration), during which all of the targets and orientations were presented once. For the practice run the same procedure was followed as described above, with the exception that the subjects were given immediate feedback by the experimenter as to the correctness of their response, and the correct identity of the target, if a mistake had been made. Also, during the practice condition, the display was unblanked immediately after the subject response so that the subject could continue to see the target zoom to its maximum size.

8.2.7 Vibration Recording

After the subjects had completed the four experiment conditions, a 100 s vibration time history was recorded on an instrumentation recorder. The parameters recorded were seat Z axis acceleration, helmet pitch axis acceleration, helmet yaw axis acceleration, and stabilization correction signals to the helmet-mounted display electronics. These records were used to compute the power spectral distributions of seat and helmet motions as well as determine the linearity and check the gain of the stabilization signals.

8.2.8 Questionnaire

At the completion of the experiment, the subjects were interviewed by the experimenter and asked to comment on the following questions:

1. Did the vibration versus no vibration conditions make a difference in your ability to recognize the targets?

2. Which target(s) was the easiest to recognize?

3. What details did you look for to help you recognize each target?

4. Did you notice any difference in the definition or clarity of the image when stabilized?

A summary of the conditions of the experiment are given in Table 8.2.1.

8.3 RESULTS

8.3.1 Central Tendency

The two quantitative performance measures in the experiment were the accuracy of target recognition and the size of the visual angle subtended by the target at the time of recognition. The visual angle at recognition was computed using a mathematical relationship empirically determined between elapsed time and the subtended angle of the target on the display. The mean and standard deviation of the magnitude of the subtended visual angles at recognition are shown in Table 8.3.1 for each target and experimental condition. Each mean data score represents the averaged scores of ten subjects for four presentations (orientations) of each target. Pooled means for each target and experimental condition are also shown. (The standard deviation for the pooled means were compiled across the individual data points of each subject.) For ease of comparison, the mean data in Table 8.3.1 are shown as histograms in Figure 8.3.1.

Differences in data means were observed between the four experiment conditions (control, vibration, and stabilization), and the magnitude of these differences varied with the type of target. Generally, subjects tended to recognize the "covered truck" (mean angle = 2.19 degrees) and

TABLE 8.2.1. EXPERIMENT ST.1: EFFECTS OF VIBRATION AND IMAGE STABILIZATION ON IMAGERY

Purpose:	To determine the effects of whole-body vibration on the perception of unstabilized and stabilized target imagery presented on the helmet-mounted display.
Method:	Measure subtended angle of targets at time of identification when target images zoomed, with increasing subtended angles. Measure accuracy of target identification.
Subjects:	10S (S1, S3, S4, S5, S7, S8, S11, S12, S13, S14)
Visual Material:	Visual tape zoom imagery 6 military vehicle targets 4 orientations each target Zoom range 0.64-6.4 degrees in 20 s Textured background Average target luminance 2.1 cd/m^2 Average background luminance 48.4 cd/m^2 Image stabilization provded via feedback of helmet pitch acceleration to modulate CRT deflection.
Vibration:	Vertical, Z axis sinusoidal at 4.0 Hz (1.0 m/s^2 rms) Modified helicopter seat Seat Z/helmet pitch/helmet yaw acceleration recorded

TABLE 8.3.1. MEAN AND STANDARD DEVIATION OF VISUAL ANGLES (DEGREES) SUBTENDED BY TARGET IMAGES ON THE HELMET-MOUNTED DISPLAY AT THE TIME OF RECOGNITION

Target Type	Experimental Conditions				Mean (all conditions)
	Control 1	Vibration w/o stab.	Stabilization	Control 2	
Uncovered truck	3.34*	4.40	4.01	2.83	3.64
	(1.21)+	(1.27)	(0.98)	(0.72)	(1.29)
Covered truck	2.06	2.44	2.30	1.96	2.19
	(0.56)	(0.60)	(0.48)	(0.38)	(0.55)
Sherman tank	3.76	4.43	4.17	3.46	3.45
	(1.53)	(1.26)	(1.58)	(1.21)	(1.49)
M-60 tank	2.74	3.41	3.17	2.31	2.91
	(1.02)	(1.37)	(1.17)	(1.03)	(1.23)
Half-track	3.28	4.08	4.15	2.96	3.62
	(1.13)	(1.16)	(1.30)	(0.66)	(1.29)
Mobile gun	2.39	2.56	2.61	2.31	2.49
	(0.98)	(0.97)	(1.34)	(0.65)	(1.05)
Mean (All targets)	2.93	3.55	3.40	2.64	3.13
	(1.25)	(1.40)	(1.40)	(1.16)	(1.36)

*Values in degrees subtended angle at the observer's eye

+Standard deviations shown in brackets under mean value

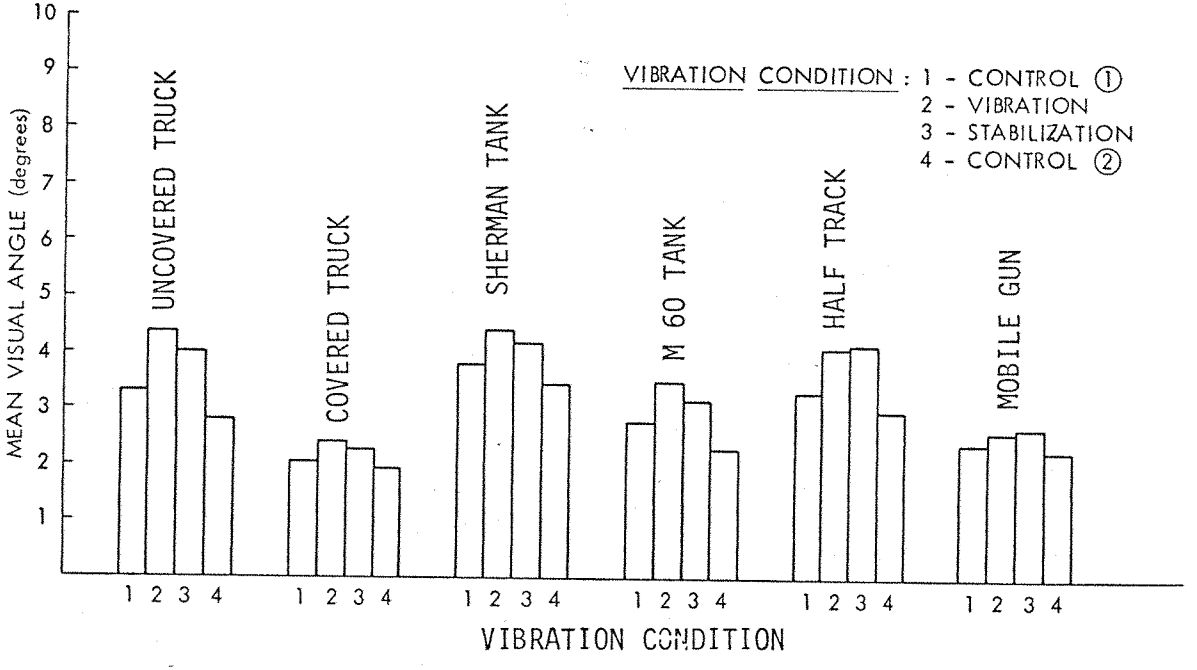

Figure 8.3.1. Histogram of Mean Visual Angle to Recognize Targets as a Function of Target Type and Vibration/Stabilization Condition (Experiment ST.1)

"mobile gun" (mean angle = 2.47 degrees) earlier than the "uncovered truck" (mean angle = 3.64 degrees), "Sherman tank" (mean angle = 3.95 degrees), or "half-track" (mean angle = 3.62 degrees). Also, the mean subtended angles for the vibration without image stabilization condition were alsways greater than those for the control conditions. The vibration with stabilization condition tended to cause a decrease in the mean subtended angles at recognition for the "uncovered truck," "covered truck," "Sherman tank," and "M-60 tank," but a slight increase in the subtended angles for the "half-track" and "mobile gun." Out of an overall total of 960 presentations, the grand mean subtended angle was 3.13 degrees with a standard deviation of 1.36 degrees.

8.3.2 Analysis of Variance (Subtended Angle)

An analysis of variance was carried out for the subtended angle performance data using a mixed effects, three factor analysis of variance with subjects as randomized blocks. The three factors were: experiment conditions (four levels), target type (six levels), and target orientation (four levels). A summary of this analysis is shown in Table 8.3.2. The main effects of target type and vibration condition were highly significant ($p<.001$). The main effect of target orientation alone was not statistically significant; however, the interaction of target orientation and target type was highly significant ($p<.001$). Target type and vibration condition ($p<.01$), and the interaction of all three factors ($p<.01$), were also found to be statistically significant.

8.3.3 Comparison of Means

A comparison of the mean subtended angles at recognition was performed for each vibration condition with mean angles pooled across targets. The Dunn's multiple comparison procedure was used for this analysis (Kirk, 1968, pages 79-81). The analysis showed that differences between the means for the two vibration conditions and the combined means of the two control conditions were statistically significant ($p<.05$). However, the difference in the means for the two control

TABLE 8.3.2. ANALYSIS OF VARIANCE SUMMARY FOR TARGET VISUAL ANGLES IN EXPERIMENT ST.1

Treatments
S = Subjects
A = Target Orientation
B = Target Type
C = Vibration/Stabilization Condition

Source	SS	DF	MS	F Ratio	p
S	178.89746	9	19.87749	19.57706	<.001
A	2.99414	3	0.99805	1.61463	ns
B	408.62305	5	81.72461	23.23779	<.001
C	128.53516	3	42.84505	12.42453	<.001
A × B	90.35938	15	6.02396	5.43881	<.001
A × C	5.62207	9	0.62467	0.98904	ns
B × C	30.35645	15	2.02376	2.27779	<.01
A × B × C	54.79688	45	1.21771	1.76488	<.01
Residual	868.12109	855	1.01535		
A × S	16.68945	27	0.61813		
B × S	158.25977	45	3.51688		
C × S	93.10742	27	3.44842		
A × B × S	149.52441	135	1.10759		
A × C × S	51.15918	81	0.63159		
B × C × S	119.94434	135	0.88848		
A × B × C × S	279.43652	405	0.68997		
Total	1768.30566	959	1.84391		

conditions and the difference in the means for the two control vibration conditions (i.e., with and without stabilization) were not statistically significant.

8.3.4 Probability of Target Recognition

Probability density functions were computed for each experimental condition and target type from the data pooled across subjects and target orientations. This analysis procedure provided an estimate of

the probability of target recognition as a function of the visual angle subtended by the target on the helmet-mounted display. A cumulative probability distribution was then determined by integrating the probability density function. Shown in Figure 8.3.2 are six sets of cumulative probability distributions for each target type. Within each target set are shown the three distributions for the average of the control conditions, the vibration condition without stabilization, and the vibration condition with stabilization.

From Figure 8.3.2, the effects of vibration and stabilization can be compared with the no vibration control condition. The effect of vibration is seen here to lower the probability of target recognition at any given subtended angle. In most cases, a slight improvement was provided by the stabilization system used in the experiment.

8.3.5 Target Identification Accuracy

Table 8.3.3 gives a collation of the target identification errors, categorized by target type and vibration condition. Each entry indicates the total number of incorrect identifications out of 40 presentations. The greatest number of errors were made during the first control condition (27 errors out of 240 presentations) while, surprisingly, the least number of errors were made during vibration without image stabilization condition (15 errors out of 240 presentations). There also appears to be a large difference in the number of errors between the two control conditions (27 errors versus 17 errors). During the overall experiment, 80 errors were made out of a total of 960 presentations for an overall error rate of 8.3 percent.

8.3.6 Analysis of Variance (Accuracy)

A Friedman two-way analysis of variance was used as a nonparametric statistical test for the number of recognition errors distributed across experimental conditions (vibration, stabilization, control). This analysis failed to show any significant contribution of experimental condition to the variance of the error scores. A Wilcoxon matched-pairs signed ranks test of the errors made between the two

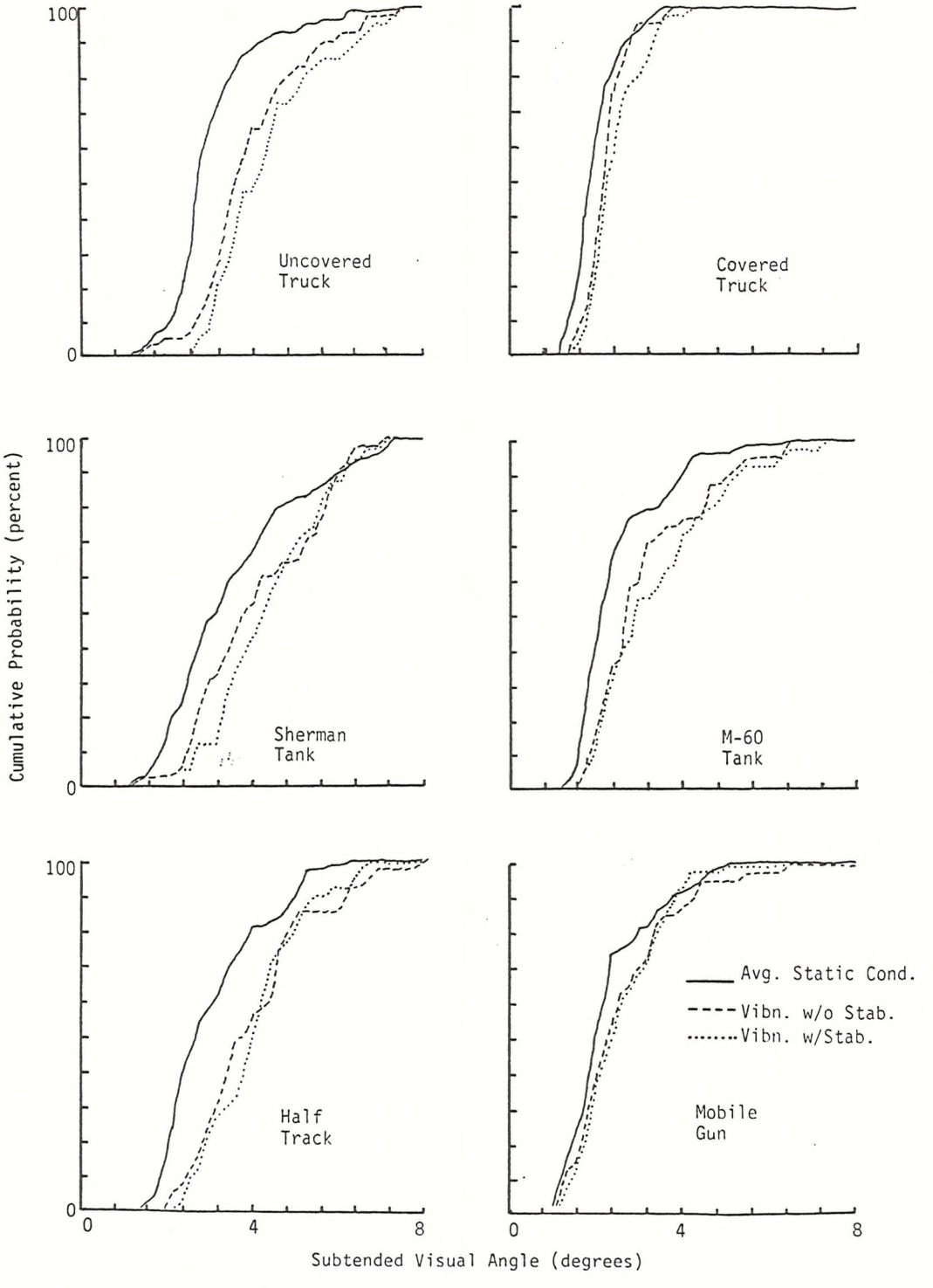

Figure 8.3.2. Cumulative Probability of Target Recognition as a Function of Target Type and Vibration/ Stabilization Conditions

TABLE 8.3.3. OCCURRENCE OF TARGET IDENTIFICATION ERRORS BY TARGET TYPE AND EXPERIMENTAL CONDITION

Target Type	Experimental Conditions				Mean (all conditions)
	Control 1	Vibration w/o stab.	Stabilization	Control 2	
Uncovered truck	7	6	7	8	28
Covered truck	2	2	0	1	5
Sherman tank	4	2	7	2	15
M-60 tank	7	2	6	4	19
Half track	4	1	1	0	6
Mobile gun	3	2	0	2	7
Total (All Targets)	27	15	21	17	Grand Total 80

control conditions indicated that the number of errors committed in the second control condition were significantly less ($p<.005$) than those committed in the first control condition. This difference in accuracy indicated that a learning or practice effect may have been present which helped the subjects to gain greater accuracy during the course of the experiment.

Inspection of Table 8.3.3 shows that the accuracy of target recognition (inverse of the number of errors) varied considerably as a function of target type. Most of the errors (28 errors out of 160 presentations) were committed when the "uncovered truck" was presented on the display and the least number of errors when the "covered truck" was presented. A Friedman two-way analysis of variance of the errors by target-type pooled across experimental conditions was statistically significant ($p<.05$) denoting that the error distributions were consistent across most subjects.

8.3.7 Confusion of Targets

Table 8.3.4 shows a summary confusion matrix for the errors made in target identification, where each row is the target being presented and each column is the number of times that target was wrongly identified as the target under the column. Inspection of Table 8.3.4 indicates that 67 of the 80 total errors made in the experiment were due to confusions between the "uncovered" and "covered trucks" and between the "Sherman" and "M-60 tanks." It is interesting to note, however, that in the case of the trucks, the "uncovered truck" was identified incorrectly as the "covered truck" almost five times more frequently than the "covered truck" was misidentified as the "uncovered truck."

8.3.8 Relationship of Accuracy and Subtended Angle Performance Measures

Spearman rank order correlation tests were performed on the summary target recognition accuracy and subtended angle data to test the relationship of the number of errors committed by target type versus the visual angle subtended by the target at recognition.

TABLE 8.3.4. TOTAL INCIDENCE OF CONFUSIONS BETWEEN INDIVIDUAL TARGETS

Target Presented	Target by Which Presented Target Identified						Total Errors
	Uncovered Truck	Covered Truck	Sherman Tank	M-60 Tank	Half Track	Mobile Gun	
Uncovered truck	--	19	0	0	9	0	28
Covered truck	4	--	0	0	1	0	5
Sherman tank	1	0	--	12	0	2	15
M-60	0	0	19	--	0	0	19
Half track	4	0	0	1	--	1	6
Mobile gun	2	0	2	3	0	--	7
Total Errors (All Targets)							80

Tests were conducted for each of the four experimental conditions, but failed to show any correlation with statistical significance. It can, therefore, be concluded that there was no observed relationship between the recognition accuracy of a target and the magnitude of the visual angle subtended by the target when recognized.

8.3.9 Results of the Questionnaire

In reply to the question (1) concerning the effect of vibration on their ability to recognize the targets, 5 of the 10 subjects (S1, S3, S4, S5, S12) stated that there was a definite increase in the difficulty of recognizing the targets under the vibration (without image stabilization) condition. Subject S3 noted that the increase in difficulty appeared to be target dependent. Three subjects (S7, S13, S14) thought that there were slight degradations in target visibility due to the vibration, and two subjects (S8, S11) stated that they felt there was no increase in difficulty at the vibration levels being used.

In response to question (2) concerning which targets were easiest to recognize, all subjects agreed that the "mobile gun" and/or the "covered truck" were the easiest to recognize. The "mobile gun" was distinguished from the other targets because it had: (a) a distinctive line (barrel) along the length of the vehicle; (b) a shadow of the overhang of the gun barrel; and (c) the absence of the star which was present on the other vehicles. The "covered truck" was recognized by the canopy over the truck bed and the transverse lines in the canopy caused by the canopy stays. Four subjects (S3, S7, S11, S14) stated that the tank targets could be identified as tanks at small visual angles but that it was difficult to distinguish between the two tanks (i.e., "Sherman" versus "M-60") until the visual angle became much larger. Most of the subjects agreed that the two tank targets were the most difficult to distinguish and caused the greatest confusion. Two subjects (S7, S14) noted that they observed that the "Sherman tank" was darker or appeared to have more contrast relative to the background than the "M-60 tank."

The responses to question (3) regarding the features used to distinguish between the targets are given in Table 8.3.5.

When the subjects were asked if they noticed any difference in the definition or clarity of the image when it was stabilized on the display, 8 of the 10 subjects (S1, S3, S4, S7, S8, S11, S12, S14) noted that it was easier to see the targets when the image was stabilized. It was added that the target appeared to be recognizable at an earlier time in the zoom run than for the display that was not stabilized. One subject (S12) stated that the stabilized image appeared to be blurred, but was still easier to recognize than the unstabilized display. Another subject (S14) thought that the overall target definition was the same in both the unstabilized and stabilized presentations, but the distinguishing features were easier to spot in the stabilized display. Subject S8 commented that he felt that the seat vibration level had actually been increased for the unstabilized display presentation. Out of the remaining two subjects, Subject S13 noticed only a very small improvement while Subject S5 did not notice any difference between the unstabilized and stabilized displays.

Various responses were given when the subjects were asked if they had any other comments (question 5). The following is a list of the most pertinent comments.

Subject S1	Became tired toward the end of the experiment. Legs became very tired. Targets did not have form until at larger subtended angle.
Subject S3	Did not like the display blanking between runs, image appeared blurred when first turned on, but became more focussed after the target zoomed in for a while.

TABLE 8.3.5. FEATURES USED BY SUBJECTS TO RECOGNIZE TARGETS (FROM QUESTIONNNAIRE)

Target	Features Recognized by Subjects
Uncovered	Absence of canopy/supports over truck bed (as compared with covered truck). Ledges or seat in truck bed. Combination of star on bonnet and seat in bed.
Covered truck	Reflection of light from canopy over truck bed. Transverse lines of canopy supports over truck bed.
Sherman tanks	Location of turret in center of tank. Reflection of light from turret. Hatch on top of turret. Edges more rounded than M-60 tank. Darker than M-60 tanks.
M-60 tank	Location of turret toward rear of tank. Turret larger than Sherman tanks. Top surface of tank appears larger than Sherman tank. Less contrast of target to background than Sherman tank.
Half track	Long lines along length of vehicle. Star on front, but no truck bed. Hatch in rear.
Mobile gun	Gun barrel along length of vehicle. Overhang of barrel and shadow of overhang on background. Absence of star.

Subject S4	Did not like the green display.
Subject S8	Felt that he was learning all the time and improving his response time (i.e., recognizing targets at smaller subtended angles).
Subject S11	Bright green picture caused too much contrast, so could not pick up image detail. Contrast seemed to be reduced when the image was stabilized and targets were easier to see.
Subjects S5, S7, S12, S13, S14	No comments

8.3.10 Power Spectral Distributions

Power spectral densities were computed from the recorded time histories of the seat Z axis, helmet pitch axis, and helmet yaw axis acceleration. The motion of the helmet in the pitch axis due to the input sinusoidal motion was largely sinusoidal but with some harmonic activity. The mean helmet pitch acceleration due to the 4.0 Hz, 1.0 m/s^2 rms seat Z motion was 5.94 rad/s^2 rms (SD = 1.37). The mean 8.0 Hz and 12 Hz harmonic components of helmet pitch motion were 0.92 rad/s^2 rms (SD = 0.38), and 0.29 rad/s^2 (SD = 0.11), respectively. The mean estimated harmonic distortion (as defined in Section 5.2) of the helmet pitch acceleration was 21.6 percent (SD = 8.2 percent). Similarly, the components of motion at 4.0 Hz, 8.0 Hz, and 12.0 Hz in the yaw axis were 0.77 rad/s^2 rms (SD = 0.31), 0.14 rad/s^2 rms (SD = 0.05), 0.18 rad/s^3 rms (SD = 0.04), respectively. The mean estimated harmonic distortion of acceleration in the yaw axis was 37.6 percent (SD = 24.2 percent). A summary of the analysis of the power spectral densities are given in Table 8.3.6.

8.3.11 Stabilization Gain Settings

Table 8.3.6 gives the mean gains of the stabilization system as adjusted by the subjects to obtain the "clearest" or "most distinct"

TABLE 8.3.6. HARMONIC ANALYSIS OF SEAT Z AND HELMET PITCH AND YAW ACCELERATIONS AND MEAN STABILIZATION GAIN SETTINGS (EXPERIMENT ST.1)

	Seat Z				Helmet Pitch				Helmet Yaw					
Subject	Frequency Components (m/s2 rms) 4.0 Hz	8.0 Hz	12.0 Hz	Total* Harmonic Duration (percent)	Frequency Components (m/s2 rms) 4.0 Hz	8.0 Hz	12.0 Hz	Total* Harmonic Duration (percent)	Frequency Components (m/s2 rms) 4.0 Hz	8.0 Hz	12.0 Hz	Total* Harmonic Duration (percent)	Gain** Settings Mean	SD
1	.874	.028	.010	7.8	6.58	0.51	0.35	13.0	1.24	0.14	0.21	19.7	8.29	0.46
3	.840	.032	.010	7.4	4.81	1.42	0.27	31.9	0.88	0.09	0.14	21.3	7.54	0.49
4	.909	.058	.000	9.6	4.63	0.82	0.29	21.8	0.29	0.23	0.25	94.4	7.46	0.31
5	.941	.049	.014	9.6	5.46	1.50	0.22	31.2	0.47	0.17	0.20	56.9	7.20	0.60
7	.931	.039	.010	8.8	6.40	0.77	0.16	16.1	0.88	0.10	0.14	22.5	10.15	1.01
8	.934	.035	.014	8.5	4.68	0.79	0.11	21.9	1.16	0.08	0.14	18.6	8.99	0.99
11	.849	.039	.014	10.1	4.34	1.18	0.42	33.2	0.49	0.14	0.21	52.0	7.36	1.41
12	.937	.076	.017	10.2	8.01	0.42	0.46	11.1	0.98	0.19	0.22	23.7	9.07	0.57
13	.851	.050	.000	9.3	6.51	1.16	0.33	21.3	0.71	0.07	0.12	28.5	6.98	1.43
14	.842	.060	.010	9.6	7.99	0.62	0.33	14.3	0.63	0.15	0.18	39.4	7.92	0.98
$\bar{x}$	.891	.047	.010	9.09	5.94	0.92	0.29	21.6	0.77	0.14	0.18	37.6	8.10	
σ	.043	.015	.006	0.95	1.37	0.38	0.11	8.2	0.31	0.05	0.04	24.2		1.26***

*As defined in Section 5.2 for a bandwidth of 0-20 Hz.

**Mean and standard deviation of four trials.

***Overall standard deviation for all gain settings taken individually.

image appearance. The mean values were calculated from four trial settings. A theoretical gain of 9.82 was required to achieve an absolute space-stabilized presentation using the pitch accelerations of the helmet as measured by the rotational accelerometer. With the exception of one subject (S7) the stabilization gains were slightly less than the ideal theoretical gain.

8.4 DISCUSSION

8.4.1 Effects of Vibration

From the results presented above, it can be concluded that whole-body vibration can degrade the perception of pictorial imagery presented in the helmet-mounted display. On the average, there was 27.9 percent increase in the subtended angle necessary to recognize the targets. A general degrading effect of vibration on display visibility was expected based upon the findings of the legibility experiments using alphanumeric characters reported in Chapter 4, especially since the 4.0 Hz vibration frequency had the greatest effect upon the legibility of numeric characters. The extent that vibration affected performance was dependent upon target type; for example, vibration caused a mean increase of 43 percent in the visual angle to recognize the uncovered truck, but only a 9 percent increase for the covered truck. Generally, the targets which were easiest to recognize under static conditions (i.e., having the smallest subtended angles at recognition) were also least affected by vibration. The vibration appeared to have accentuated any difficulty in target recognition experienced under static conditions. These factors may account for the significant interaction between the effects of target type and experiment condition shown in the analysis of variance.

Using the mean helmet pitch acceleration data computed from the power spectral densities of the individual subjects, the mean peak-to-peak angular displacement of the display image in space at 4.0 Hz was estimated to be 1.52 degrees (SD = 0.36); similarly, the mean estimated peak-to-peak yaw displacement was 0.20 degrees (SD = 0.080).

Assuming that the eyes were approximately stable in space at 4.0 Hz (due to the vestibulo-ocular reflex), the corresponding peak-to-peak displacement of the nodal image of the display on the retina was approximately 1.5 degrees vertically and 0.2 degrees horizontally. Since the magnitude of the vertical displacement is on the order of the visual angle subtended by the target, it is probable that nodal images of the target area significantly overlapped the background areas; consequently, the superimposition of the darker target scene over the background scene of higher luminance reduced the contrast of the high spatial frequency details in the target and/or perhaps completely obscured these details. Under these conditions, the overall contrast of the target to the background would have been effectively reduced from 96 percent to 4 percent. As a result of these effects of vibration, larger subtended visual angles were required to discriminate the distinguishing features of the targets.

8.4.2 Image Stabilization

The simple image stabilization system provided only slight improvements (average 6.1 percent) in the subtended angle performance of subjects, although this improvement was not significant nor consistent across subjects or targets. The intended function of the stabilization network was to reduce the relative motion of the eye and the display in the pitch axis, so as to cause the display image to remain stable on the retina. In order to do this, helmet pitch acceleration signals were processed and used to position the image on the CRT equal to and in the opposite direction of the pitch motion of the helmet. However, the particular approach used for stabilization was only an approximation; and it was known prior to the experiment that the quality of the stabilization would be compromised by several factors, including improper setting of the gain in the stabilization circuit and nonsinusoidal movement of the helmet due to harmonic distortion of the helmet pitch acceleration. Two additional factors not related to the stabilization circuit, but which may have degraded performance, were the persistence of the CRT phosphor and image displacement errors due to helmet yaw movement. The following sections discuss the nature of these factors which probably tended to compromise the quality of the stabilization system.

8.4.3 Stabilization Error Sources

8.4.3.1 Errors Due to Harmonic Distortion

Because the helmet pitch motion contained harmonic components, an optimum stabilization of the image could not be achieved. The simple gain-inverter method used to process the helmet pitch acceleration signals caused an over-amplification of the harmonic components of the 4.0 Hz motions (i.e., 6 dB for 8 Hz, 9.5 dB for 12 Hz, and 12 dB for 16 Hz, etc.). For subjects having harmonic distortion in helmet pitch acceleration of greater than 30 percent, stabilization errors (displacement) of greater than 27 percent may have resulted. For example, the analysis of the power spectral distribution of helmet pitch acceleration for subject S11 (Table 8.3.6) showed that the 4.0 Hz, 8.0 Hz, and 12.0 Hz frequency components were 4.34 rad/s^2 rms, 1.18 rad/s^2 rms, and 0.42 rad/s^2 rms, respectively. The harmonic distortion for a bandwidth of 0 to 20 Hz was 33.2 percent. The equivalent peak-to-peak angular displacements of the helmet were 1.11 degree (4.0 Hz), 0.30 degree (8.0 Hz), and 0.11 degree (12.0 Hz). With the optimum adjustment of stabilization gain for the 4.0 Hz motion, residual displacements of 0.30 degree at 8.0 Hz and 0.11 degree at 12.0 Hz would result. Consequently, the adjustment of stabilization gain had to be a compromise between the 4.0 Hz, 8.0 Hz, and 12.0 Hz (plus other harmonic) components of motion. This factor may account for the reason that the stabilization gains generally were adjusted at levels lower than the theoretical gain for 4.0 Hz (i.e., 9.82). Regardless of the gain setting, the stabilization was not exact and residual motion was present.

8.4.3.2 Errors Due to Helmet Yaw

The movement of the helmet in the yaw axis due to the seat Z motion was sufficiently large to affect performance in both the unstabilized and stabilized conditions. (No attempt was made in this experiment to stabilize the display image in the yaw axis although it could be easily implemented via the same method used for the pitch axis.) Benson and Barnes (1978) have shown that, as in the case of pitch axis

motion, the vestibulo-ocular reflex should cause the eyes to remain stable in the head yaw axis at a frequency of 4.0 Hz. Accordingly, the mean peak angular displacement of the helmet in the yaw axis of 0.77 rad/s^2 would have caused an estimated peak-to-peak displacement of the image on the retina of approximately 11.9 minutes-of-arc. This displacement in yaw most likely reduced the perceived horizontal resolution of the display, thereby compromising the fidelity of any stabilization provided to the pitch axis.

8.4.3.3 Phosphor Persistence

A video field was scanned by the raster on the cathode-ray tube every 20 ms (i.e., 25 Hz frame rate with two fields per frame). Within this interval, the phosphor luminance intensity at a particular point on the faceplate decayed to a nominal value of 18 percent of its initial value (as derived from Figure A.3.1.2, Appendix A.3.1). Since the complete raster was being translated continuously on the CRT to compensate for helmet pitch motion, portions of successive video fields were written on phosphor screen locations occupied by fields immediately preceding it. For a mean helmet pitch acceleration of 5.94 rad/s^2 rms, the peak velocity of the movement on the raster (for space stabilization) was approximately 19 deg/sec. Therefore, after 20 m/s, the raster was repositioned at locations up to 0.38 degree from the previous raster postion. In the early part of the target zoom (i.e., target subtended angle of 0.64 degree) it is likely that significant portions of video fields representing the target (with an average luminance of 2.1 cd/m^2) were being scanned over areas of the phosphor scene previously occupied by the background with an average luminance of 48.4 cd/m^2. During the interval of 20 ms the previous background scene decayed to approximately 8.7 cd/m^2, thereby completely obscuring or masking the 2.1 cd/m^2 average luminance values of the target. The degrading effect of this factor was not overcome until the target size became large enough so that the interfield afterglow and image translation on phosphor screen were insignificant relative to the spatial modulation aspects of the target details. The artifact of the phosphor persistence probably severely compromised the advantages of the stabilization approach in reducing display image

motion on the retina, yielding only the slight improvements observed in performance relative to the unstabilized display condition. For a 4.0 Hz vibration frequency, a factor of ten increase in the phosphor decay rate was needed during image stabilization to eliminate the problems caused by the long persistence phosphor used in the helmet-mounted display.

8.4.4 Subjective Effects of Image Stabilization

From the discussion above, it can be seen that there were several factors which compromised the performance of the stabilization approach used in the experiment. The three main factors were harmonic distortion in the helmet pitch motion causing improper adjustments of the stabilization gain, displacements due to yaw axis motion, and phosphor persistence. Notwithstanding these problems, the stabilization system did render some improvements in subtended angle performance. The subjects comments reinforced the value of image stabilization by indicating that the stabilized image was more desirable to view on the display than the unstabilized. It is the author's opinion that a long term effect of fatigue also may have been reduced considerably by the stabilization of the display.

8.5 SUMMARY

This experiment has shown that vertical, Z axis sinusoidal whole-body vibration can affect the perception of target imagery presented on a helmet-mounted display. The main effect of the vibration was to increase the visual angle subtended by the target before the target was recognized. A simple technique for stabilizing the helmet-mounted display image was demonstrated, but provided only slight improvements in the subtended visual angles required to recognize targets. The effectiveness of the stabilization approach was compromised mainly by CRT phosphor persistence. Other factors degrading the quality of the image stabilization were shown to result from harmonic distortion present in the helmet pitch acceleration signals, and the effects of helmet yaw axis motion.

If the helmet-mounted display is to be used in flight under similar vibration conditions and in applications where time for target recognition must be minimum, stabilization of the helmet-display image will be required. It is felt that the quality of image stabilization performance using feedback from a helmet pitch accelerometer can be improved significantly by using a continuous, true double integration of the helmet pitch signals. This approach would eliminate the effects of harmonic distortion and the need to adjust the stabilization gain as a function of vibration frequency. Further improvements can be made by providing yaw stabilization as well, but for these stabilization approaches to be optimum, phosphor persistence must be reduced to allow the luminance to decay between video fields (i.e., decay to at least 1.0 percent of the initial intensity within 20 msec). Additional aspects of image motion stabilization approaches will be considered in the next chapter.

Chapter 9
SUMMARY AND CONCLUSIONS

9.1 SUMMARY OF EXPERIMENTAL FINDINGS

9.1.1 Vibration, Display Factors, and Reading Performance

The results of the experiments reported in this thesis have shown that vertical sinusoidal vibration of seated subjects (Z axis) can seriously degrade their ability to perceive visual material presented on a helmet-mounted display. The magnitude and nature of the degraded performance was a function of the frequency and level of vibration and the display conditions under which the visual materials were presented. There were wide variations in the absolute reading performances of subjects, but generally, vibration between 4.0 Hz and 5.6 Hz produced the greatest decrements in perception. At each vibration frequency, increases in the level of vibration caused proportional increases in the number of reading errors. In the character legibility studies, static and dynamic reading errors decreased as the subtended angle formed by the character on the retina increased. Characters presented with a low luminance background (provided either by the raster or an external source) reduced the number of reading errors as compared to either a dark background or high luminance background viewing conditions. Whole-body vibration also increased the subtended angle required to recognize targets presented in pictorial imagery. The magnitude of the effect of vibration on target recognition was dependent upon the features of the target.

9.1.2 Dynamic Behaviour

The dynamic studies showed that sinusoidal vertical motion of the seat applied to the Z axis of seated subjects caused sinusoidal rotational motions of the head and helmet predominantly in the pitch axis. There were also rotational movements of the helmet on the head. Head and helmet motion contained significant harmonic components for frequencies of 4.0 Hz and less. The transmission of vibration to the head and helmet varied widely across subjects. A mean seat vibration of

6.4 Hz produced the greatest helmet pitch movement, and 7.5 Hz the greatest helmet to head movement. The maximum head pitch motion occurred at a mean frequency of 5.5 Hz. Head orientation also affected the transmission of vibration to the head and the coupling of the helmet to the head. The movements of the helmet in pitch axis were shown to be linearly related to seat Z acceleration with the exception of those frequencies between 5.6 and 11.2 Hz.

The rotational motion of the head and helmet caused apparent nodal images of the helmet display images. At seat vibration frequencies from 2.8 to 4.0 or 5.6 Hz, the angular separation these images corresponded to the peak-to-peak angular displacement of the helmet in the pitch axis, signifying that, while the display image was oscillating in space, the eyes were remaining stable in space. This behaviour was attributed to the compensatory reflexive response of the eye mediated by the angular stimulation of the vestibular end organs (i.e., the vestibulo-ocular reflex). The observed nature of the displacement of nodal images was explained by comparing helmet pitch behaviour with the frequency response of the vestibulo-ocular reflex.

9.1.3 Mechanisms Degrading Reading Performance

The degrading effects of whole-body vibration on the perception of the helmet-mounted display were ascribed to the dynamic displacement of the display image on the retina of the eye. Reading performance was found to be correlated with the predictive model proposed by O'Hanlon and Griffin (1971) using helmet pitch displacements of subjects for vibration frequencies of 4.0 Hz and below, and helmet pitch on head pitch displacements at frequencies of 5.6 Hz to 16 Hz. This finding implied that there was a roll-off in the vestibulo-ocular reflex at frequencies above 5.6 Hz. This finding was reinforced by the performance of reading a panel-mounted display viewed at 1.5 m during whole-body vibration.

Even with the formation of distinct nodal images, reading performance of characters degraded with increasing vibration levels. It was likely that the increased velocity of the display images reduced the

"dwell time" of the image over a small region of retinal receptors. This situation provided an inadequate period of time for the light quanta from the display to be integrated by the retinal receptors, thereby causing the modulation contrast of the high spatial frequency detail of the image to be reduced below threshold.

The effects of nodal image formation were somewhat different for the imagery display. For target images located in complex backgrounds, nodal image formation probably degraded rather than assisted display visibility. In this case the low contrast, high spatial frequency detail of the target overlapped with itself and was superimposed on other detail in the background, thereby confusing the appearance of the image presentation. Only until the spatial details of the targets became large relative to the displacement of the image on the retina did the features of the targets become discerned adequately for recognition.

9.1.4 Field Trials

Field trials using the helmet-mounted display yielded negative results in that no reading errors were produced by the two pilot/subjects during any flight condition or character sizes which was presented. However, the nature of these results were consistent with laboratory findings given the helicopter vibration levels and the display background luminance conditions.

9.1.5 Image Stabilization

A simple image stabilization system was developed to reduce the relative movement of the display image on the retina. The system used a closed loop feedback of the helmet pitch acceleration to move the image on the display in a direction opposite to the movement of the helmet and by an amount determined by the feedback gain adjusted by each subject. The stabilization system was liked by the subjects, but the data did not indicate that it caused a significant improvement in the performance of subjects in a target recognition task. It was decided that the performance of the system was compromised by long

phosphor persistence and inaccuracies in stabilization due to gain errors of the stabilization network for the harmonics of helmet pitch acceleration.

9.2 IMPLICATIONS OF EXPERIMENTAL RESULTS

9.2.1 Limitations of Laboratory Findings

The results of the experimental investigations above were obtained using a single monocular helmet-mounted display system, specific visual material, laboratory vibration apparatus, and sinusoidal vibration conditions. Based upon the review of the literature, different vibration and seating conditions can significantly alter the transmission of vibration to the head. Similarly, different helmets and helmet-mounted display configurations (with their unique mechanical properties) are likely to affect differently helmet and head movement during vibration. Each of these factors can influence the nature of reading performance using the helmet-mounted display. For these reasons, the data in this thesis should not be interpreted as representing the absolute performance expected from operators. Nevertheless, the data do represent some of the dimensions, factors, and trends in the performance of operators. Likewise, the mechanisms affecting performance in the laboratory studies reported herein are likely to be similar for many applications of the helmet-mounted display in a vibration environment.

9.2.2 Nature of Aircraft Vibration and Effect on Helmet-Mounted Display Performance

It can be assumed from the experimental findings above that whole-body vibration of either a random or deterministic nature, within the frequency range of 2.0 Hz to 11.2 Hz and applied in the vertical direction to the Z axis of seated operators will produce rotational motions of the head and helmet. These motions, in turn, may affect the operator's ability to perceive information presented on a helmet-mounted display.

In the present helmet-mounted display, the limiting resolution of the display at the eye in the vertical dimension was estimated to be about 6 minutes-of-arc per cycle (Figure 4.4.5), given the luminance conditions, optical design, and CRT spot size used in the experiments. Displacements of the display image on the retina on the order of the limiting angular resolution may reduce the perceived resolution by a factor of two. Accordingly, from Table 6.3.3, the estimated nodal image displacement (assuming linearity) of about 6 minutes-of-arc would occur during vertical seat acceleration levels of about 0.40 m/s^2 rms, 0.12 m/s^2 rms, and 0.08 m/s^2 rms for vibration frequencies of 2.8 Hz, 4.0 Hz, and 5.6 Hz, respectively. From Figure 2.5.2, it can be seen that vertical motions of a representative fixed-wing aircraft at these frequencies are well within the acceleration ranges to produce image displacements of this order. However, these vibration levels were not measured at the seat-pilot interface; therefore, additional effects of the transmissibility of this vibration through the seat to the pilot can be expected.

In the helicopter experiment (H.2) (Chapter 7), a maximum vertical seat acceleration of about 1.0 m/s^2 was observed at 17 Hz in the Sea King helicopter during the 70 knots flight condition. Under similar flight conditions in Experiment H.1, no errors were produced in reading numeric characters presented on the helmet-mounted display. The results of H.1 were found to be consistent with the results of Experiment LG.3 for similar vibration and reading conditions. Griffin (1972) observed a vertical seat acceleration of about 0.05 m/s^2 rms at 7 Hz in the Scout helicopter. Based upon the findings of Experiment LG.1 (i.e., Figure 4.2.3), this vibration level and frequency will have little affect on display perception. It can be concluded from this discussion that predominant vibrations in these helicopter aircraft were generally at higher frequencies and lower amplitudes than are likely to affect perception of the helmet-mounted display. However, low frequency vibration (i.e., between 2.0 Hz and 5.6 Hz) may still be present from nonharmonic sources, such as buffeting and atmospheric turbulence, which may cause sufficient movements of the head to affect reading performance. Furthermore, because of the anticipated degrading effects of even small helmet pitch motions on

the perceived resolution of the display, it is likely that imagery presentations will be affected more severely than symbolic presentations by low vibration levels.

9.2.3 Displays of Symbolic Information

9.2.3.1 Display Factors and Dynamic Factors

The results of the experiments above tend to involve two sets of factors; first, the mechanisms which cause the display image to move on the retina and second, the psychophysiological factors of perception governed by the adaptation and accommodation states of the eye and the spatial and modulation characteristics of the visual material. The results of Experiments LG.3 and LG.4 tend to show that the appropriate changes in the spatial and luminance characteristics of the visual material reduce considerably the effect of whole-body vibration, in spite of the motion of the image on the retina. Consequently, there are two major recommendations which can be made regarding the operational use of the helmet-mounted display for presenting symbolic material. The first is that an attempt should be made to reduce the magnitude of helmet pitch motion due to vibration of the seat. The second is that the display luminances and visual material should be manipulated to reduce the effects of image displacement on the retina.

9.2.3.2 Vibration Isolation of Seat

Vibration isolation of the seat or seating configuration and restraint systems may be designed to reduce the effects of vibration. Also the seat back to operator interface seems to have a large effect on vibration transmission to the head (Section 2.5.3.4 and 5.2.3.2, BD.2). The vibration frequencies of major concern are between 2.8 Hz and 11.2 Hz, or more specifically 4.0 and 5.6 Hz. It would be most desirable to tune a vibration isolation system to attenuate vibration transmissibility to the head over this frequency range.

9.2.3.3 Spatial Frequency Considerations

The effects of whole-body vibration on display legibility can be reduced for the presentation of symbolic information by increasing the subtended visual angle of the characters. The ideal size of the characters will be dependent upon the vibration factors and the contrast modulation transfer function of the display. From the results of Experiment LG.3 (Section 4.4) for a display limiting resolution of about 10 cycles per degree vertically and 15 cycles per degree horizontally, character widths of at least 20 minutes-of-arc were needed to provide optimum definition of 5 x 7 numeric characters, under static conditions (i.e., corresponding to a character height of 28 minutes-of-arc). But even at character heights of 27 minutes-of-arc, some reading errors were observed under the worst case vibration and viewing conditions (i.e., 4.0 Hz, 1.0 m/s^2 rms, and dark background). The results of Hemingway and Erickson (1969) and Laycock (1978) suggest that further increases in character height should be accompanied by an increase in resolution. If 7 x 9 dot matrix character are used, the minimum horizontal dimension should be 28 minutes-of-arc (i.e., 4 minutes-of-arc per element), thereby requiring a vertical subtended angle of 36 minutes-of-arc. In this case, the number of scan lines forming the vertical dimension of the character could be increased to 12 scan lines before resolution becomes limiting. A character height of 36 to 48 minutes-of-arc composed of 12 to 14 TV scan lines was recommended also by Laycock (1978) for helmet-mounted display operation in a low altitude, high speed flight environment.

9.2.3.4 Display Luminance Considerations

The results of Experiments LG.3 and LG.4 (Section 4.4. and 4.5) suggest that a dark background should be avoided for the display of symbolic information in a vibrating environment. For a night viewing situation, the results show that a raster background of about 1.0 cd/m^2 should be provided while the character-to-background contrast should be maintained at 0.96. For a daylight viewing condition, the luminance of the characters at the eye and the transmittance of

the ambient light through the visor and/or display combiner optics should be adjusted also to maintain a contrast of 0.96. In addition, transmittances of the visor and combiner should be adjusted to meet the criteria established by Cohen (1973) and Cohen et al. (1974) (i.e., $0.3 \leq L_{\Delta} \leq 10.0$, Section 2.4.5, and $C_{max} \geq 0.23$, Section 2.4.4).

For example, given a typical CRT luminance (L_{CRT}) of 1000 cd/m^2, optical transmittance (t_0) of 0.80 and ambient luminance (L_S) of 10,000 cd/m^2, a combiner transmittance (t_c) of 0.022 and reflectance (r_c) of 0.978 and visor transmittance ($t_v = t'_v$) of 0.15 would produce, theoretically, the desired contrast. Under these conditions $L_{\Delta} = 0.54$ and $C_{max} = 0.92$ and, according to Cohen, these values will allow adequate visibility of both the display presentation and the outside scene. L_{Δ} can be adjusted upward, if necessary, by reducing the transmittance of the visor over the nondisplay eye.

9.2.3.4 Character Font Considerations

The confusions of some characters in the legibility experiments indicate the need to exercise some care in selecting character fonts. Since characters will be grouped in operational displays, and image overlap may occur due to vibration, characters should be chosen whose distinctive features minimize confusion under these conditions.

9.2.4 Displays of Imagery

As discussed above, the nodal images formed by sinusoidal vibration significantly degraded the quality of pictorial image presentation. There are few approaches for offsetting this effect. One approach may be to increase the optical or electronic (i.e., CRT) magnification of the display so as to make the resolution elements and targets appear larger relative to nodal image displacements. Although this approach may provide some improvements, large magnifications most likely would be needed (e.g., for a two-to-one improvement in perceived resolution the magnification must increase by at least a factor of two). With a fixed display field-of-view, increasing the image scale size to compensate for the loss in perceived resolution will be offset by a concommitant loss in scene field-of-view.

The other alternative is to reduce the motion of the display image on the retina. Again, isolation of the seat from the vibrating aircraft structures may reduce some of the motion transmitted to the head, otherwise some form of image stabilization must be used. Possible techniques for image stabilization are discussed below.

9.2.5 Image Stabilization

The results of Experiments LG.1 (Section 4.2), LG.2 (Section 4.3), and SD.2 (Section 6.3) lead to the recommendation that vibration stabilization should be provided over a frequency range of 2.0 Hz to 16.0 Hz to cover the regions wherein vertical whole-body vibration has been shown to degrade display visibility. Generally, the frequencies between 2.8 Hz to 8.0 Hz have the greatest impact on reading performance and the largest retinal image displacements. At these frequencies the vestibulo-ocular reflex is providing some space stabilization to the eyes while the display image is oscillating in the pitch axis with the helmet. For this frequency region, retinal image displacements may be reduced by also causing the display image to be stabilized in space. For the vibration frequencies exceeding the bandwidth of the VOR (nominally 8.0 Hz to 16.0 Hz), the motion of the display image on the retina is due to the rotational displacement of the helmet on the head. Here retinal image displacements may be reduced by causing the display image to move in accordance with the displacement differences between the helmet and head. For fixed-wing aircraft, image stabilization only up to 8.0 Hz may be needed, depending upon the power spectral distribution of the vertical vibration. For rotary wing aircraft, stabilization may have to be tuned to the predominant frequencies of the resulting deterministic vibration.

Image stabilization of the display should be provided for both the pitch and yaw axes. The findings of Experiments SD.2 (Section 6.3) and ST.1 (Section 8.2) suggest that peak-to-peak image displacements of up to 123 minutes-of-arc in pitch and 20 minutes-of-arc in yaw can be anticipated for vertical Z axis sinusoidal vibration of 1.0 m/s^2 rms between 2.8 and 8.0 Hz. Harmonics of the fundamental frequencies of seat vibration can also be anticipated in the motion of the head and helmet for frequencies of 4.0 Hz and below.

9.2.5.1 Image Stabilization Techniques

Generally, methods for stabilizing the helmet-mounted display image can be categorized as either active or passive. Passive techniques use the mechanical properties of components or materials comprising the head-coupled display system in order to achieve image stabilization. Active techniques add special elements to the system to transduce movements of the display, head, helmet, or eyes and use this information to activate or control other elements for orienting the display image relative to the eye. Figure 9.2.1 outlines some approaches for achieving image stabilization. Tables 9.2.1 and 9.2.2 list advantages and disadvantages of these approaches which may be considered in selecting the appropriate approach for operational use.

9.2.5.2 Phosphor Characteristics

For those stabilization approaches which electronically displace the image on the CRT, the results of Experiment ST.1 (Section 8.4) suggest that the interfield luminances decay to an extent that the residual luminance from one field will have little effect on the contrast details of successive fields. A phosphor which decays to about 1 percent of its initial value during one field interval is recommended.

9.3 RECOMMENDED AREAS FOR FUTURE RESEARCH

9.3.1 Reading Task

One problem which emerged during the experimental program was associated with the character reading task. It was found that most subjects were unsuccessful in pacing their reading of the numeric characters under the more severe vibration conditions. Reading rates often fell well below the one character per second rate although subjects were advised frequently to maintain their pace to equal the pulse rate of the tone generator. It was likely that the number of reading errors committed by the subjects under these conditions did not fully represent the difficulty of the task (i.e., the error rate was too low). If the subjects had been paced by some other method which precluded a

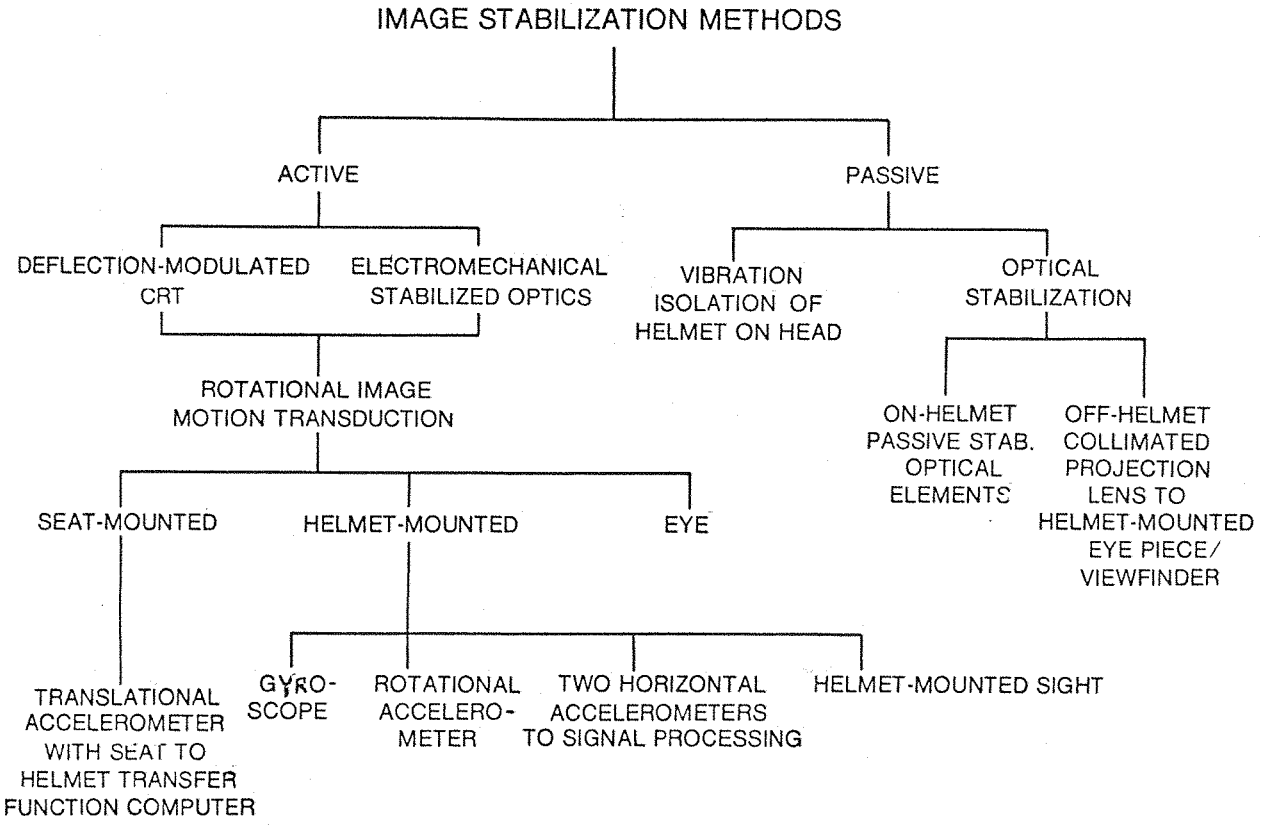

Figure 9.2.1. Helmet-Mounted Display Image Stabilization Methods

TABLE 9.2.1. ADVANTAGES AND DISADVANTAGES OF PASSIVE IMAGE STABILIZATION METHODS

Method	Advantages	Disadvantages
vibration isolation of helmet on head (or display optics on helmet)	-nonfrangible	-may increase helmet mass, form factor -difficult to isolate at low frequency with large head displacements -difficult to isolate over large frequency range -may alter protection requirements during ejection (e.g., windblast, impact) -must "tune" design to each operator
optical stabilization		
on helmet (passive stabilization of optical elements)	-minimum adjustment required -nonfrangible	-increased mass/weight of optical assembly -affected by normal head movements -poor high frequency response
off helmet (collimated projection lens to helmet-mounted eyepiece/ viewfinder)	-minimum adjustment required -nonfrangible -reduced helmet mass (CRT located off helmet) -ideal space stabilization	-restricted head movement -display image does not move with with the head for off-axis operation -significant crewstation modifications may be required

TABLE 9.2.2. ADVANTAGES AND DISADVANTAGES OF ACTIVE IMAGE STABILIZATION METHODS

Method	Advantages	Disadvantages
electromechanical stabilized optics	-minimum adjustment required -nonfrangible	-requires external motion transducer -increases size/mass of optics -electromechanical actuators increase mass and bulk of helmet-mounted unit -must adjust gain/phase of transducer feedback loop
deflection-modulated CRT	-easy to implement in HMD electronics -no impact on optics	-requires external motion transducer -sensitive to phosphor effects (e.g., persistence) -must adjust gain/phase of transducer feedback loop
display rotational motion transduction		
seat-mounted (translational accelerometer in seat with seat to helmet transfer function computer)	-minimum impact on helmet -nonfrangible	-must assume transfer function of seat-to-helmet -complexity of additional computation -cannot compensate for intrasubject transmissibility effects of posture, muscle tension, and head orientation
helmet/display mounted	-measures helmet-motion directly	-adds mass/bulk to helmet
rotational accelerometer	-simplest direct measure of helmet/display rotational acceleration	-frangible, bulky transducers required -double integration required
translational accelerometer (must use at least two to transduce rotation acceleration)	-small, lightweight transducers -less frangible than rotational accelerometer	-requires signal processing to derive rotational motion -double integration required
gyroscope	-nonfrangible	-large mass increase to helmet -single integration required (rate gyro) -special power suplies required
helmet-mounted sight (helmet position sensor)	-may already be incorporated with helmet-mounted display	-complex, expensive -poor angular resolution -required high update and throughput rates -phase compensation required

voluntary adjustment of reading rate, such as presenting one character at a time, error rates probably would have been greater. However, if such a presentation method were used, the presentation time should be long enough to include several cycles of oscillation of the seat. Also, the rate at which the character luminance decreases at turn off should be gradual to prevent a high contrast afterimage from forming on the retina after each character is blanked.

9.3.2 Characteristics of Head/Helmet Motion

Further research is needed to characterize the behaviour of helmet-movement on the head. The stability of the helmet on the head may be the major factor causing retinal image displacements at vibration frequencies exceeding the bandwidth of the vestibulo-ocular reflex. The results of the dynamic experiments reported herein were inconclusive about the presence of a helmet-to-head resonance nor could the bizarre nonlinear behaviour of the helmet movement on the head be explained at some frequencies. The effect of helmet fit, helmet-to-head suspension method, and mass loadings on the helmet should be considered in future investigations.

9.3.3 Random Vibration

The laboratory experiments reported above were conducted with controlled single frequency sinusoidal motions of the seat. In turn, these vibration conditions tended to set up steady-state motions of the head, helmet, and eye. Nodal images were formed on the retina at the zero velocity points of the display image. The location of these nodal images on the retina was approximately the same for each vibration cycle, causing a single character (or picture element) on the display to appear as two distinct characters or picture elements to the subject. If random vibration were applied to the seat containing some of the same frequencies as the single vibration frequencies used in the laboratory experiments above, then it is likely that "nodal-type" images would also be formed at the zero velocity points of the excursions of the display image on the retina, as mediated by the same

helmet pitch and VOR mechanisms cited previously for the single frequency input. In case of the random motion, however, successive nodal points would not occur at the same locations on the retina. Under these conditions, a distinct appearance of this display image would occur only if there were sufficient "dwell time" of the image across retinal receptors to integrate sufficient luminous energy to perceive the image. Depending upon the spectral content of the vibration input (i.e., power in low frequencies), greater degradation of display visibility may occur due to the absence of distinct nodal images during random vibration than under single frequency conditions with equivalent rms vibration levels.

Since the random motion is prevalent in the fixed-wing aircraft environments in which the helmet-mounted display is to be applied, it is recommended that further research investigate the nature of the effects of whole-body random motion on the perception of the helmet-mounted display. If possible, vibration frequencies between 1.0 Hz and 5.6 Hz should be emphasized in these investigations to correspond with the vibration responses of many fixed-wing aircraft.

9.3.4 Imagery

In the experiments above, the effects of vibration on the perception of pictorial imagery were investigated for only one vibration frequency and level (i.e., 4.0 Hz and 1.0 m/s^2 rms in Experiment ST.1). Since the presentation of sensor imagery is a primary application of the helmet-mounted display, more research is needed to extend these results to other sinusoidal vibration frequencies, levels, and to random vibration environments. As discussed in Section 9.1.3 previously, formation of nodal images probably does not facilitate perception of imagery on the helmet-mounted display. In this case, vibration level (for fixed spatial detail of the target) may have little effect. There may be a significant interaction between the vibration level (i.e., producing various displacements of nodal images) and the size and spatial details of the targets and their backgrounds, depending upon how the target overlaps itself and the background.

9.3.5 Interaction of Background Luminance and Contrast on Display Perception

It was apparent from Experiments LG.3 (Section 4.4.1) and LG.4 (Section 4.4.2) that luminances of the background and the character to background contrast had a significant influence on the way that vibration affected reading performance. From the discussions in Section 4.4.4 and 4.5.4, it was proposed that these factors influenced, photochemical adaptation of eye, pupil diameter, lens accommodation, contrast sensitivity, and optical aberrations of the eye. In addition to the profound effects of contrast and background luminance on reading performance, there also seemed to be an effect on subjective factors, such as maintaining focus of the image and perhaps fatigue (e.g., subjects commented often that they did not like to look at the green image). Since the proposed applications of the helmet-mounted display are for both night/low ambient luminance, and daylight/high ambient luminance viewing conditions, further study is needed to understand the way that these factors, along with vibration, influence reading performance and fatigue. For example, it may be inappropriate to collimate the HMD to optical infinity for operation at night due to the difficulty in maintaining accommodation to optical infinity under low luminance levels. Perhaps high spatial frequency images should be superimposed over the display (CRT) scene to insure that sufficient spatial detail is available to elicit the appropriate accommodation response of the eye. Also, the spectral emmissivity characteristics of the phosphor may be adjusted to aid accommodation to collimated images.

9.3.6 Stabilization

In spite of the passive improvements in reading performance during vibration provided by manipulating the spatial and luminance characteristics of the display (that is, for single characters or symbolic information), vibration will degrade perception of the helmet-mounted display as long as there is relative movement of the display image on the retina (resulting from other than the normal physiological nystagmus). The only alternative is to adopt some means for reducing

this movement. A simple approach for stabilizing the image has been demonstrated (Experiment ST.1, Section 8) and improvements to this design have been recommended. As a next step, these recommendations should be incorporated into an improved stabilization system and assessed using both character legibility and pictorial target recognition tasks. The stabilization techniques should be evaluated across a range of appropriate discrete vibration frequencies and random motion environments. Methods should be developed for readily adjusting the gain and phase characteristics of the stabilization system, and correcting for drifts so that system alignments (boresights) remain intact. Filtering algorithms must be established for isolating the rotational movements of the head which are voluntary from those involuntary movements produced by vibration inputs. Finally, a trade-off of the various stabilization mechanizations must be performed to identify the best approach (or approaches) for the specific applications. Factors in a trade-off analysis should include: weight, form factor on helmet, frangibility, ease of adjustment, cost, complexity, accuracy of stabilization, quality of image presentation, and impact on existing helmet-mounted display designs.

9.4 FINAL CONCLUSIONS

The original objectives of this thesis were to investigate the ways whole-body vibration affected perception of the helmet-mounted display, to identify the mechanisms causing degradation, and to develop methods for reducing or overcoming these debilitating effects. It is felt that through the experimental programme which has been reported herein and within the constraints of the specific vibration variables studied, these objectives have been met. The results above show that whole-body vibration will effect the perception of the helmet-mounted display. These results, therefore, confirm the original hypothesis of this thesis. The results also agree generally with the literature regarding the dynamic nature of the human operator during vibration and the nature of compensatory mechanisms such as the vestibulo-ocular reflex. The results support the posit by Benson and Barnes (1978) that vibration producing head rotation will affect perception of a head-coupled display at some frequencies. The results also extend the

findings of Laycock (1978) regarding the legibility of characters on the helmet-mounted display during whole-body vibration.

The research reported herein implies that under some aircraft vibration conditions, the performance of operators can be degraded by whole-body vibration. The extent of the degradation will depend upon the nature of the vibration environment, operator characteristics, the type of presentation, and other display factors (e.g., contrast, background luminance). The harmful effects of vibration can be reduced, however, by reducing the transmission of vibration to the head, selecting optimum display factors, and reducing the displacement of the image on the retina by some stabilization process.

Further research is needed to extend these results to lower vibration frequencies and random motion environments commensurate with the nature of vibration in fixed-wing aircraft. Other work is needed to optimize approaches for image stabilization.

The vibration problems which have been shown to affect the helmet-mounted display can be overcome, given a knowledge of the display-operator characteristics and development of appropriate compensation mechanisms. These efforts, however, have come late in the development of the head-coupled display technology, which began in 1961. This happening emphasizes the need to begin investigations of the human factors aspects of environmental stressors, such as vibration, early in the design of all visual displays. Accordingly, the design criteria and recommendations for reducing the effects of environment stressors should be included in the evolution of the display technology, incorporated into prototype designs, and evaluated in simulated operational environments prior to the final development stages of a display system.

REFERENCES

ABBOTT B A (1968). Evaluation of a night vision display system for helicopter operation--Study II, flight test of the total low light level television system. Bell Helicopter Co., Fort Worth, Texas, Report No. 599-527-001, January 1968.

ABBOTT B A (1969). A head-mounted night vision display system for helicopter operation, final technical report. Bell Helicopter Company, Fort Worth, Texas, Report No. 299-099-3, November 1969.

ALEXANDER C (1972). Performance changes due to the single and dual frequency vibration of reading material. MSc thesis. University of Southampton.

ANONYMOUS (1973). Helmet-mounted display (HMD) manual, model RC/HMD-201. Hughes Aircraft Company, Culver City, California, January 1973.

ANONYMOUS (1974). Guide for the evaluation of human exposure to whole-body vibration. International Organization for Standardization, ISO 2631-1974(E).

ANONYMOUS (1975a). Vibration and combined stresses in advanced systems. North Atlantic Treaty Organization, Advisory Group for Aerospace Research and Development, AGARD conference proceedings, AGARD-CP-145, March 1975.

ANONYMOUS (1975b). The effects of buffeting and other transonic phenomena on maneuvering combat aircraft. North Atlantic Treaty Organization, Advisory Group for Aerospace Research and Development, Advisory Report AGARD-AR-82, July 1975.

ANONYMOUS (1975c). Vibration and shock vocabulary, International Organization for Standardization, ISO 2041-1975(E/F).

BARNES G R (1976). Vestibulo-ocular responses to head turning movements and their functional significance during target acquisition. PhD thesis, University of Surrey, November 1976.

BARNES G R (1979a). Vestibulo-ocular function during coordinated head and eye movements to acquire visual targets. Journal of Physiology 287, pp 127-147.

BARNES G R (1979b). The effects of aircraft vibration on vision. Paper to U.K. Informal Group on Human Response to Vibration, Institute of Aviation Medicine, Farnborough, September 24-26, 1979.

BARNES G R, BENSON A J and PRIOR A R J (1978). Visual vestibular interaction in the control of eye movement. Aviation, Space and Environmental Medicine 49(4), pp 557-564.

BARNES G R and RANCE B H (1974). Transmission of angular acceleration to the head in the seated human subject. Aerospace Medicine 45(4), pp 411-416.

BARNES G R and RANCE B H (1975). Head movement induced by angular oscillation of the body in the pitch and roll axes. Aviation, Space and Environmental Medicine 46(8), pp 987-993.

BARNES G R and SMITH R (1980). The effects of image movement across the stationary retina on visual discrimination. Submitted for publication.

BENDAT J S and PIERSOL A G (1971). Random Data: Analysis and Measurement Procedures. (Wiley-Interscience, New York).

BENSON A J (1972). Effect of angular oscillation in yaw on vision. Aerospace Medical Association Annual Scientific Meeting, May 8-11, 1972, Bal Harbour, Florida, pp 43-44.

BENSON A J (1974). Modification of the response to angular accelerations by linear accelerations. In: Handbook of Sensory Physiology. H H Kornhuber Ed. (Springer-Verlag, Berlin).

BENSON A J and BARNES G R (1978). Vision during angular oscillation: the dynamic interaction of visual and vestibular mechanisms. Aviation, Space and Environmental Medicine 49(1), pp 340-345.

BIRT J A and FURNESS T A (1974). Visually-coupled systems. Air University Review 20(3), pp 28-40.

BIRT J A and TASK H L Ed. (1973). Proceedings of a Symposium on Visually-Coupled Systems: Development and Applications. Brooks Air Force Base, Texas, November 8-10, 1972, USAF Aerospace Medical Division, Brooks AFB, Texas, Technical Report No. AMD-TR-73-1, September 1973.

BRIDGEMAN B, HENDRY D and STARK L (1975). Failure to detect displacement of the visual world during saccadic eye movements. Vision Research 15, pp 719-722.

BROADBENT D E (1958). Perception and Communication. (Pergamon, Oxford).

BROWN H T (1964). Evaluation of a head worn audio-visual aid. Hughes Aircraft Company, Fullterton, California, Report No. FR 64-10-333, November 1964.

BROWN J L (1965). Flicker and intermittent stimulation. In: Vision and Visual Perception, C H Graham, Ed. (John Wiley, New York), pp 251-320.

BROWN J L and MUELLER C G (1965). Brightness discrimination and brightness contrast. In: Vision and Visual Perception, C H Graham, Ed. (John Wiley, New York), pp 208-250.

BURNETT K T (1971). The status of human perceptual characteristic data for electronic flight display design. North Atlantic Treaty Organization, Advisory Group on Aerospace Research and Development, Conference Proceedings, AGARD-CP-96, October 1971.

CAMPBELL F W and GREEN D G (1965a). Optical and retinal factors affecting visual resolution. Journal of Physiology 181, pp 576-593.

CAMPBELL F W and GREEN D G (1965b). Monocular versus binocular acuity. Nature 208, pp 191-192.

CAMPBELL F W and GUBISH R W (1966). Optical quiality of the human eye. Journal of Physiology 186, p 558.

CAMPBELL F W and WESTHEIMER G (1959). Factors involving accommodation responses of the human eye. Journal of the Optical Society of America 49, pp 568-571.

CHISUM G T (1975). Head-coupled display visual design considerations. Aviation, Space and Environmental Medicine 46(11), pp 1373-1377.

COERMANN, R (1940). Investigations into the effect of vibration on the human body. Luftfahrtmedizin 4, pp 73-117.

COHEN B (1971). Vestibulo-ocular relations. In: Control of Eye Movements, P Back-Y-Rita and C C Collins, Eds. (Academic Press, London), pp 105-148.

COHEN B J (1973). Integrated helmet-mounted sight/display program--computer assisted analysis of day/night visual requirements. Honeywell, Inc., Minneapolis, Minnesota, Special Study Report IHMS/D-SR5, July 1973.

COHEN B J and MARKOFF J I (1972). Integrated helmet-mounted sight/display program--special human factors report. Honeywell Systems and Research Division, Minneapolis, Minnesota, Report IHMS/D-SR1, December 1972.

COHEN B J, BLOOMFIELD J R and MC ALLEESE K J (1974). Helmet-mounted displays--an experimental investigation of display luminance and contrast. Honeywell Inc., Minneapolis, Minnesota, August 1974.

COLLINS A M (1973). Decrements in tracking and visual performance during vibration. Human Factors 15(4), pp 379-393.

CORNSWEET T N (1970). Visual Perception. (Academic Press, New York).

CROOK M N, HOFFMAN A C, WESSELL N Y, WULFECK J W and KENNEDY J L (1947a). Preliminary studies of the effects of vibration, illumination and type size on legibility of numerals. USAF Aero Medical Laboratory, Wright-Patterson AFB, Ohio, Technical Report No. TSEAA-694-1F.

CROOK M N, HOFFMAN A C, WESSELL N Y, WULFECK J W and KENNEDY J L (1947b). Further studies of the effect of vibration and other factors on legibility of numerals. USAF Aero Medical Laboratory, Wright-Patterson AFB, Ohio, Technical Report No. TSEAA-694-1K.

CROOK M N, HARKER G S, HOFFMAN A C and KENNEDY J L (1948). Studies of the effects of typographical spacing on the legibility of numerals under vibration. USAF Material Command, Memo Report MCREXD-694-1Q.

CROOK M N, HARKER G S, HOFFMAN A C, WULFECK J W and KENNEDY J L (1949). A determination of amplitude thresholds for the visual perception of vibration. USAF Air Material Command, Memo Report MCREXD-694-1R.

CROOK M N, NARKER C S, HOFFMAN A C and KENNEDY J L (1950). Effect of amplitude of apparent vibration, brightness, type size on numeral reading. Air Force Aero Medical Laboratory, Wright-Patterson AFB, Ohio, Technical Report AFTR 6246.

DAVIDSON M L (1968). Perturbation approach to spatial brightness interaction in human vision. Journal of the Optical Society of America 58, pp 1300-1309.

DEAN R D, MC GLOTHEN G L and MONROE C L (1964). Performance and physiological effects of CH-46a noise and vibration. The Boeing Company, Seattle, Washington, Report No. D2-90583.

DENNIS J P (1963). A survey of experimental data on the effects of whole-body vibration and of vibration of the visual object upon visual performance. Occupational Psychology 37(4), pp 277-282.

DENNIS J P (1965a). Some effects of vibration upon visual performance. Journal of Applied Psychology 49(4), pp 245-252.

DENNIS J P (1965b). The effect of whole-body vibration on a visual performance task. Ergonomics 8, pp 193-205.

DRAZIN D H (1962). Factors affecting vision during vibration. Research 15, pp 275-280.

ERICKSON R A (1978). Line criteria in target acquisition with television. Human Factors 20(5), pp 573-588.

ERICKSON R A and HEMINGWAY J C (1970). Image identification on television. Naval Weapons Center, China Lake, California, Technical Report NWC TP 5025, September 1970.

EVANS D W (1980). The effects of vibration on target acquisition. MSc thesis, Wright State University.

FARRELL R J and BOOTH J M (1975). Design handbook for imagery interpretation equipment. Boeing Aerospace Company, Seattle, Washington, December 1975.

FECHNER G (1861). Euber einige verhaltnisse des binocularen sehens. Abh. Kon. Sachs. Gesells. Wiss., 5, pp 336-564.

FEDDERSEN W E (1962). Simulation evaluation of a head mounted orientation display. Bell Helicopter Company, Fort Worth, Texas, Technical Report No. D228-421-012, May 1962.

FEHR E R (1973). Optimized optical link for helmet-mounted display. USAF Aerospace Medical Research Laboratory, Wright-Patterson AFB, Ohio, Technical Report AMRL-TR-73-20, September 1973.

FESTINGER L (1971). Eye movements and perception. In: Control of Eye Movements, P Back-Y-Rita and C C Collins, Eds. (Academic Press, London), pp 259-273.

FLEISHMAN E A and HEMPEL W E (1955). The relation between abilities and improvement with practice in a visual discrimination reaction task. Journal of Experimental Psychology 49, pp 301-312.

FUCHS A F (1971). The saccadic system. In: Control of Eye Movements, P Back-Y-Rita and C C Collins, Eds. (Academic Press, London), pp 343-361.

FURNESS T A (1969). The application of helmet-mounted displays to airborne reconnaissance and weapon delivery. Proceedings of symposium for Image Display and Recording, Air Force Avionics Laboratory, Wright-Patterson AFB, Ohio, Technical Report TR-69-241, April 1969, AD 700515.

FURNESS T A (1978). Visually-coupled information systems. ARPA Conference on Biocybernetic Applications for Military Systems, Chicago, Illinois, April 5-7, 1978.

GASSOWSKI L N (1941). Illumination of the retina of the nonutilized eye during work at monocular visual apparatuses. Problemy Fiziologicheskoi Optiki 1, pp 33-42.

GIBSON J E (1965). Adaptive and learning control systems. In: System Engineering Handbook, R E Machol Ed. (McGraw-Hill, New York).

GIBSON K S and TYNDALL E P T (1923). Visibility of radiant energy. Scientific Paper Bureau of Standards, No. 475, 19, 3, August 11, 1923, pp 131-191.

GINSBURG A P (1978). Visual information processing based on spatial filters constrained by biological data. USAF Aerospace Medical Research Laboratory, Wright-Patterson AFB, Ohio, Technical Report AMRL-TR-78-129, December 1978.

GOULD J D (1976). Looking at pictures. In: Eye Movements and Psychological Processes, R A Monty and J W Senders, Eds. (Lawrence Erlbaum, Hillsdale, New Jersey), Part V, Chapter 2, pp 323-345.

GRAHAM C H (1965). Visual space perception. In: Vision and Visual Perception, C H Graham, Ed. (Wiley, New York), pp 504-547.

GRANIT R and HARPER P (1930). Comparative studies on the peripheral and central retina: II. Synaptic reactions in the eye. American Journal of Physiology 95, pp 211-227.

GRETHER W F (1971). Vibration and human performance. Human Factors 13(3), pp 203-216.

GRIFFIN M J (1972a). The transmission of triaxial vibration to pilots in the Scout AH MKI helicopter. University of Southampton, Institute of Sound and Vibration Technical Report No. 58, Southampton, August 1972.

GRIFFIN M J (1972b). Whole-body vibration and human vision. PhD thesis, University of Southampton, November 1972.

GRIFFIN M J (1973). A survey of human response to vibration in Great Britain. University of Southampton, Institute of Sound and Vibration Technical Report No. 60, Southampton.

GRIFFIN M J (1974). A study of vibration, pilot vision and helicopter accidents. AGARD Conference on Vibration and Combined Stresses in Advanced Systems, No. 145, pp 22-23, April 1974.

GRIFFIN M J (1975a). Vertical vibration of seated subjects: effects of posture, vibration level, and frequency. Aviation, Space and Environmental Medicine 46(3), pp 269-276.

GRIFFIN M J (1975b). Levels of whole-body vibration affecting human vision. Aviation, Space and Environmental Medicine 46(8), pp 1033-1040.

GRIFFIN M J (1975c). A study of vibration, pilot vision and helicopter accidents. Advisory Group on Aerospace Research and Development, Conference Report AGARD-CR-145, March 1975.

GRIFFIN M J (1976a). Vibration and Visual Acuity. In: Infrasound and Low Frequency Vibration, W Tempest Ed. (Academic Press), Chapter 10, pp 263-298.

GRIFFIN M J (1976b). Eye motion during whole-body vertical vibration. Human Factors 18(6), pp 601-606.

GRIFFIN M J (1976c). Subjective equivalence of sinusoidal and random whole-body vibration. Journal of the Acoustical Society of America 60(5), pp. 1140-1145.

GRIFFIN M J and LEWIS C H (1978). A review of the effects of vibration on visual acuity and continuous manual control. Part I: visual acuity. Journal of Sound and Vibration 56(3), pp 383-413.

GRIFFIN M J, LEWIS C H, PARSONS K C and WHITHAM E M (1978). The biodynamic response of the human body and its application to standards. Presented at AGARD Aerospace Medical Panel 35th Specialist's Meeting on "Models and Analogues for the Evaluation of Human Dynamic Response and Protection." November 6-10, 1978, Paris, AGARD Conference Proceedings, AGARD-CP-253, June 1979.

GRIFFIN M J and WHITHAM E M (1978). Individual variability and its effect on subjective and biodynamic response to whole-body vibration. Journal of Sound and Vibration 58(2), pp 239-250.

GRIMSTER W F, HOLLIDAY C D and HERRICK C S (1974). Sea King pilot vibration. Westland Helicopters Ltd., Research Paper No. 463, part 2.

GUEDRY F E, LENTZ J M and JELL R M (1978). Visual-vestibular interactions: 1. influence of peripheral vision on suppression of the vestibulo-ocular reflex and visual acuity. Naval Aerospace Medical Research Laboratory, Technical Report NAMRL-1246, Pensacola, Florida.

GUIGNARD J C (1965). Vibration. In: A Textbook of Aviation Physiology, J A Gillies, Ed. (Pergamon, Oxford), Chapter 29, pp 813-894.

GUIGNARD J C and GUIGNARD E (1970). Human response to vibration: a critical survey of published work. University of Southampton, Institute of Sound and Vibration Memorandum No. 373, Southampton.

GUIGNARD J C and IRVING A (1960). Effects of low frequency vibration in man. Engineering (London) 190, pp 364-367.

GUIGNARD J C and KING P F (1972). Aeromedical aspects of vibration and noise. North Atlantic Treaty Organization, Advisory Group for Aerospace Research and Development, AGARDograph No. 151.

GUTMANN J C, SYNDER H L, FARLEY W W and EVANS J E (1979). An experimental determination of the effect of image quality on eye movements and search for static and dynamic targets. USAF Aerospace Medical Research Laboratory, Wright-Patterson AFB, Ohio, Technical Report No. AMRL-TR-79-51. August 1979.

HAIG C (1941). The course of rod dark adaptation as influenced by intensity and duration of preadapting to light. Journal of General Physiology 24, pp 735-751.

HALL R J and MILLER J W (1960). Feasibility study for a monocular head-mounted display. Hughes Aircraft Company, Culver City, California, Special Technical Document 5060-70, September 1960.

HALL R J and MILLER J W (1963). Head-mounted electrocular display: a new display concept for specialized environments. Aerospace Medicine 34(4), April 1963.

HECHT S (1934). Vision II. The nature of the photoreceptor process. In: Handbook of General Experimental Psychology, C Murchimsun, Ed. (Clark University Press, Worchester, Mass.), pp 704-828.

HEMINGWAY J C and ERICKSON R A (1969). Relative effects of raster scan lines and image subtense on symbol legibility on television. Human Factors 11(4), 331-338.

HERSHBERGER M L and GUERIN D F (1975). Binocular rivalry in helmet-mounted display applications. USAF Aerospace Medical Research Laboratory, Wright-Patterson AFB, Ohio, Technical Report AMRL-TR-75-48.

HOFFMAN C S and GREENING C P (1967). Effect of blur and size on target recognition. Aerospace Medicine 38, pp 156-158.

HUDDLESTON J H F (1970). Tracking performance on a visual display apparently vibrating at one to ten hertz. Journal of Applied Psychology 54(5), pp 401-408.

HUGHES R L, CHASON L R and SCHWANK S C H (1973). Psychological considerations in the design of helmet-mounted displays and sights. USAF Aerospace Medical Research Laboratory, Wright-Patterson AFB, Ohio, Technical Report AMRL-TR-73-16, August 1973.

HURT G J (1963). Rough-air effect on crew performance during a simulated low-altitude high-speed surveillance mission. National Aeronautics and Space Administration, Langley, Virginia, Technical Note D-1924.

JACOBS R S, TRIGGS T J and ALDRICH J W (1971). Helmet-mounted display/sight system study, Volume 1. USAF Flight Dynamics Laboratory, Wright-Patterson AFB, Ohio, Technical Report No. AFFDL-TR-70-83, March 1971.

JARRETT D N (1978). Helmet slip during simulated low-level high speed flight. Royal Aircraft Establishment, Farnborough, Technical Report 78018, February 1978.

JOHNSON C (1976). Effects of luminance and stimulus distance on accommodation and visual resolution. Journal of the Optical Society of America, 66, pp 138-142.

JOHNSON J (1958). Image intensifier symposium. U.S. Army Night Vision Laboratory, Fort Belvoir, Virginia, AD 220160, October 1958.

JONES G M (1971). Organization of neural control in the vestibulo-ocular reflex arc. In: Control of Eye Movements, P Back-Y-Rita and C C Collins, Eds. (Academic Press, London), pp 497-518.

JONES G M (1976). The vestibular system for eye movement control. In: Eye Movements and Psychological Processes, R A Monty and J W Senders, Eds. (Lawrence Erlbaum, Hillsdale, New Jersey), Part 1, Chapter 1, pp 3-17.

JUST M A and CARPENTER P A (1976). Eye fixations and cognitive processes. Cognitive Psychology 8, pp 441-480.

KELLY D H (1961). Visual responses to time-dependent stimuli. I. Amplitude sensitivity measurements. Journal of the Optical Society of America 51, pp 422-429.

KENNEDY K W and KROEMER K H E (1973). Excursion of head, helmet and helmet attached reticle under $+G_z$ forces. USAF Aerospace Medical Research Laboratory, Wright-Patterson AFB, Ohio, Technical Report AMRL-TR-72-127, May 1973.

KIRK R E (1968). Experimental Design: Procedures for the Behavioural Sciences. (Brooks/Cole, Belmont, California).

KOCIAN D F and PRATT P D (1972). Development of a helmet-mounted visor display. Proceedings of a symposium on visually-coupled systems: development and applications, Brooks Air Force Base, Texas, November 8-10, 1972. USAF Aerospace Medical Division, Brooks AFB, Texas, Technical Report AMD-TR-73-1, September 1973.

KÖNIG A and BRODHUN E (1889). Experimentelle untersuchugen ueber die psychophysische fundamentalformel in Bezug auf den Gesichtssin. Sitzungsberg. Preuss Akad. Wiss. 27, pp 641-644.

KRAUSKOPF J (1957). Effect of retinal image motion on contrast thresholds for maintained vision. Journal of the Optical Society of America 47(8), pp 740-744.

KROEMER K H E and KENNEDY K W (1973). Involuntary head movements and helmet-motions during centrifuge runs with up to +6 G_z. Aerospace Medicine 44(6), pp 639-644.

LACEY L A (1975). Effect of raster scan lines, image subtense, and target orientation on aircraft identification on television. Naval Weapons Center, China Lake, California, NWC TP 5763, May 1975.

LAYCOCK J (1976). A review of the literature appertaining to binocular rivalry and helmet-mounted displays. Royal Aircraft Establishment, Farnborough, Technical Report 76101, July 1976.

LAYCOCK J (1977). A laboratory investigation of the effect of stimulus parameters on binocular rivalry in helmet-mounted displays. Royal Aircraft Establishment, Farnborough, Technical Report 77028, February 1977.

LAYCOCK J (1978). A preliminary investigation of the legibility of alphanumeric characters on a helmet-mounted display. Royal Aircraft Establishment, Farnborough, Technical Memo FS 155, January 1978.

LEVELT W J M (1968). On Binocular Rivalry. (Mouton, The Hague).

LEVISON W H (1978). Model for human controller performance in vibration environments. Aviation, Space and Environmental Medicine 49(1), pp 321-327.

LEWIS C H (1977). Frequency of whole-body vibration and reading performance. Paper to U. K. Informal Group on Human Response to Vibration, VOP Bostrom, Northampton, September 7-9 (1977).

LEWIS C H (1978a). The effects of vibration on the performance of human operators in continuous manual control systems. PhD thesis, University of Southampton, August 1978.

LEWIS C H (1978b). The effect of character size on the legibility of alpha-numerics in vibration environments. Paper presented at the U.K. Informal Group Meeting on Human Response to Vibration. N.I.A.E., Silsoe, Bedfordshire, September 1978.

LEWIS C H (1979a). Personal communications regarding dynamic nature of modified helicopter seat and its effect on reading performance during whole-body vibration.

LEWIS C H (1979b). The interaction of the effects of vibration, in three axes, and seating conditions on the reading of numeric displays. Paper presented to U.K. Informal Group on Human Response to Vibration, R.A.E./I.A.M., Farnborough, September 1979.

LEWIS C H and GRIFFIN M J (1979a). The effect of character size on the legibility of numeric displays during vertical whole-body vibration. Journal of Sound and Vibration 67(4), pp 562-565.

LEWIS C H and GRIFFIN M J (1979b). Predicting the effects of vibration frequency, combinations of frequencies and viewing distance on the reading of numeric displays. (Submitted to the Journal of Sound and Vibration).

LICHTY W R (1974). An engineering model holographic visor helmet-mounted display. Hughes Aircraft Company, Culver City, California, Report No. P76-18, C8918, October 1974.

LUDVIGH E J and MILLER J W (1953). A study of dynamic visual acuity. Kresge Eye Institute and U.S. Naval School of Aviation Medicine, Joint Project No. NM 001075.01.01, Report I.

LURIA S M and STRAUSS M S (1975). Eye movements during search for coded and uncoded targets. Perception and Psychophysics 17(3), pp 303-308.

MARTIN W, TASK H L, WOODRUFF K R and PINKUS A (1976). A study of element density and active to total area ratio requirements for matrix displays. Air Force Avionics Laboratory, Wright-Patterson AFB, Ohio, Technical Report No. AFAL-TR-75-235, February 1976.

MC CORMICK E J (1976). Human Factors in Engineering and Design (McGraw-Hill, New York).

MEDDICK R D L and GRIFFIN M J (1976). The effect of two-axis vibration on the legibility of reading material. Ergonomics 19(1), pp 21-33.

MEIRY J L (1965). The vestibular system and human dynamic space orientation. ScD thesis, Massachusetts Institute of Technology.

MEIRY J L (1971). Vestibular and proprioceptive stabilization of eye movements. In: Control of Eye Movements, P Back-Y-Rita and C C Collins, Eds. (Academic Press, London), pp 483-496.

MERCER C A (ca. 1972). Data analysis. Unpublished report. Institute of Sound and Vibration Research, University of Southampton.

MERCER C A (1973). Development of data analysis in sound and vibration. Journal of Sound Vibration 28(3), pp 631-642.

MILLER E F (1956). Ocular pursuit of a target moving in an apparent circular path. U.S. Naval School of Aviation Medicine, Research Project NM 001-110-102, Report No. 1.

MILLER J W (1958). Study of visual acuity during ocular pursuit of moving test objects. II. Effects of direction of movement, relative movement, and illumination. Journal of the Optical Society of America, 48, pp 8034+.

MILLER J W and LUDVIGH E J (1953). Dynamic visual acuity when the required pursuit is in the vertical plane. Kresge Eye Institute and U.S. Naval School of Aviation Medicine, Joint Project No. NM 001-110-501, Report No. 2.

MILLER J W and LUDVIGH E (1962). The effect of relative motion on visual acuity. Survey of Ophthalmology 7(2), pp 83-116.

MORRIS D F (1966). The effects of whole-body vibration on numeral reading and compensatory tracking under low intensity red and white lighting. The Boeing Company, Wichita, Kansas, Report No. D3-7008, April 1966.

O'HANLON J G and GRIFFIN M J (1971). Some effects of the vibration of reading material upon visual performance. University of Southampton, Institute of Sound and Vibration Research Technical Report No. 49, May 1971.

OHLBAUM (1976). Mechanical resonance of the eye in vivo. USAF Aerospace Medical Research Laboratory, Wright-Patterson AFB, Ohio, Technical Report No. AMRL-TR-75-113.

OVERINGTON I (1976). Vision and Acquisition. (Pentech Press, London).

PARSONS K C (1979). The effect of whole-body rotational vibration on passenger comfort. PhD thesis, University of Southampton.

PATEL A S (1966). Spatial resolution by the human visual system. The effect of mean retinal illuminance. Journal of the Optical Society of America 56, pp 689-694.

PRADKO F, ORR T R and LEE R A (1965). Human vibration analysis. Society of Automotive Engineers, Mid-Year Meeting, Chicago, Illinois, May 17-21, 1965.

PRATT P D (1976). Advanced helmet reticle assembly. USAF Aerospace Medical Research Laboratory, Wright-Patterson AFB, Ohio, Technical Report No. AMRL-TR-73-11, July 1976.

RANCE B H (1978). Personal Communication. Head rotational movement due to vertical G_z motion.

RICHARDS W (1969). Saccadic suppression. Journal of the Optical Society of America, 59(5), pp 617-623.

RIGGS LORIN A (1965). Visual acuity. In: Vision and Visual Perception, C H Graham, Ed. (John Wiley, New York), pp 321-349.

ROBINSON D A (1968). The oculomotor control system: a review. Proceedings of the IEEE 56(6), pp 1032-1049.

ROBINSON D A (1976). The physiology of pursuit eye movements. In: Eye Movements and Psychological Processes, R A Monty and J W Senders, Eds. (Lawrence Erlbaum, Hillsdale, New Jersey), Part 1, Chapter 2, pp 19-31.

ROGERS J G and CAREL W L (1973). Development of design criteria for sensor displays. Office of Naval Research, Washington, D.C., Annual Report on Contract No. N00014-72-C-0451, NR213-107, December 1973.

ROSELL F A and WILLSON R H (1973). Recent psychophysical experiments and the display signal-to-noise ratio concept. In: Perception of Displayed Information, L M Biberman, Ed. (Plenum Press, New York), pp 167-231.

ROWLANDS G F (1977). The transmission of vertical vibration to the heads and shoulders of seated men. Royal Aircraft Establishment, Farnborough, Technical Report TR 77068, May 1977.

ROWLANDS G F and ALLEN G R (1969). The rotational eye movements needed to correct for vibration of the head. Royal Aircraft Establishment, Farnborough, Technical Memorandum EP 427, August 1969.

RUBENSTEIN L and TAUB H A (1967). Visual acuity during vibration as a function of frequency, amplitude and subject display relationship. Aerospace Medical Research Laboratory, Wright-Patterson AFB, Ohio, Technical Report 66-181.

SCANLAN L A and CAREL W L (1976). Human performance evaluation of matrix displays: literature and technology review. USAF Aerospace Medical Research Laboratory, Wright-Patterson AFB, Ohio, Technical Report AMRL-TR-76-39, June 1976.

SCHNITZLER A D (1973). Analysis of noise required contrast and modulation in image detecting and display systems. In: Perception of Displayed Information, L M Biberman, Ed. (Plenum Press, New York), pp 119-166.

SCOTT F and HOLLANDA P A (1970). The informative value of sampled images as a function of the number of scans per scene object. Photographic Science and Engineering 14, pp 21-27.

SEKULER R (1974). Spatial vision. Annual Review of Psychology 25, pp 195-232.

SELF H C (1972). The construction and optics problems of helmet-mounted displays. Proceedings of a Symposium on visually-coupled systems: development and applications. Brooks AFB, Texas, November 8-10, 1972. USAF Aerospace Medical Division, Technical Report No. AMD-TR-73-1, September 1973.

SEMPLE C A, HEAPY R J, CONWAY E J and BURNETTE K T (1971). Analysis of human factors data for electronic flight display systems. USAF Flight Dynamics Laboratory, Wright-Patterson AFB, Ohio, Technical Report AFFDL-TR-70-174, April 1971.

SHERR S (1973). Fundamentals of Display Systems Design. (John Wiley and Sons, New York.)

SHOENBERGER R W (1972). Human response to whole-body vibration. Perceptual and Motor Skills 34, pp 127-160.

SHONTZ W D and TRUM G A (1969). Perceptual processes and current helmet-mounted display concepts: a review of the literature. Honeywell Inc., Minneapolis, Minnesota, Life Sciences Technical Note TN-1, April 1969.

SHURTLEFF D A (1974). Legibility research. Proceedings of the Society for Information Display 15(2), pp 41-51.

SIEGEL S (1956). Nonparametric Statistics for the Behavioral Sciences. (McGraw-Hill Kogakusha, Tokyo).

SPEAKMAN J D (1971). Crew station vibration environments during low-altitude, high speed flight. Proceedings of the Air Force Systems Command 1971 Science and Engineering Symposium, October 1971, Dayton, Ohio.

SPEAKMAN J D, BONFILI H F, HILLE H K and COLE J N (1971). Crew exposure to vibration in the F-4C aircraft during low-altitude, high speed flight. USAF Aerospace Medical Research Laboratory, Wright-Patterson AFB, Ohio, Technical Report AMRL-TR-70-09, January 1971.

STARK L, YOUNG L R, TAUB R, TAUB A and KATONA P G (1966). Biological control systems--a critical review and evaluation. National Aeronautics and Space Administration, Technical Report CR-577, September 1966.

STILES W S and CRAWFORD B H (1933). The luminous efficiency of rays entering the eye pupil at different points. Proceedings of the Royal Society (London) 112B, pp 428-450.

STROTHER D D and UPTON H W (1971). Head-mounted display/control system in V/STOL operations. Presented at 27th Annual National V/STOL Forum of the American Helicopter Society, Washington, D.C., May 1971.

SYNDER H L (1976). Visual search and image quality: final report. USAF Aerospace Medical Research Laboratory, Wright-Patterson AFB, Ohio, Technical Report AMRL-TR-76-89, December 1976.

SYNDER H L, KEESEE R, BEAMON W S and ASCHENBACH J R (1974). Visual search and image quality. USAF Aeropsace Medical Research Laboratory, Wright-Patterson AFB, Ohio, Technical Report AMRL-TR-73-114, October 1974.

TASK H L (1979). An evaluation and comparison of several measures of image quality for television displays. USAF Aerospace Medical Research Laboratory, Wright-Patterson AFB, Ohio, Technical Report AMRL-TR-79-7, January 1979.

TASK H L and HORNSETH J P (ca. 1974). Feasibility of a flexible fiber optics bundle for helmet-mounted displays. USAF Aerospace Medical Research Laboratory, Wright-Patterson AFB, Ohio, unpublished technical report.

TASK H L and VERONA R W (1976). A new measure of television quality relatable to observer performance. USAF Aerospace Medical Research Laboratory, Wright-Patterson AFB, Ohio, Technical Report AMRL-TR-76-73, August 1976.

TASK H L, KOCIAN D F and BRINDLE J H (1980). Helmet-mounted displays: design considerations. In: Advancement on Visualization Techniques, North Atlantic Treaty Organization, Advisory Group on Aerospace Research and Development, AGARDograph No. 255, October 1980.

TATHAM N O (1976). An investigation of head aiming during simulated aircraft vibration conditions. Royal Aircraft Establishment, Farnborough, Technical Memo FS 74.

TAYLOR J H (1969). Factors underlying visual search performance. Scripps Institution of Oceanography, San Diego, California, Report No. 69-22, November 1969.

TEICHNER W H and KREBS M J (1972). Estimating the detectability of target luminance. Human Factors 14(6), pp 511-519.

THOMAS J C (1965). Use of piezoaccelerometer in studying eye dynamics. Journal of the Optical Society of America 55, pp 534-537.

TULUNAY-KEESEY U and JONES R M (1976). The effect of micromovements of the eye and exposure duration on contrast sensitivity. Vision Research 16, pp 481-488.

UPTON H W (1962). Eyeglass display projector feasibility study. Bell Helicopter Company, Fort Worth, Texas, Report No. 8007-099-012, February 1962.

VAN COTT H P and WARRICK M J (1972). Man as a system component. In: Human Engineering Guide to Equipment Design, H P VanCott and R G Kinkade, Eds. (U.S. Government Printing Office, Washington, D.C.), pp 18-39.

von GIERKE H E and CLARKE N P (1971). Effects of vibration and buffeting on man. In: Aviation Medicine, H W Randel, Ed. (Williams and Wilkins, Baltimore), 2nd Edition, Chapter 10, pp 198-223.

VOS J J, LAZET A and BOWMAN M A (1956). Visual contrast thresholds in practical problems. Journal of the Optical Society of America 46, pp 1065-1068.

WALD G (1945). Human vision and the spectrum. Science 101, pp 653-658.

WESTHEIMER G (1965). Visual acuity. Annual Review of Psychology, 1965.

WILLIAMS L G (1966). Target conspicuity and visual search. Human Factors, February 1966, pp 80-92.

WILLIAMS L G (1967). The effects of target specification on objects fixated during visual search. Acta Psychologica 27, pp 355-360.

WILSON R V (1974). Display collimation under whole-body vibration. Human Factors 16(2), pp 186-195.

WOODSON W E (1954). Human Engineering Guide for Equipment Designers. (University of California Press, Los Angeles).

WYSZECKI G and STILES W S (1967). Color Science: Concepts and Methods. Quantitative Data and Formulas. (Wiley, New York).

YOUNG L R (1971). Pursuit eye tracking movements. In: Control of Eye Movements, P Back-Y-Rita and C C Collins, Eds. (Academic Press, London), pp 429-443.

YOUNG L R and SHEENA D (1975). Survey of eye movement recording techniques. Behavior Research Methods and Instrumentation 7(5), pp 397-429.

Appendix A.3.1
DESCRIPTION OF HELMET-MOUNTED DISPLAY SYSTEM

A.3.1.1 Introduction

This appendix gives the description and theory of operation of the helmet-mounted display system used in the experiments reported in this thesis. Another appendix (A.3.2) describes the imaging performance of the HMD.

A.3.1.2 Model Designation

The helmet-mounted display system described herein is the model RC/HMD-202 Helmet-Mounted Display System. This display system was developed for the United States Air Force by the Hughes Aircraft Company, Culver City, California.

A.3.1.3 Description of Components

The helmet-mounted display system consists of three units or subsystems: display electronics unit, control panel unit, and helmet-mounted unit. Each of these units is described below.

A.3.1.3.1 Helmet-Mounted Unit

The helmet-mounted unit is that portion of the helmet-mounted display which is attached to the helmet. It contains a cathode-ray tube/cable assembly and optics assembly. The display is a monocular display in that it is viewed with only one eye. The helmet mounted unit can be affixed to either side of the helmet, and accordingly can be viewed with either the left or right eye. In the experiments reported in this thesis, the helmet-mounted unit was attached to the right side of a modified United States Air Force flight helmet (HGU 2A/P). The helmet-mounted unit was positioned on the helmet so that a tinted (neutral density) helmet visor could be lowered over both the display and nondisplay eyes of the observer. The light transmission of the tinted visor was 15 percent. The helmet-mounted unit increased the

mass of the flight helmet by 520 gm for a total helmet and helmet-mounted display mass of 2255 gm including approximately 0.25 m of the cable. Table A.3.1.1 gives the weight contributions of each component of the helmet-mounted unit and helmet. The helmet-mounted unit also shifts the overall center-of-gravity of the flight helmet by approximately 32.4 gm toward to the right side of the helmet.

a) CRT Assembly. The CRT was a modified general purpose microspot miniature display tube (Ferranti 02B/97D2). The exceptional performance of the tube was obtained by the use of electromagnetic deflection, special electro-optics, and a micrograin phosphor. The manufacturer's published data sheet on the CRT is contained in Table A.3.1.2. The diameter of the active phosphor screen size as 19 mm with an overall tube outside diameter of approximately 26.5 mm. A small electronic circuit was added to the tube and potted with silicon rubber next to the terminal pins of the tube. This circuit provided the final video drive voltages to the control grid. The CRT employed a yellowish-green P-1 type phosphor (designated D2 by the manufacturer) with the spectral emission characteristics shown in Figure A.3.1.1. The peak radiant energy output was at a wavelength of approximately 525 nm. The typical phosphor persistance characteristics are shown in Figure A.3.1.2. The typical resolution characteristics of the CRT, when used in conjunction with the display electronics unit, are discussed in Appendix A.3.2. The CRT was driven by the display electronic unit with a 7 kV anode potential.

b) Optics Assembly. The CRT was housed in an optics assembly. A schematic diagram of the optical design is shown in Figure A.3.1.3. Once an image was generated on the CRT, the optics magnified, collimated, and projected the image onto a combiner which reflected the image into the eye of the observer. When observed through the optics, the 19 mm diameter of the cathode-ray tube subtended a visual angle of 30 degrees. The image was collimated to optical infinity. The diameter of the optical exit pupil

TABLE A.3.1.1. BREAKDOWN OF WEIGHT OF COMPONENTS IN HELMET-MOUNTED UNIT

Component	Mass (gm)
Helmet-mounted unit	
cathode-ray tube + 0.25 m cable	220
optics assembly including latch	300
	520
Helmet (USAF HGU 2A/P)	
with communications headset	1735
receptacle for helmet-mounted unit	
insertable liner-foam pads	
Total mass on head	2255

through which the entire field-of-view could be seen was 15 mm. The size of the exit pupil was designed to minimize the effects of helmet slip on the head during high sustained Gz accelerations (Kennedy and Kroemer, 1973).

The fore and aft (X axis) position of the exit pupil was adjusted over the subject's eye by releasing two screws holding the optics barrel to the latching mechanism after which the barrel could slide freely in the latching assembly (±25 mm). Rotation of the barrel provided some flexibility in positioning the exit pupil in the vertical axis. The exit pupil was positioned in the side-to-side (Y axis) direction by releasing four screws which held the latch receptacle to the helmet. Because the overall size of the exit pupil was large relative to the entrance pupil of the eye, precision adjustment of the exit pupil was not required.

TABLE A.3.1.2. MANUFACTERER'S CHARACTERISTICS OF CATHODE-RAY TUBE USED IN HELMET-MOUNTED DISPLAY (FERRANTI LTD. SPECIAL COMPONENTS DEPARTMENT, BULLETIN ON 02B/97 MICROSPOT CATHODE-RAY TUBE, DATED OCTOBER 1974)

FERRANTI

Microspot Cathode Ray Tubes

02B/97

Previously 1B/97

The 02B/97 is a general purpose miniature display tube. It combines high brightness and high resolution with small size and weight. The tube, complete with deflection coil, is encapsulated in a mumetal shield. Applications include helmet display, spot injection, phototypesetting —

Deflection	Magnetic – integral deflection coil
Focus	Electrostatic – accelerator type
Screen	Aluminized phosphor A5, A6, D2, Q8, T4, and V4
Faceplate	Optical quality

Screens

All screens are aluminized.
Ferranti phosphors A5, A6, D2, Q8, T4 and V4 are recommended for use with this tube. For the characteristics of these, please refer to the individual data sheets in the 'Phosphor data' section of the Micospot Handbook.

Other phosphors may be supplied to special order but it should be noted that not all types are suitable for use with this tube.

Faceplate

This is made from optical quality glass. Optically polished to:

Thickness	2 mm
Flatness	5 fringes D line
Flatness of completed tube	30 fringes D line concave

Refractive indices

N_D	1·50632
N_F	1·51217
N_G	1·51677

External Finish

This tube is supplied with flying leads for gun, final anode and coil as standard, code letter KA. Other finishes may be supplied to special order.

Mumetal Shield

The tube complete with deflection coil is encapsulated in a mumetal shield.

Precision Mounting

An alternative version of this tube has the outside diameter and front end of the mumetal shield precision machined and accurately located with reference to the faceplate. Tolerances up to those shown in the drawing on page 4 can be provided. This system enables the tube faceplate to be accurately referenced to external optics and is equivalent to precision collaring in a larger CRT.

Electrical Ratings (absolute) and Characteristics

	Min	Max	Typical Operation		
Heater voltage ..	—	—	6·3	6·3	V
Heater current ..	—	—	0·3	0·3	A
First anode voltage ..	200	600	300	300	V
First anode current ..	—	±10	0	0	μA
Focus anode voltage..	500	1500	—	—	V
Focus anode voltage for focus*	—	—	0·65 to 1·0	1·0 to 1·4	kV
Focus anode current†	—	—	0·9 × I_k	0·9 × I_k	
Final anode voltage ..	4·5	8·5	5	7·5	kV
Grid voltage for visual cut-off	—	—	−30 to −70	−30 to −70	V
Heater-cathode voltage					
Heater positive ..	—	200	—	—	V
Heater negative ..	—	200	—	—	V
Grid-cathode resistance	—	1·5	—	—	MΩ
Capacitance					
$C_{g\text{-all}}$	—	12	—	—	pF
$C_{k\text{-all}}$	—	8	—	—	pF

*To ensure that the tube can be taken through focus it is advisable for the voltage range of the focus supply to be greater than the quoted range. Note should be taken of the current flowing to this electrode when designing the focus supply.
†The cathode current is shared between the focus and final anodes, approximately 10% of the cathode current reaches the final anode and screen.

Deflection Coil (X and Y windings similar)

Winding		Single ended
Inductance	X	145 μH ±10%
	Y	125 μH ±10%
Resistance	X	1·8Ω ± 10%
	Y	1·7Ω ± 10%
Deflection sensitivity at 5 kV* ..		0·77A ±10% for 9·5 mm deflection
Deflection sensitivity at 7·5 kV* ..		1·0A ± 10% for 9·5 mm deflection
Orthogonality X to Y		±2°

*Sensitivity can be increased by 10% where hysteresis is no problem.

Environment

This tube will meet the following requirements of BS2011.

Dry heat	+70°C
Damp heat	+40°C and 95% R.H.
Low temperature	−40°C
Shock	100g, half sine wave 6 ms pulse
Vibration	5 Hz to 5 kHz, amplitude 2·54 mm or 5g, whichever is the lesser.
Bump	40g
Mould growth	Standard test
Salt mist	Severity 1
Driving rain	Duration 1 hour

Ordering

If the standard tube is required the type number must be followed by the code for the phosphor type required. This in turn must be followed by the code for the desired external finish. Thus if this tube is required with an A5 phosphor and flying leads the full type number is 02B/97A5KA. If a precision shielded tube is required the details should be specified and the tube will be given a number of the form 02B/1xxx. Full details of the coding system are given in the general section 'Nomenclature' in the Microspot Handbook.

Note

This data sheet should be read in conjunction with the general information section and phosphor data section of the Microspot Handbook.

TABLE A.3.1.2. MANUFACTERER'S CHARACTERISTICS OF CATHODE-RAY TUBE USED IN HELMET-MOUNTED DISPLAY (FERRANTI LTD. SPECIAL COMPONENTS DEPARTMENT, BULLETIN ON 02B/97 MICROSPOT CATHODE-RAY TUBE, DATED OCTOBER 1974) (continued)

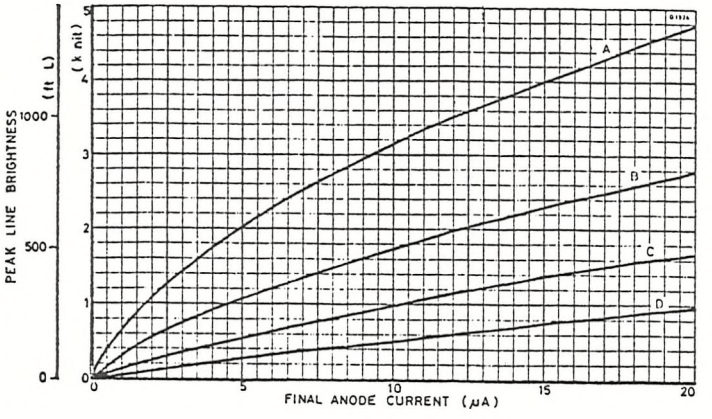

Typical Light Output Characteristics

Curves A and B ..	Phosphor D2
C and D ..	Phosphor A5
Writing speed ..	.. 0·1 mm/μs
Refresh rate	50 Hz
V_{a1}	300V
V_{a3} curves A and C ..	7·5 kV
B and D ..	5 kV

A dc. spot brightness of 12,000 nits can be obtained at 7·7 kV with typical grid drives of 5V for A5 phosphor and 4V for D2 phosphor.

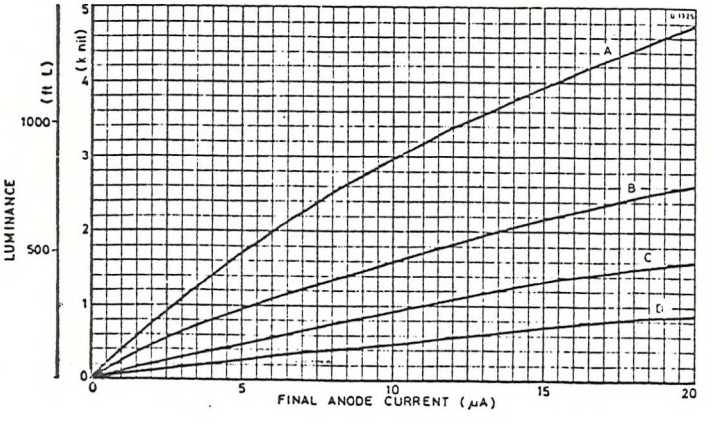

Typical Luminance Characteristics

Curves A and B ..	Phosphor D2
C andD ..	Phosphor A5
Raster size ..	10 × 10 mm
Refresh rate	50 Hz
V_{a1}	300V
V_{a3} curves A and C ..	7·5 kV
B and D ..	5 kV

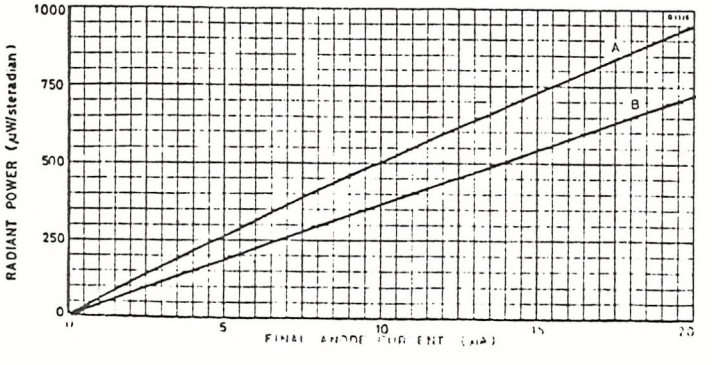

Typical Radiant Power Characteristics

Phosphor	Q8
Raster size ..	10 × 10 mm
Writing speed ..	.. 0·1 mm/μs
Refresh rate	50 Hz
V_{a1}	300V
V_{a3} curve A	7·5 kV
B	5 kV

TABLE A.3.1.2. MANUFACTERER'S CHARACTERISTICS OF CATHODE-RAY TUBE USED IN HELMET-MOUNTED DISPLAY (FERRANTI LTD. SPECIAL COMPONENTS DEPARTMENT, BULLETIN ON 02B/97 MICROSPOT CATHODE-RAY TUBE, DATED OCTOBER 1974) (continued)

Typical Resolution Characteristics

Line width measured at half power

Phosphors	A5, D2, Q8
Writing speed	0·1 mm/μs
V_{a1}	300V
V_{a3} curve A	5 kV
B	7·5 kV

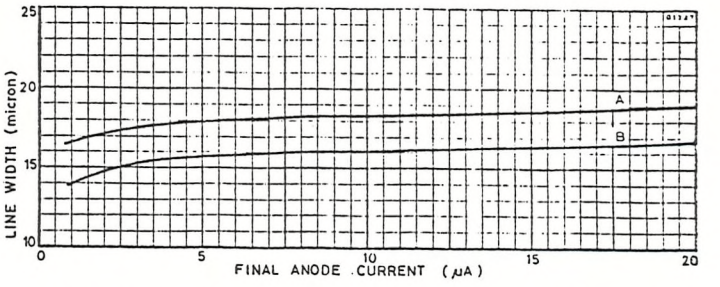

Typical Deflection Defocusing Characteristic

Spot diameter measured at half power.

Spot refocused at each point

V_{a1}	300V
V_{a3}	7·5 kV

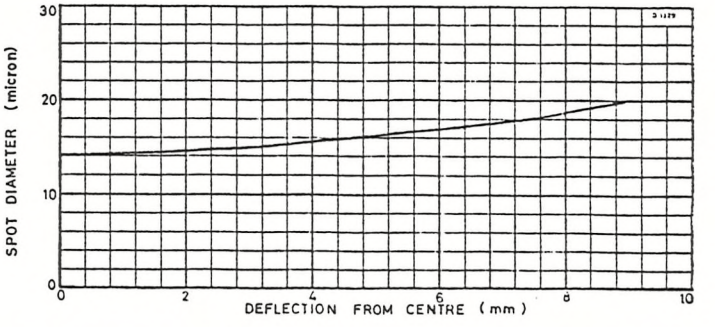

Typical Deflection Linearity Characteristics

V_{a3} curve A	7·5 kV
B	5 kV

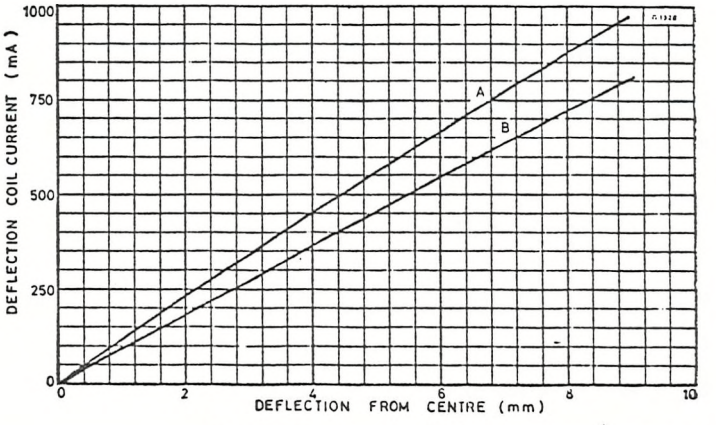

Typical Grid Drive Characteristics

Curve A	I_{a3} at V_{a3} = 7·5 kV
B	I_{a3} at V_{a3} = 5 kV
C	I_k at V_{a3} = 5/7·5 kV
V_{a1}	300V

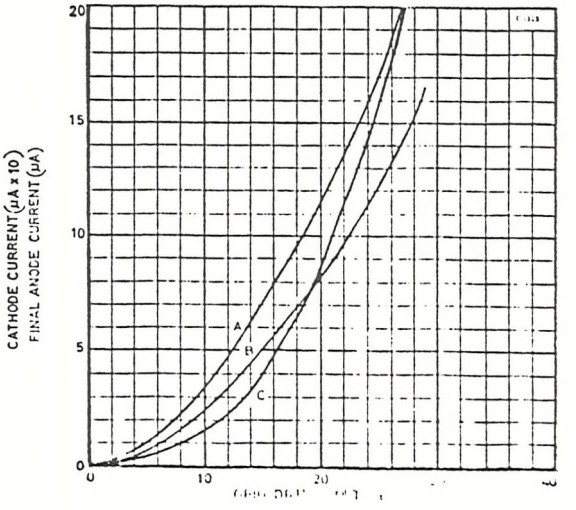

TABLE A.3.1.2. MANUFACTERER'S CHARACTERISTICS OF CATHODE-RAY TUBE USED IN HELMET-MOUNTED DISPLAY (FERRANTI LTD. SPECIAL COMPONENTS DEPARTMENT, BULLETIN ON 02B/97 MICROSPOT CATHODE-RAY TUBE, DATED OCTOBER 1974) (continued)

Outline Drawings

Standard tube

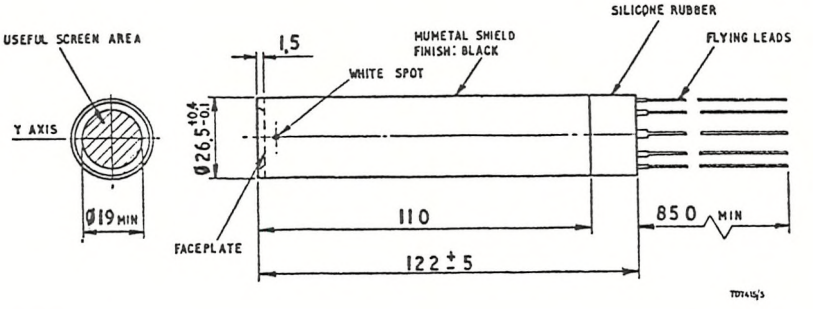

Precision shielded tube

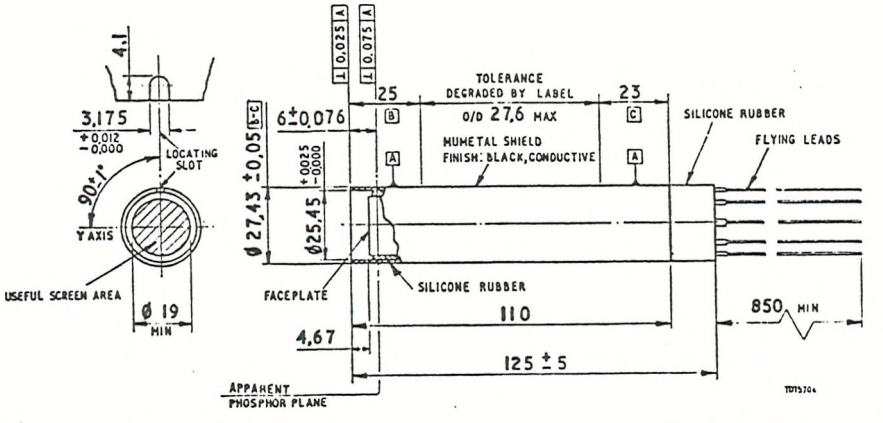

Weight excluding leads

Standard tube	120g
Precision tube	230g

Dimensions in millimetres

Connections

Flying leads a3	7/0·125 mm PTFE insulated 1·375 mm O.D.
others	19/0·15 mm PTFE insulated 1·0 mm O.D.
Heaters	Brown
Cathode	Yellow
Grid	Green
First anode	Blue
Focus anode	Grey
Final anode	Red
Deflection coil X	Black and violet
Y	Orange and white

For down and left deflection when viewed on tube face black and orange leads should be positive.

On the standard tube a white spot indicates top, and on the precision tube the slot is on the left.

FERRANTI LTD., SPECIAL COMPONENTS DEPARTMENT, GEM MILL, CHADDERTON, OLDHAM OL9 8NP Tel. 061 624 0515
Ferranti Electric Inc., East Bathpage Road, Plainview, N.Y. 11803 Tel. (516) 293 8383
[illegible] 22 [illegible] 6

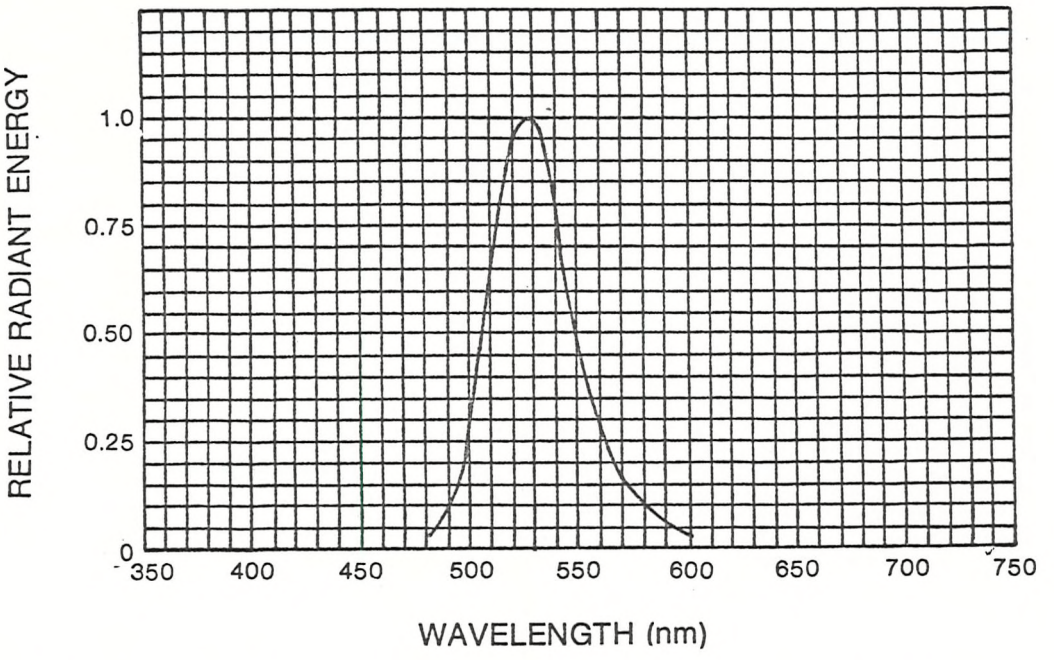

Figure A.3.1.1. Phosphor Spectral Emission Characteristics (Ferranti Ltd. Special Components Department Bulletin on 02 Phosphor, October 1975)

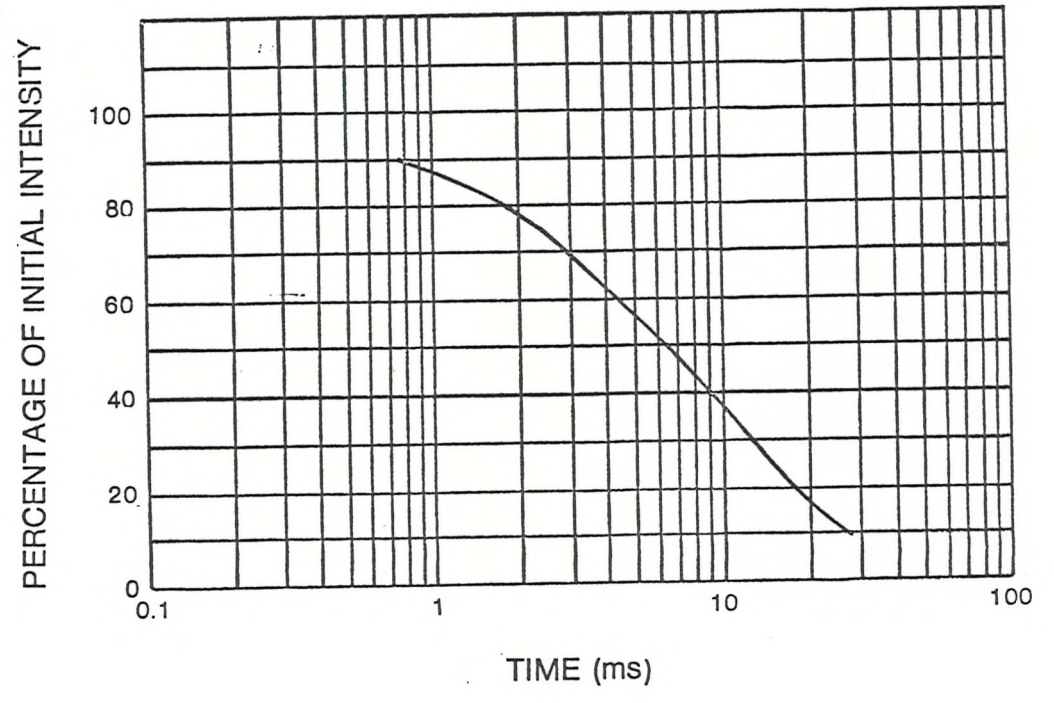

Figure A.3.1.2. Phosphor Persistence Characteristics (Ferranti Ltd. Special Components Department Bulletin on 02 Phosphor, October 1975)

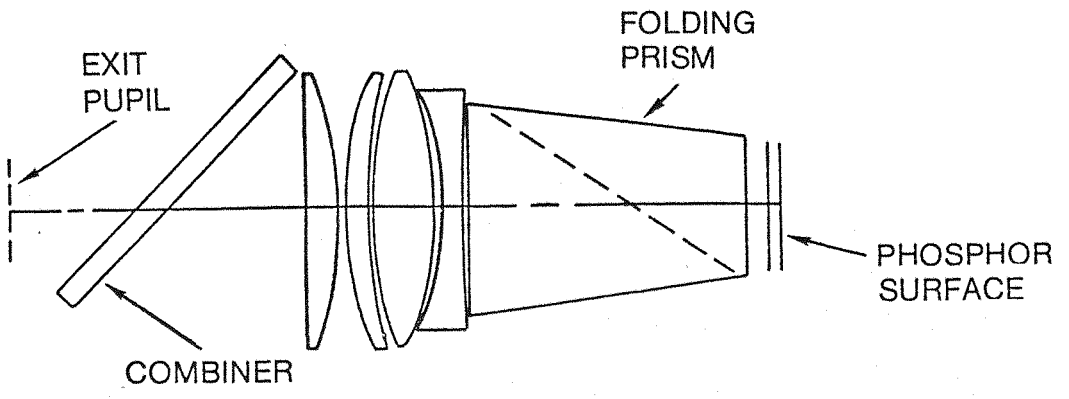

Figure A.3.1.3. Design of Optical Elements Used in Helmet-Mounted Unit

A.3.1.3.2 Display Electronics Unit

The display electronics unit generated the power supply voltages, deflection, and video signals to operate the cathode-ray tube. The unit consisted of several printed circuit modules and power supplies which are described in detail in the operation and maintenance manual (Helmet-Mounted Display Manual Model RC/HMD-201, January 1973). The display electronics unit employed linear amplifiers to control the deflection of the electron beam within the cathode-ray tube. The unit also contained a reticle target generator (i.e., here a reticle is defined as a set of horizontal and vertical lines which intersect). Screwdriver adjustments were provided in the unit for setting the size, position, and luminance of a reticle as well as the focus, horizontal, and vertical hold (oscillator frequency) and horizontal and vertical gain of the deflection amplifiers.

The display electronics unit required a supply voltage of 115 VAC, 400 Hz single phase, 80 w, and composite video or synchronization signals.

A.3.1.3.3 Control Panel Unit

The control panel interfaced with the display electronics unit and provided controls for the remote adjustment of the image brightness

and video gain (contrast). A switch was added to the control panel to provide manual blanking of the display image.

A.3.1.3.4 Modifications of the Helmet-Mounted Display System

A special modification was made to the display electronics unit. This modification replaced the miniature screwdriver potentiometers used to adjust the deflection gain with calibrated 10 turn potentiometers which were incorporated in a remote control box. The modification simplified the adjustments to character size for Experiments LG.3, LG.4, and H.1.

A.3.1.4 Theory of Operation

Figure A.3.1.4 is a functional schematic diagram of the helmet-mounted display system. Composite video signals containing video (picture or symbols) and synchronization (timing) signals were input into the display electronics unit. The sync separation network stripped the sync from the video signal and provided synchronization to the horizontal and vertical sweep oscillators. The outputs of the sweep oscillators were sawtooth waveforms for controlling the x and y position of the CRT beam such that the CRT beam scanned a raster of lines across the phosphor faceplate of the CRT. The deflection signals were amplified by linear deflection amplifiers (linear current output to voltage input) and coupled to the deflection coils in the CRT (helmet-mounted unit) via the cable assembly. The size of the scanning raster on the CRT was adjusted by setting the gain of the deflection amplifiers. The video signals were amplified by the video amplifier and coupled to the final video driver which was potted at the rear of the CRT. The output signal from the final video driver excited the control grid of the CRT where the intensity of the scanning beam was modulated. Retrace blanking signals were provided to the CRT cathode to blank the beam during horizontal and vertical retrace. The reticle generator provided the signals to present a reticle image on the CRT. The reticle could be displayed with or without external video input signals. For the experiments reported in this thesis, the horizontal and vertical oscillators were adjusted so that a standard 625 line

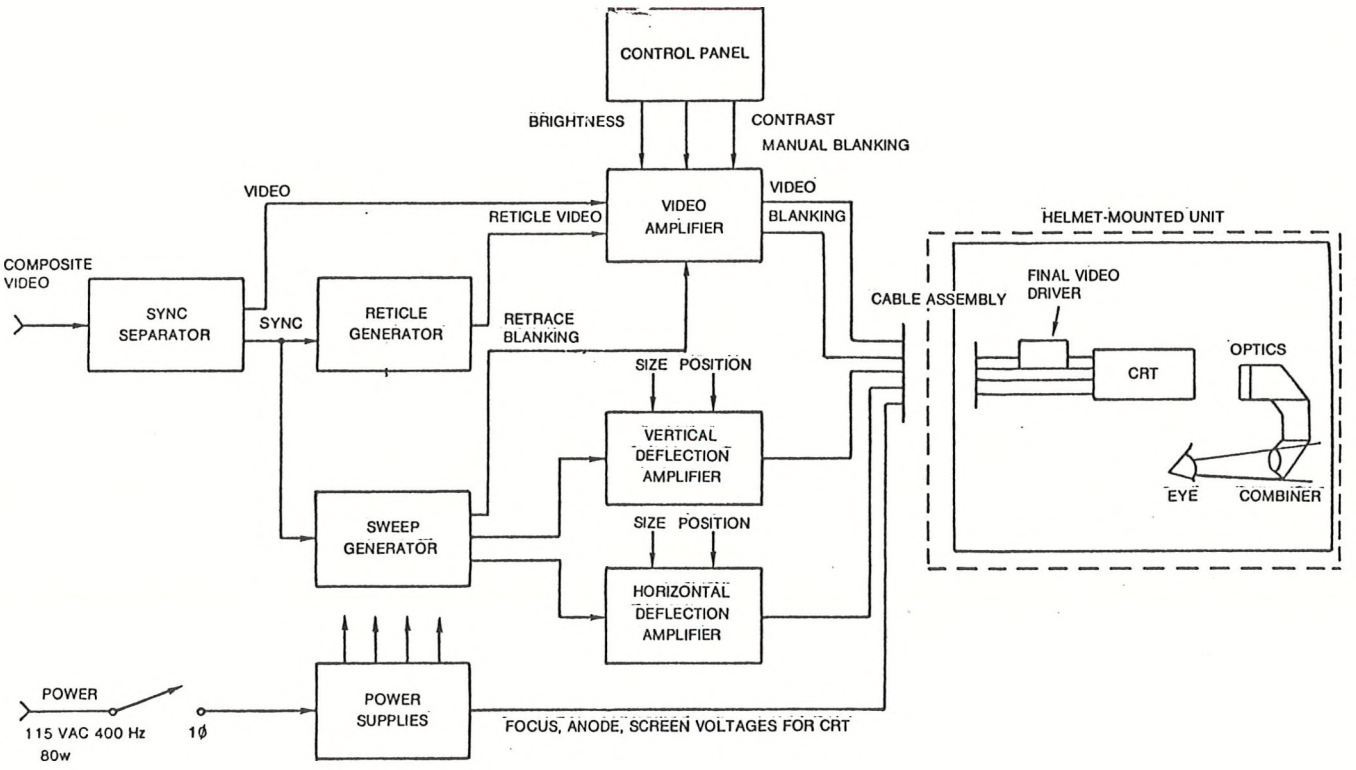

Figure A.3.1.4. Functional Schematic Diagram of Helmet-Mounted Display

raster with 2:1 interlace would be produced on the CRT. The image on the CRT was relayed through the optics assembly where it was magnified and collimated and then projected via the optical combiner into the right eye of the subject. The presentation on the display appeared to the subject as a virtual image of the original CRT image.

A.3.1.5 Subtended Visual Angle of CRT Image

The subtended angle of the displayed image was adjusted by setting the gains of the deflection amplifier. The relationship between the magnitude of the visual angle (δ) subtended by an object on the display is given by the equation

$$\delta = 1.58\ I$$

where I = the size of the object on the CRT in millimeters and δ is the subtended visual angle in degrees.

Appendix A.3.2
IMAGE QUALITY OF THE HELMET-MOUNTED DISPLAY

A.3.2.1 Modulation Transfer Function Theory

The quality of the image generated by the helmet-mounted display and presented to the subject's eye can be described using modulation transfer functions. The modulation transfer function (MTF) of a linear system is a measure of the system's capacity to transfer spatial information. The modulation contrast or modulation response is that amplitude of a sinusoidal spatial pattern which is produced or transmitted through the system relative to an input sinusoidal spatial pattern or signal. Mathematically, the MTF is the Fourier transform of the point spread function, where the luminance across the point represents a Guassian distribution. An expression for the MTF of a system (M_0) (Sherr, 1973; and Hershberger and Guerin, 1975) is

$$M_0 = e^{-2(\pi\sigma N)^2} \qquad \text{A.3.2.1}$$

where

σ = standard deviation of the luminance distribution (assumed Gaussian) across a point (i.e., CRT spot) and is equal to the radius of the spot where the luminance has fallen to .60 of its maximum value; and

N = sine wave spatial frequency in cycles per unit distance.

A.3.2.2 Linearity of Video Input to Output

For the expression of MTF above to be valid, the HMD system must be linear; that is, a linear relationship must exist between the amplitude of the output signal versus the input signal across all spatial frequencies. The linearity of the luminance output of the CRT used herein, as a function of the input video signal level, is shown in Figure A.3.2.1 for three settings of video gain. From this figure, the video signal to luminance transfer characteristics appear to be

linear across a wide range of input signals and contrast control settings.

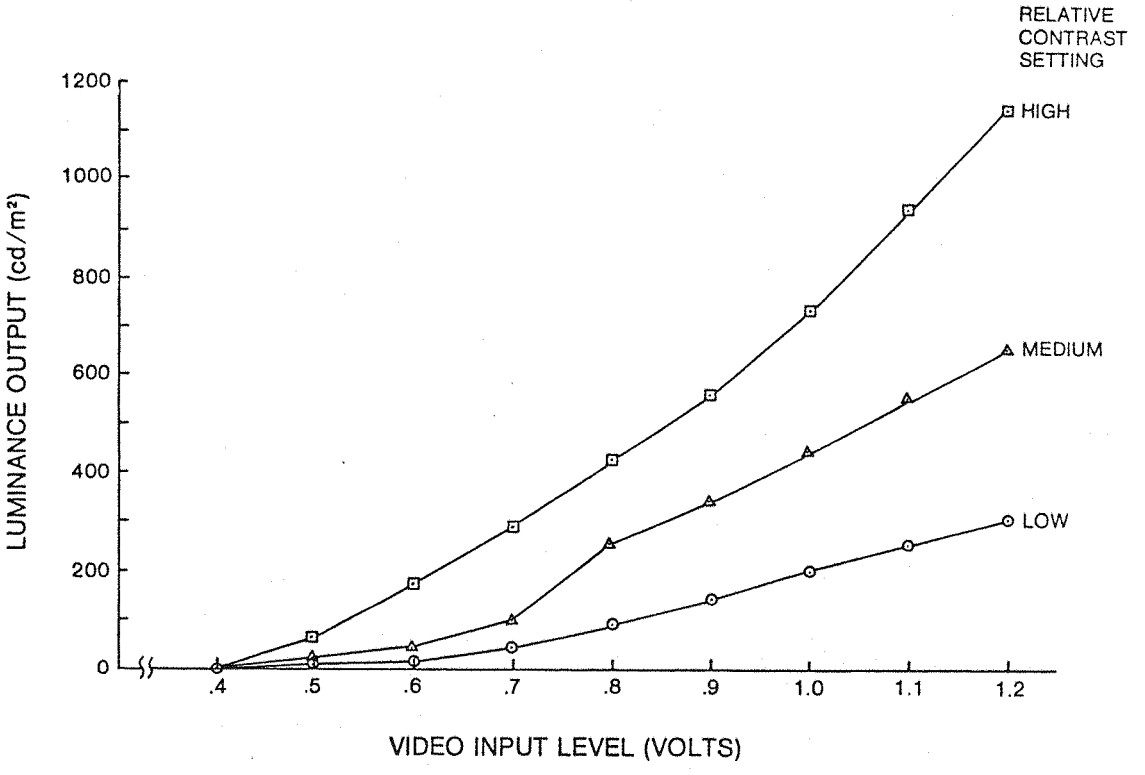

Figure A.3.2.1. Luminance Output of the Cathode-Ray Tube as a Function of Video Level for Three Contrast (Video Gain) Settings

A.3.2.3 MTF of CRT--Horizontal Axis

A modulation transfer function for the horizontal axis of the CRT used in the HMD (i.e., along the scan lines) is shown in Figure A.3.2.2. The MTF in this figure represents the normalized response of the CRT as a percentage of the amplitude of a sinusoidal spatial input signal. The response is plotted as a function of the spatial frequency in cycles per millimeter on the CRT faceplate. The specific MTF shown is an estimate of the actual CRT response used in the experiments in this thesis.

This MTF was derived using Equation A.3.2.1 and a value of $\sigma = 12$ μm which was determined empirically for a similar helmet display system

by the United States Air Force Aerospace Medical Research Laboratory, Wright-Patterson Air Force Base (Task and Verona, 1976).

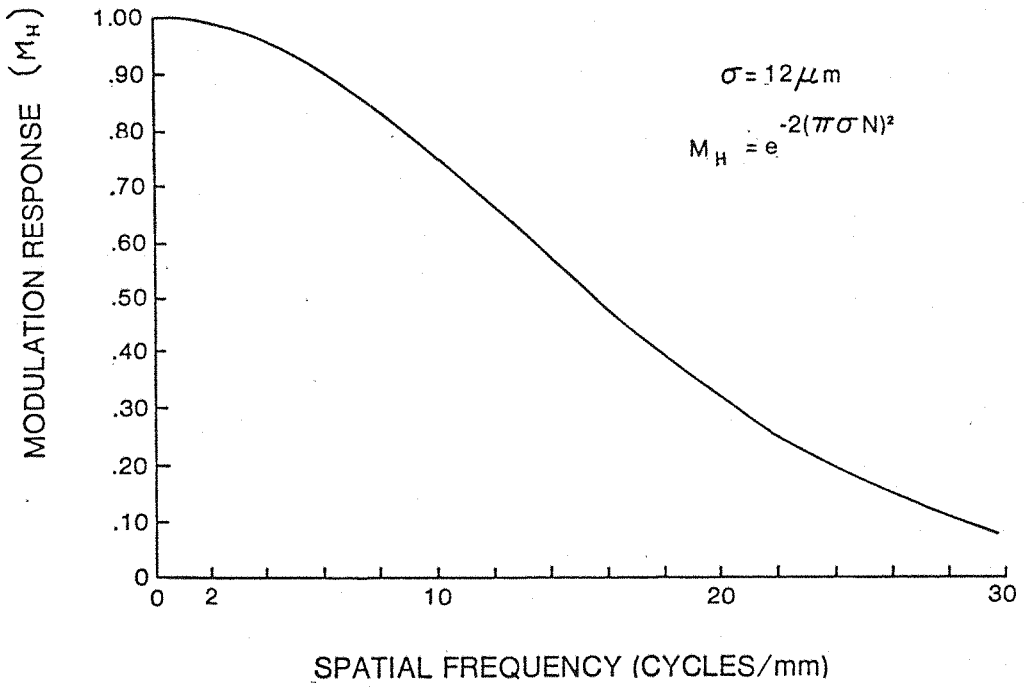

Figure A.3.2.2. Theoretical Modulation Transfer Function in the Horizontal Axis of the CRT Used in the Helmet-Mounted Display

A.3.2.4 MTF of CRT--Vertical Axis

The quality of the CRT image in the vertical dimension (i.e., across scan lines) is a function of the amount of overlap of the adjacent scan lines in the raster. The modulation which the display can produce in the vertical axis (m_V) is given by the expression (Sherr, 1970):

$$m_V = 1 - \frac{2e^{-(r_0^2/2\sigma^2)}}{1+e^{-(4r_0^2/2\sigma^2)}}$$

where

r_0 = 1/2 distance of the separation of adjacent scanning lines,

and

σ = one half width of the scanning line when the luminance across the line has decreased to 60 percent of the peak value.

In terms of modulation contrast (Cm_V) the equation above can be rewritten

$$Cm_V = \frac{1 + e^{-(1/2N^2\sigma^2)} - 2e^{-(1/8N^2\sigma^2)}}{1 + e^{-(1/2N^2\sigma^2)} + 2e^{-(1/8N^2\sigma^2)}} \qquad \text{A.3.2.2}$$

Based upon equation A.3.2.2 and σ = 12 µm, the modulation contrast as a function of spatial frequency is shown in Figure A.3.2.3. It should be noted that for vertical modulation, two scan lines are required to constitute one spatial frequency cycle (i.e., N = ½ cycle = $\frac{1}{2r_0}$).

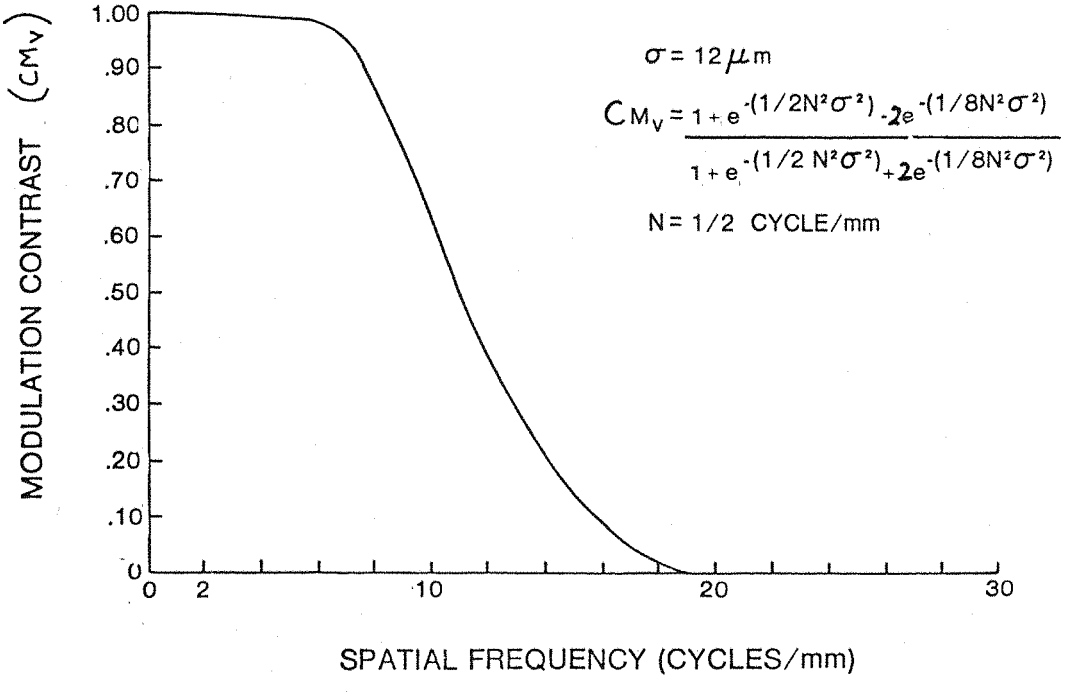

Figure A.3.2.3. Theoretical Modulation Contrast in the Vertical Axis Produced by the Scan Lines on the Cathode-Ray Tube

A.3.2.5 MTF of Optics

The image quality properties of the optics assembly also can be represented by a modulation transfer function. In Figure A.3.2.4, the MTF has been calculated from the diffracting limiting performance of the optical elements as reported by Fehr (1973). The performance is for on-axis viewing only. As the input object is displaced toward the periphery of the field-of-view, the MTF will degrade slightly. Similarly, as the eye is displaced toward the edge of the exit pupil, the image quality will also degrade somewhat. The MTF for the optical assembly applies for both the vertical and horizontal axes.

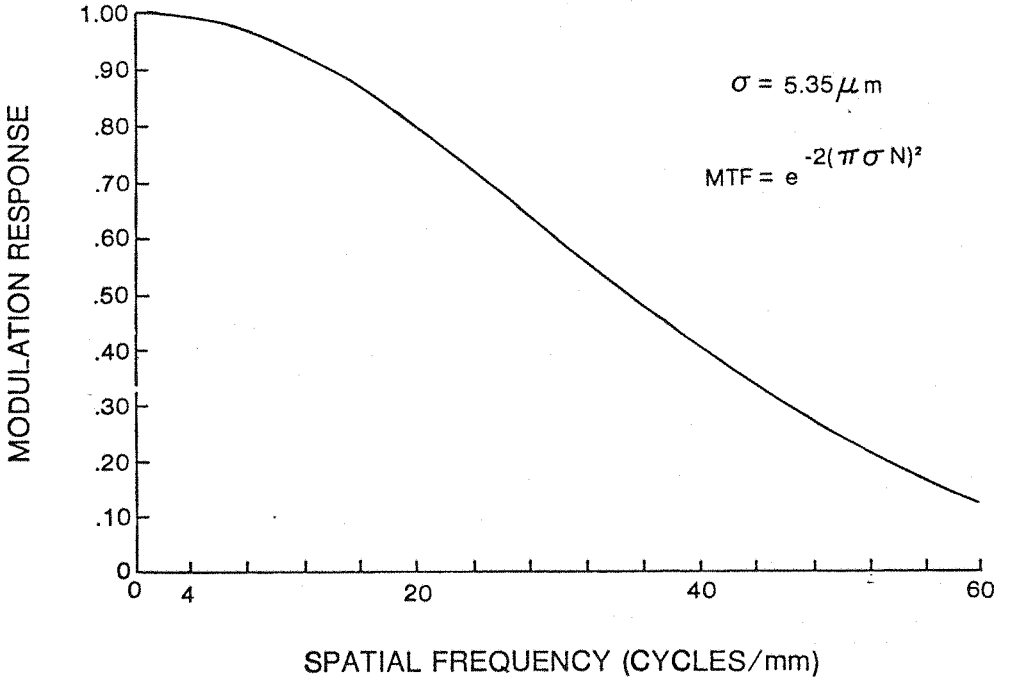

Figure A.3.2.4. Theoretical Modulation Transfer Function of the Projection Optics Used in the Helmet-Mounted Display

A.3.2.6 Overall System MTF

One of the advantages of the MTF approach to image quality analysis is that the performance of the overall system (i.e., electronics, CRT assembly, and optics assembly) can be computed by multiplying the

individual MTFs of each component. Again, this procedure will only be valid if the system is linear. In Section A.3.2.2, it was shown that the combined CRT and display electronics exhibited linear properties. Furthermore, since conventional optical elements were used, the behaviour of the optics assembly can be expected to be linear. The overall system MTF in the horizontal axis is, therefore, the product of the MTFs of the CRT and optics, as shown below:

$$M_{\text{horz. system}} = M_{CRT} \cdot M_{\text{optics}} = e^{-3.405 \times 10^{-3} N^2} \qquad \text{A.3.2.3}$$

where

$$M_{CRT} = e^{-2.84 \times 10^{-3} N^2}$$

and

$$M_{\text{optics}} = e^{-.565 \times 10^{-3} N^2}$$

Using Equation A.3.2.3, the theoretical system MTF is plotted in Figure A.3.2.5 showing the modulation response of the system as a function of spatial frequency in terms of the number of cycles per degree subtended visual angle. From this curve the HMD performance can be assessed in conjunction with the visual capabilities of the subjects. Since, technically the modulation response for the CRT in the vertical axis is not a real modulation transfer function (i.e., ratio of output to input sinusoidal signals), the system MTF for the vertical dimension can only be approximated by the relationships Cm_V and M_{optics}. Accordingly, estimated vertical modulation transfer function of the system is plotted in Figure A.3.2.5.

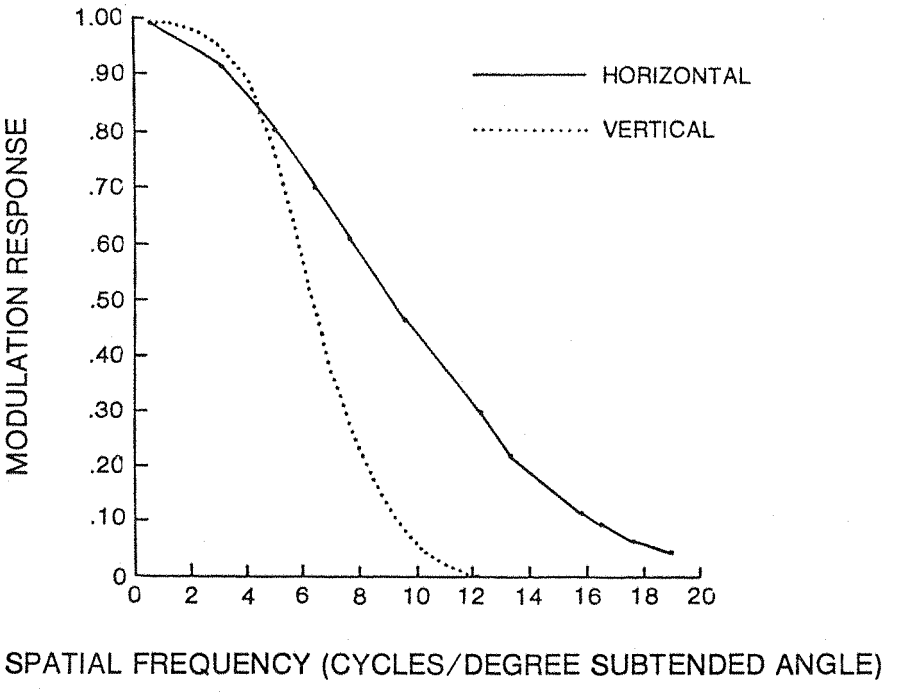

Figure A.3.2.5. Theoretical System Modulation Transfer Functions

Appendix A.3.3
LIST OF CONTRAINDICATIONS FOR PARTICIPATION IN VIBRATION EXPERIMENTS

Listed below are the physical, medical, and psychological conditions which would render persons unfit for participating in whole-body vibration experiments.

- Age under 4 years
- Infectious disease
- Fever
- Active skin disease
- Mental defect or disorder requiring supervision under the Mental Health Acts
- History of a suicidal attempt
- Any neurological disorder involving coarse tremor of the limbs or head, unsteadiness of gait, or wasting of muscles
- Deafness or history of ear surgery
- Blindness, Glaucoma; History of eye surgery
- Notifiable occupational disease
- History of coughing up, vomiting, or passing blood
- History of ulceration of the stomach or gastrointestinal tract requiring medical or surgical treatment
- History of haemorrhoids (piles); rectal or vaginal prolapse
- History of blood pressure or heart disease requiring control by drugs under medical supervision
- Intermittent pain, blanching, or numbness of fingers
- History of back injury or "strain" requiring surgical treatment, traction, support, or manipulation
- Any internal prosthetic device
- Surgical operation within the past 6 months
- Pregnancy later than 26 weeks, multiple pregnancy, or pregnancy and a history of miscarriage

Appendix A.3.4

APPLICATION/DECLARATION FOR PARTICIPATION
IN VIBRATION EXPERIMENTS

APPLICATION TO TAKE PART AS A SUBJECT IN VIBRATION EXPERIMENTS

Name: _____ (Mr./Mrs./Miss/)

Date of Birth: _____ Tel. No. _____

Are you in good health? Yes/No

If No, please explain: _____

Have you ever suffered from a serious illness or accident? Yes/No

If Yes, please give particulars: _____

Are you at present under medical treatment or suffering any disability affecting your daily life? Yes/No

If Yes, please give particulars: _____

Please read the list of conditions on the preceding page which would render you unfit for these experiments.

DECLARATION

I, _____, hereby volunteer to be an experimental subject in a vibration experiment (ref. no.) to be conducted by _____ during the period _____ to _____ 19__. My replies to the above questions are correct to the best of my belief, and I understand that they will be treated as confidential by the experimenter. The purpose of the experiment and the nature of the vibration to be used have been explained by the experimenter.

I understand that I may at any time withdraw from the experiment and that I am under no obligation to give reasons for withdrawal or to attend again for experimentation.

I undertake to obey the regulations of the laboratory and instructions of the experimenter regarding safety, subject only to my right to withdraw declared above.

Signature of Subject: _____

Date: _____

Signature of Experimenter: _____

Date: _____

Appendix A.4.1
COMPUTER PROGRAMS FOR ANALYSES OF VARIANCE AND SIMPLE MAIN EFFECTS (Lewis, 1978a)

The programs listed on the following pages are written in FORTRAN IV-PLUS. A number of system subroutines are used for input and output data. These are listed below.

CALL TYPE
Type a new line to terminal.

CALL TYPE ('&**')
Type to terminal character string between ' ', (& indicates a new line).

CALL TYPEI(K)
Type interger to terminal.

CALL TYPER(V)
Type floating point value to terminal.

CALL ASKN(A, '&***')
Read next job parameter as a file name. If the name is not found the message supplied is printed on the terminal and the program waits for the user to type a file name.

CALL ASKI(K, '&***')
Read next job parameters as an integer. If not supplied print a message and wait for user to type in an integer.

CALL ASKR(B, '&***')
As ASKI except uses a real value.

CALL INPUT(A, CB, M)
Open input file. Read control block to CB. M is a marker used by the IN subroutine to indicate the end of the file.

CALL OUTPUT(B)
Open output file for OUT subroutine.

CALL INS(A, 0, 0)
Start reading input file at block 0 number 0.

Assign 100 to M - 100 is the label that the program will jump to if you request a value beyond the end of the file.

CALL INEND(A)
Close input file.

CALL OUTEND(B, CB)
Close output file with CB as its control block.

A.4.1.1 2 FACTOR ANALYSIS OF VARIANCE WITH RANDOMIZED BLOCKS.

note: data is input in serial form as a single data file.

********** LISTING OF PDEVLIST **********

```
FORTRAN IV-PLUS V02-04G                    11:18:05    12-MAY-78          PAGE 1
                /RO/TR:ALL/WR

0001            DIMENSION AA(300),BB(300),CB(128)
0002            DIMENSION ZABS(1080),ZAB(270)
0003            CALL TYPE('&ANALYSIS OF VARIANCE')
0004            CALL ASKI(NS,'&NO. OF SUBJECTS/BLOCKS, S = ')
0005            CALL ASKI(NA,'&NO. OF LEVELS OF FACTOR A = ')
0006            CALL ASKI(NB,'&NO. OF LEVELS OF FACTOR B = ')
0007            CALL ASKN(AA,'&INPUT FILE =  ')
0008            CALL ASKN(BB,'&OUTPUT FILE = ')
0009            NABS=NA*NB*NS
0010            NAB=NA*NB
0011            NAS=NA*NS
0012            NBS=NB*NS
0013            CALL INPUT(AA,CB,M1)
0014            ASSIGN 999 TO M1
0015            CALL INS(AA,0,0)
0016            X=0.0
0017            ABS=0.0
0018            S=0.0
0019            AS=0.0
0020            AB=0.0
0021            BS=0.0
0022            A=0.0
0023            B=0.0
0024            I=1
0025    10      CALL IN(AA,ZABS(I))
0026            X=X+ZABS(I)
0027            ABS=ABS+ZABS(I)*ZABS(I)
0028            I=I+1
0029            GO TO 10
0030    999     X=X*X/NABS
0031            DO 20 I=1,NAB
```

```
0032     20       ZAB(I)=0.0
0033              DO 40 I=0,NS-1
0034              T=0.0
0035              DO 30 J=1,NAB
0036              K=J+(I*NAB)
0037              ZAB(J)=ZAB(J)+ZABS(K)
0038     30       T=T+ZABS(K)
0039     40       S=S+T*T/NAB
0040              CALL OUTPUT(BB)
0041              CALL PSAVE
0042              CALL PSCLR
0043              CALL TYPE('&B X A  COLUMN TOTALS - OVER S SUBJECTS')
0044              CALL TYPE
0045              CALL TYPE
0046              M=0
0047              DO 600 J=1,NB
0048              DO 600 I=1,NA
0049              M=M+1
0050              CALL TYPE
0051              CALL TYPEI(J,I)
0052              CALL TYPER(ZAB(M))
0053              CALL OUT(BB,ZAB(M))
0054     600      CONTINUE
0055              CALL TYPE
0056              CALL TYPE
FORTRAN IV-PLUS V02-04G                    11:18:05    12-MAY-78          PAGE 2
XNOVA.FTP         /RO/TR:ALL/WR

0057              DO 50 I=1,NAB
0058     50       AB=AB+ZAB(I)*ZAB(I)/NS
0059              DO 70 I=1,NA
0060              T=0.0
0061              II=NA*(NB-1)+I
0062              DO 60 J=I,II,NA
0063     60       T=T+ZAB(J)
0064     70       A=A+T*T/NBS
0065              DO 90 I=0,NB-1
0066              T=0.0
0067              II=I*NA
0068              DO 80 J=II+1,II+NA
```

```
0069     80      T=T+ZAB(J)
0070     90      B=B+T*T/NAS
0071             DO 120 I=0,NS-1
0072             II=I*NAB
0073             DO 110 J=II+1,II+NA
0074             T=0.0
0075             JJ=NA*(NB-1)+J
0076             DO 100 K=J,JJ,NA
0077     100     T=T+ZABS(K)
0078     110     AS=AS+T*T/NB
0079     120     CONTINUE
0080             DO 140 I=0,NBS-1
0081             II=I*NA
0082             T=0.0
0083             DO 130 J=II+1,II+NA
0084     130     T=T+ZABS(J)
0085     140     BS=BS+T*T/NA
0086     200     CONTINUE
0087             DFTOT=NABS-1
0088             DFSUB=NS-1
0089             DFTRT=NAB-1
0090             DFA=NA-1
0091             DFB=NB-1
0092             DFAB=DFA*DFB
0093             DFRES=DFSUB*DFTRT
0094             DFAS=DFA*DFSUB
0095             DFBS=DFB*DFSUB
0096             DFABS=DFA*DFB*DFSUB
0097             SSTOT=ABS-X
0098             SSSUB=S-X
0099             SSTRT=AB-X
0100             SSA=A-X
0101             SSB=B-X
0102             SSAB=AB-A-B+X
0103             SSRES=ABS-S-AB+X
0104             SSAS=AS-A-S+X
0105             SSBS=BS-B-S+X
0106             SSABS=ABS-AB-AS-BS+A+B+S-X
0107             SMTOT=SSTOT/DFTOT
0108             SMSUB=SSSUB/DFSUB
```

```
0109            SMTRT=SSTRT/DFTRT
0110            SMA=SSA/DFA
0111            SMB=SSB/DFB
0112            SMAB=SSAB/DFAB
FORTRAN IV-PLUS V02-04G                 11:18:05    12-MAY-78          PAGE 3
XNOVA.FTP       /RO/TR:ALL/WR

0113            SMRES=SSRES/DFRES
0114            SMAS=SSAS/DFAS
0115            SMBS=SSBS/DFBS
0116            SMABS=SSABS/DFABS
0117            FSUB=SMSUB/SMRES
0118            FTRT=SMTRT/SMRES
0119            FA=SMA/SMRES
0120            FB=SMB/SMRES
0121            FAB=SMAB/SMRES
0122            FAS=SMA/SMAS
0123            FBS=SMB/SMBS
0124            FABS=SMAB/SMABS
0125            CALL TYPE('&    ABS          AB           A            B            X')
0126            CALL TYPE
0127            CALL TYPE
0128            CALL TYPER(ABS,AB,A,B,X)
0129            CALL TYPE
0130            CALL TYPE
0131            CALL TYPE('&    S            AS           BS     ')
0132            CALL TYPE
0133            CALL TYPE
0134            CALL TYPER(S,AS,BS)
0135            CALL TYPE
0136            CALL TYPE
0137            CALL ASKI(III,'&TYPE 0 FOR ANOVA SUMMARY TABLE ')
0138            CALL PSCLR
0139            CALL TYPE('&ANOVA SUMMARY TABLE')
0140            CALL TYPE
0141            CALL TYPE
0142            CALL TYPE('&SOURCE          SS           DF           ')
0143            CALL TYPE('MS            F   ')
0144            CALL TYPE
0145            CALL TYPE
```

```
0146              CALL TYPE('&SUBJECTS  ')
0147              CALL TYPER(SSSUB,DFSUB,SMSUB,FSUB)
0148              CALL TYPE
0149              CALL TYPE('&TREATMENTS')
0150              CALL TYPER(SSTRT,DFTRT,SMTRT,FTRT)
0151              CALL TYPE
0152              CALL TYPE('&    A     ')
0153              CALL TYPER(SSA,DFA,SMA,FAS)
0154              CALL TYPE
0155              CALL TYPE('&    B     ')
0156              CALL TYPER(SSB,DFB,SMB,FBS)
0157              CALL TYPE
0158              CALL TYPE('&    AB    ')
0159              CALL TYPER(SSAB,DFAB,SMAB,FABS)
0160              CALL TYPE
0161              CALL TYPE('&RESIDUAL  ')
0162              CALL TYPER(SSRES,DFRES,SMRES)
0163              CALL TYPE
0164              CALL TYPE('&    AS    ')
0165              CALL TYPER(SSAS,DFAS,SMAS)
0166              CALL TYPE
0167              CALL TYPE('&    BS    ')
0168              CALL TYPER(SSBS,DFBS,SMBS)
FORTRAN IV-PLUS V02-04G                 11:18:05    12-MAY-78          PAGE 4
XNOVA.FTP       /RO/TR:ALL/WR

0169              CALL TYPE
0170              CALL TYPE('&    ABS   ')
0171              CALL TYPER(SSABS,DFABS,SMABS)
0172              CALL TYPE
0173              CALL TYPE
0174              CALL TYPE('&TOTAL     ')
0175              CALL TYPER(SSTOT,DFTOT,SMTOT)
0176              CALL TYPE
0177              CALL TYPE
0178              CALL TYPE
0179              CALL ASKI(III,'&TYPE 0 TO CONTINUE COMPUTATION ')
0180              CALL PSCLR
0181              CALL PSRES
0182              CALL OUTEND(BB,CB)
0183              CALL INEND(AA)
0184              END
```

A.4.1.2 3 FACTOR ANALYSIS OF VARIANCE WITH RANDOMIZED BLOCKS.

note: data is input in serial form as a single data file.

********** LISTING OF PDEVLIST **********


```
0001            DIMENSION AA(300),BB(300),CB(128)
0002            DIMENSION ZABCS(15,15,2,10),ZABC(15,15,2)
0003            DIMENSION D(17),SS(17)
0004            CALL TYPE('&3 FACTOR ANALYSIS OF VARIANCE')
0005            CALL ASKI(NS,'&NO. OF SUBJECTS/BLOCKS, S = ')
0006            CALL ASKI(NA,'&NO. OF LEVELS OF FACTOR A = ')
0007            CALL ASKI(NB,'&NO. OF LEVELS OF FACTOR B = ')
0008            CALL ASKI(NC,'&NO. OF LEVELS OF FACTOR C = ')
0009            CALL ASKN(AA,'&INPUT FILE = ')
0010            CALL ASKN(BB,'&OUTPUT FILE = ')
0011            CALL ASKI(IG,'&TYPE 1 FOR ANOVA ONLY ',0)
0012            CALL INPUT(AA,CB,M1)
0013            ASSIGN 999 TO M1
0014            CALL INS(AA,0,0)
0015            X=0.0
0016            ABS=0.0
0017            S=0.0
0018            AS=0.0
0019            AB=0.0
0020            BS=0.0
0021            A=0.0
0022            B=0.0
0023            ABCS=0.0
0024            C=0.0
0025            CS=0.0
0026            ABC=0.0
0027            AC=0.0
0028            BC=0.0
0029            T=0.0
0030            P=0.0
0031            I=1
0032            J=1
```

```
0033              K=1
0034              L=1
0035     10       CALL IN(AA,ZABCS(I,J,K,L))
0036              IF(L.EQ.1)ZABC(I,J,K)=0.0
0037              ZABC(I,J,K)=ZABC(I,J,K)+ZABCS(I,J,K,L)
0038              T=T+ZABCS(I,J,K,L)
0039              ABCS=ABCS+ZABCS(I,J,K,L)*ZABCS(I,J,K,L)
0040              I=I+1
0041              IF(I.LE.NA)GO TO 10
0042              I=1
0043              J=J+1
0044              IF(J.LE.NB)GO TO 10
0045              J=1
0046              K=K+1
0047              IF(K.LE.NC)GO TO 10
0048              K=1
0049              L=L+1
0050              S=S+T*T/(NA*NB*NC)
0051              X=X+T
0052              T=0
0053              GO TO 10
0054     999      X=X*X/(NA*NB*NC*NS)
0055              D(17)=NA*NB*NC*NS-1
0056              SS(17)=ABCS-X
FORTRAN IV-PLUS V02-04G                    11:56:41     12-MAY-78          PAGE 2
XNOVA3.FTP        /RO/TR:ALL/WR

0057              D(1)=NS-1
0058              SS(1)=S-X
0059              IF(IG.EQ.1)GO TO 20
0060              CALL TYPE
0061              CALL TYPE('&A X B X C  COLUMN TOTALS - OVER S SUBJECTS')
0062              CALL TYPE
0063              CALL TYPE
0064     20       CONTINUE
0065              CALL OUTPUT(BB)
0066              DO 50 K=1,NC
0067              DO 50 J=1,NB
0068              DO 50 I=1,NA
```

```
0069              IF(IG.EQ.1)GO TO 30
0070              CALL TYPE
0071              CALL TYPEI(I,J,K)
0072              CALL TYPER(ZABC(I,J,K))
0073     30       CONTINUE
0074              CALL OUT(BB,ZABC(I,J,K))
0075              ABC=ABC+ZABC(I,J,K)*ZABC(I,J,K)/NS
0076     50       CONTINUE
0077              CALL TYPE
0078              CALL TYPE
0079              DO 80 I=1,NA
0080              T=0
0081              DO 70 L=1,NS
0082              P=0
0083              DO 60 K=1,NC
0084              DO 60 J=1,NB
0085     60       P=P+ZABCS(I,J,K,L)
0086              AS=AS+P*P/(NB*NC)
0087     70       T=T+P
0088     80       A=A+T*T/(NB*NC*NS)
0089              D(2)=NA-1
0090              SS(2)=A-X
0091              D(10)=(NA-1)*(NS-1)
0092              SS(10)=AS-A-S+X
0093              DO 110 J=1,NB
0094              T=0
0095              DO 100 L=1,NS
0096              P=0
0097              DO 90 K=1,NC
0098              DO 90 I=1,NA
0099     90       P=P+ZABCS(I,J,K,L)
0100              BS=BS+P*P/(NA*NC)
0101     100      T=T+P
0102     110      B=B+T*T/(NA*NC*NS)
0103              D(3)=NB-1
0104              SS(3)=B-X
0105              D(11)=(NB-1)*(NS-1)
0106              SS(11)=BS-B-S+X
0107              DO 140 K=1,NC
0108              T=0
0109              DO 130 L=1,NS
```

```
0110                P=0
0111                DO 120 J=1,NB
0112                DO 120 I=1,NA
0113      120       P=P+ZABCS(I,J,K,L)
0114                CS=CS+P*P/(NA*NB)
0115      130       T=T+P
0116      140       C=C+T*T/(NA*NB*NS)
0117                D(4)=NC-1
0118                SS(4)=C-X
0119                D(12)=(NC-1)*(NS-1)
0120                SS(12)=CS-C-S+X
0121                DO 170 I=1,NA
0122                DO 170 J=1,NB
0123                T=0
0124                DO 160 L=1,NS
0125                P=0
0126                DO 150 K=1,NC
0127      150       P=P+ZABCS(I,J,K,L)
0128                ABS=ABS+P*P/NC
0129      160       T=T+P
0130      170       AB=AB+T*T/(NC*NS)
0131                D(5)=(NA-1)*(NB-1)
0132                SS(5)=AB-A-B+X
0133                DO 200 I=1,NA
0134                DO 200 K=1,NC
0135                T=0
0136                DO 190 L=1,NS
0137                P=0
0138                DO 180 J=1,NB
0139      180       P=P+ZABCS(I,J,K,L)
0140                ACS=ACS+P*P/NB
0141      190       T=T+P
0142      200       AC=AC+T*T/(NB*NS)
0143                D(6)=(NA-1)*(NC-1)
0144                SS(6)=AC-A-C+X
0145                DO 230 J=1,NB
0146                DO 230 K=1,NC
0147                T=0
```

```
0148              DO 220 L=1,NS
0149              P=0
0150              DO 210 I=1,NA
0151     210      P=P+ZABCS(I,J,K,L)
0152              BCS=BCS+P*P/NA
0153     220      T=T+P
0154     230      BC=BC+T*T/(NA*NS)
0155              D(7)=(NB-1)*(NC-1)
0156              SS(7)=BC-B-C+X
0157              D(8)=(NA-1)*(NB-1)*(NC-1)
0158              SS(8)=ABC-AB-AC-BC+A+B+C-X
0159              D(9)=(NA*NB*NC-1)*(NS-1)
0160              SS(9)=ABCS-S-ABC+X
0161              D(13)=(NA-1)*(NB-1)*(NS-1)
0162              SS(13)=ABS-AB-AS-BS+A+B+S-X
0163              D(14)=(NA-1)*(NC-1)*(NS-1)
0164              SS(14)=ACS-AC-AS-CS+A+C+S-X
0165              D(15)=(NB-1)*(NC-1)*(NS-1)
0166              SS(15)=BCS-BC-BS-CS+B+C+S-X
0167              D(16)=(NA-1)*(NB-1)*(NC-1)*(NS-1)
0168              SS(16)=ABCS-S-ABC+X
FORTRAN IV-PLUS V02-04G                  11:56:41     12-MAY-78          PAGE 4
XNOVA3.FTP        /RO/TR:ALL/WR

0169              DO 240 M=10,15
0170     240      SS(16)=SS(16)-SS(M)
0171              CALL TYPE
0172              CALL TYPE('&BASIC QUANTITIES')
0173              CALL TYPE
0174              CALL TYPE('&      A           B           C')
0175              CALL TYPE
0176              CALL TYPER(A,B,C)
0177              CALL TYPE
0178              CALL TYPE('&      AB          AC          BC          ABC')
0179              CALL TYPE
0180              CALL TYPER(AB,AC,BC,ABC)
0181              CALL TYPE
0182              CALL TYPE('&      AS          BS          CS')
0183              CALL TYPE
0184              CALL TYPER(AS,BS,CS)
0185              CALL TYPE
```

```
0186            CALL TYPE('&      ABS          ACS          BCS')
0187            CALL TYPE
0188            CALL TYPER(ABS,ACS,BCS)
0189            CALL TYPE
0190            CALL TYPE('&      ABCS         S            X')
0191            CALL TYPE
0192            CALL TYPER(ABCS,S,X)
0193            CALL TYPE
0194            CALL ASKI(III,'&TYPE 0 FOR ANOVA SUMMARY TABLE  ')
0195            CALL PSAVE
0196            CALL PSCLR
0197            CALL TYPE('&                ANOVA SUMMARY TABLE')
0198            CALL TYPE
0199            CALL TYPE('&      SOURCE       SS           DF           MS')
0200            CALL TYPE('            F RATIO')
0201            CALL TYPE
0202            DO 250 M=1,17
0203            SM=SS(M)/D(M)
0204            XM=M
0205            CALL TYPE
0206            CALL TYPER(XM,SS(M),D(M),SM)
0207            IF(M.GT.8)GO TO 250
0208            MM=M+8
0209            F=SM/(SS(MM)/D(MM))
0210            CALL TYPER(F)
0211     250    CONTINUE
0212            CALL TYPE
0213            CALL TYPE
0214            CALL TYPE('&                SOURCE KEY')
0215            CALL TYPE
0216            CALL TYPE('&1=SUBJECTS   2=A    3=B    4=C    5=AB    6=AC    7=BC')
0217            CALL TYPE
0218            CALL TYPE('&8=ABC    9=RESIDUAL    10=AS    11=BS    12=CS    13=ABS')
0219            CALL TYPE
0220            CALL TYPE('&14=ACS    15=BCS    16=ABCS    17=TOTAL')
0221            CALL TYPE
0222            CALL ASKI(III,'&         TYPE 0 TO CONTINUE  ')
0225            CALL INEND(AA)
0226            CALL OUTEND(BB,CB)
0227            END
```

A.4.1.3 SIMPLE MAIN EFFECTS AND TREND ANALYSES>

note: the input file for this program is the output file from either of the previous 2 analysis of variance programs.

********** LISTING OF FDEVLIST **********

```
FORTRAN IV-PLUS V02-04G                    12:13:01     12-MAY-78          PAGE 1
XSMF.FTP          /RO/TR:ALL/WR

0001                DIMENSION YF(300),CB(128),MXL(6),MXQ(6)
0002                CALL TYPE('&SIMPLE MAIN EFFECTS')
0003                CALL ASKN(YF,'&INPUT FILE = ')
0004                CALL ASKI(NP,'&NO. OF TREATMENT LEVELS OF FACTOR A = ')
0005                CALL ASKI(NS,'&NO. OF SUBJECTS = ')
0006                CALL ASKR(SMAS,'&A X S INTERACTION MEAN SQUARE = ')
0007                IF(NP.GT.4)GO TO 4
0008                MXL(1)=-3
0009                MXL(2)=-1
0010                MXL(3)=1
0011                MXL(4)=3
0012                MXQ(1)=1
0013                MXQ(2)=-1
0014                MXQ(3)=-1
0015                MXQ(4)=1
0016                ICL=20
0017                ICQ=4
0018                GO TO 6
0019           4    IF(NP.GT.5)GO TO 5
0020                MXL(1)=-2
0021                MXL(2)=-1
0022                MXL(3)=0
0023                MXL(4)=1
0024                MXL(5)=2
0025                MXQ(1)=2
0026                MXQ(2)=-1
0027                MXQ(3)=-2
0028                MXQ(4)=-1
0029                MXQ(5)=2
0030                ICL=10
```

```
0031              ICL=14
0032              GO TO 6
0033     5        MXL(1)=-5
0034              MXL(2)=-3
0035              MXL(3)=-1
0036              MXL(4)=1
0037              MXL(5)=3
0038              MXL(6)=5
0039              MXQ(1)=5
0040              MXQ(2)=-1
0041              MXQ(3)=-4
0042              MXQ(4)=-4
0043              MXQ(5)=-1
0044              MXQ(6)=5
0045              ICL=70
0046              ICQ=84
0047     6        CONTINUE
0048              CALL INPUT(YF,CB,M)
0049              ASSIGN 99 TO M
0050              CALL INS(YF,0,0)
0051              CALL TYPE
0052              CALL TYPE('&      SOURCE          SS           DF          ')
0053              CALL TYPE(' MS           F RATIO')
0054              NTREAT=1
0055     7        SSA=0
0056              SA=0
FORTRAN IV-PLUS V02-04G                  12:13:01     12-MAY-78          PAGE 2
XSMF.FTF          /RO/TR:ALL/WR

0057              BL=0
0058              BQ=0
0059              DO 10 I=1,NP
0060              CALL IN(YF,Y)
0061              SSA=SSA+Y*Y
0062              SA=SA+Y
0063              IF(NP.LT.4.OR.NP.GT.6)GO TO 10
0064              BL=BL+MXL(I)*Y
0065              BQ=BQ+MXQ(I)*Y
0066     10       CONTINUE
0067              DFA=NP-1
```

```
0068            DFL=1
0069            DFDEP=NP-2
0070            SSA=(SSA/NS)-(SA*SA/(NS*NP))
0071            SMA=SSA/DFA
0072            FA=SMA/SMAS
0073            IF(NP.LT.4.OR.NP.GT.6)GO TO 20
0074            SSL=BL*BL/(ICL*NS)
0075            SSQ=BQ*BQ/(ICQ*NS)
0076            SSDEP=SSA-SSL
0077            SMDEP=SSDEP/DFDEP
0078            FL=SSL/SMAS
0079            FQ=SSQ/SMAS
0080            FDEP=SMDEP/SMAS
0081    20      CONTINUE
0082            CALL TYPE
0083            CALL TYPE('&TREATMENT')
0084            CALL TYPEI(NTREAT)
0085            CALL TYPER(SSA,DFA,SMA,FA)
0086            IF(NP.LT.4.OR.NP.GT.6)GO TO 80
0087            CALL TYPE('&LINEAR REG.')
0088            CALL TYPER(SSL,DFL,SSL,FL)
0089            CALL TYPE('&QUADRATIC  ')
0090            CALL TYPER(SSQ,DFL,SSQ,FQ)
0091            CALL TYPE('&NONLINEAR  ')
0092            CALL TYPER(SSDEP,DFDEP,SMDEP,FDEP)
0093            RCO=100*SSL/SSA
0094            CALL TYPE('&PERCENTAGE LINEARITY OF TREATMENT EFFECT =')
0095            CALL TYPER(RCO)
0096    80      NTREAT=NTREAT+1
0097    90      GO TO 7
0098    99      CALL TYPE
0099            CALL INEND(YF)
0100            END
```

A.4.1.4 SPLIT PLOT ANALYSIS OF VARIANCE.

note: the 2 factor analysis of variance program is run first on the data.. The input file for this program is then formed from the basic quantities output from the 2 factor analysis.

********** LISTING OF PDEVLIST **********

```
FORTRAN IV-PLUS V02-04G                    12:23:39    12-MAY-78          PAGE 1
XSPLOT.FTP      /RO/TR:ALL/WR

0001            DIMENSION F(300),CB(128),Q(30)
0002            CALL TYPE('&SPLIT PLOT ANOVA SUMMARY')
0003            CALL ASKN(F,'&ANOVA OUTPUT 1, 2 AND COMBINED =')
0004            CALL ASKI(NB,'&NO. OF LEVELS OF TREATMENT B =')
0005            CALL ASKI(NC,'&NO. OF LEVELS OF TREATMENT C =')
0006            CALL ASKI(NS,'&NO. OF SUBJECTS/BLOCKS =')
0007            CALL INPUT(F,CB,M)
0008            ASSIGN 999 TO M
0009            CALL INS(F,0,0)
0010            I=1
0011    10      CALL IN(F,Q(I))
0012            I=I+1
0013            GO TO 10
0014    999     CALL INEND(F)
0015            NS=NS/2
0016            NA=2
0017            SSA1=Q(6)-Q(5)
0018            SSA2=Q(14)-Q(13)
0019            SSBS1=Q(8)-Q(4)-Q(6)+Q(5)
0020            SSBS2=Q(16)-Q(12)-Q(14)+Q(13)
0021            SSCS1=Q(7)-Q(3)-Q(6)+Q(5)
0022            SSCS2=Q(15)-Q(11)-Q(14)+Q(13)
0023            SSBCS1=Q(1)-Q(2)-Q(7)-Q(8)+Q(3)+Q(4)+Q(6)-Q(5)
0024            SSBCS2=Q(9)-Q(10)-Q(15)-Q(16)+Q(11)+Q(12)+Q(14)-Q(13)
0025            AS=Q(22)
0026            ABCS=Q(17)
0027            A=Q(5)+Q(13)
0028            B=Q(20)
0029            AB=Q(4)+Q(12)
```

```
0030              C=Q(19)
0031              AC=Q(3)+Q(11)
0032              ABS=Q(24)
0033              ACS=Q(23)
0034              BC=Q(18)
0035              ABC=Q(2)+Q(10)
0036              X=Q(21)
0037              SSTOT=ABCS-X
0038              SSSUB=AS-X
0039              SSA=A-X
0040              SSSUBWG=AS-A
0041              SSWSUB=ABCS-AS
0042              SSB=B-X
0043              SSAB=AB-A-B+X
0044              SSBS=ABS-AB-AS+A
0045              SSC=C-X
0046              SSAC=AC-A-C+X
0047              SSCS=ACS-AC-AS+A
0048              SSBC=BC-B-C+X
0049              SSABC=ABC-AB-AC-BC+A+B+C-X
0050              SSBCS=ABCS-ABC-ABS-ACS+AB+AC+AS-A
0051              DFSUB=NA*NS-1
FORTRAN IV-PLUS V02-04G                    12:23:39    12-MAY-78          PAGE 2
XSPLOT.FTP        /RO/TR:ALL/WR

0052              DFA=NA-1
0053              DFSUBWG=NA*(NS-1)
0054              DFWSUB=NS*NA*(NB*NC-1)
0055              DFB=NB-1
0056              DFAB=(NA-1)*(NB-1)$SUS
0057              DFBS=NA*(NS-1)*(NB-1)
0058              DFC=NC-1
0059              DFAC=(NA-1)*(NC-1)
0060              DFCS=NA*(NS-1)*(NC-1)
0061              DFBC=(NB-1)*(NC-1)
0062              DFABC=(NA-1)*(NB-1)*(NC-1)
0063              DFBCS=NA*(NS-1)*(NB-1)*(NC-1)
0064              DFTOT=NA*NB*NC*NS-1
0065              CDFB=1
0066              CDFAB=NA-1
```

```
0067              CDFBS=NA*(NS-1)
0068              DFA1=NS-1
0069              DFBS1=(NS-1)*(NB-1)
0070              DFCS1=(NS-1)*(NC-1)
0071              DFBCS1=(NS-1)*(NB-1)*(NC-1)
0072              PSA1=SSA1/DFA1
0073              PSA2=SSA2/DFA1
0074              PSBS1=SSBS1/DFBS1
0075              PSBS2=SSBS2/DFBS1
0076              PSCS1=SSCS1/DFCS1
0077              PSCS2=SSCS2/DFCS1
0078              PSBCS1=SSBCS1/DFBCS1
0079              PSBCS2=SSBCS2/DFBCS1
0080              IF(PSA1.GT.PSA2)FA1=PSA1/PSA2
0081              IF(PSA1.LE.PSA2)FA1=PSA2/PSA1
0082              IF(PSBS1.GT.PSBS2)FBS1=PSBS1/PSBS2
0083              IF(PSBS1.LE.PSBS2)FBS1=PSBS2/PSBS1
0084              IF(PSCS1.GT.PSCS2)FCS1=PSCS1/PSCS2
0085              IF(PSCS1.LE.PSCS2)FCS1=PSCS2/PSCS1
0086              IF(PSBCS1.GT.PSBCS2)FBCS1=PSBCS1/PSBCS2
0087              IF(PSBCS1.LE.PSBCS2)FBCS1=PSBCS2/PSBCS1
0088              PSTOT=SSTOT/DFTOT
0089              PSSUB=SSSUB/DFSUB
0090              PSA=SSA/DFA
0091              PSSUBWG=SSSUBWG/DFSUBWG
0092              PSWSUB=SSWSUB/DFWSUB
0093              PSB=SSB/DFB
0094              PSAB=SSAB/DFAB
0095              PSBS=SSBS/DFBS
0096              PSC=SSC/DFC
0097              PSAC=SSAC/DFAC
FORTRAN IV-PLUS V02-04G                  12:23:39     12-MAY-78          PAGE 3
XSPLOT.FTP      /RO/TR:ALL/WR

0098              PSCS=SSCS/DFCS
0099              PSBC=SSBC/DFBC
0100              PSABC=SSABC/DFABC
0101              PSBCS=SSBCS/DFBCS
0102              FA=PSA/PSSUBWG
```

```
0106            FAC=PSAC/PSCS
0107            FBC=PSBC/PSBCS
0108            FABC=PSABC/PSBCS
0109            CALL PSAVE
0110            CALL PSCLR
0111            CALL TYPE
0112            CALL TYPE
0113            CALL TYPE('&ANOVA SUMMARY TABLE')
0114            CALL TYPE
0115            CALL TYPE
0116            CALL TYPE
0117            CALL TYPE('&       SOURCE          SS            DF          ')
0118            CALL TYPE('MS           F              DF(CONS.)')
0119            CALL TYPE
0120            CALL TYPE
0121            CALL TYPE('&BETWEEN SUBJECTS')
0122            CALL TYPER(SSSUB,DFSUB,PSSUB)
0123            CALL TYPE
0124            CALL TYPE('&          A       ')
0125            CALL TYPER(SSA,DFA,PSA,FA)
0126            CALL TYPE
0127            CALL TYPE('&S  WITHIN GROUPS')
0128            CALL TYPER(SSSUBWG,DFSUBWG,PSSUBWG)
0129            CALL TYPE
0130            CALL TYPE('&WITHIN SUBJECTS ')
0131            CALL TYPER(SSWSUB,DFWSUB,PSWSUB)
0132            CALL TYPE
0133            CALL TYPE('&          B       ')
0134            CALL TYPER(SSB,DFB,PSB,FB,CDFB)
0135            CALL TYPE
0136            CALL TYPE('&          AB      ')
0137            CALL TYPER(SSAB,DFAB,PSAB,FAB,CDFAB)
0138            CALL TYPE
0139            CALL TYPE('&          BS      ')
0140            CALL TYPER(SSBS,DFBS,PSBS)
0141            CALL TYPE('              ')
0142            CALL TYPER(CDFBS)
0143            CALL TYPE
0144            CALL TYPE('&          C       ')
0145            CALL TYPER(SSC,DFC,PSC,FC,CDFB)
0146            CALL TYPE
```

```
0147            CALL TYPE('&          AC      ')
0148            CALL TYPER(SSAC,DFAC,PSAC,FAC,CDFAB)
0149            CALL TYPE
0150            CALL TYPE('&          CS      ')
0151            CALL TYPER(SSCS,DFCS,PSCS)
0152            CALL TYPE('             ')
0153            CALL TYPER(CDFBS)
FORTRAN IV-PLUS V02-04G                 12:23:39    12-MAY-78          PAGE 4
XSPLOT.FTP      /RO/TR:ALL/WR

0154            CALL TYPE
0155            CALL TYPE('&          BC      ')
0156            CALL TYPER(SSBC,DFBC,PSBC,FBC,CDFB)
0157            CALL TYPE
0158            CALL TYPE('&          ABC     ')
0159            CALL TYPER(SSABC,DFABC,PSABC,FABC,CDFAB)
0160            CALL TYPE
0161            CALL TYPE('&          BCS     ')
0162            CALL TYPER(SSBCS,DFBCS,PSBCS)
0163            CALL TYPE('             ')
0164            CALL TYPER(CDFBS)
0165            CALL TYPE
0166            CALL TYPE
0167            CALL TYPE('&       TOTAL      ')
0168            CALL TYPER(SSTOT,DFTOT,PSTOT)
0169            CALL TYPE
0170            CALL TYPE
0171            CALL TYPE
0172            CALL ASKI(IFO,'&FINISHED ?')
0173            CALL TYPE
0174            CALL TYPE
0175            CALL TYPE('&TEST FOR HOMOGENEITY OF ERROR TERMS')
0176            CALL TYPE
0177            CALL TYPE
0178            CALL TYPE('&       SOURCE          SS          DF          ')
0179            CALL TYPE('MS          F MAX.')
0180            CALL TYPE
```

```
0181              CALL TYPE
0182              CALL TYPE('&SUBJECTS AT A1  ')
0183              CALL TYPER(SSA1,DFA1,PSA1,FA1)
0184              CALL TYPE
0185              CALL TYPE('&SUBJECTS AT A2  ')
0186              CALL TYPER(SSA2,DFA1,PSA2)
0187              CALL TYPE
0188              CALL TYPE('&       BS AT A1  ')
0189              CALL TYPER(SSBS1,DFBS1,PSBS1,FBS1)
0190              CALL TYPE
0191              CALL TYPE('&       BS AT A2  ')
0192              CALL TYPER(SSBS2,DFBS1,PSBS2)
0193              CALL TYPE
0194              CALL TYPE('&       CS AT A1  ')
0195              CALL TYPER(SSCS1,DFCS1,PSCS1,FCS1)
0196              CALL TYPE
0197              CALL TYPE('&       CS AT A2  ')
0198              CALL TYPER(SSCS2,DFCS1,PSCS2)
0199              CALL TYPE
0200              CALL TYPE('&      BCS AT A1  ')
0201              CALL TYPER(SSBCS1,DFBCS1,PSBCS1,FBCS1)
0202              CALL TYPE
0203              CALL TYPE('&      BCS ST A2  ')
0204              CALL TYPER(SSBCS2,DFBCS1,PSBCS2)
0205              CALL TYPE
0206              CALL TYPE
0207              CALL ASKI(IFO,'&FINISHED ?')
0208              CALL PSCLR
0209              CALL PSRES
FORTRAN IV-PLUS V02-04G                  12:23:39    12-MAY-78          PAGE 5
XSPLOT.FTP        /RO/TR:ALL/WR

0210              END
```

Appendix A.4.2
MEASUREMENT OF LUMINANCE AND CONTRAST OF VISUAL MATERIAL PRESENTED ON THE HELMET-MOUNTED DISPLAY

Because the helmet-mounted display produces a virtual image, it is difficult to measure directly the luminance characteristics of the images perceived by the subject. For the character legibility experiments discussed in Chapter 4, the dimensions of the characters were less than 0.3 mm in height when generated on the CRT phosphor faceplate, although the visual angle subtended by the character was as great as 30 minutes-of-arc when viewed through the optics. Direct measurement of character luminance on the CRT required special purpose microphotometric equipment which was unavailable to the author. As an alternative approach, the image luminance was measured indirectly using a brightness matching technique. Figure A.4.2.1 shows a diagram of the apparatus used for this measurement. First, the right half of the CRT faceplate in the helmet-mounted unit was masked with black plastic tape allowing only the characters on the left half of the visual field to be seen by the eye. A rear projection screen was positioned approximately 0.3 m in front of the helmet-mounted unit of the HMD. A 500 watt slide projector was located behind the rear projection screen and used to project a field of white light onto the screen. A green Wratten gelatin filter (Kodak No. 61) was placed on the rear projection screen. The subtended angle of the Wratten film was equivalent to the the subtended angle of the opaque or dark region of the CRT. The spectral transmission characteristics of the filter approximated the spectral emissivity characteristics of the P1 phosphor on the CRT (i.e., Figure A.3.1.1).

Similarly, the area on projection screen left of the filter was masked, preventing light from the slide projector from entering the HMD. Again, the area of the opaque region was equivalent to the subtended angle of the region within the HMD visual field wherein the characters were presented. [Hereafter, the left portion (opaque) of the field will be called the test field and the right portion (filter) called the reference field.]

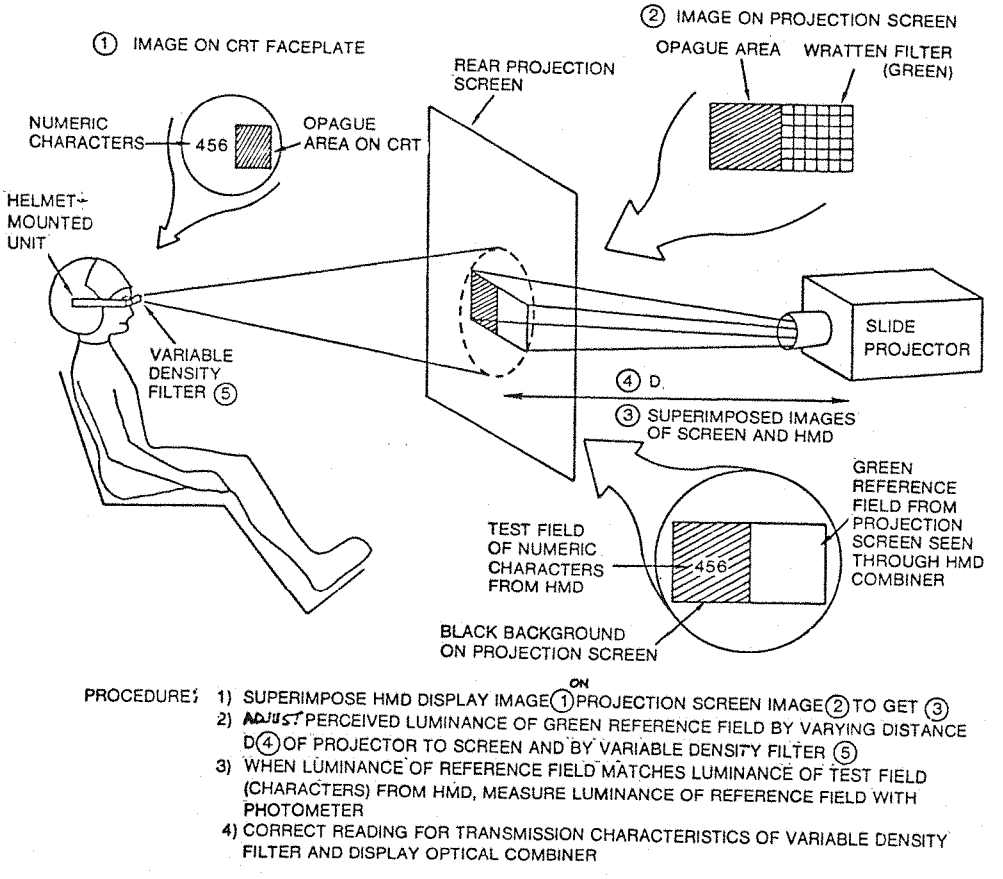

Figure A.4.2.1. Apparatus for Measuring Perceived Luminance of Helmet-Mounted Display Images

In order to perform the measurement, the helmet display was operated in a "see-through" mode, that is the transmittance of the variable density filter was adjusted so that light from the reference field of the peak projection screen could be seen through the optical combiner of the HMD. The position of the display was adjusted such that the right field of the HMD and the reference (right) field of the rear projection screen were superimposed. Likewise, the left (test) fields were superimposed. The luminance level of the reference field as seen through the display was then adjusted by both the variable transmission filter of the optics assembly and changing the distance of the projector to the screen, until the perceived luminance of the reference field apparently matched that of the characters or test field. Having accomplished these adjustments, the luminance of the reference

field through the variable density filter was measured using a spot photometer. (Exposure photometer, Salford Electrical Instruments, Ltd.). This luminance reading was then adjusted for the additional light attenuation due to the optical combiner of the helmet-mounted unit. The resulting luminance level was then assumed to be the apparent luminance of the characters at the specific brightness and contrast control settings and video input level conditions during which the measurement was taken. Several samples were taken and averaged for each luminance reading.

For those display conditions when the backgrounds of the characters were not zero, the luminance measurement was performed twice, once for the characters and once for the background. This also applies to the display of imagery when the light and dark portions of the target and its background were measured independently.

The luminance contrast for the characters and targets were computed from the luminance measured above using the formula (McCormick, 1976):

$$C = \frac{L_1 - L_2}{L_1} \times 100\%$$

where

L_1 = brighter of two contrasting areas, and

L_2 = darker of two contrasting areas.

Appendix A.4.3
ADJUSTMENT AND MEASUREMENT OF SUBTENDED VISUAL ANGLES OF IMAGES PRESENTED ON THE HELMET-MOUNTED DISPLAY

The dimensions of the raster image on the CRT faceplate can be set by adjusting the gain of the horizontal and vertical deflection amplifiers. Since the visual material in this thesis (i.e., characters, reticle, and imagery) were generated with a scanning raster on the CRT, changing the size of the raster also changed the subtended angle of the images presented within the raster.

Direct measurement of the size of the images on the CRT faceplate was not possible due to the small sizes of the character (i.e., less than 0.3 mm); therefore, two alternate means were devised for measuring the dimensions of the virtual image of the CRT faceplate as seen by the subject. The first method was to superimpose the image from the display on a chart located some distance from the display. The chart contained areas of specified dimensions over which the characters or other images of the display could be superimposed.

The viewing distance from the chart to the display was then adjusted until the vertical or horizontal subtended angle of the image in the display fit a specific dimension of the chart. The angular size (δ) of the character in minutes-of-arc was then computed by

$$\delta \cong \sin^{-1}\left(\frac{h}{d}\right) \times 60 \text{ minutes-of-arc}$$

where h is the dimension on the chart over which the vertical image was superimposed and d is the viewing distance.

Another method for measuring subtended angle was devised for the larger subtended angles of the target images in Experiment ST.1 (Chapter 8). Here the chart with fixed dimensions described above was replaced with a cathode-ray oscilloscope. The output of signals from a sine wave oscillator were input into the vertical amplifier input of the oscilloscope producing a sinusoidal pattern on the scope CRT. The height or amplitude of the sinusoidal pattern was controlled by the

gain adjustment of the oscillator. The rms output of the oscillator was measured by a digital voltmeter. The gain inputs to the oscilloscope were adjusted such that the output of the digital voltmeter was in the units of height of the peak-to-peak amplitude of the sinusoidal waveform on the scope. The helmet-mounted unit of the HMD was located at a fixed distance (500 mm) from the scope. The subtended angle of the image on the display was then measured by superimposing the virtual image from the helmet-mounted display on the oscilloscope faceplate then adjusting the amplitude of the sinusoidal pattern until it measured exactly the size of the image on the HMD. The height (h) of the wave form (in millimeters) was then read from the digital voltmeter and used to compute the subtended angle of the HMD image (δ):

$$\delta = 2 \tan^{-1} \left(\frac{h}{1000}\right) \times 60 \text{ minutes-of-arc}$$

The combination of the two methods above provided the means of calibrating the gain controls for the deflection amplitude in the electronics unit. Hereafter, since the size of the characters in the input video signals did not vary, the character height and/or image size was set directly by adjusting the gain controls on the deflection amplifiers. The modification to the display electronics unit discussed in Appendix A.3.1 (Section A.3.1.3.4) provided remote control of the deflection amplifier gains. These controls were calibrated so that specific character sizes could be set directly.

Appendix A.4.4

INSTRUCTIONS TO SUBJECTS FOR EXPERIMENT LG.1

(PANEL-MOUNTED AND HELMET-MOUNTED DISPLAYS)

EXPERIMENT LG.1: INSTRUCTIONS TO SUBJECTS (PANEL-MOUNTED DISPLAY)

You will be participating in an experiment to measure character legibility on three different displays while your seat is being vibrated at different frequencies and levels. During this session of the experiment, you will be viewing a panel-mounted display.

Your task is to read different arrays of random numbers presented on the display. Each array has 50 numbers arranged in 5 rows and 10 columns. You will read one array for each vibration condition. The total duration of each run is approximately 1 minute. There are a total of 52 runs in this session.

The arrays are to be read from left to right beginning with the top line and progressing to the bottom line. Your reading rate is to be paced by the tone or beep which you will hear. Please read one number for each beep that you hear. Please state the number at the time you hear the beep. Try to be as accurate as possible. If you are unsure about a number, give your best guess and continue on to the next number with the next beep. Do not go back.

In between the runs the display will be blanked. You are to begin reading the characters when the experimenter says "begin" and continue until you have read all of the numbers in the array. You will have two practice runs before the experiment begins.

You may stop the experiment at any time by pressing the large red button on your right. You may also withdraw from the experiment at any time.

Do you have any questions?

EXPERIMENT LG.1: INSTRUCTIONS TO SUBJECTS (HELMET-MOUNTED DISPLAY)

You will be participating in an experiment to measure character legibility on three different displays while your seat is being vibrated at different frequencies and levels. During this session of the experiment, you will be viewing a helmet-mounted display. (This display is attached to a special helmet you will be wearing during the experiment. This display is viewed with only your right eye; however, keep both eyes open at all times while viewing the display during the experiment.)

Your task is to read different arrays of random numbers presented on the display. Each array has 50 numbers arranged in 5 rows and 10 columns. You will read one array for each vibration condition. The total duration of each run is approximately 1 minute. There are a total of 52 runs in this session.

The arrays are to be read from left to right beginning with the top line and progressing to the bottom line. Your reading rate is to be paced by the tone or beep which you will hear. Please read one number for each beep that you hear. Please state the number at the time you hear the beep. Try to be as accurate as possible. If you are unsure about a number, give your best guess and continue on to the next number with the next beep. Do not go back.

In between the runs the display will be blanked. You are to begin reading the characters when the experimenter says "begin" and continue until you have read all of the numbers in the array. You will have two practice runs before the experiment begins.

You may stop the experiment at any time by pressing the large red button on your right. You may also withdraw from the experiment at any time.

Do you have any questions?

Appendix A.4.5
INSTRUCTIONS TO SUBJECTS FOR EXPERIMENT LG.2
(LINE AND ARRAY DISPLAY FORMTS)

INSTRUCTIONS TO SUBJECTS (ARRAY DISPLAY FORMAT)

You will be participating in an experiment to measure your ability to read numeric characters presented on a helmet-mounted display while your seat is being vibrated at different frequencies and levels. The experiment is divided into two parts. In this part of the experiment you will be viewing random numbers presented in an array format on the display. Each array has 50 numbers arranged in 5 rows and 10 columns. Your task is to read the numbers in the array from left to right beginning with the top line and progressing to the bottom line. Your reading rate is to be paced by the tone or beep which you will hear. Please state the number at the time you hear the beep. Try to be as accurate as possible. If you are unsure about a number, give your best guess and continue on to the next number with the next beep. Do not go back. While you are reading the arrays, keep both eyes open. (Note that the helmet-mounted display is viewed with only your right eye; however, keep both eyes open during this experiment.) Also keep a relaxed, upright posture; do not stiffen muscles in your legs, back, or neck during the experiment runs. Keep your head and eyes pointing straight ahead.

In between the runs the display will be blanked. You are to begin reading the characters when the experimenter says "begin" and continue until you have read all of the numbers in the array. You will have two practice runs before the experiment begins. You will read one array for each vibration condition. The duration of each run is approximately 1 minute. There are a total of 32 runs in this part of the experiment.

You may stop the experiment at any time by pressing the large red button on your right. You may also withdraw from the experiment at any time.

Do you have any questions?

INSTRUCTIONS TO SUBJECTS (LINE DISPLAY FORMAT)

You will be participating in an experiment to measure your ability to read numeric characters presented on a helmet-mounted display while your seat is being vibrated at different frequencies and levels. The experiment is divided into two parts. In this part of the experiment you will be viewing random numbers arranged in a row or line format. Each line will contain 10 numbers. Your task is to read the numbers in the line from left to right as each line is presented. Your reading rate is to be paced by the tone or beep which you will hear. Please state the number at the time you hear the beep. Try to be as accurate as possible. If you are unsure about a number, give your best guess and continue on to the next number with the next beep. Do not go back. While you are reading the lines, keep both eyes open. (Note that the helmet-mounted display is viewed with only your right eye; however, keep both eyes open during this experiment.) Also keep a relaxed, upright posture; do not stiffen muscles in your legs, back, or neck during the experiment runs. Keep your head and eyes pointing straight ahead.

In between the runs the display will be blanked. You are to begin reading the characters when the experimenter says "begin" and continue until you have read five lines (of 10 numbers each) for each experiment run. You will have two practice runs before the experiment begins. The duration of each run is approximately 1 minute. There are a total of 32 runs in this part of the experiment.

You may stop the experiment at any time by pressing the large red button on your right. You may also withdraw from the experiment at any time.

Do you have any questions?

Appendix A.4.6
INSTRUCTIONS TO SUBJECTS FOR EXPERIMENT LG.3
(CHARACTER SIZE)

INSTRUCTIONS TO SUBJECTS (CHARACTER SIZE)

You will be participating in an experiment to measure your ability to read numeric characters presented on a helmet-mounted display while your seat is being vibrated at different frequencies and levels. During this experiment, you will be viewing random numbers arranged in a row or line format. The size of the characters will be adjusted during the experiment. Each line will contain 10 numbers. Your task is to read the numbers in the line from left to right as each line is presented. Your reading rate is to be paced by the tone or beep which you will hear. Please state the number at the time you hear the beep. Try to be as accurate as possible. If you are unsure about a number, give your best guess and continue on to the next number with the next beep. Do not go back. While you are reading the lines, keep both eyes open. (Note that the helmet-mounted display is viewed with only your right eye; however, keep both eyes open during this experiment.) Also keep a relaxed, upright posture; do not stiffen muscles in your legs, back, or neck during the experiment runs. Keep your head and eyes pointing straight ahead.

In between the runs the display will be blanked. You are to begin reading the characters when the experimenter says "begin" and continue until you have read 5 lines (or 10 numbers) for each experiment run. You will have two practice runs before you begin.

You may stop the experiment at any time by pressing the large red button on your right. You may also withdraw from the experiment at any time.

Do you have any questions?

Appendix A.5.1
THEORETICAL CONSIDERATIONS FOR THE COMPUTATION OF TRANSFER FUNCTIONS

A.5.1 THEORETICAL CONSIDERATIONS

A.5.1.1 Introduction

In its simplest form, the transmission of vibration through the body to the head can be represented by the ratio of the amplitude of the movement of the head or helmet (in one of several axes) to the movement of the vibrating input structure, in this case, vertical Z axis seat motion. If the vibration input is deterministic [that is, one where the magnitude of the seat displacement, velocity, or acceleration can be predicted from its state at a previous time (given frequency, amplitude, and phase)], then theoretically, for a linear system, the time varying output of the system y(f) is related to the input x(f) by the equation:

$$\frac{y(f)}{x(f)} = A(f)$$

where y(f) and x(f) are deterministic and A is defined at each frequency (f). In the equation above, A(f) is defined as a discrete quantity for each f and is independent of the amplitude of x(f). The experiments conducted in this thesis use sinusoidal vibration in order to simplify analysis and interpretation of the data results.

However, because of the imperfections within the vibration and instrumentation systems used in experiments, a pure sinusoidal vibration motion cannot be assumed. Usually a combination of compound harmonic motion exists along with noise due to vibration drive electronics and instrumentation. Figure A.5.1.1 is a simple block diagram representing the transmission of a time varying input motion x(f) to the head or helmet of the subject. x(f) is the measured input of seat motion due to the original drive signal x'(f).

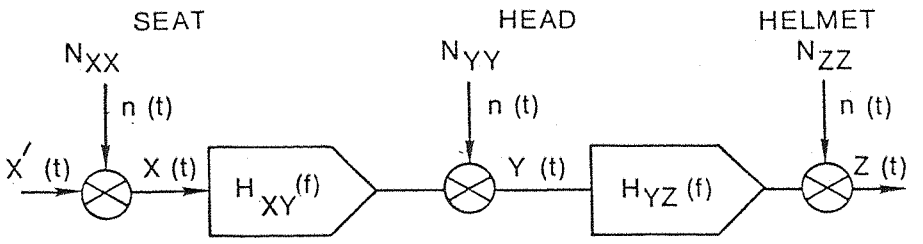

Figure A.5.1.1. Transmission of Time Varying Input Motion to the Head and Helmet of a Subject

The measured response of the head is y(t) and the measured response of the helmet is z(t). In this illustration, the relationship of head to seat motion is represented by the transfer function $H_{xy}(f)$ and the helmet to head motion relationship is represented by the transfer function $H_{yz}(f)$. N_{xx}, N_{yy}, and N_{zz} represent random noise sources due to imperfections in the experiment setting. If x(f), y(f), and z(f) are stationary ergodic processes (Bendat and Piersol, 1971, pages 12, 86-88), and $H_{xy}(f)$ and $H_{yz}(f)$ are approximately linear motion transfer relationships, then linear systems analysis procedures can be used for characterizing the system. The assumptions that the motions x(f), y(f), and z(f) are stationary and ergodic is highly likely because of the deterministic nature of the original input signal x'(f) (e.g., sinusoidal in laboratory experiments and deterministic in helicopter field trials). The assumption of linearity may only be validated by some empirical analyses of the system itself; however, several experiments have found the transmission of vertical vibration to the head of seated subjects to be reasonably linear (e.g., Pradko et al., 1965).

A.5.1.2 Root Mean Square Values

If these assumptions are valid, then the general intensity of motion of the seat, head, and helmet can be described in terms of root mean square values Ψ_x, Ψ_y, Ψ_z, where

$$\Psi_x^2 = \lim_{T\to\infty} \int_0^T x^2(t)\, dt$$

$$\Psi_y^2 = \lim_{T\to\infty} \int_0^T y^2(t)\, dt$$

$$\Psi_z^2 = \lim_{T\to\infty} \int_0^T z^2(t)\, dt$$

and T is the period over which the sample is taken (or in the case of a true rms voltmeter reading, the time constant).

From a practical standpoint, an approximation to the magnitudes of the transfer functions $H_{xy}(f_0)$ and $H_{yz}(f_0)$ can be obtained at a given frequency f_0 by the following relationships

$$\left\{H_{xy}(f_0)\right\} \sim \frac{\Psi_y}{\Psi_x} \text{ at } f_0 \text{ (head to seat transfer ratio)}$$

A.5.1.1

$$\left\{H_{yz}(f_0)\right\} \sim \frac{\Psi_x}{\Psi_y} \text{ at } f_0 \text{ (helmet to head transfer ratio)}$$

Note also that another relationship $\left\{H_{xz}(f_0)\right\} \sim \frac{\Psi_z}{\Psi_x}$ at f_0

can also be defined for the helmet to seat motion. The ratio of the rms values can only provide an approximation to the transfer characteristics at f_0 since the noise sources (N_{xx}, N_{yy}, N_{zz}) and spurious harmonics contribute to these signals.

Using the relationships above, an analysis of the transmissibility characteristics of the subjects can be made in the time domain. This approach would be implemented by taking true rms readings of the

accelerometer transducers indicating the head, helmet, and seat accelerations, then computing by the ratio of the rms values the various approximations to the transfer functions. In order to characterize the nature of the transfer functions across some range of frequencies, several combinations of time histories would have to be measured at discrete frequencies in order to establish an overall representation of transmissibility across a vibration frequency range.

A.5.1.3 Frequency Domain Analysis (Power Spectral Density Function)

Another method for representing the response of the subjects to the input motion is by analyzing input and output motions in the frequency domain. Known as spectral analysis, this approach provides an estimate of the energy density of a random time varying process within various frequency bands. Because the signals x(f), y(f), and z(f) described above are contaminated with noise, the analysis becomes a statistical problem wherein it is possible only to know the average of the signal level and establish some measure of the reliability or accuracy of the average. Again, if the processes represented by x(f), y(f), and z(f) are stationary and ergodic, a power spectral density function can be computed from the time varying data, which describes the frequency composition of the data in terms of the spectral density of its mean-squared value. The power spectral density function can be computed by taking the Fourier transform of the autocorrelation function $R(\tau)$ where

$$R_x(\tau) = \lim_{T\to\infty} \frac{1}{T}\int_0^T x(t)\, x(t+\tau)\, dt$$

and τ = time displacement and T = period of observation. In the case of the input vibration motion x(t), the power spectral density function $G_{xx}(f)$ is given by

$$G_{xx}(f) = 2\int_{-\infty}^{\infty} R_x(\tau)e^{-j2\pi f\tau}\, d\tau$$

Similarly, G_{yy} and G_{zz} can be obtained.

Inversely, the root mean square value of x(t) over a bandwidth of 0 Hz to B Hz can be obtained by taking the positive square root of the integral of the power spectral density function:

$$\Psi_x = \left[\int_0^B G_{xx}(f)\, df \right]^{1/2} \qquad \text{A.5.1.2}$$

One main advantage of the analysis using the power spectral density function over the ratio of rms values is that the frequency composition of both the input and output is shown. Harmonic content is also evident. From this, the amount of power (signal intensity) can be estimated at each frequency of the output due to the power of the input. The transfer function can then be estimated by the following relationship:

$$\left\{ H_{xy}(f) \right\} = \left[\frac{G_{yy}(f)}{G_{xx}(f)} \right]^{1/2} \qquad \text{A.5.1.3}$$

A further extension of the use of the PSD analysis comes when the input frequency is swept across a frequency band of interest during a single time history record. The function $\left\{ H_{xy}(f) \right\}$ could then be defined as a continuous frequency response function wherein gain or amplitude of the energy plus noise relative to the input is defined continuously across the frequency band interest (e.g., f_0 to f_1). In this case only the magnitude of the frequency response is calculated and the $\left\{ H_{xy}(f) \right\}_{f_0}^{f_1}$ contains contributions from N_{yy}.

Although the function $\left\{ H_{xy}(f) \right\}_{f_0}^{f_1}$ relates some basic characteristics of the physical system, the function is still contaminated with contributions from the noise source N_{yy}. Also, only the magnitude of the frequency response is computed. The determination of the phase response chracteristics of the physical system requires a knowledge of the joint properties of the input and output signals.

A.5.1.4 Frequency Domain Analysis (Cross Spectral Density Function)

The cross spectral density function (CSD) is one means of characterizing the joint properties of two random (type) signal sources. The CSD is related to the cross correlation function $\left[R_{xy}(\tau)\right]$. If x(t) and y(t) are input and output time histories (which are stationary and ergodic) taken in a signal record of time (T), the cross correlation function $\left[R_{xy}(\tau)\right]$ is defined as

$$R_{xy}(\tau) = \lim_{T\to\infty} \frac{1}{T}\int_0^T x(t)\, y(t+\tau)\, dt$$

The cross spectral density function $G_{xy}(f)$ is the Fourier transform of the cross correlation function.

$$G_{xy}(f) = 2\int_{-\infty}^{\infty} R_{xy}(\tau)\, e^{-j2\pi f\tau}\, d\tau$$

The cross spectral density function is complex, having a real part C_{xy} (i.e., the coincident spectral density function) and an imaginary part Q_{xy} (quadrature spectral density function). Using polar notation

$$G_{xy} = |G_{xy}(f)|\, e^{-j\theta_{xy}(f)}$$

where

$$|G_{xy}(f)| = \sqrt{C_{xy}^2(f) + Q_{xy}^2(f)}$$

is the magnitude of $G_{xy}(f)$ and

$$\theta_{xy}(f) = \tan^{-1}\left[\frac{Q_{xy}(f)}{C_{xy}(f)}\right]$$

is the phase angle. The transfer function $H_{xy}(f)$ is the ratio of the cross power of the output to the input relative to the auto power of the input or

$$H_{xy}(f) = \frac{G_{xy}(f)}{G_{xx}(f)} = \left|\frac{G_{xy}(f)}{G_{xx}(f)}\right| e^{-j\theta_{xy}(f)} \qquad \text{A.5.1.4}$$

The magnitude or modulus of the transfer function is

$$|H_{xy}(f)| = \left|\frac{G_{xy}(f)}{G_{xx}(f)}\right|$$

and the phase response is $\theta_{xy}(f)$. The special feature of using cross spectral analysis is that both the gain and phase relationships between the inputs and outputs can be defined. Furthermore, the linear response of the system is more closely discerned since only that portion of the output signal which is correlated with the input signal is shown in $H_{xy}(f)$. Likewise, the effects of the noise source such as N_{yy} are eliminated because there would be little or no correlation of the noise of the output $y(t)$ with the noise or signal of the input $x(t)$. At the same time, the harmonic response of the system could not be shown since the output response of the system at any particular frequency could only be related to the input at that same frequency. Therefore, the unique properties to the physical systems being measured (in this case the head and helmet to seat input) can be characterized by looking at both the transfer functions computed by auto spectral (Equation A.5.1.3) and cross spectral (Equation A.5.1.4) techniques.

A.5.1.5 Coherence Function

Another useful relationship in quantifying the goodness of the transfer function computations above is the coherence function $\gamma_{xy}^2(f)$, given by

$$\gamma_{xy}^2(f) = \frac{|G_{xy}(f)|^2}{G_{xx}(f)\, G_{yy}(f)} \qquad \text{A.5.1.5}$$

$\gamma_{xy}^2(f)$ is a real valued quantity that indicates the degree to which the output signal is correlated with the input signal at any particular frequency. If the value for $\gamma_{xy}^2(f)$ is very low, the computation of $H_{xy}(f)$ using the cross spectral method is invalid. Normally, $\gamma_y^2(f)$ should be >0.5 (Mercer, 1972). From Equations A.5.1.3, A.5.1.4, and A.5.1.5, it can be seen that

$$\gamma_{xy}^2(f) = \frac{|H_{xy}(f)|_{CSD}}{\{H_{xy}(f)\}_{PSD}} \qquad \text{A.5.1.6}$$

As $\gamma_{xy}^2(f) \to 1$ then $\{H_{xy}(f)\}^{PSD} \to |H_{xy}(f)|^{CSD}$.

A.5.1.6 Confidence Intervals

Using the coherence function $\gamma_{xy}^2(f)$ and the power spectral density functions in the input and output signals $\left[G_{xx}(f),\ G_{yy}(f)\right]$, the confidence interval for an estimated transfer function $\hat{H}_{xy}(f)$ can be determined by computing the quantity $\hat{r}(f)$ (Bendat and Piersol, 1971, pages 201-208)

$$\hat{r}(f) = \left\{ \frac{2}{n-2} F_{2,\ n-2:\alpha} \left[1 - \hat{\gamma}_{xy}(f)\right] \frac{\hat{G}_{yy}(f)}{\hat{G}_{xx}(f)} \right\}^{1/2*} \qquad \text{A 5.1.7}$$

*positive square root

where

n = number degrees of freedom of each spectral estimate (i.e., $n = 2B_eT$ where B_e = resolution bandwidth and T length of time history)

$F_{2,\ n-2:\alpha}$ = 100 α percentage point of an F distribution with $n_1 = 2$ and $n_2 = n-2$ degrees of freedom

$\hat{G}_{xx}(f)$ = computed power spectrum estimate of input x(t)

$\hat{G}_{yy}(f)$ = computed power spectrum estimate of output y(t)

$\hat{\gamma}_{xy}^2(f)$ = estimate of the ordinary coherence function between the input x(t) and the output y(t)

From the equation above, the confidence interval (1-α) about the real modulus $|H(f)|$ can be shown in terms of the estimates of the modulus $|\hat{H}(f)|$ determined empirically and the factor $\hat{r}(f)$ at each frequency (f) by

$$|\hat{H}(f)| - \hat{r}(f) \leq |H(f)| \leq |\hat{H}(f)| + \hat{r}(f)$$

Likewise, the confidence interval (1-α) for the phase response $\phi(f)$ at each frequency is given by

$$\hat{\phi}(f) - \Delta\hat{\phi}(f) \leq \phi(f) \leq \hat{\phi}(f) + \Delta\hat{\phi}(f)$$

where $\hat{\phi}(f)$ is the estimate of the phase response determined empirically from $\hat{H}_{xy}(f)$ and $\Delta\hat{\phi}(f)$ where

$$\Delta\hat{\phi}(f) = \sin^{-1}\left[\frac{\hat{r}(f)}{|\hat{H}(f)|}\right] \qquad \text{A.5.1.8}$$

A.5.1.7 Statistical Degrees-of-Freedom

In order to minimize the value of $\hat{r}(f)$ and hence, increase the confidence of the estimated values for H(f), the number of degrees of freedom for the spectral density computations must be kept large. For example, 104 degrees of freedom are needed to estimate the accuracy of H(f) within ±1dB, at a confidence level of 90 percent. As either the requirements for confidence level or accuracy increase, so do the requirements for the number of degrees of freedom. Table A.5.1.1 summarizes the degrees of freedom needed to obtain various accuracies and confidence levels in spectral density measurements.

TABLE A.5.1.1. DEGREES OF FREEDOM AS FUNCTION OF ACCURACY AND CONFIDENCE LEVEL (Mercer, 1973)

Confidence Level	Accuracy			
	±5dB	±2.5dB	±1dB	±0.5dB
40%	--	3	11	42
60%	2	5	28	105
80%	4	11	63	250
90%	5	18	104	410
96%	8	27	161	640
98%	10	34	207	820

A.5.1.8 Fast Fourier Transforms

An alternative method of computing the estimated power spectral density and cross spectral density functions described above is by making direct use of the Fourier transform. If X(f) denotes the Fourier transform of the time history x(t) and X*(t) denotes its complex conjugate, then the power spectral density functions can be represented by

$$G_{xx}(f) = \lim_{T\to\infty} 2\,\frac{X(f)\,X^*(f)}{T} \qquad \text{A.5.1.9}$$

Likewise, the power spectral density function for y(t) can be represented by

$$G_{yy}(f) = \lim_{T\to\infty} 2\,\frac{Y(f)\,Y^*(f)}{T} \qquad \text{A.5.1.10}$$

where Y*(f) is the complex conjugate of the Fourier transform Y(f) of the time history y(t). The cross spectral density function can be derived also using the Fourier transforms of the x(t) and y(t) records.

$$G_{xy}(f) = \lim_{T\to\infty} 2\,\frac{X(f)\,Y^*(f)}{T} \qquad \text{A.5.1.11}$$

This latter method for computing the spectral density estimate was used for the analyses described in this thesis. High speed digital data acquisition and digital computing systems and Fast Fourier Transform (FFT) computation techniques have made the direct Fourier approach described in Equations A.5.1.9, A.5.1.10, and A.5.1.11 above much more practical than the auto correlation and cross correlation procedures described earlier. For these reasons, the Fast Fourier Transforms were used for analyzing the experimental data reported in this thesis. Figure 5.1.4 (Chapter 5) describes in diagram form the data manipulation and analysis procedures used to compute the various spectral density and transfer functions reported herein.

A.5.1.9 Relationships of Bandwidth, Degrees-of-Freedom, Sampling Rate, and Number of Samples

In order to gain the needed confidence levels and accuracies for computing the CSD and PSD using the Fast Fourier transform technique, successive slices of the time history must be taken. If only one sample were taken for a time T which approaches infinity, the Expressions A.5.1.9, A.5.1.10, and A.5.1.11 would have only two degrees of freedom. The statistical accuracy of the estimates is improved by taking ensemble averages of successive slices of the sampled time history and averaging across adjacent frequency bands. Using this approach, the number of degrees of freedom (DOF) in any particular estimate of the power spectral density or cross spectral density (and transfer function) is given by the equation

$$\text{DOF} = 2\left(\frac{2N}{L} - 1\right) \qquad \text{A.5.1.12}$$

where N is the number of samples in the time history and L is the number of samples used to compute each Fourier transform. (L is always a power of 2.) The actual frequency resolution B_e of the PSD or CSD can be computed by

$$B_e = \frac{S}{L} \qquad \text{A.5.1.13}$$

where S is the sampling rate and L is the transform length as above. Substituting Equation A.5.1.13 into Equation A.5.1.12, the DOF can be related to frequency resolution and sample rate as follows

$$DOF = 2\left[2N\left(\frac{R}{S}\right) - 1\right] \qquad \text{A.5.1.14}$$

In most cases, it is desirable to fix the sampling rate at no less than twice the maximum frequency component of interest within the time history (Bendat and Piersol, 1971, pages 228 to 231). If S is selected, then in order to increase resolution B_e, (i.e., decrease the width of each adjacent frequency band within the PSD and CSD), then a proportional increase in the number of samples (N) is needed. The required record length would be determined by the relationship $T = \frac{N}{S}$. The specific sampling rates, degrees of freedom, and resolution are reported in the description of each experiment, and are indicated on the plots of the data.

A.5.1.10 An Example From Chapter 5

In experiment BD.5 (Chapter 5, Section 5.5), it was desired to establish transfer functions of vertical Z axis seat motion to the motion of the head and helmet in the pitch axis. The maximum frequency of interest was 60 Hz, and the desired resolution of the transfer function was B_e = 0.5 Hz. It was also desired that the accuracy of the estimated transfer function to be within ±1dB of the actual transfer function. From Table A.5.1.1 at least 161 degrees of freedom were required to maintain a confidence of at least 96 percent. In order to prevent aliasing of the sampled data, the time histories of vibration motions were filtered with a low pass filter with a bandwidth of 60 Hz (-3dB). Accordingly, the sampling frequency (S) was set at 120 samples/s. With the desired bandwidth (B_e = 0.5 Hz) and the sampling rate (S = 120 samples/s) established, the transform length (L) was determined to be 256 samples (L must be adjusted to the nearest power of 2 greater than the ratio of S to R). The number of samples (N) required was

computed from Equation A.5.1.14 to be 10,432 or about 87 s of data samples at 120 samples/s. Since the vibration input was a swept sine wave, and the period of the sweep from 0 to 60 Hz was 100 s, the number of samples acquired was increased to 12,000 corresponding to a sampling period of 100 s. The resulting DOF was then recomputed to be 184.

Appendix A.5.2
SPECIFICATIONS OF VIBRATION MEASUREMENT
AND RECORDING COMPONENTS

Figure A.5.2.1 shows an interconnection diagram of the transducers, amplifiers, and recording equipment used to measure the vibration motions reported in Chapter 5 of this thesis.

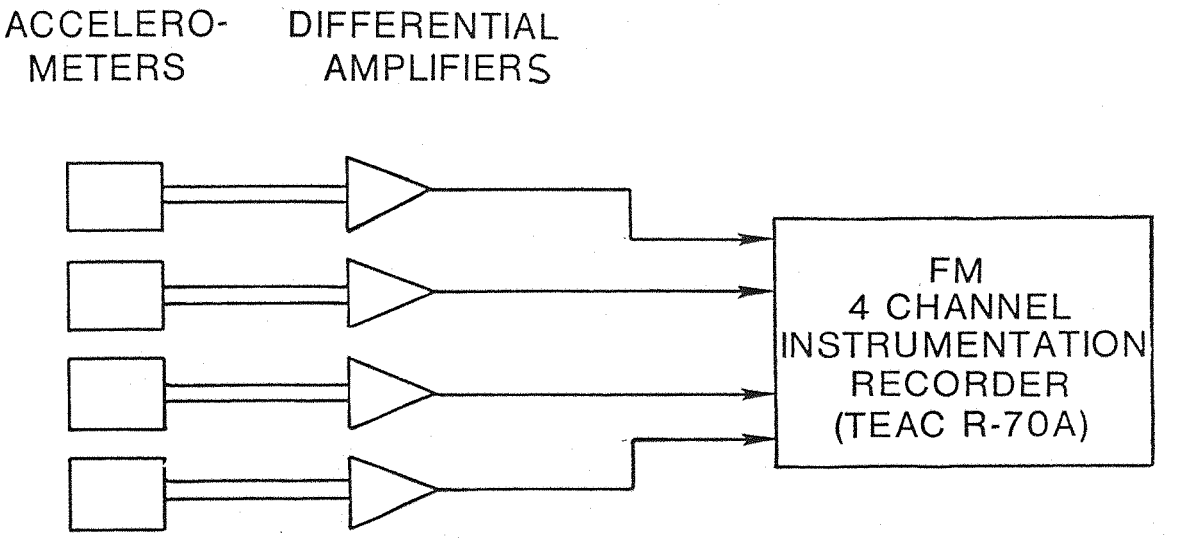

Figure A.5.2.1. Vibration Measurement Instrumentation

The rotational motions (i.e., head pitch, roll, yaw, and helmet pitch, and yaw) were measured by rotational accelerometers (Schaevitz ASMP-100). The translational motions (i.e., seat Z, seat back Z, seat back X, head Z, and display Z) were measured by translational accelerometers (Endevco 2265-20). Specifications of these accelerometers are given in Table A.5.2.1.

The signals from these transducers were amplified by instrumentation amplifiers designed and fabricated at the Institute of Sound and Vibration Research, University of Southampton. The outputs of the amplifiers were recorded by an FM instrumentation recorder (TEAC R-70A). Table A.5.2.2 gives the specifications of the recorder. The recorded signals from the accelerometers were then analyzed by replaying the tape recordings into the Data Analysis Center Facilities described in Section 3.5.

TABLE A.5.2.1. TECHNICAL SPECIFICATION OF ACCELEROMETERS

Type	Translational Accelerometer (Endevco 2265-20)	Rotational Accelerometer (Schaevitz ASMP-100)
Range	±20 g	±100 rad/s^2
Sensitivity	30 mv/g	10 $mv/rad/s^2$
Natural Frequency	1000 Hz	50 Hz
Damping	0.01 to 0.05	0.65
Cross Axis Frequency	1.5 mv/g	10 mv/g
Hysteresis	±0.6 mv/g	±2 $mv/rad/s^2$
Linearity	±0.6 mv/g	±5 $mv/rad/s^2$
Frequency Response	0-200 Hz ±1.5 mv/g	--
Operating Temperature	-18 to +65°C	-40 to +93.3°C
Mass	6 gm	56 gm

TABLE A.5.2.2. TECHNICAL SPECIFICATIONS OF INSTRUMENTATION RECORDER (TEAC MODEL R-70A)

Tracks	4
Channels	4
Tape Speed	4.75 cm/s ±1%
Wow and Flutter	0.5% rms or less (at 0.1 to 250 Hz)
Frequency Response (FM)	DC to 625 Hz (+1.0, -2.0 dB)
Signal to Noise Ratio (FM)	35 dB rms or more
Harmonic Distortion (FM)	3% or less (at 20 Hz)
Crosstalk	less than noise level between channels
Drift	±2%

Appendix A.5.3

DYNAMIC TRANSFER FUNCTIONS FOR INDIVIDUAL SUBJECTS
(EXPERIMENT BD.5)

This appendix contains the moduli and phases of the transfer functions for individual subjects as determined in Experiment BD.5. These transfer functions are given in Figures A.5.3.1 through A.5.3.8 as shown below:

Transfer Function	Figure	
	Modulus	Phase
$\frac{\ddot{Z}_{head}}{\ddot{Z}_{seat}}$	A.5.3.1	A.5.3.2
$\frac{\ddot{\theta}_{head}}{\ddot{Z}_{seat}}$	A.5.3.3	A.5.3.4
$\frac{\ddot{\theta}_{helmet}}{\ddot{Z}_{seat}}$	A.5.3.5	A.5.3.6
$\frac{\ddot{\theta}_{helmet}}{\ddot{\theta}_{head}}$	A.5.3.7	A.5.3.8

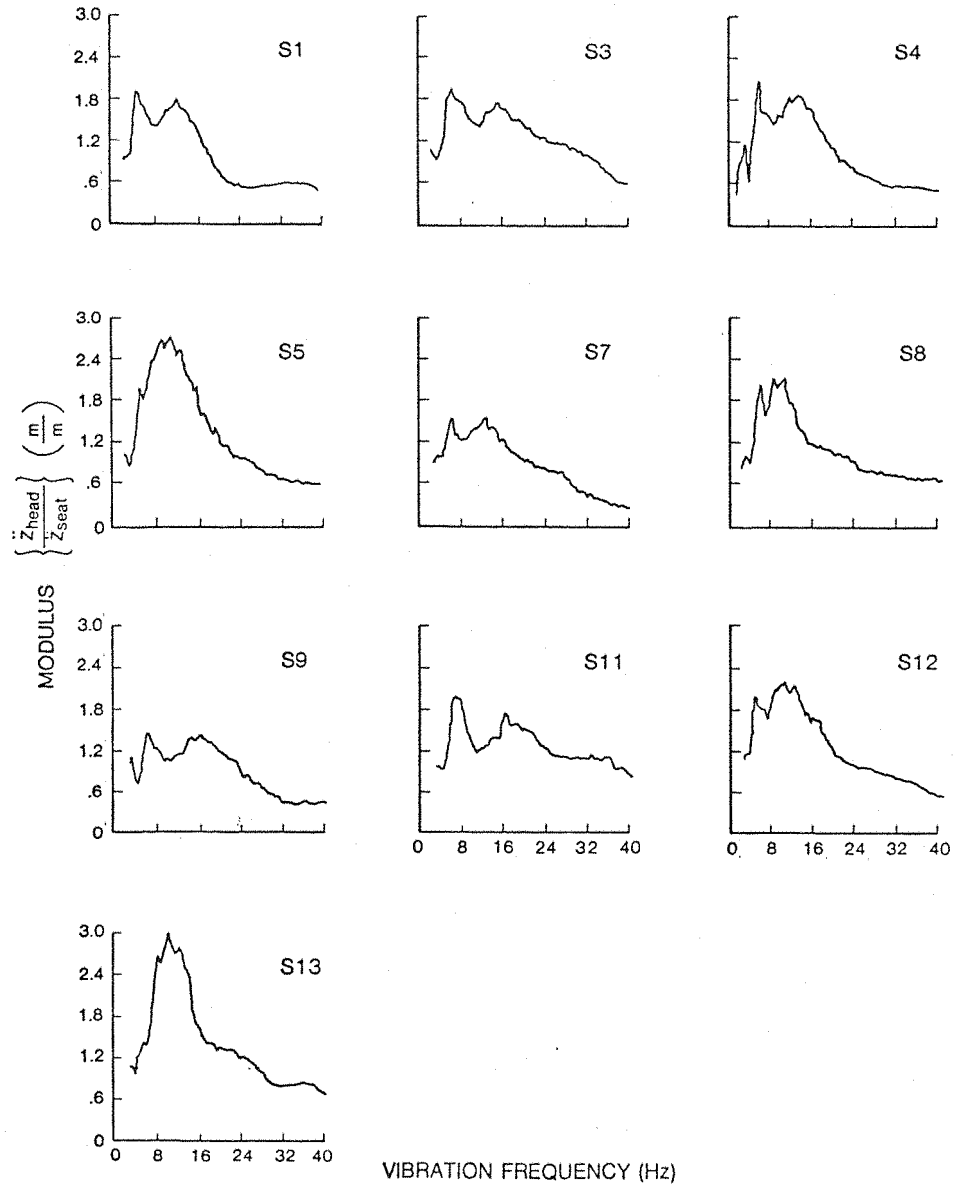

Figure A.5.3.1. Moduli of Head Z Axis to Seat Z Axis Transfer Functions for Individual Subjects (B_e = 0.5 Hz, DOF = 184, Experiment BD.5)

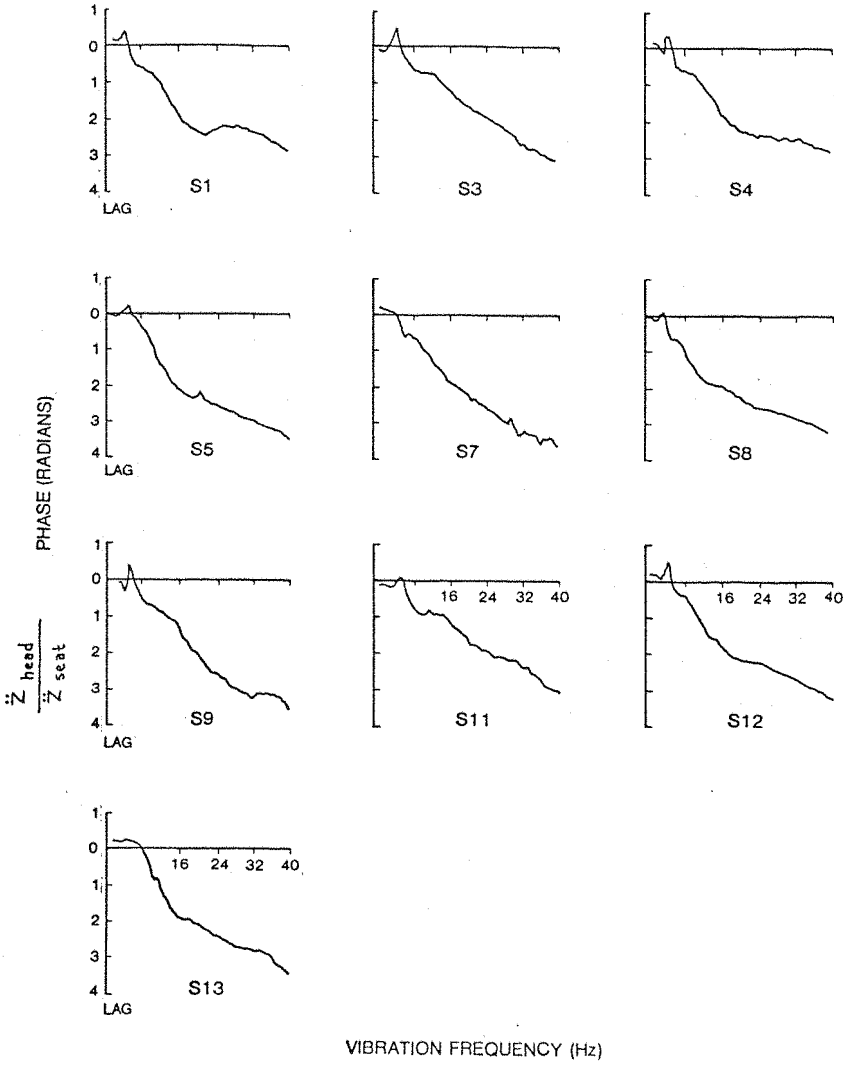

Figure A.5.3.2. Phase of Head Z Axis to Seat Z Axis Transfer Functions for Individual Subjects (B_e = 0.5 Hz, DOF = 184, Experiment BD.5)

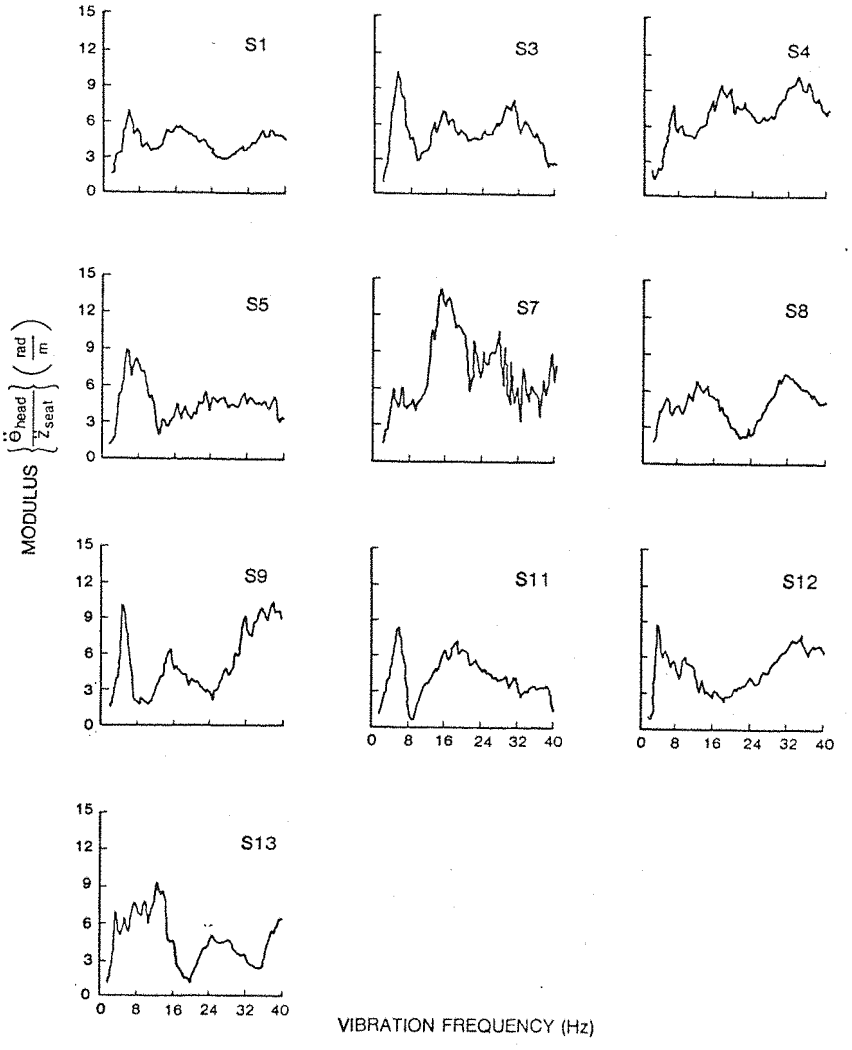

Figure A.5.3.3. Moduli of Head Pitch Axis to Seat Z Axis Transfer Functions for Individual Subjects (B_e = 0.5 Hz, DOF = 184, Experiment BD.5)

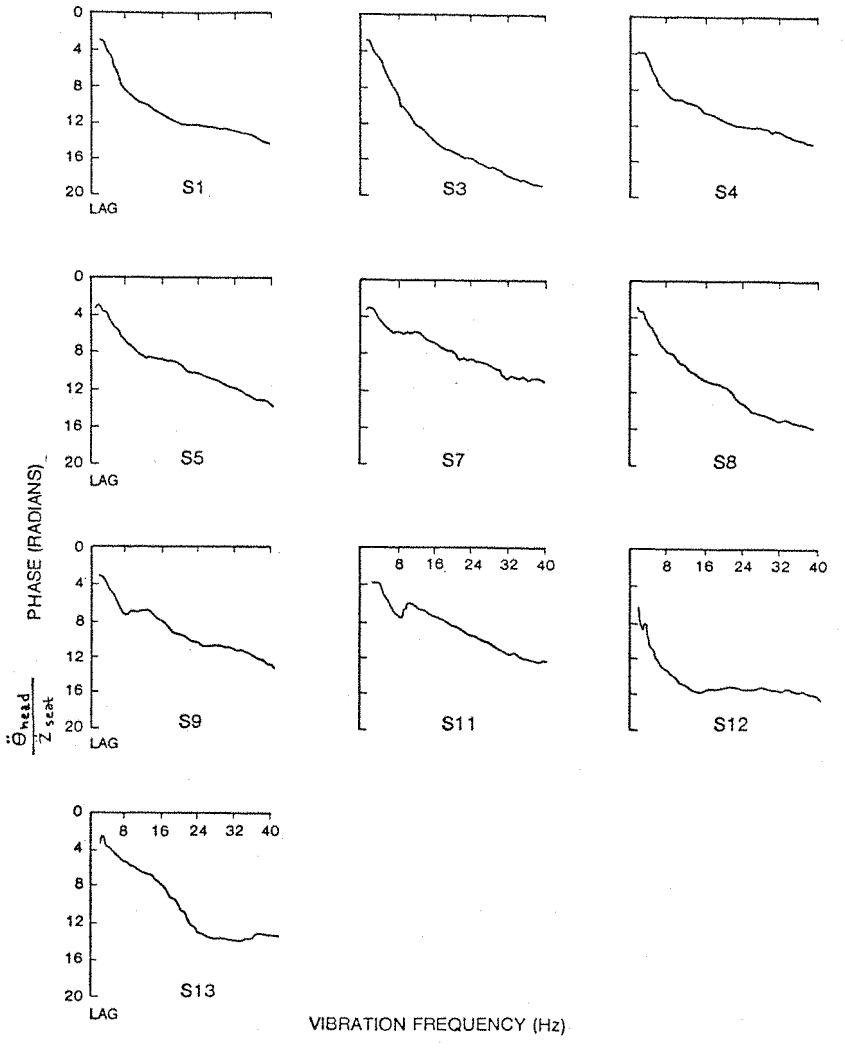

Figure A.5.3.4. Phase of Head Pitch Axis to Seat Z Axis Transfer Functions for Individual Subjects (B_e = 0.5 Hz, DOF = 184, Experiment BD.5)

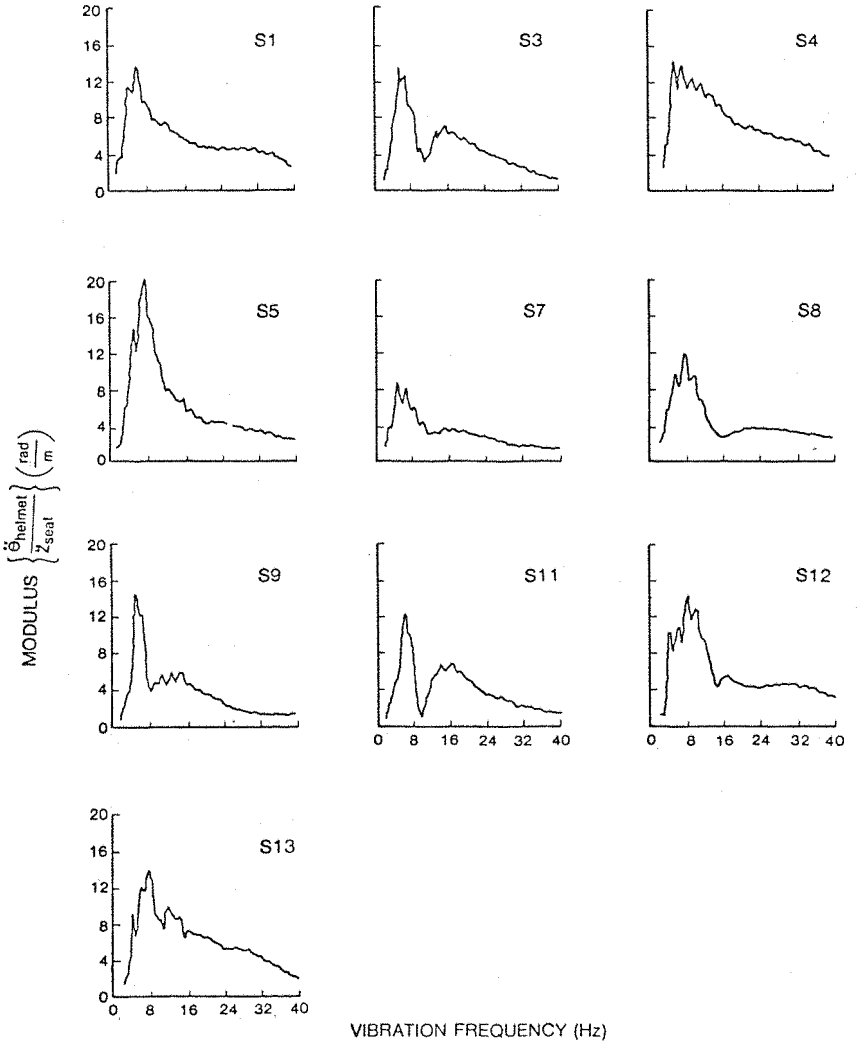

Figure A.5.3.5. Moduli of Helmet Pitch Axis to Seat Z Axis Transfer Functions for Individual Subjects (B_e = 0.5 Hz, DOF = 184, Experiment BD.5)

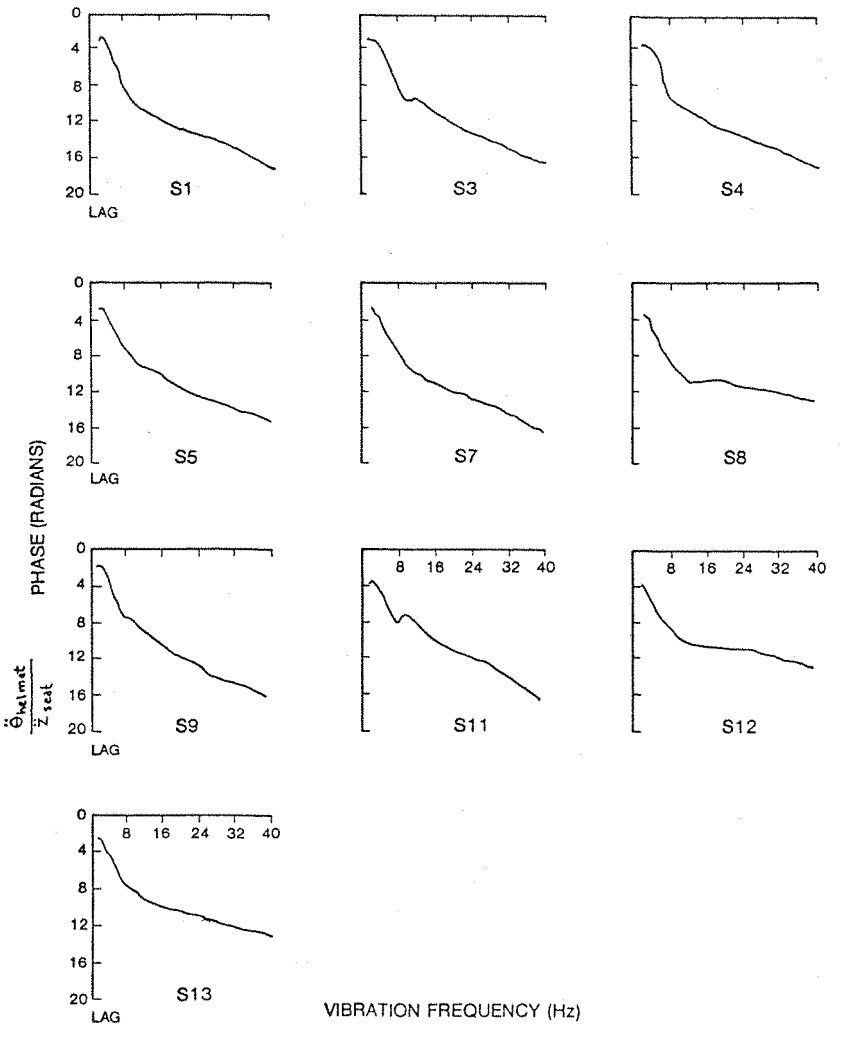

Figure A.5.3.6. Phase of Helmet Pitch Axis to Seat Z Axis Transfer Functions for Individual Subjects (B_e = 0.5 Hz, DOF = 184, Experiment BD.5)

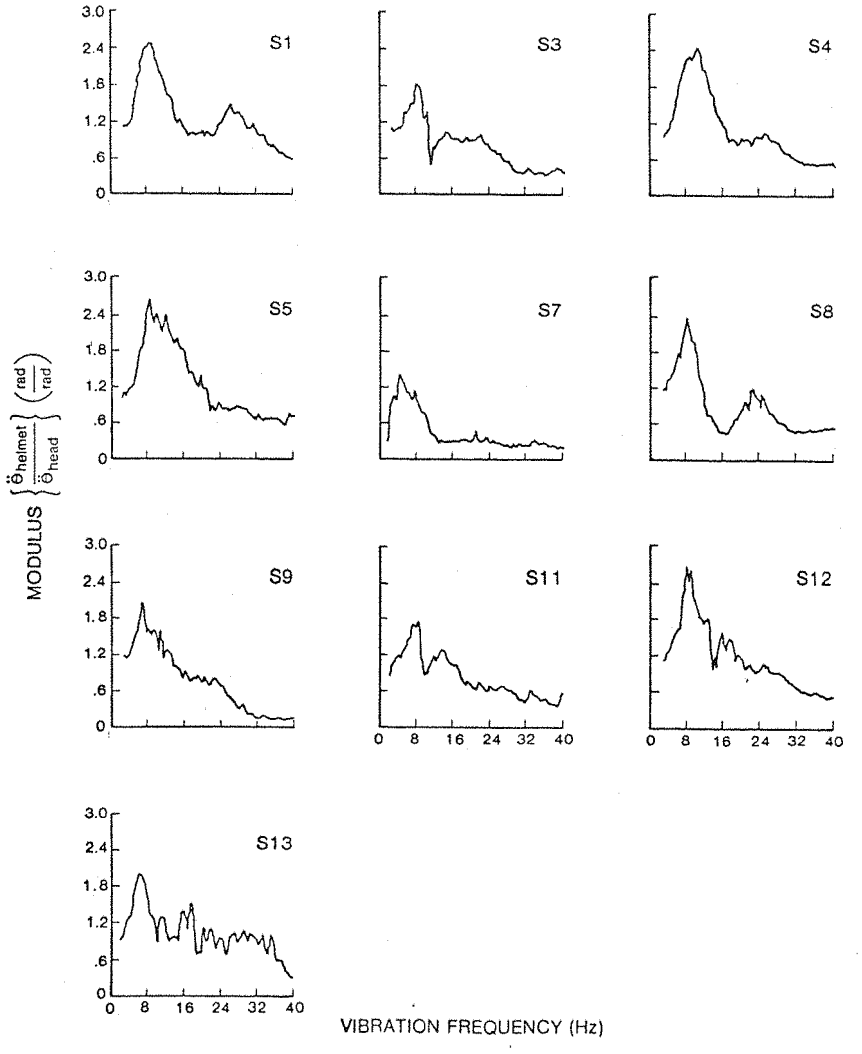

Figure A.5.3.7. Moduli of Helmet Pitch Axis to Head Pitch Axis Transfer Functions for Individual Subjects (B_e = 0.5 Hz, DOF = 184, Experiment BD.5)

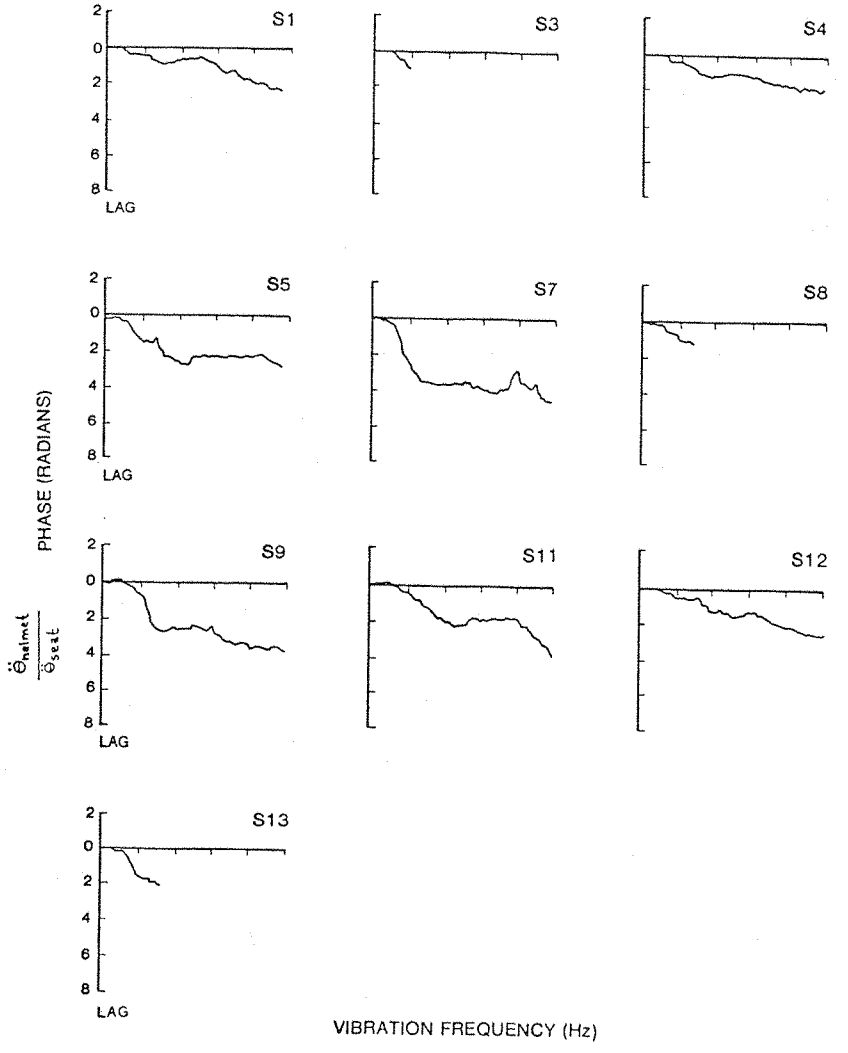

Figure A.5.3.8. Phase of Helmet Pitch Axis to Head Pitch Axis Transfer Functions for Individual Subjects (B_e = 0.5 Hz, DOF = 184, Experiment BD.5)

Appendix A.5.4

MODULI OF TRANSFER FUNCTIONS FOR SUBJECTS S3 and S8
AT SIX HEAD ORIENTATION ANGLES
(EXPERIMENT BD.7)

This appendix contains the moduli of transfer functions for Subjects S3 and S8 at various head orientation angles as determined in Experiment BD.7. These moduli are given in Figures A.5.4.1 through A.5.4.8 as shown below:

Modulus	Figure S3	Figure S8
$\frac{\ddot{\theta}_{head}}{\ddot{Z}_{seat}}$	A.5.4.1	A.5.4.2
$\frac{\ddot{\theta}_{helmet}}{\ddot{Z}_{seat}}$	A.5.4.3	A.5.4.4
$\frac{\ddot{\theta}_{helmet}}{\ddot{\theta}_{head}}$	A.5.4.5	A.5.4.6
$\frac{\ddot{\phi}_{helmet}}{\ddot{Z}_{seat}}$	A.5.4.7	A.5.4.8

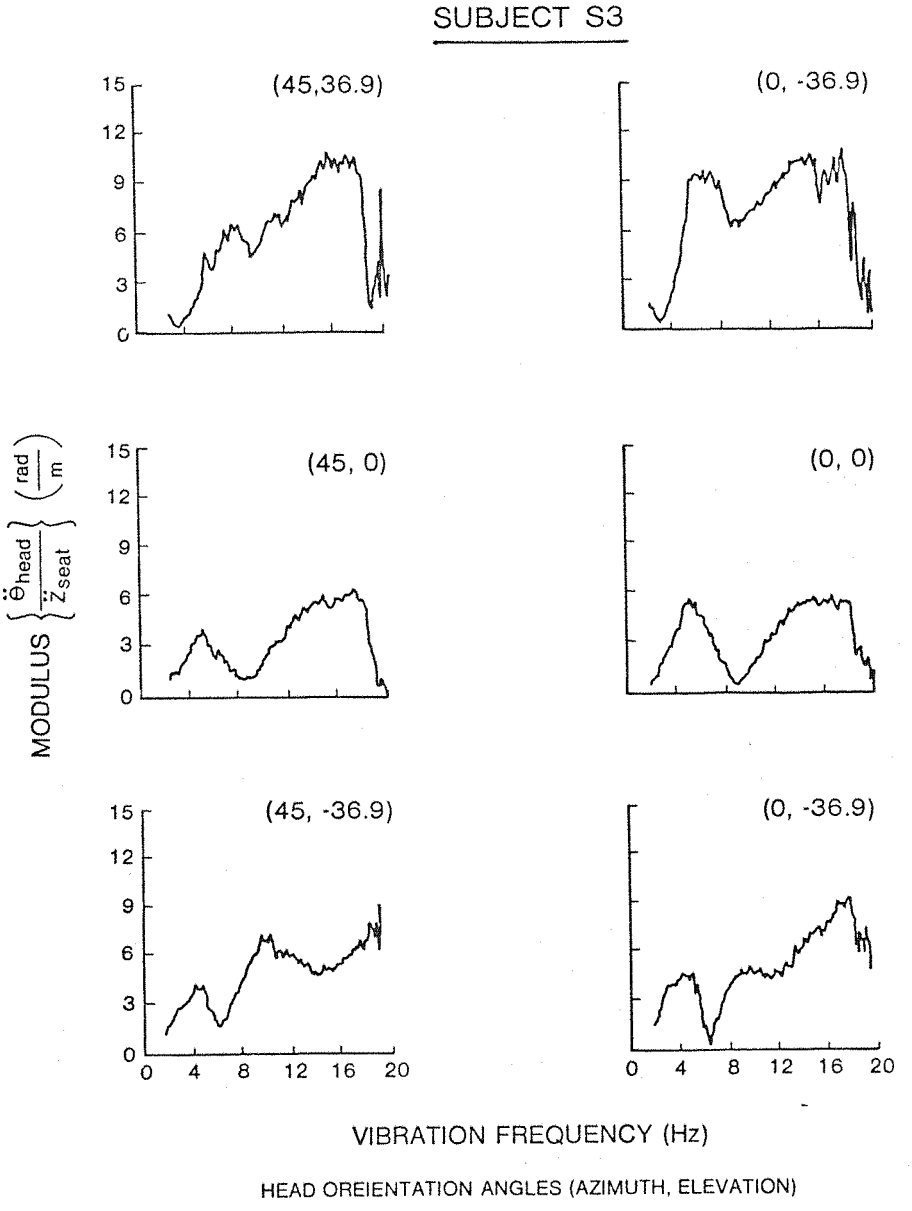

Figure A.5.4.1. Moduli of Head Pitch to Seat Z Axis Transfer Functions for Subject S3 at Six Head Orientation Angles (B_e = 0.2 Hz, DOF = 68, Experiment BD.7)

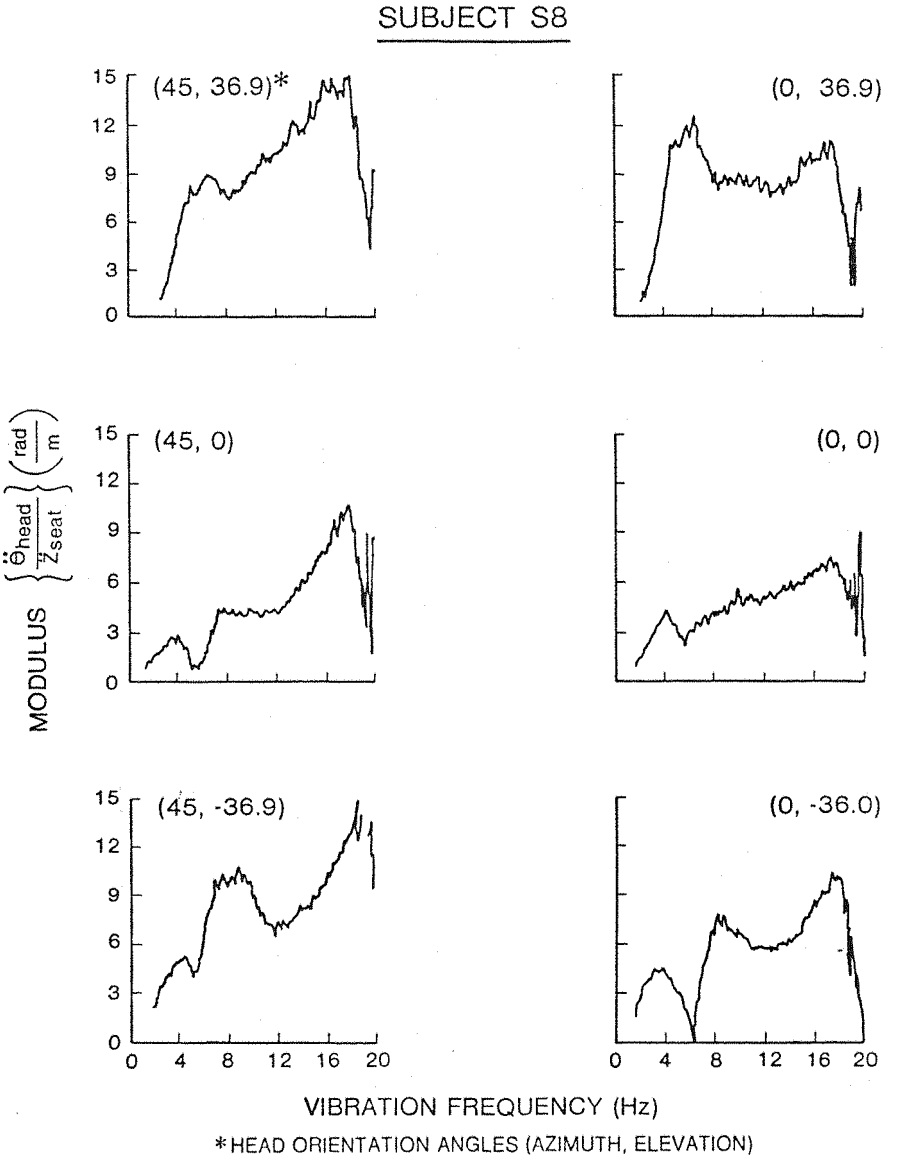

Figure A.5.4.2. Moduli of Head Pitch to Seat Z Axis Transfer Functions for Subject S8 at Six Head Orientation Angles (B_e = 0.2 Hz, DOF = 68, Experiment BD.7)

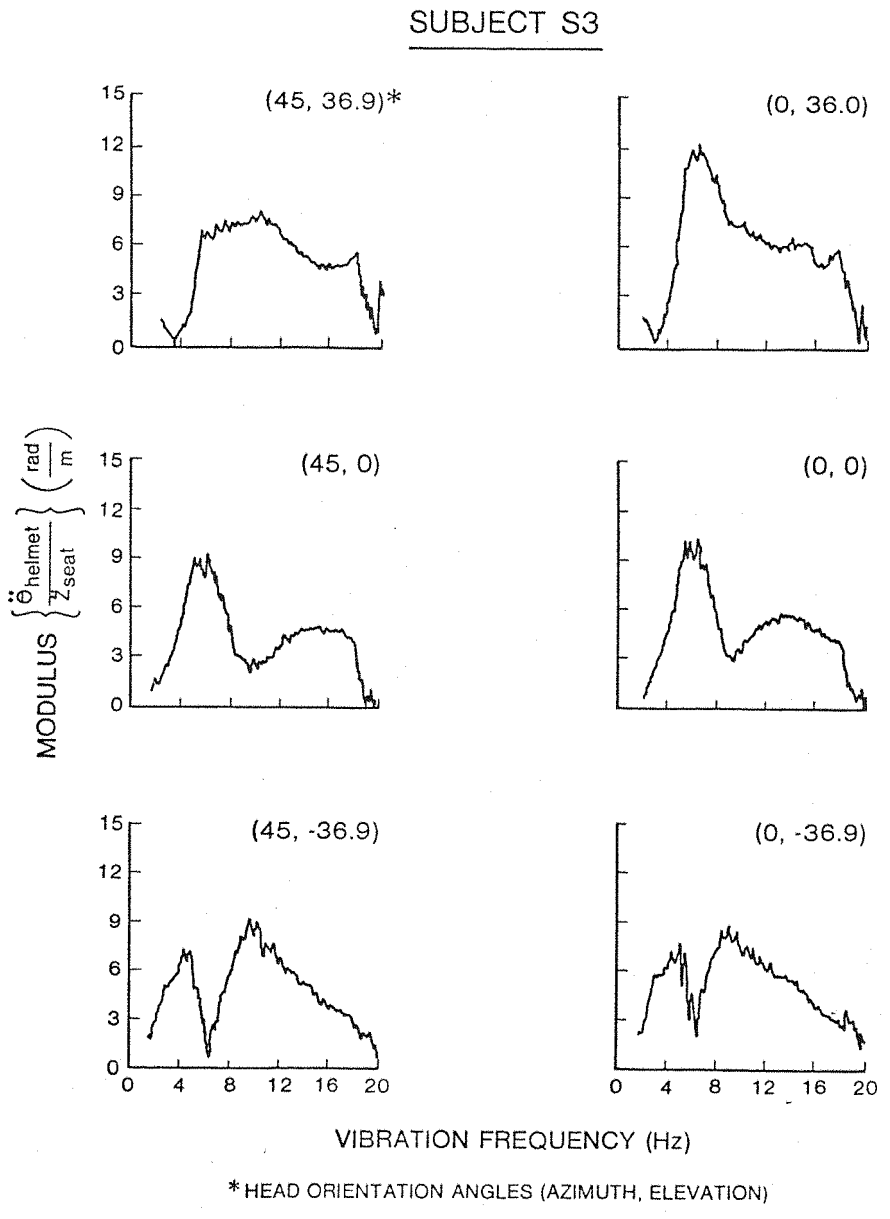

Figure A.5.4.3. Moduli of Helmet Pitch to Seat Z Axis Transfer Functions for Subject S3 at Six Head Orientation Angles (B_e = 0.2 Hz, DOF = 68, Experiment BD.7)

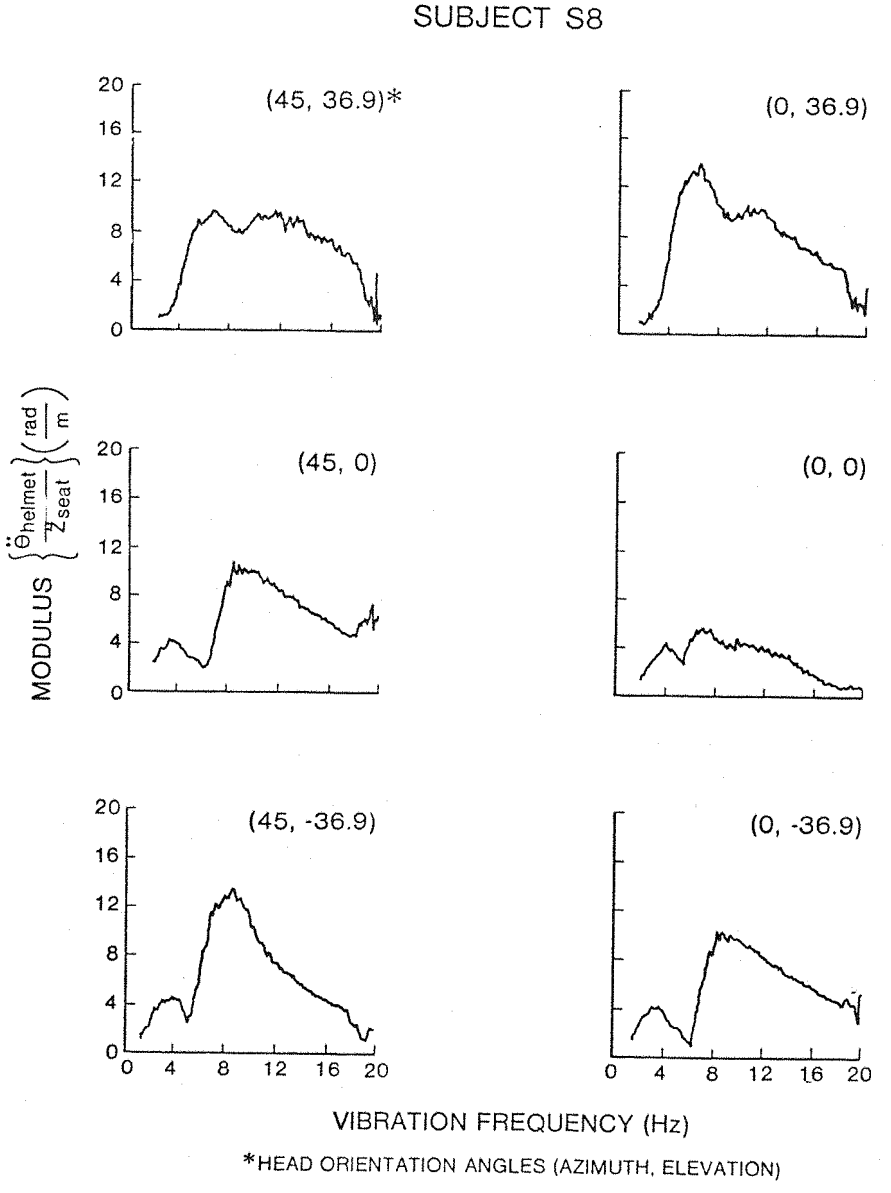

Figure A.5.4.4. Moduli of Helmet Pitch to Seat Z Axis Transfer Functions for Subject S8 at Six Head Orientation Angles (B_e = 0.2 Hz, DOF = 68, Experiment BD.7)

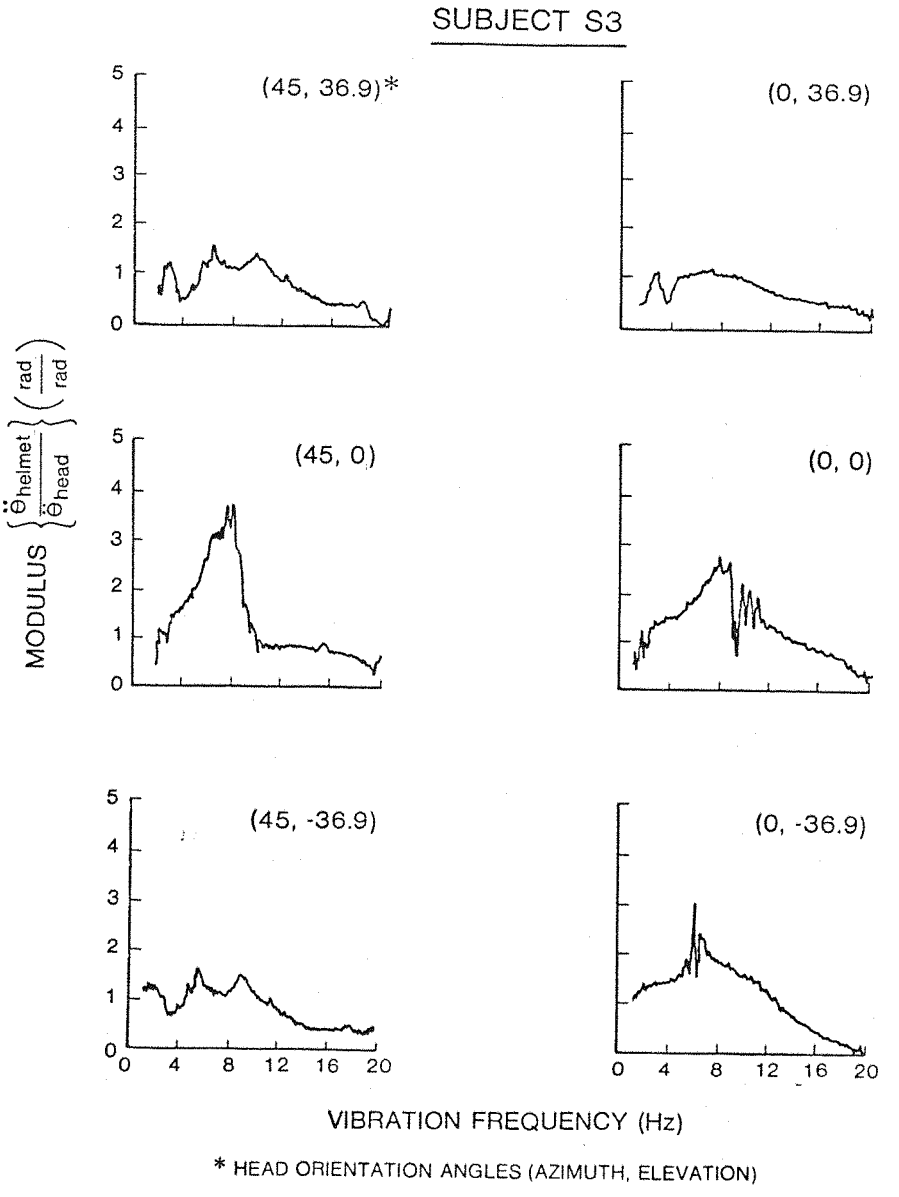

Figure A.5.4.5. Moduli of Helmet Pitch to Head Pitch Transfer Functions for Subject S3 at Six Head Orientation Angles (B_e = 0.2 Hz, DOF = 68, Experiment BD.7)

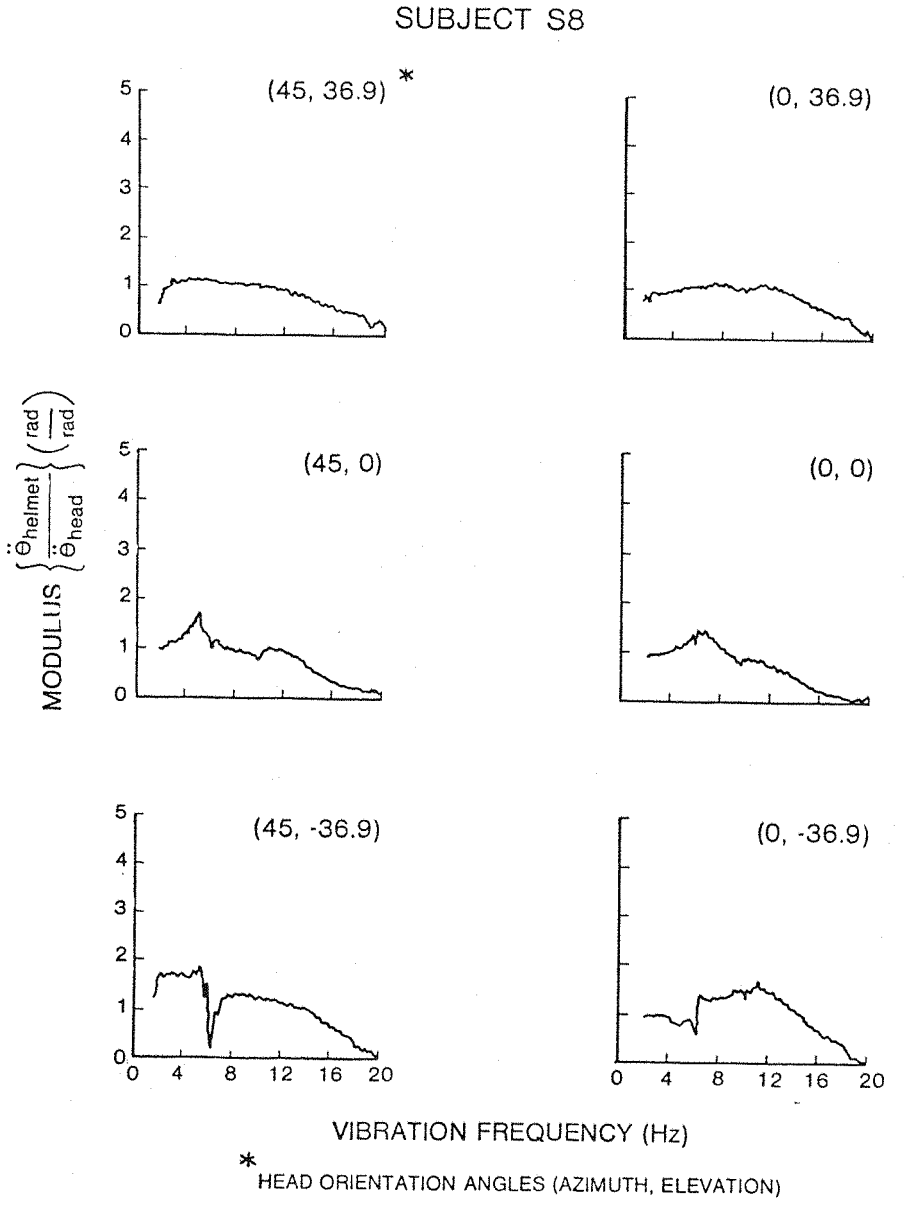

Figure A.5.4.6. Moduli of Helmet Pitch to Head Pitch Transfer Functions for Subject S8 at Six Head Orientation Angles (B_e = 0.2 Hz, DOF = 68, Experiment BD.7)

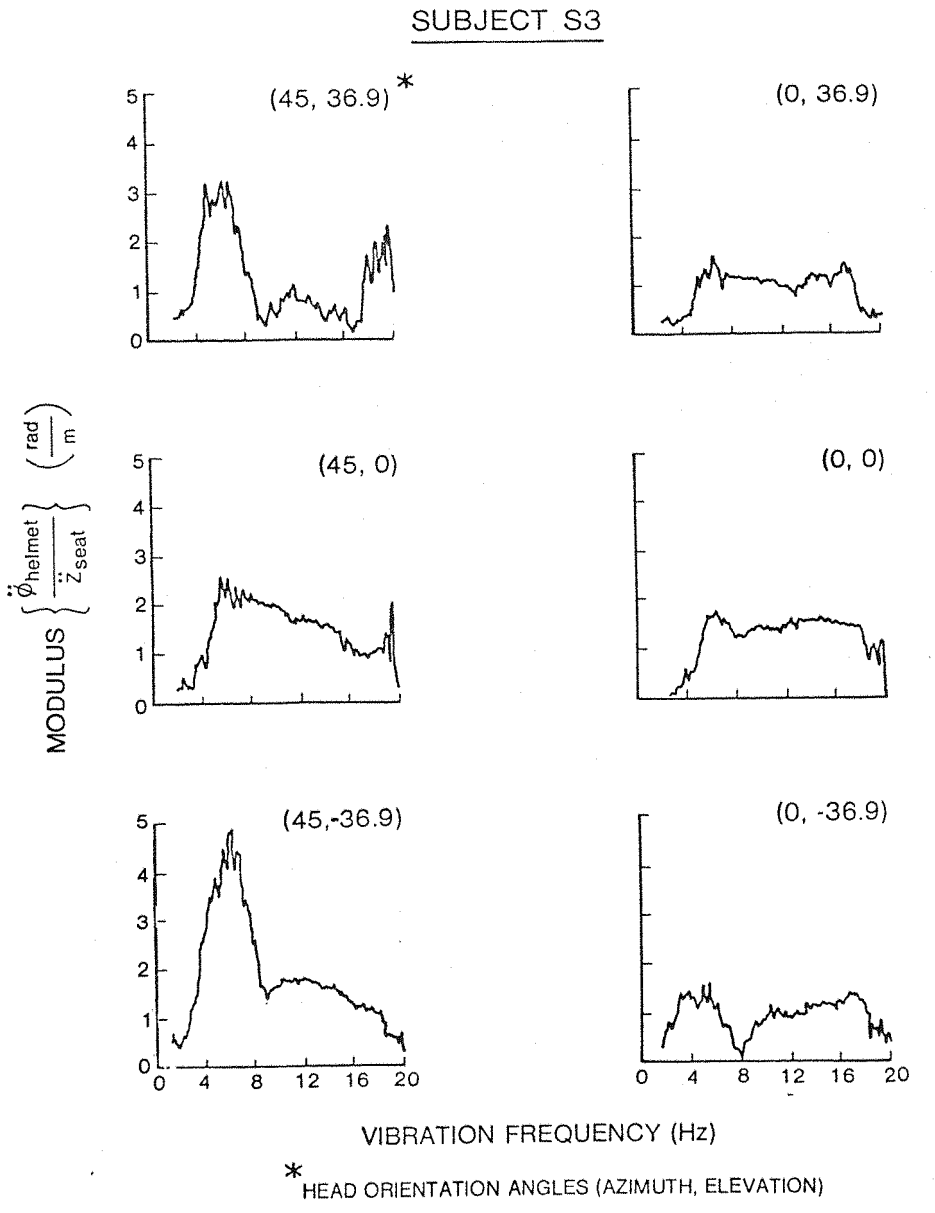

Figure A.5.4.7. Moduli of Helmet Yaw to Seat Z Axis Transfer Functions for Subject S3 and Six Head Orientation Angles (B_e = 0.2 Hz, DOF = 68, Experiment BD.7)

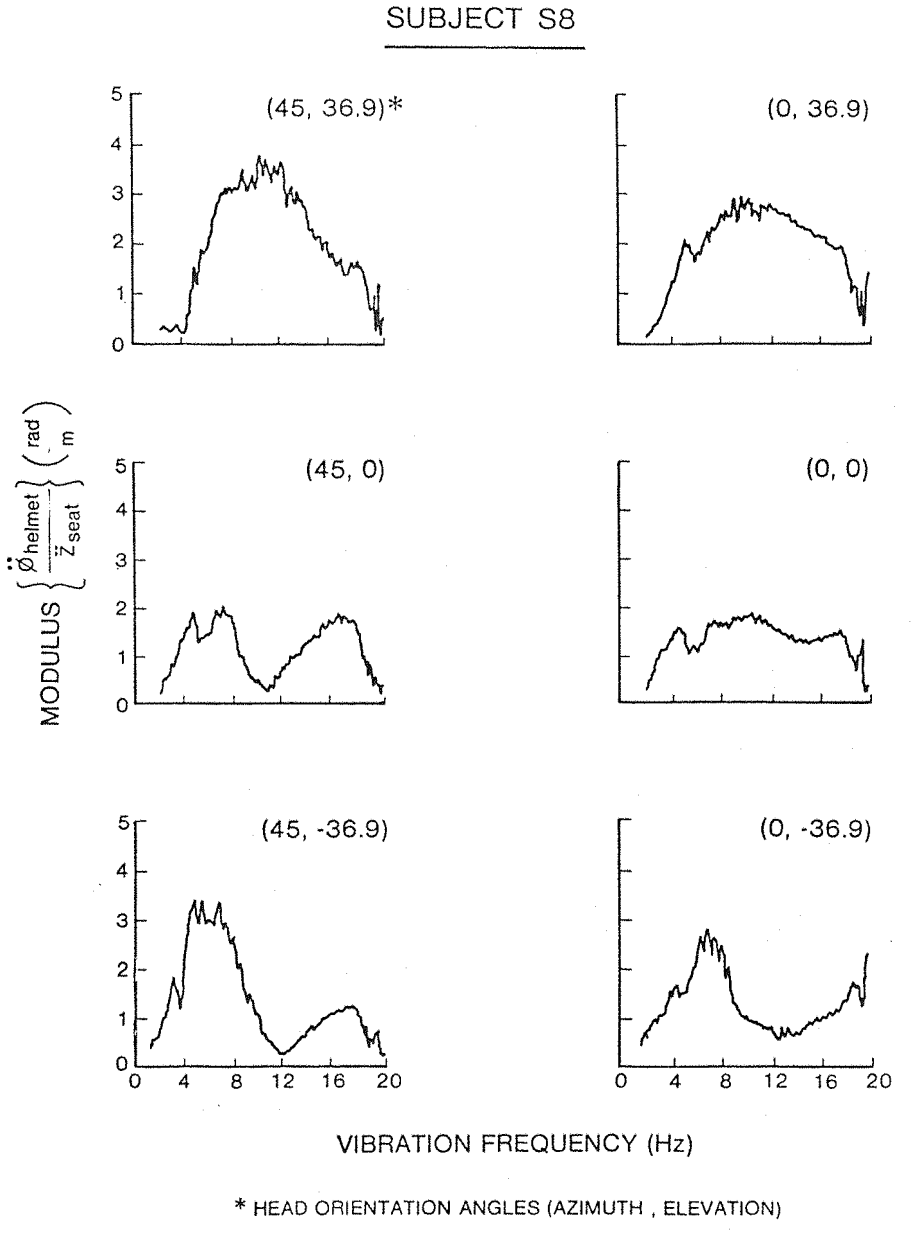

Figure A.5.4.8. Moduli of Helmet Yaw to Seat Z Axis Transfer Functions for Subject S8 and Six Head Orientation Angles (B_e = 0.2 Hz, DOF = 68, Experiment BD.7)